Addis Ababa University

Addis Ababa Institute of Technology

School of Graduate Students

School of Mechanical and Industrial Engineering

Thermal Engineering stream

Transient Computational Model of Ice Slab Formation Using Solar PV System for Milk Cooling

A thesis submitted to the school of Graduate Studies of Addis Ababa University in partial fulfilment of the requirements of the Degree of Masters of Science in Mechanical Engineering (Thermal)

By

Ayele Mengist Semane

Advisor: Dr. Ing. Demiss Alemu

Addis Ababa, Ethiopia

July 2020

Declaration

This is to certify that the thesis presented by Ayele mengist semane, titled as "Transient computational model of ice slab formation using solar PV system for milk cooling" and submitted to the School of Mechanical and Industrial Engineering in the partial fulfillment of the requirements for the award of the degree of masters of science in Thermal Engineering with the regulations of the university, and meet accepted standards with respect to originality and quality.

Ayele mengist semane	_____	_____
Name	Signature	Date

This thesis has been submitted for examination with approval as a university advisor.

Dr. Ing. Demiss Alemu (Ph.D.)	_____	_____
Advisor	Signature	Date

Addis Ababa University

Addis Ababa Institute of Technology

School of Mechanical and Industrial Engineering

School of Graduates Students

Transient computational model of ice slab formation using solar PV system for milk cooling

By

Ayele mengist semane

Approved by Board of Examiners

Dr. Ing. Demiss Alemu	_____	_____
Advisor	Signature	Date
Dr. Tilahun Nigussie	_____	_____
Internal Examiner	Signature	Date
Dr. Yilma Taddese	_____	_____
External Examiner	Signature	Date
Dr. Yilma Taddese	_____	_____
Dean of SMiE	Signature	Date
Dr. Ermias Tesfaye	_____	_____
Director of Post Graduate Program	Signature	Date

TABLES OF CONTENT

LIST OF TABLES

LIST of FIGURES

NOMENCLATURE

S	$Solid\ phase\ change\ material\ (ice\ slab)$
L	$Liquid\ phase\ change\ material\ (water)$
T	$Temperature\ [k]$
T_r	$Reference\ temperature\ [k]$
T_f	$Freezing\ and\ freezing\ temperature\ [k]$
G	The intensity of solar irradiance, W/m^2
G_r	The reference intensity of solar irradiance
K_V	Temperature coefficient of the open circuit voltage
K_i	Temperature coefficient of the short circuit current
U	Overall heat transfer coefficient
t	$Time\ [sec]$
V	$Volume\ [m^3]$
v	$Velocity\ [m/s]$
m	$Mass\ [kg]$
Lt	$Solidification\ thickness\ of\ ice\ [m]$
h	$Thickness\ of\ the\ capsule\ [m]$
$f(T)$	Liquid fraction $[-]$
Q_L	$Latent\ heat\ of\ fusion\ [J/kg]$
H	$Enthalpy\ [J/kg]$
Q	$Conduction\ heat\ transfer\ [w]$
h_l	$Convective\ heat\ transfer\ coefficient\ [w/m^2K]$
E	$Energy$
St	$Stephan\ number$
$X(t)$	$Solidliquid\ interface\ position\ [m]$

sl	$Solid-liquid\ region$
i_b	$Interface\ node\ index$
p	$Location\ of\ moving\ interface$
i,j	$Coordinate\ value$
erf	$Error\ function$
$erfc$	$Complementary\ error\ function$
eff	$Effective$
n	$Old\ value\ (at\ time\ t) of\ the\ dependent\ variable$
$n+1$	$New\ value\ (at\ time\ t+\Delta t) of\ the\ dependent\ variable$
b	$Beam$
d	$Diffuse$
rt	$Ratio\ of\ hourly\ to\ daily\ diffuse\ solar\ radiation$
Ho	Extraterrestrial solar radian
G_{SC}	$Solar\ constant$
P	$Parallel$
s	$Series$
PV	$Photovoltaic$
ref	$Refrigerant$
C_p	$Specific\ heat\ at\ costant\ pressure\ [J/kg.K]$
k	$Thermal\ conductivity\ [w/m.K]$
α	$Thermal\ diffusivity\ [m^2/s]$
ρ	$Density\ [kg/m^3]$
δ	$Declination\ angle$
ϕ	$Latitude\ of\ the\ site$

ω	Solar hour angle
ω_s	Sunset hour angle

ACRONYMS

PCM	$Phase\ change\ material$
TES	Thermal energy storage
FAO	$Food\ and\ agricultural\ organization$
FF	$Fill\ factor$
SC	$Short\ circuit$
OC	$Open\ circuit$
DC	$Direct\ current$
AC	$Alternative\ current$

ACKNOWLEDGMENT

The authors wish to acknowledge all individuals that contributed to this research: (1) the almighty God, (2) my adviser Dr. Ing. Demiss Alemu who give me unlimited advice, instructions, and encouragement at every step of this research. Sincerely I thank Fikadu G. PhD student for his supporting and giving valuable comments to me. I also thank all members of Addis Ababa University, AAiT, SMiE Thermal stream staffs and also big thanks to my friends those who stood beside me to accomplish this research.

Finally, I also thank my very deep gratitude to my parents and families for providing me with constant support and continuous motivation throughout all my years of study and through all the process of researching and writing this thesis.

Thank you.

ABSTRACT

Most of the Ethiopian people living around remote areas, their special daily needs are milk and milk products which needs preservation to keep from bacteria, germs and other small organisms. In case of Ethiopia specifically around rural areas using electricity are very rare due to less availability of electricity around there to cool domestic needs. For this reason, other alternative energy sources are needed which is solar PV ice formation system without battery due to its inexhaustible, renewable and non-pollutant energy sources. This research were studied to cool 50 litre of milk initially at a temperature of 4℃ during night by substituting 8.5 kilogram of slab ice to replace the amount of heat leak through the milk tank wall. Thus, in this study the mathematical model of phase change material solidification and melting by using transient explicit conduction type heat transfer equation was modeled. By using these mathematical equation the nodal temperature variation and ice crystal growth were simulated using Matlab algorism. And also the performance of ice formation at the specific location of Semera was studied using Matlab algorism. From the result, highly performed months of a year which forms required 0.04 meter ice crystal before 3PM and others form 0.037 meter ice crystal around 4PM. The result was also validated through comparison with other experimental result by considering the presence of solar radiation difference. The result is satisfied with small variation due to different solar radiation of the location. The system has the complete solution for making ice cold storage facilities in off grid areas and gives an environment friendly solution of the faced problem

CHAPTER ONE: INTRODUCTION

This chapter covers about background and justifications of the study, over views of ice formation and rural milk cooling systems, motivations of the study, problem statement and objectives of the research, scope and significance of the research, methodology, research outline and limitation of the research.

1.1. Introduction

Food is a universal need, for living humans to develop energy for live continuing. Milk and milk products are a very essential types of food in Ethiopia especially around rural areas, which needs preservation to keep from bacteria, germs and other small organisms by putting them in cold place. Mostly the refrigeration system is powered by electrical energy, however the availability of electricity in rural areas of Ethiopia is very less.

Because of, the low availability of electricity in rural areas of Ethiopia, the refrigeration system needs any other alternative energy sources and methods must be taken in to account to drive compressor and condenser fans. Some of the alternative energy sources are to use diesel engine, water, wind energies, solar thermal and solar photovoltaic systems etc. but these are very expensive and constructing them to remote areas are a difficult task except solar thermal and solar photovoltaic energy systems. So, to avoid and reduce the addressed problems, it is important to addressee the rising need for a new fuel renewable (inexhaustible or endless), nonpolluting and inexpensive energy source by utilizing solar energy.

Even though solar photovoltaic energy is renewable, nonpolluting and inexpensive energy sources, it needs a storage battery to store energy used for night and non-sunny or cloudy days. Using batteries for photovoltaic energy system needs high capital and maintenance cost, which are battery cost, charge controller cost, inverter cost and replacement costs. Additionally, environmental pollution from batteries due to their contaminating elements and limited life cycle due to very rare or very difficulties of recycling the used batteries, needs funding for purchasing and transporting the device from developed to developing countries like Ethiopia [1].

Replacing the energy storage batteries by locally available phase change materials such as water eutectic salts and honey wax is a very interesting technology to store cold and hot energy by phase transition for the purpose of using it when sunlight is readily not available

or at night. Using these system is inexpensive, needs less equipment, high portability and reliability [2]**.** Using these phase change materials depends on the areas of application, availability, and cost and its energy charging and discharging performance. Water is a good phase change material due to its availability, cost, and used to store both cold and hot energy by cooling and heating it respectively.

In refrigeration system the water adjacent to the evaporator forms ice using cylindrical, spherical or rectangular (slab) geometries during sunny days and back to water during night or cloudy days. These three geometries have different performances to change water in to ice (solidification) and back to water (melting).

1.2. Background and Justification of the Study

In Ethiopian, especially around remote areas, milk and milk products are common. Based on the above explanation these types of milk products are easily affected by bacteria, germs and other small organisms, which are the cause of human health problems. For this reason, cooling is important to keep these types of product from bacteria, germs and other small organisms. It is known that to preserve these product needs energy which is developed by one of the followings energy sources which are, electric motors, diesel engine, solar, wind, water, etc. For in case of Ethiopia specifically around rural areas using electric motor to power refrigeration system for milk product preservation is very rare due to electricity problems around there. For this reason, every individuals living around there are suffering by health problems due to using unpreserved milk products.

In some remote areas there is a possibility of water powered refrigeration system nearest to the river, however these plants can operate only two or three months throughout the year due to rain dependents of Ethiopian rivers. There is also other possibility of diesel engine powered refrigeration system around there, which is nonrenewable, exhaustible, pollutant and costy energy sources. For this reason, using diesel engine for this purpose, pollutes the environment by releasing CO_2 gas during operation, and cost of powering is high due to cost of exhaustible fuel. Using wind energy powered refrigeration system, needs high capital cost and it is not available every remote areas of Ethiopia.

The sun is an inexhaustible or endless source of energy, and the amount of solar energy an area receives depends on day time, season of the year, sky cloudiness, and closeness of the area to the earth’s equator. Ethiopia is close enough to the equator to get plenty of solar

power; in a fourth rank in the world in terms of solar heating potential, with thirteen months of sunshine [3]. So, it is important to use the technology of solar energy powered refrigeration system either Solar photovoltaic PV refrigeration system or solar thermal refrigeration system in order to solve the addressed problems.

Solar photovoltaic refrigeration system has more advantages on the refrigeration effect, due to simple operation and energy utilization rate compare to solar thermal refrigeration system [4]. Photovoltaic refrigeration system with battery, has a very expensive cost, exhaustible sources and affects the environment, however using ice to store cold energy in place of battery needs less cost, non-pollutant and inexhaustible sources of energy.

Using ice for cold energy storage device has the problems of imbalance between charging and discharging processes of the system. To produce enough ice for the specific application and discharge it within the needed time period an efficient system must be design and evaluate by using computational methods such as **Ansys fluent** and **Matlab simulations**.

Thus, to reduce health problems due to unpreserved milk products, by constructing solar PV ice slab formation system, in this research analyzing the transient computational model of ice slab formation using solar PV system, by using Matlab programing is expected to get the following merits.

- Reduce electricity consumption from grid system
- Reduce health problems due to using unpreserved milk products
- Reduced greenhouse gases due to replacing diesel engine by solar systems and batteries by ice.

Experimental, analytical and computational methods are the three-research problem solving methods. From these computational method needs less cost and easy way compare to experimental method.

For this reason, it is important to analyze the transient ice slab formation using photovoltaic system by using computational methods in order to analyze the solidification performance of the system and the developed ice thickness throughout the year to preserve milk and milk products in remote areas of Ethiopia.

1.3. Over View of Ice Formation Using PV System and Milk Cooling

1.3.1 Different Techniques of Ice Formation System

Ice formation is the transforming process of water to ice by cooling water below its freezing point temperature of 0℃. During ice formation phase change takes place due to the heat transfer process of ice formation in order to cool the process [5].

In addition to water, ice used for the phase changing medium in ice storage system to provide the system with more cooling capacity than chilled water system due to the latent heat of fusion. The thermal storage is charged by generating ice and stops generating when cooling is required. In order to build ice a chiller is required located outside the storage tank to generate ice either directly from the radiator in the tank or by pipe filled with glycol inside the tank in an ice storage system. In this system the chiller cools the glycol solution to a lower temperature and these glycol solution pumped through the pipes to freeze the water to produce ice around the coil. Thermal ice storage is more advantage than conventional chilled water system its ability to produce energy needs based on time rather than cooling requirement [6].

In Ethiopia, ice fabrication using solar energy system is not common. But around the hot areas of the country, they produce ice in traditional way by putting a plastics of water in a domestic refrigerator and they sell one kilogram ice by one birr for peoples have not a refrigerator to cool drinking water.

1.3.2 Rural Milk Cooling System

In the remote areas of Ethiopia, there is no any cooling systems for different daily products like milk, meat, fish and fruits. Due to the absence of cooling systems, the rural women uses different traditional mechanisms to keep milk and milk products from bacteria. Some of the mechanisms are putting milk and milk products outside the house during night time, adding salts and mitmita on the milk products to keep it from bacteria and other small organisms.

In developed countries they uses a modified of the shelf direct drive photovoltaic refrigerator technology, coupled with innovative cooling and energy storage devices to cool evening milk on the farm for later transport to the next morning to milk product collection centers [7]. And also there was evaporative cooling which is a physical phenomenon in

which evaporation of a liquid, typically into surrounding air, cools an object or a fluid medium either water or air in contact with it [8].

1.4. Motivation

In Ethiopia, milk and milk products processed industries are located in towns. But milk product suppliers in the country are small holder dairy farmers, located around remote areas long distance from the processed industries. They do not have electricity access from the national grid and the only available solutions around there is the diesel generator. There is a problem with the availability and the continuously increasing price of diesel fuel in the remote areas as well as all over the country due to its expensiveness.

Thus, there has not been an economical method available for farm milk cooling systems in the country for small holder dairy farmers and other mixed farmers. In Ethiopia most milk is collected from the cow, camel, and goat are half in morning and half in evening times. The dairy organizations located around small towns have organized to collect only morning milk products, but they do not accept evening milk due to a high bacteriological count, since it is collected in the evening and kept in warm place until morning. Due to the lack of on-farm cooling system, half of the milk product collected in the evening time can be either forced consumed, sold cheaply to nearby neighbors or hawkers or they can be lost or it goes to wasted. For this reason, the total of milk produced in Ethiopia's remote areas only half is processed in the industries and leads to decrease the milk productivity in the country and also the quality of the produced milk [9]. Rural milk wastage due to lack of preservation is not only evening milk, but also unused morning milk was wasted.

The motivation of this research is, due to all of the above reasons in the sides of milk product. In the sides of energy product and utilization, solar energy and ice thermal energy storage systems are becoming more and more general. This is due to the broadly increasing energy demand, because of an increasing of electricity rates. And also another great advantages of ice thermal energy storage system, due to its environmental benefits by lowering overall electricity generation from environmental malevolent sources such as coal, oil or natural gas fired power plants, to lower the overall greenhouse gas emission from these power plants. So the implementation of solar PV ice formation system around remote areas to store ice thermal energy used to cool different daily products, such as meat, fish, milk and milk products, fruits and medicines without altering the existing air conditioning systems [2]. For these reason around remote areas integrated solar PV milk

cooling and ice making system during day time is important, in order to keep the minimum milk temperature during night time by adding ice to replace the heat leak through the milk tank wall [10].

1.5. Problem Statement

In Ethiopia especially in rural areas there is no refrigeration systems to preserve domestic foods like milk and milk products. This leads to decrease the quality of milk and milk products and increase health problems due to using unpreserved milk products. According to World Bank report in 2017, more than 57% of Ethiopian population living in remote areas are live without using electricity both grid connected and off grid systems and hence they are suffering by these health problems.

There are possible cooling powered systems to preserve milk and milk products around remote areas, using diesel engine, wind, hydro and solar sources. However, using water can operate only two or three months throughout the year due to rain dependents of Ethiopian rivers, using diesel engine for this purpose, pollutes the environment by releasing CO_2 gas during operation, and cost of powering is high due to cost of exhaustible fuel, using wind energy powered refrigeration system, needs high capital cost and not available every remote areas of Ethiopia.

Even though utilizing solar PV refrigeration system for milk cooling has more advantages on the refrigeration effect, due to simple operation and energy utilization rate compare to solar thermal refrigeration system and other energy sources, it needs battery in order to keep daily cooled milk temperature at night, which is a very expensive due to high capital and maintenance cost, exhaustible or limited life cycle or not recycled, and affects the environment by releasing contaminating elements and it is not locally available. For these reason, using ice to store cold thermal energy in place of battery, is cost effective, available everywhere, inexhaustible and renewable sources of energy.

The extensive use of traditional and inefficient way of ice formation system causes high energy demand with less performance of the system and leads to decrease cooling capacity of ice. To avoid or minimize these problems and increased concerns around remote areas, transient computational model of ice slab formation using PV system could be designed to solve the problems, and to analyze the performance of the whole system specifically melting and solidification of ice.

For this research focus is given to investigate the performance of ice slab formation to size the photovoltaic panel to make the required ice.

1.6. Objective of the Research

1.6.1 General Objective

- The general objective of the research is to study and analysis the transient computational model of ice slab formation using solar PV system to produce ice in order to cool milk and milk products around selected remote areas during night.

1.6.2 Specific Objectives of the Research

The specific objectives of this research are:

- Collect and sorting solar radiation data around hot remote areas of Semera.
- Mathematical modeling of phase change material solidification and melting.
- Ice slab and milk tank design and geometrical modeling of system.
- Simulation of ice slab formation, to find ice thickness variation as a function of time and nodal temperature distribution of water.
- Analyzing the performance of slab ice solidification using solar PV system around selected hot remote areas of Semera.
- Compare (or validate) these computational results with the experimental result done by other researchers.

1.7 Significance of the Research

The majority of Ethiopian populations are living in rural areas. As we know, there is shortage of electricity in remote areas of Ethiopia. Due to this there is no refrigeration system around there to cool daily domestic products like milk and milk products. The unpreserved milk product can easily affect by bacteria and germs which are the Cause of human health problems. So, solar PV milk cooling with ice storage system plays an important role in their life. The solar ice slab formation system is expected to solve the problems of human health, battery cost and environmental impacts of the battery by replacing this ice thermal energy storage system on it by using ice thermal energy for milk cooling during night.

1.8 Scope of the Research Study

The scope of this MSc thesis is to develop the methodologies of converting solar PV cooling system with battery backup by solar PV cooling system without battery which is

slab ice formation using solar PV system. The major objectives involve simulating and modeling the ice crystal growth variation as a function of time and nodal temperature distribution of water by using Matlab programming. This research work is conducted to analysis the performance of slab ice formation using solar PV system to cool milk and milk products during night around hot remote areas.

1.9 Methodology of the Research

The methodologies and materials to achieve the objectives of transient computational model of ice slab formation using PV system for night milk cooling application in remote areas are the following:

1.9.1 Literature Survey, Data Collation and Computational Modeling

At the begging reviewing related literatures and collecting solar radiation data and sorting.

Mathematical modeling of PCM solidification using 1D transient explicit method, due to its high accuracy of the result.

Cooling load calculation and Select DC compressor based on the amount of cooling load and formulate the rpm of the selected compressor using compressor performance equation and performance coefficient values integrated with electrical energy generated from solar PV system and thus, formulate cooling capacity of the system.

Matlab program modeling of nodal temperature distribution of water and ice crystal formation with time variation. And also analyzing system performance. The chosen of Matlab program is due to its accurate result for heat transfer problems

1.9.2 Result and Discussion

Discussion is done on the results obtained from the computational simulation results and the result was compared with experimental results from literature.

1.9.3 Conclusion and Recommendation

The recommendation and conclusions are presented based on the simulation result obtained and analyzed. The simulation results were concluded and recommended accordingly, and also future works are presented in this area.

1.10. Limitations of the Research

Even though it was fully accomplished of the research successfully by giving deep attentions of the research and using different alternatives to model the system, the limitations as:

- Internet service problems, due to shortage of computer laboratory rooms and only five working days per week from Monday to Friday.
- Another limitation of the research, due to expected time limitation and budget, it was not possible to manufacture and construct solar PV powered ice slab formation system at the specific location, except simulation of the systems by using computational methods.

1.11. Layout of the Research

This research contains eight chapters where, chapter one justifies about the applications of using ice slab cold energy storage in place of battery for milk cooling during night around remote areas. And also it covers the research problems, objectives, scope and delimitation.
Chapter two explains about different literatures related to ice slab formation using solar PV system for different applications with its historical background as well. It also explains solar DC refrigeration system, principle of ice formation system using solar energy.
Chapter three deals about the details arrangement of solar PV panel and its mathematical modeling to study PV characteristics.
Chapter four deals about methodologies of the research, such as the mathematical modeling of phase change material using fixed and moving mesh methods, construction of ice and milk storage tank, total cooling load calculation, solar radiation calculation, sizing of solar PV module.
Chapter four deals about the refrigeration component selection and design and also modeling all the system components geometrically.
Chapter six includes simulation of ice slab thickness and nodal temperature of water using Matlab code and explaining its result and also validation the result with experimental values, analyzing the performance of ice slab formation using solar PV system around the selected remote areas.
Chapter Seven deals with summarizing the results of the work and indicating future works, in the conclusion and recommendation.

CHAPTER TWO

2. Literature Review

2.1 Introduction

This chapter reviews thermal energy storage systems and types, phase change materials, transient heat transfer numerical formulations, different methods of refrigeration and ice formation using solar PV systems. This chapter also covers related literatures of ice formation using solar PV system, like the thermal insulation systems of the ice storage tank, different types of ice formation geometries, control mechanisms, feasibility of ice formation using solar PV system, different mechanisms to increase thermal conductivity of phase change material, summary of different literatures and findings of the study.

2.2 Thermal Energy Storage (TES) System

There are different types of energy storage systems, these are:- mechanical energy storage system, electrical energy storage system and thermal energy storage system.

Thermal energy storage is a temporary thermal energy holding system in the form of cold or hot substance for later utilization, which is helpful to balance between supply and demand of energy. The system deals with storage of energy, by heating, cooling, solidifying, melting, or vaporizing of substance and when the process is reversed it becomes thermal energy [12].

The quantities of thermal energy storage system depends on temperature. The energy content of the system can be increase with increasing the temperature of the substance. E, is the required energy to heat a volume V of a substance from a temperature (T_1) to temperature (T_2) is given by [13].

$$E = mc(T_2 - T_1) = \rho Vc(T_2 - T_1) \dots\dots\dots\dots\dots\dots\dots\dots\dots\dots [2.1]$$

Where C, ρ *and* m: *are* specific heat, density and mass of the material respectively.

2.3 Thermal Energy Storage Process Steps

Thermal energy storage involves at least three steps to complete its process, which are charging, storing and discharging. Charging and storing may occur simultaneously and each step may occur more than once in each storage cycle [13].

In these research the slab ice is formed inside the rectangular geometry by charging from one side and discharges through the four sides of the tank.

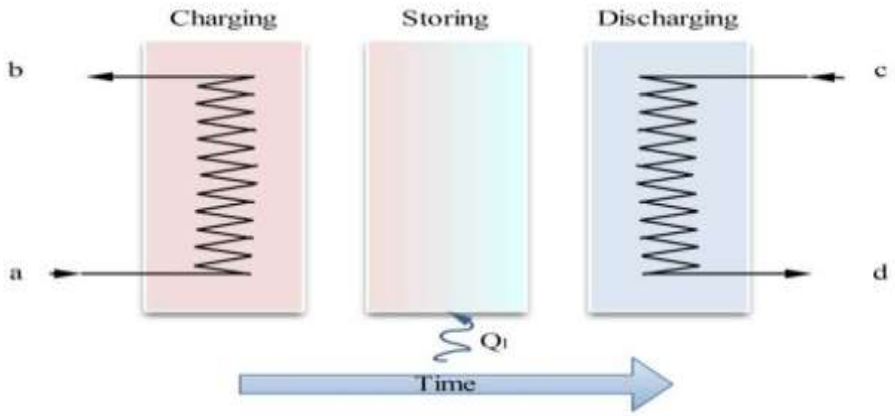

[Source, [13]]

Figure 2-1. The three processes in a general thermal energy storage system

The main types of thermal energy storage system are sensible and latent heat storage systems.

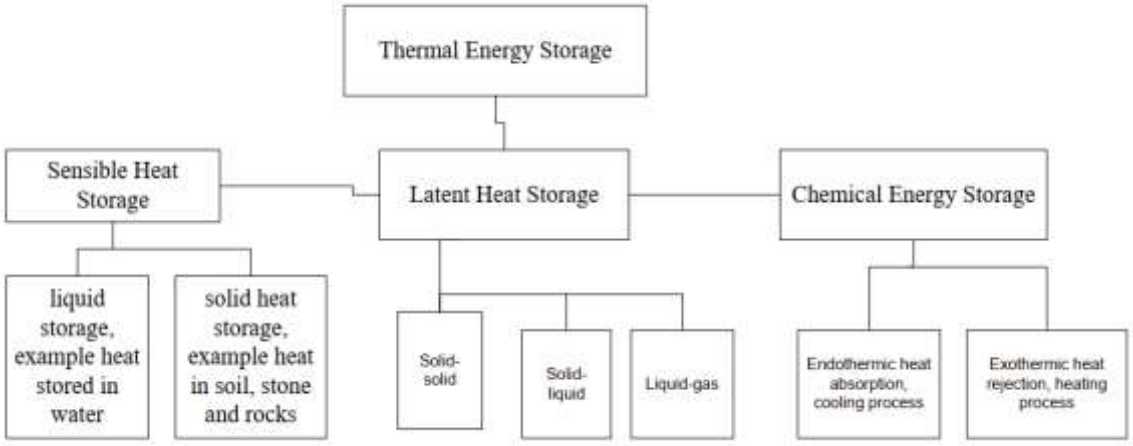

Figure 2-2 Classification of thermal energy storage based on the state of energy storage material [14]

2.3.1 Latent and Sensible Heat Storage Systems

a. Sensible Heat Storage System:-

Sensible heat storage is a thermal energy storage system by raising or lowering the temperature of liquid or solid. Water is the best sensible heat storage liquid due to it is inexpensive and has high specific heat. But above 100℃, oils, molten salts and liquid metals are also used. The system uses change in temperature of material during charging and

discharging process and heat capacity. The amount of stored heat depends on change in temperature, amount of stored material and specific heat of the medium [14].

$$Q = \int_{T_i}^{T_f} mC_P dT \quad = \quad mC_P(T_F - T_i) \ldots\ldots\ldots\ldots\ldots\ldots\ldots\ldots\ldots\ldots\ldots\ldots\ldots [2.2]$$

$Q =$ Amount of thermal energy stored/released in the form of sensible heat (KJ)

$m =$ The mass of material used to store thermal energy (kg)

$C_P =$ the specific heat of the material to store thermal energy $\left({}^{KJ}/_{Kg°C}\right)$

T_F and $T_i =$ final and initial temperature (°C), respectively

b. Latent heat storage system:-

Latent heat storage is a thermal energy storage system based on the heat absorption or released during the phase change time of the storage material from liquid to solid or solid to liquid, liquid to gas or gas to liquid [14].

$$Q = \int_{T_i}^{T_f} mC_P dT + ma_m \Delta h_m + \int_{T_m}^{T_f} mC_P dT \ldots\ldots\ldots\ldots\ldots\ldots\ldots\ldots\ldots\ldots\ldots\ldots\ldots\ldots [2.3]$$

$Q =$ Amount of thermal energy stored or released in the form of latent heat (KJ)

$C_P =$ Specific heat of the material to store thermal energy $\left({}^{KJ}/_{Kg°C}\right)$

$m =$ mass of material used to store thermal energy (kg)

$\Delta h_m = Heat\ of\ fussion\ per\ unit\ mass\ (KJ/kg)$

$T_i, T_F\ and\ T_m = Initial, Final\ and\ Melting\ temperature\ (°C) respectively$

2.4 Materials for Phase Change Process (PCM)

Phase change materials are both hot and cold temperature, thermal energy storage substances that absorb and release energy during the heating and reverse cooling process when phase change takes place. For cold temperature storage phase change materials such as ice, which changes from liquid to solid absorbs energy and changes from solid to liquid releases that absorbed energy. On the other hand for hot temperature storage phase change materials, changes from solid to liquid absorbs energy and changes from liquid to solid phase releases that absorbed energy. The amount of that energy released and absorbed is called latent heat [12].

2.4.1 Classification of (PCM) Phase Change Material Process

The nature of solidification phase change can take many changes. The classification depends on the state of small portion of the phase change material region, representing a single degree of freedom in the numerical discretization. The three classification of phase changes are:-

a. Distinct case: - in this case the phase change region consists of distinct liquid and solid phases separated by a smooth continuous front. The state of the system is characterized by the position of the interface. Example, pure metals rapid solidification or freezing of water [15].
b. Alloy case: - in this case the phase change region has a crystalline structure consisting columnar and/or equi-axed grains and the solid/liquid interface is a complex shape. Example the solidifications of most metal alloys [15]
c. Continuous case: - in this case there is no distinct interface between the solid and liquid phases and the solid liquid phases are fully dispersed throughout the phase change region. Example, solidifications of polymers, wax, or glasses [15].

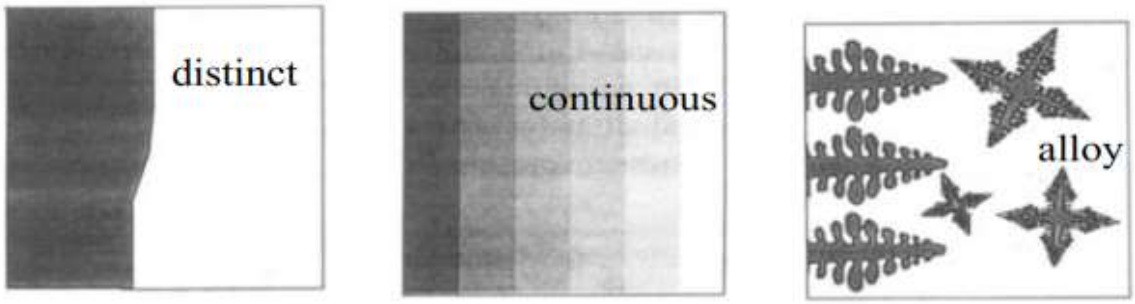

Figure 2-3. Classification of PCM solidification process [source, [15]].

2.5 Transient Heat Transfer Numerical Formulation

There are two formulations of numerical transient heat transfer problems, which are explicit or forward difference and implicit or backward difference.

2.5.1 Forward Difference (Explicit Formulation)

Fixed grid or forward difference method is a grid of a spatial nodes used to discretize the given problem and is the simplest method for solving thermal heat conduction problems involving with phase change process.

In this method the derivative is evaluated at the begging of the time step or at the n^{th} step. In other way under this formulation, the temperature of future time increment is expressed

in terms of the surrounding nodal temperature at the beginning of the time increment. The explicit formulation the nodal temperatures $T_{i,j}^{n+1}$ explicitly in terms of the previous nodal temperature $T_{i,j}^{n}$. In this formulation the calculation proceeds directly from one time increment to the next until the temperature distribution is calculated at the desired final state [16].

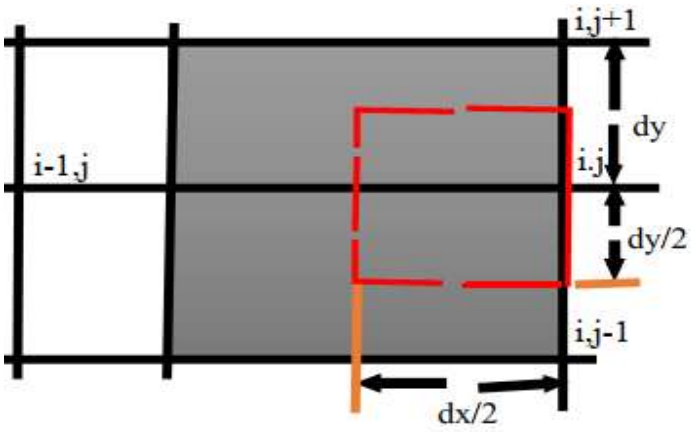

Figure 2-4 Schematic of node at plane surface

Where, n, old value (at time t) of the dependent variable

$n+1$, The new value (at t+Δt) of the dependent variable.

Fixed grid method has major advantages which solves multidimensional problems efficiently without difficulties.

Fixed grid method also can classified in to three classes, which are Enthalpy based method, Effective heat capacity method and the heat source method in capable to solve the moving fronts of solidification or melting of phase change materials [17].

a. Enthalpy Based Method

This method used to evaluate latent heat storage systems of diffusion phase change material melting or solidification problems based on direct solutions of fixed grid or forward difference equations. In this method, in the energy equation total enthalpy can be considered the primary dependent variable rather than temperature. The enthalpy H, in general sense can be defined as follows:

$$H(T) = \int_{T_{ref}}^{T} \rho C(T) dT \ldots\ldots\ldots\ldots\ldots\ldots\ldots\ldots\ldots\ldots\ldots\ldots\ldots\ldots\ldots\ldots\ldots\ldots [2.4]$$

b. Effective Heat Capacity Method

In this method enthalpy is evaluated by using effective heat capacity and temperature derivatives. The effective heat capacity method considers the effects of enthalpy and its progress in time by considering the effective heat capacity through thermal phase change process.

a. The Heat Source Method

In this method, the enthalpy can be separates in to two parts, which are sensible and latent heat terms. The latent heat is the source term due to the latent parts of the enthalpy.

2.5.2 Backward Difference (Implicit Formulation)

In this method the derivative is evaluated at the $(n+1)^{th}$ time step or at the begging of end of time step. In other way, under this formulation, the equation is formulated by computed the space derivatives in terms of the temperature at the n+1 time increment. In this formulation the time derivative moves backward from the times for heat conduction in to the node. The backward difference formulation does not permit the explicit calculation of the T^{n+1} in terms of T^{n}. Rather, a whole set of equations must be written for the entire nodal system and solved simultaneously to determine the temperatures T^{n+1} [16].

2.6 Refrigeration System

Refrigeration system is the process of cooling a space by removing heat and transferring it to the nearest surrounding. The primary objective of all refrigeration system is producing and maintaining the space temperature lower than the surrounding temperature [17]. The refrigerator is used to cool or thermal storing of the substance such as fresh food to keep from spoiled and decayed. The refrigerator runs by supplying electrical power through inverter.

Generally, refrigeration systems are classified into three main groups based on the compressor powering mechanisms and compression system to increase refrigerant pressure, these are:

Compression refrigeration system, vapour absorption refrigeration system, and gas cycle refrigeration system.

2.6.1 Solar DC Compression Refrigeration System

Compression refrigeration system can be powered by solar photovoltaic, solar thermo electric or solar thermo mechanical systems.

a. Solar photovoltaic refrigeration system: - Photo voltaic (PV) involve the direct conversion of solar radiation to direct current (DC) electricity using semi conducting materials. Based on this concept, the operation of a PV-powered solar refrigeration cycle is simple. Solar photovoltaic panels produce DC electrical power that can be used to operate a DC motor, which is coupled to the compressor of a vapor compression refrigeration system.

In this system, the refrigeration effect can be powered by either direct current without an inverter or alternative current with inverter from a solar photovoltaic system. The system consists of compressor, expansion valve, photovoltaic cell, DC/AC motor, condenser, evaporator, battery and solar regulator [18].

b. Solar photovoltaic panel: - photovoltaic modules converts' solar energy in to electrical energy with maximum power point tracking system to drive the refrigerator compressor, pump and fan and it is regulated by controller. During daytime the PV panel receives solar energy and this solar energy turns in to direct-current electric power which is also can be converted in to an alternative current electric power by inverter to drive AC compressor, pump and fan of the refrigerator components [19].

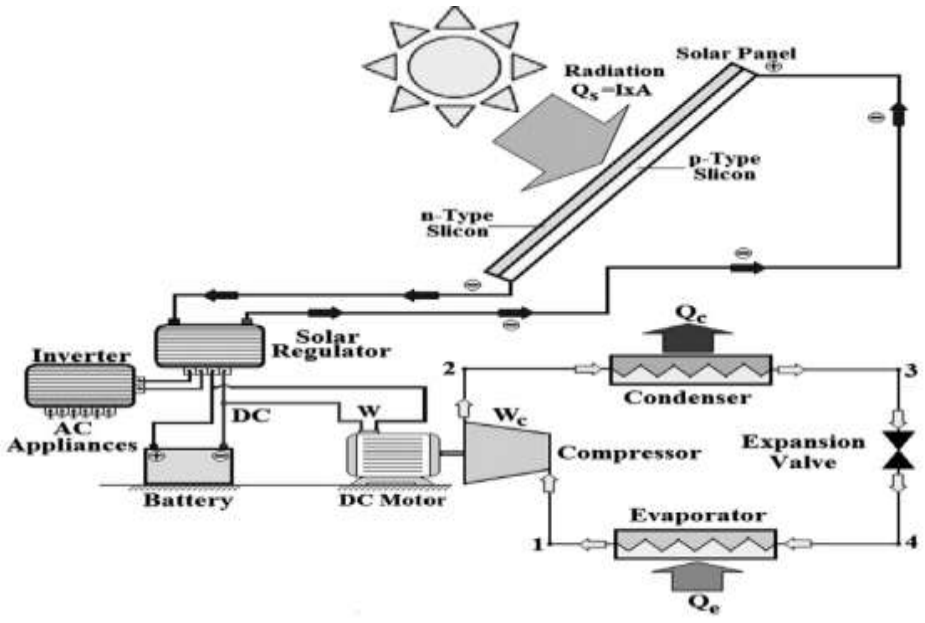

Figure 2-5. Schematic Diagram of a Solar PV Powered DC Refrigerator [Source, [17]]

2.6.2 Solar DC Compression Refrigerator with Ice Storage

Solar photovoltaic refrigeration system without battery, by using cold latent heat storage or hot latent heat storage system depending on application can also use for refrigeration systems for numerous reasons. Battery can be adopted and connected with controller to maintain the stability of electric energy supply and conversion in the most optimized way. Batteries are essential component in solar PV refrigeration system to store energy and to solve the intermittent of solar energy. However, using batteries in the system increases running and investment costs and reduce the system energy conversion efficiencies. Thus, ice storage technology has a great role to save energy [20].

Ice thermal energy storage technology is used to shift the demand of electricity from on-peak period to off-peak hours and reduces the peak demand. The system utilizes a storage medium to store cold energy produced during off-peak hours and these stored energy is used during peak hours for different applications. There are two classifications of ice cold thermal energy storage systems based on the ways of delivering ice in to the storage tank. These are:

Dynamic system: - in this system, ice is produced outside the storage tank and removed continuously from ice making tank.

Static system: - in this system, ice making pipe is installed inside the storage tank and ice can produced inside the storage tank and removed when it is melted [21].

The reason to use ice as a cold thermal energy storage system, is due to it's an excellent medium to store thermal energy and to deliver cooling energy in a short period of time. The other benefits using water as the phase change material to form ice are: due to its low cost, high latent heat, high specific heat, high volumetric capacity, non-volatility and stability.

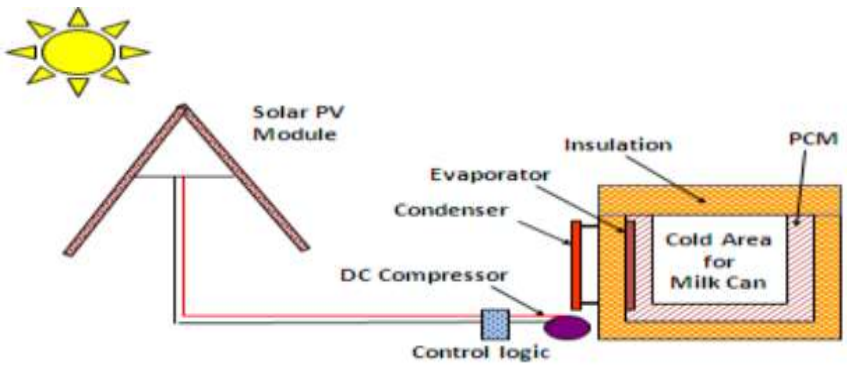

[Source, [7]]

Figure 2-6 Diagram of solar refrigerator with VSDC compressor and E-W fixed tracking

2.6.3 Principle of Solar PV Ice Formation System

The principle of ice formation using solar PV system for different applications, geometries, locations of ice storage tank relative to evaporator and load, and mechanisms are similar except charging and discharging performance of the system. The most common solar PV ice maker system consists of AC/DC compressor, condenser, expansion device, evaporator, and ice storage tank.

The compressor of the system compresses the refrigerant inside the pipe to increase its pressure. The compressor can be powered by AC/DC electric power generated by the solar PV panel. The compressed refrigerant enters in to the condenser and it condenses by releasing heat to the surrounding. Then the condensed refrigerant enters in to the expansion device and its pressure and temperature decreases drastically. These cold refrigerant feeds in to the evaporator and it is vaporized. Depending on the mechanism and arrangement of the system, heat exchanger takes place between the cold refrigerant inside the evaporator tube and the water within the storage tank. The water begins to freeze and forms ice on the evaporator tube surface [19].

2.7 Related Literatures Studied in This Area

George D. (1989) [11], he studied the ice thickness by traditionally has been calculated using a method in which the thickness is assumed proportional to the square root of the accumulated freezing degree days. Particularly for newly formed thin ice this method over predicts ice thickness. Consideration of thermal resistance between top of the ice and the atmosphere results in a method which predicts linear growth with time for thin ice and transitions to the thickness half growth at large thickness.

Piia Lamberg. (2004) [22], he studied the solidification process at the constant end wall temperature in the finned two-dimensional phase change material storage temperature distribution of the fin and solid-liquid phase interface location by using a simplified analytical model. The author uses the heat capacity numerical method to compare the analytical results and he got a satisfactory estimation of the fin temperature and solid liquid phase interface with the fin length less than 0.06m and the storage cell of length to height ratio less than 6m. Using the analytical model rather than the two dimensional numerical model the error is 10%.

Petros. J et al (2009) [1], investigated batteryless solar photovoltaic powered ice maker system experimentally by the use of new concept of dedicated controller and four DC drive compressors**.** Under this study the system is done by providing easy compressor startup, maximum power tracking and power management system and can produce large quantity of ice up to 17kg from 440Wp PV panel on a good day.

Anish Modi et al. (2009) [23], studied technically feasibility of Photovoltaic refrigerator with battery bank under a normal operating condition to convert an existing 165 litre refrigerator working on grid electricity and it performed similar task. However, for a sustainable system large storage battery bank or large capacity PV module are needed and it makes the system economically unfeasible due to their high initial cost. Under this study the RETScreen simulation indicates that, PV refrigeration system with battery is not economically feasible without the initial financial incentive or government subsidy**.**

Xie. J. et al. (2014) [24], studies the arrangements and materials of thin layer ring on ice formation and they found a most significant effect on the formation. However, the thickness of thin layer rings had no clear effects on the formation of ices**.**

Y. Yusufoglu et al. (2015) [25]**,** they incorporating phase change material for cooling of residential buildings to increase refrigerator efficiency or performance and to reduce harmful emissions by reducing energy consumption**.** The researcher studied experimentally based on four different PCMs, two different refrigerator models, different condenser surface area, different location of PCM on the evaporator, amount of PCM melting/freezing during compressor on/ off period and PCM packaging plays an important role to save energy**.**

Asmaa Ahmed M. (2015) [26]**,** in this study, the performance of vapor compression refrigerator powered by solar PV system, direct current motor with and without thermal storage and with and without loading through indoor and outdoor tests were investigated experimentally and theoretically. The theoretical model is used to size the large cooling capacity solar PV driven refrigerator. Operation of refrigerator without PCM have higher coefficient of performance, however where there is a lack of solar energy refrigerator begins to loss its thermal energy faster than when PCM is installed and nothing to compensate it until solar energy is available. The coefficient of the refrigerator under PCM – full load condition at indoor condition is higher than that of the outdoor condition. Due

to different surrounding ambient temperatures, the product stored in a refrigerator reached required storage temperature first.

Vu Van Truong. (2015) [27]**,** studied the effects of volume change due to density difference between the solid and liquid phase changes on solidification processes of phase change material, by using direct numerical simulation techniques. The solidification interface is represented by connected points. He used a front tracking finite difference method and validated the result through comparison with exact solutions of one and two dimensional solidification problems. The validation results are satisfied and support the method. To demonstrate the effects of density change on the solidification process of phase change material, numerical computation were performed both cases of without and with density changes. The numerical result indicates that, the shrinkage such that the latent heat of fusion greater than one, reduces the solidification rate and the latent heat of fusion is less than one, increase the solidification rate.

Victor Torres-Toledo. Et al, (2015) [28], studied the transient performance and the effects of ambient temperature on a small milk cooling system using pv, battery and charge controller system, both experimentally and computationally, at three different ambient temperatures of 20ºC, 30ºC and 40ºC**.** In this research they studied the developments of milk temperature and energy consumption experimentally and computationally at three different ambient temperatures to size the PV system at a specific location. They used 3kg ice to cool 17litries of milk with two DC refrigerator operating at -10 ºC to produce ice and 4 ºC to preserve milk. From the result there was 30% COP reduction between 20 ºC and 40 ºC and the total daily energy consumption increases 100%. The specific energy consumption per litre of milk was between 30wh/L and 58wh/L**.**

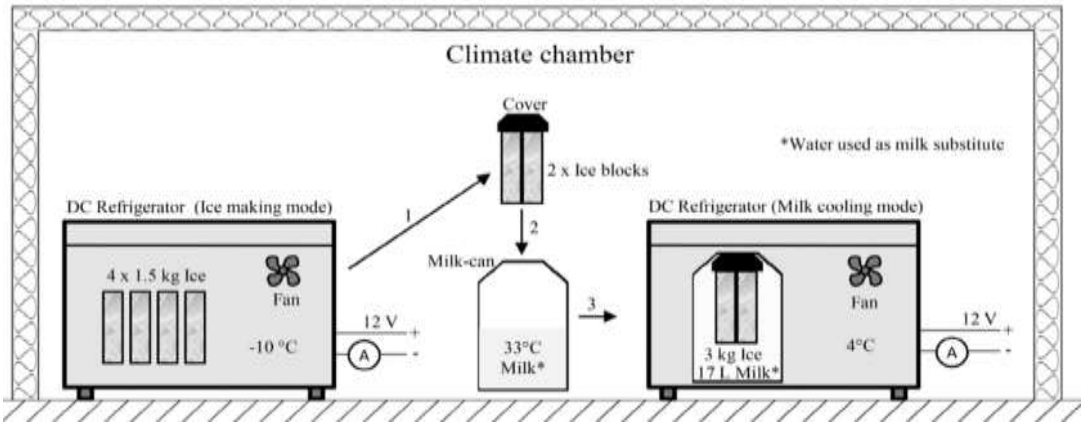

Figure 2-7 Schematic diagram of ice crystal formation with milk cooling system [[28]]

The above figure shows, Experimental setup and working principle of the employed refrigerator units operating in ice making and cooling mode, tested under constant voltage in a climate chamber at 20ºC, 30ºC and 40ºC ambient temperatures.

They investigated phase change phenomena and the effects of different heat transfer fluid inlet temperatures on ice formation around a horizontal tube in the rectangular vessel both experimentally and analytically. From the result, they obtained the following [21]

- From experiment nucleation occurs at all axial measuring stations and nucleation first starts at the entrance region and propagates along the tube.
- The heat transfer fluid inlet temperature affects the start of the phase change of water and nucleation time. Nucleation time decreases with decreasing of heat transfer fluid inlet temperature and increases with the axial distance for all HTFT.
- The ice thickness formed at the bottom and top sides of the tube is different, but at the right and left sides the ice thickness is close to each other, from this natural convection affects ice thickness around the tube. Ice thickness around the tube decreases at all points with increasing of heat transfer fluid inlet temperatures.
- For all heat transfer fluid inlet temperatures, the ice thickness calculated by mathematical model reasonably agrees with the experimental data.

Ismail, K. et al, (2016) [29], studied the effects of adding fins on the tube surface to reduce the freezing time and improving solidification process. By increasing fin geometries such that fin thickness, diameter and length to increase the heat transfer area, they found finned tube improved solidification process and reduced freezing time without considering fabrication cost of fins. In conclude the fin tubes produced about four time more ice than the normal tubes**.**

Victor Torres et al. (2016) [30]**,** were developed and analyzed the commercial freezer and an innovative adaptive control unit with the help of simulations and experiments to adapt compressor operation with the available solar energy, to produce ice efficiently by photovoltaic energy**.** The original control system and temperature sensor was replaced by the new system. They studied 12kg ice production per day with the selected parameters of 600Wp PV array and 65Ah of battery capacity at 24V. From one-year simulation the result showed that the ice maker stores a total of 50kg ice, is able to deliver 12kg ice for 89% of the days of typical weather year at selected location.

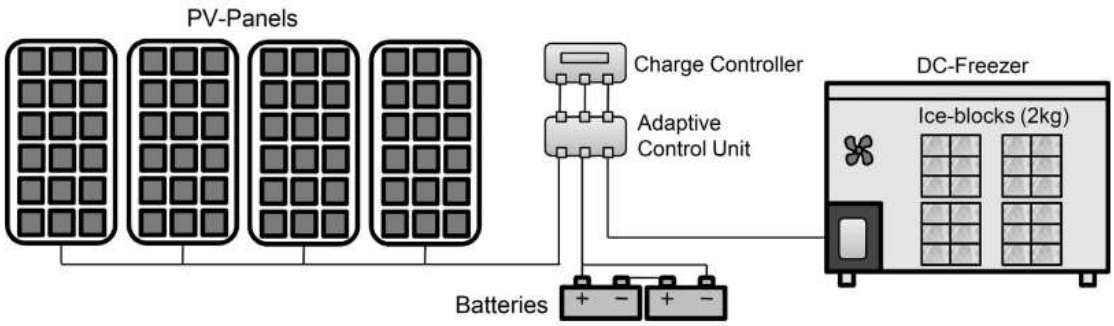

Figure 2-8 Diagram of PV ice-maker based on a DC-freezer and adaptive control [[30]]

Y. F. Xu et al. (2016) [20], studied structure optimization design analysis by theoretical calculation and experimental tests to improve energy utilization efficiency and exergy efficiency of an ice storage air conditioning system powered by distributed photovoltaic system**.** In this study co-integrated heat exchanger and immersed evaporator were implemented to reduce the high energy losses in the ice making process of ice slide machine and in the photo-electric conversion process, and also the discharging process was takes place by a special type of solenoid valve. From the result they obtained that the exergy efficiency improved from 90% to 97.45% in ice making process, the energy efficiency improved from 51.31% to 75.02%, the system exergy efficiency increased from 43.91% to 57.33% and the system energy efficiency increased from 4.64% to 8.14%**.**

Jannesari et al. (2017) [31]**,** investigated the effects of the parameters of thin layer rings and annular fins numerically and optimized by taguchi method using around coils to find the optimal combination. Utilized nine combinations of models are carried out by combining different levels of each factor, they found that the formation of ice by using annular fins and rings corresponded 21% and 34% higher than from the regular bar tube. In general, finned and ringed tubes increasing by 15%. The numerical result is verified by the two other researchers of analytical results.

S. Bakhshipour et al. (2017) [32], they studied the refrigeration cycle incorporated with PCM and without PCM heat exchanger numerically and the parametric effects which are tube length and diameter, PCM thickness and refrigerant mass flow rate and type. The PCM heat exchanger is located after the condenser and before the expansion valve in the refrigeration cycle and the coefficient of performance of the cycle is investigated. The computational fluid dynamics simulation, considers the flow inside the pipe is one dimension in the axial extension and the surrounding PCMs are considered two

dimensional. Numerical simulation is carried out using Matlab programming and the simulation result shows that in a refrigeration cycle of a refrigerator incorporating PCM causes an improvement in the convection procedure and the results increases by 9.58% in coefficient of performance by decreasing the refrigerant outlet temperature of the condenser. The geometrical and refrigerant properties have a positive effect on system performance and COP, but the PCM thickness must be optimum for better performance of the system.

Hani Hussein Sait, 2018 [33], studied the performance of ice formation **e**xperimentally in a flooded tube to investigate the behavior of liquid adjacent to the freezing surface and the formed ice subjected to stirred water, recirculated water and stagnant water. From the result the flooded tube with recirculated water have best performance. With the starting overall heat transfer coefficient of 1096W/m^2 k, 7.9g/m^2 s amount of ice was produced. He also analyzed the discharge cycle, and obtain 7.1kg of ice was sufficient to hold a load for 110 min for a 927w unit**.**


[Source, [33]]

Figure 2-9 Schematic diagram of flooded test section of this system

Several researchers studied the effects of freezing of falling film on varies geometries, which are on immersed cold-tube banks, around horizontal tube, on inline horizontal tubes and on circular horizontal tubes etc. They found that ice formation and heat transfer rate decreased with increased ice thickness due to the low thermal conductivity of ice layer. The four solutions to increase the heat transfer rate in PCM such as water are increase tube surface area by adding extended fins or thin layer rings, using encapsulated ice instead of accumulated ice layer, to get liquid ice add an additive to the PCM and use nano-fluid to increase solid heat transfer coefficient.

2.7.1 Summary of Previous Works

To summarize all the literatures explained above: The different mechanisms of solar pv refrigeration system with and without ice storage systems were investigated and analyzed analytically, computational and experimentally. Photovoltaic refrigerator with battery is

not feasible and it is economically feasible by incorporating PCM in place of batteries and structure optimization of the system increases refrigerator efficiency or performance. The effects of different ambient temperature on different freezing system using PV, battery and charge controller system were studied. From this result the higher ambient temperature reduces coefficient of performance and increases daily energy consumption. The phase change phenomena and the effects of different heat transfer fluid inlet temperatures and natural convection on ice formation were investigated.

Several researchers studied the effects of freezing of falling film on varies geometries or parametric effects, which are on immersed cold-tube banks, around horizontal tube, on inline horizontal tubes and on circular horizontal tubes etc. They found that ice formation and heat transfer rate decreased with increased ice thickness due to the low thermal conductivity of ice layer than the tube material. The four solutions to increase the heat transfer rate in PCM such as water are increase tube surface area by adding extended fins or thin layer rings, using encapsulated ice instead of accumulated ice layer, to get liquid ice add an additive to the PCM and use nano-fluid to increase solid heat transfer coefficient.

In this study, analyzing the performance of ice slab formation by using selective systems and mechanisms which are energy efficient slab geometries, encapsulated ice, high heat conduction materials of thin ring copper tube evaporator attached to the two parallel and vertical tank sides, and using co-integrated heat exchangers can operate without battery. The cooled thermal energy installation is based on the static system, which is the ice making pipe is installed in the storage tank where the formation and melting of ice takes place inside the tank. In this study also simulating and analyzing the ice thickness growth variation as a function of time and nodal temperature distribution within the system.

In this study the computational model was developed based on using the monthly average solar radiation data other than the representative days and also the cooling capacity was developed from compressor performance equation and performance coefficient values integrated with electrical energy generated from solar PV system.

The system is design and analysis its performance based on Ethiopian solar radiation, specifically around Semera located 350 kilometers far from Addis Ababa.

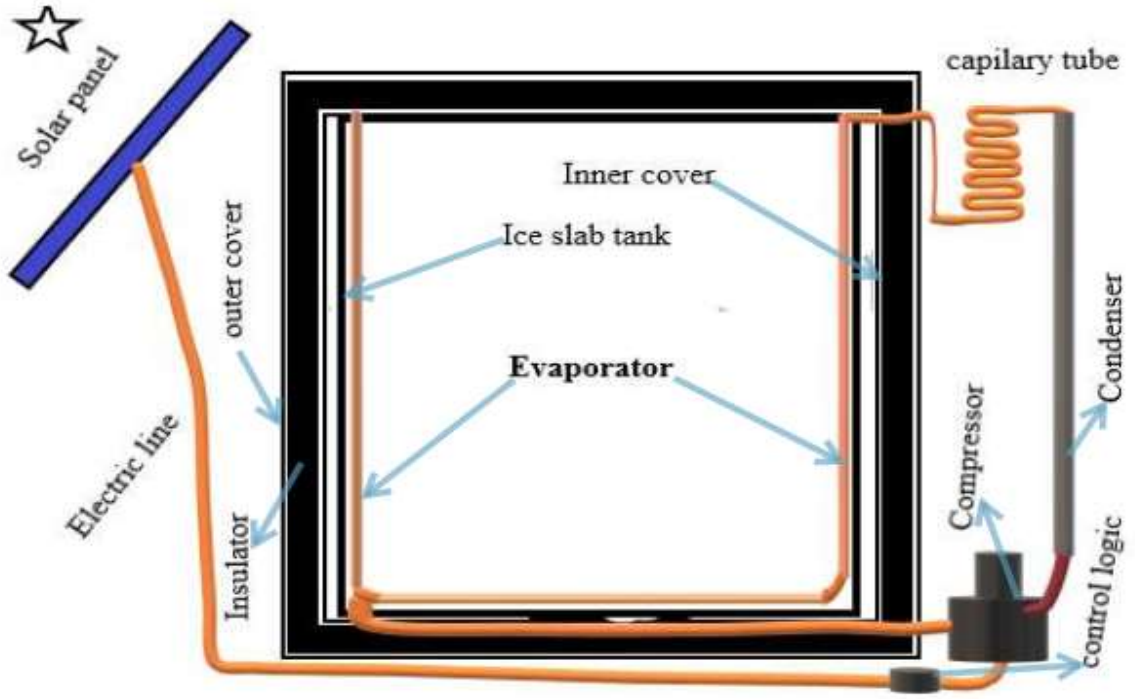

Figure 2-10 Schematic of 2D section view of ice slab formation using solar PV system

CHAPTER THREE

3 Details Arrangement and Mathematical Modeling of PV Cell

3.1 Introduction

This chapter explains about photovoltaic cell, photovoltaic module, photovoltaic array and arrangement of the system components, PV conversion system, PV cell types and mathematical modeling to study the I-V, P-V and P-I characteristic curve, the power curve and maximum power point or the working point by using solar radiation data at the selected location to form ice slab to cool milk and milk products.

3.2 PV Panel Arrangement and Power Generating Principle

Photovoltaic cells are semiconductor devices to convert incident solar radiation in to useful form of electrical energy. The principle of electricity generating using PV cell system, when sunlight strikes a PV cell the photons of the absorber removes the electron from the atoms of the cell. Then free electron move through the cell, creating and filling a holes in the cell. Then, these electron movement and holes can generate electricity. The physical process that a PV cell converts sunlight into electricity is called the photovoltaic effect [34].

The size of photovoltaic array to supply the required energy for a particular load application primarily depends on metrological conditions of environments which is the amount of incident solar radiation. In order to produce the required energy at the lowest costs the selection of the individual PV component is important because of the transient behavior of the metrological condition.

3.2.1 Photovoltaic Cell Arrangement

Solar cells are the building blocks of a PV array in the system. These are formed from silken and other semiconductor materials. A thin semiconductor wafer is particularly treated to form an electrical field, in one side positive and in the other side is negative. When light strikes semiconductor material, electrons are collided loose from the atoms. If an electrical circuit is made attaching a conductor to both sides of a semiconductor, electron flow will start causing an electric current [35].

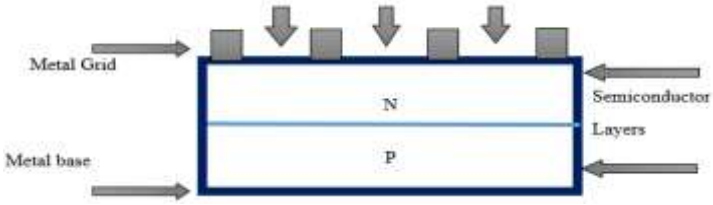

[Source, [35]].

Figure 3-1. Structure of solar Photovoltaic cell

3.2.2 Photovoltaic Module Arrangement

Photovoltaic module is formed by connecting many solar cells in series and parallel. The voltage generated by a single PV cell is very low, which is around 0.5V. For this reason, a number of solar PV cells are connected both in series and parallel connections to achieve the desired output. In the case of partial shielding, diodes may be needed to avoid opposite current in the array. Ventilation system is needed behind the panel to control efficiency decreasing at high temperature [35].

3.2.3 Photovoltaic Array Arrangement

The power produced by a single module is not sufficient to meet the needed power for practical purposes. The modules are connected in series for more voltage rating or to get an increased voltage and then connect in parallel to the specification current or an increased current. The connection of the module in an array is same as that of cells in a module [35].

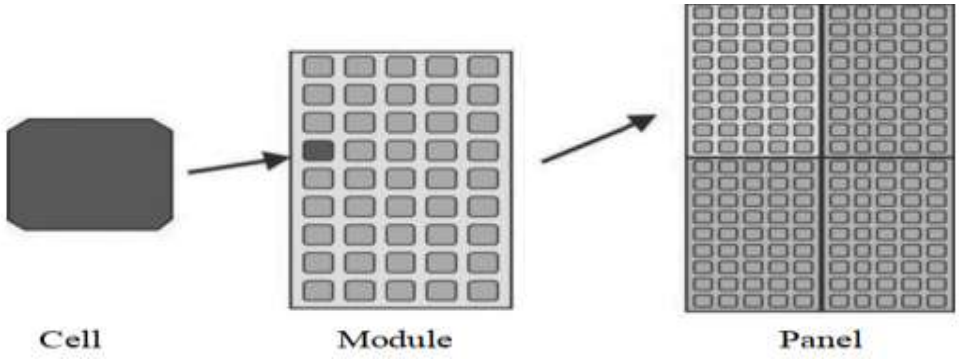

Figure 3-2 Solar photovoltaic system [Source, Samlexsolar, 2004]

3.3 Mathematical Modeling of Solar Photovoltaic Panel

3.3.1 Equivalent Circuit

A PV module consists of a number of solar cells connected in series and parallel to obtain the desired voltage and current output levels. The series and parallel resistance photovoltaic modeling yields more perfect and practical than the series resistance model without considering the expense of longer computational time. This model is modified by adding

an extra diode to represent the recombination of effect of the charge carriers. In general the two diode method modeling of solar PV cell is more accurate but it needs much longer computational time. For simplicity the single diode model is used for this research. This model offers a good compromise between simplicity and accuracy with the basic structure consisting of a current source and a parallel diode [35].

3.3.2 Modeling of Solar Photovoltaic Cell

The photovoltaic solar cell modeling is developed using circuit equation including the effects of temperature change and solar irradiation. Solar PV cell can be represented by a current source connected in parallel with a diode, since it generates current when it is irradiated and acts as a diode when it is not. The equivalent circuit model also includes a shunt and series resistance represented by R_{Sh} *and* R_S respectively. Photovoltaic solar cell can be modeled ideally and non-ideally or practical modeling.

a. Ideal Modeling of Solar Photovoltaic Cell

An ideal solar cell can be modeled by a current source connected in parallel with a rectifying diode and equation can be expressed as follows [36] [37]:

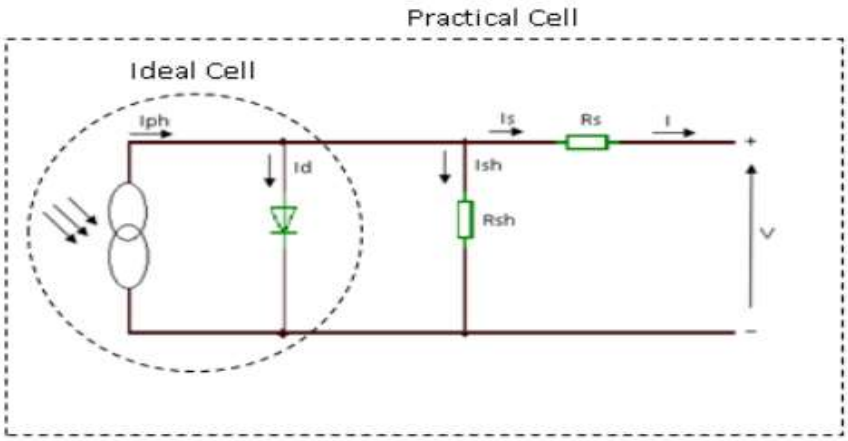

Figure 3-3 General model of solar PV cell in a single diode model

Using general model and by applying Kirchhoff's low on the common node of the current can be expressed as follows:

$$I_{cell} = I_{ph} - I_D, \qquad but, \quad I_D = I_O\left[exp^{\left(\frac{qV}{nKT_C}\right)} - 1\right] \ldots\ldots\ldots\ldots\ldots\ldots\ldots\ldots\ldots\ldots [3.1]$$

$$I_{cell} = I_{ph} - I_O\left[exp^{\left(\frac{qV_d}{nKT_C}\right)} - 1\right] \ldots\ldots\ldots\ldots\ldots\ldots\ldots\ldots\ldots\ldots\ldots\ldots\ldots\ldots\ldots [3.2]$$

$I_o = I_{load}$: $dark\ saturation\ current, it\ strongly\ depends\ on\ cells\ temperature$

$$I_O = \left[I_{Or} * \left(\frac{T_C}{T_r}\right)^3\right] exp\left[\frac{qE_g}{kn} * \left(\frac{1}{T_r} - \frac{1}{T_C}\right)\right] \ldots\ldots\ldots\ldots\ldots\ldots\ldots\ldots\ldots\ldots\ldots\ldots [3.3]$$

Where, $I_{cell} = I_{load}$: $Load\ current\ and\ q$: $charge\ on\ the\ electron$ $[1.602 * 10^{-19}\ C]$

I_{ph}: $Generated\ current$, Mainly depends on G, G_r: The intensity of solar irradiance and cells operating temperature: T_C and T_r

$$I_{ph} = \left[I_{phr} + K_i * (T_C - T_r)\right] * \left(\frac{G}{G_r}\right) \ldots\ldots\ldots\ldots\ldots\ldots\ldots\ldots\ldots\ldots\ldots\ldots [3.4]$$

I_{phr}: The photovoltaic current under standard conditions at G_r and T_r

K_i: Temperature coefficient of the short circuit current

G: The intensity of solar irradiance, W/m^2

G_r: The reference intensity of solar irradiance $= 1000\mathrm{W}/m^2$

k : $Boltzman\ constant$ $[1.38 * 10^{-23}\ J/K]$

T_r : $Reference\ cell\ operating\ temperature$

$V_d = V_{load}$: $Terminal\ voltage\ [V]$ E_g: $band\ gab\ of\ semiconductor\ material$

n: $Ideality\ factor\ equal\ to$ 1.1 T_C : $operating\ temperature\ of\ cell\ [K]$

$$T_C = \left[\frac{NOCT - 20}{0.8}\right] * G + T_a \ldots\ldots\ldots\ldots\ldots\ldots\ldots\ldots\ldots\ldots\ldots\ldots\ldots\ldots [3.5]$$

NOCT: Nominal operating cell temperature

T_a: Ambient air temperature

I_{or}: $reverse\ dark\ saturation\ current\ at\ temperature\ reference\ T_r$

$$I_{or} = \left[\frac{I_{scr,cell}}{exp\left(\frac{V_{ocr,cell}}{nV_t}\right) - 1}\right] \ldots\ldots\ldots\ldots\ldots\ldots\ldots\ldots\ldots\ldots\ldots\ldots\ldots\ldots [3.6]$$

$thermal\ voltage, V_t = \frac{KT}{q}$

$I_{scr,cell}$- Short circuit current of photovoltaic cell under standard conditions at $T_r\ and\ G_r$

$V_{ocr,cell}$- Open circuit voltage of photovoltaic cell under standard conditions at $T_r\ and\ G_r$

The open circuit voltage and short circuit current are important parameters associated with I-V characteristics curve of solar panel. These parameters are subjected to variations in atmospheric conditions. The short circuit current and open circuit voltage can be calculate under different atmospheric conditions.

$$I_{sc,cell} = \left[I_{SCr,cell} + K_i * (T_C - T_r)\right] * \left(\frac{G}{G_r}\right) \dots\dots\dots\dots\dots\dots\dots\dots\dots\dots\dots\dots\dots [3.7]$$

$$V_{oc,cell} = \left[V_{OCr,cell} + K_V * (T_C - T_r)\right] \dots\dots\dots\dots\dots\dots\dots\dots\dots\dots\dots\dots\dots [3.8]$$

$I_{sc,cell}$- Short circuit current of photovoltaic cell under operating conditions at $T_C\ and\ G$

$V_{oc,cell}$- Open circuit voltage of photovoltaic cell under operating conditions at $T_C\ and\ G$

K_V: Temperature coefficient of the open circuit voltage

b. Non - Ideal Modeling of Solar Photovoltaic Cell

Practical modeling of solar PV cells differ from the ideal PV solar cell modeling. In practical or non-ideal solar cell modeling also contains series (R_S) and parallel or shunt (R_{Sh}) resistances [36].

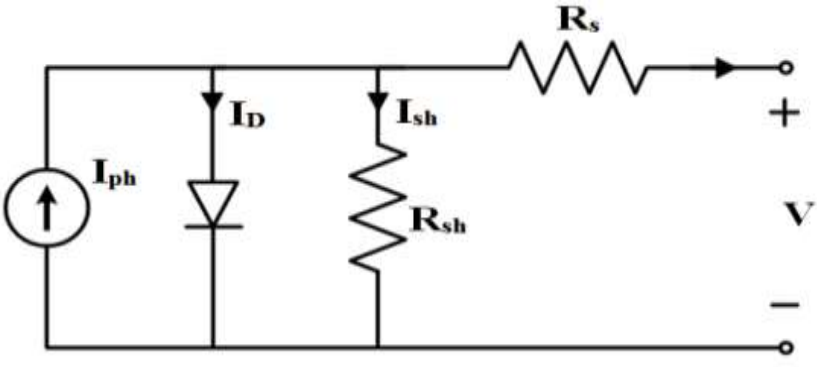

[Source, [36]]

Figure 3-4 a practical single diode equivalent circuit of PV cell

$$I_{cell} = I_{ph} - I_D - I_{sh}, \quad and, \quad I_D = I_O\left[exp^{\left(\frac{qV_d}{nKT}\right)} - 1\right] \dots\dots\dots\dots\dots\dots\dots [3.9]$$

$$I_{cell} = I_{ph} - I_O\left[exp^{\left(\frac{qV_d}{nKT}\right)} - 1\right] - I_{sh} \ldots\ldots\ldots\ldots\ldots\ldots\ldots\ldots\ldots\ldots\ldots [3.10]$$

$$V_{sh} = V_d \ \ and \ \ V_d = V + I_{cell}R_s \ldots\ldots\ldots\ldots\ldots\ldots\ldots\ldots\ldots\ldots\ldots\ldots [3.11]$$

$$where, V_d = terminal\ voltage, V = cell\ output\ voltage,$$

$$R_{sh}\ and\ R_s = shunt\ \ and\ series\ resistance\ respectivily,$$

$$V_{sh} = voltage\ across\ shunt\ resistance\ and\ I_{sh} = shunt\ current$$

$$I_{sh} = \frac{V_{sh}}{R_{sh}} = \frac{V_d}{R_{sh}} = \frac{V + I_{cell}R_s}{R_{sh}} \ldots\ldots\ldots\ldots\ldots\ldots\ldots\ldots\ldots\ldots\ldots [3.12]$$

Then, by substituting equation [3.12] in to equation [3.10] we get:

$$I_{cell} = I_{ph} - I_O\left[exp^{\left(\frac{qV_d}{nKT}\right)} - 1\right] - \frac{V + I_{cell}\,R_s}{R_{sh}} \ldots\ldots\ldots\ldots\ldots\ldots [3.13]$$

3.3.3 Mathematical Modeling of Photovoltaic Module

Practically, output power from single solar PV cell is not enough to apply any application. For this reason, in order to increase capability of solar photovoltaic system, solar PV cell must be arranged in series and parallel features. To increase total voltage of the module, cells have to be connected in series $V_{Out} = V_1 + V_2 + V_3..,$ connecting PV cells in parallel to increase total current ($I_{Out} = I_1 + I_2 + I..,$).

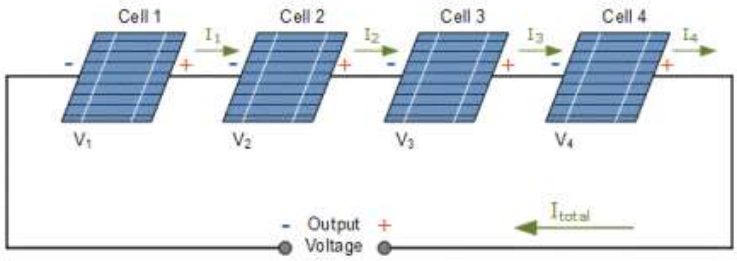

Figure 3-5 Representation of connecting Solar PV cells in series [Source, [36]]

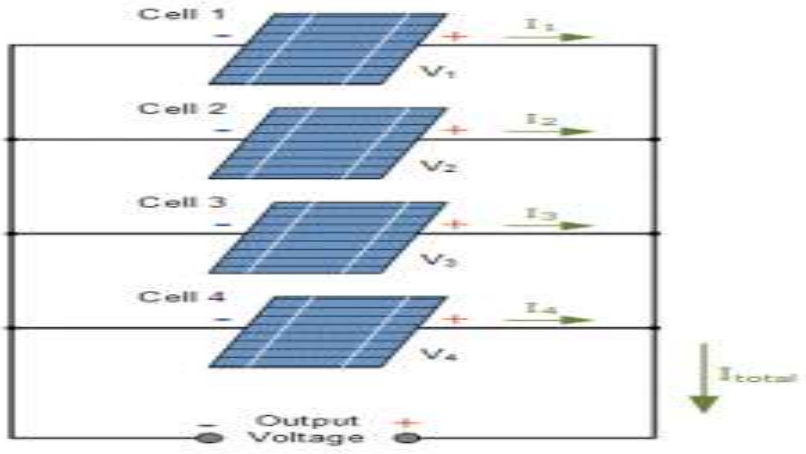

Figure 3-6 Representation of connecting Solar PV cells in parallel [Source, [36]]

By considering N_P is the number of solar PV cells connected in parallel and N_S number of PV solar cells connected in series. The relationship between voltage and current produced by photovoltaic module can be expressed as follows [38].

$$I_{ph,module} = N_p I_{ph}, \quad and \;\; I_{O,module} = N_p I_O \dots\dots\dots\dots\dots\dots\dots\dots [3.14]$$

$$n_{module} = N_S n, \quad and \;\; R_{S,module} = \frac{N_S}{N_p} R_S \dots\dots\dots\dots\dots\dots\dots\dots [3.15]$$

$$R_{Sh,module} = \frac{N_p}{N_{Sh}} R_{Sh}, \quad and \;\; I_{SC,module} = N_p I_{SC} \dots\dots\dots\dots\dots\dots [3.16]$$

$$V_{OC,module} = N_S V_{OC} \dots\dots\dots\dots\dots\dots\dots\dots\dots\dots [3.17]$$

Then, by substituting equation [3.14 – 3.15] in to equation [3.13] we get:

$$I_{cell} = N_p I_{ph} - N_p I_O \left[exp^{\left(\frac{qV_d}{N_S nKT}\right)} - 1 \right] - \frac{V + I_{cell} \frac{N_S}{N_p} R_s}{R_{sh}} \dots\dots\dots [3.18]$$

3.3.4 Mathematical Modeling of Photovoltaic Array

The modules in a solar photovoltaic system are typically connected in arrays. Solar PV cell array consists of M_p parallel branches with M_s modules in series in each branch as shown in figure bellow [37]:

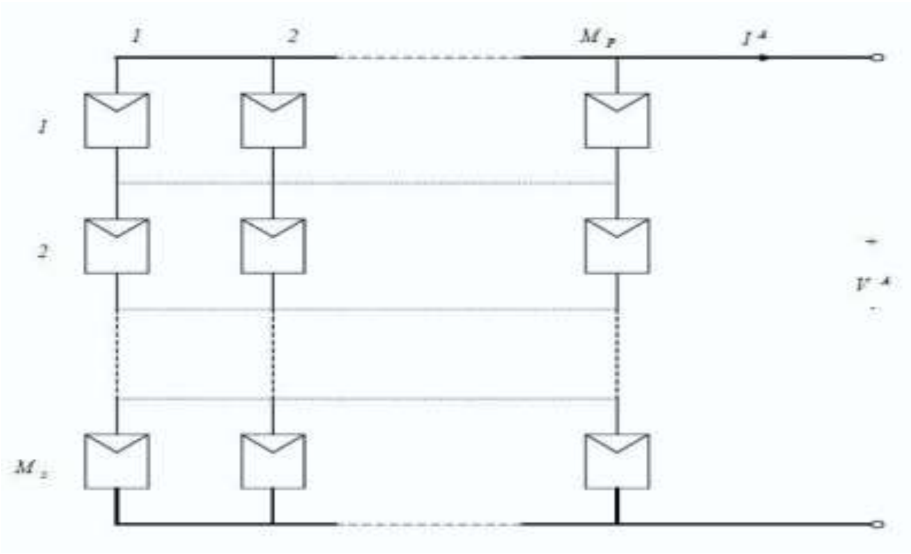

[Source, [36]]

Figure 3-7 solar cell array consists of M_p parallel branches with M_s series modules, V^A applied voltage and I^A, total current of the array

Figure 3.7, shows solar PV cell array consists of M_p parallel branches with M_s modules in series in each branch, V^A, is the applied voltage at the array's terminals and I^A is the total current of the array.

$$(I)^A = \sum_{i=0}^{M_p} I_i \ldots\ldots\ldots\ldots\ldots\ldots\ldots\ldots\ldots\ldots\ldots\ldots\ldots\ldots\ldots\ldots\ldots\ldots [3.19]$$

Where, A is the branch number.

If modules are identical and ambient irradiation is the same on all modules, then arrays current can be expressed as follows:

$$I^A = M_P I^M \ldots\ldots\ldots\ldots\ldots\ldots\ldots\ldots\ldots\ldots\ldots\ldots\ldots\ldots\ldots\ldots\ldots\ldots\ldots\ldots [3.20]$$

Maximum power point (MPP) represents the working point, at which solar PV cell can deliver maximum power for a given radiation intensity.

Corresponding values of V_{MPP} and I_{MPP} can be estimated from V_{OC} and I_{OC} as follows [39]:

$$V_{MPP} = (0.8)V_{OC} \text{ And } I_{MPP} = (0.8)I_{OC} \ldots\ldots\ldots\ldots\ldots\ldots [3.21]$$

Another essential characteristic of solar panels are the fill factor, which represents how square the voltage/current characteristics of the panel. Solar PV panels have a fill factor

(FF) between 0.4 and 0.8 in general, and an ideal PV panels have a fill factor of 1.0. It can be expressed as follows [36]:

$$FF = \frac{P_{max}}{V_{OC} I_{SC}} \dots \dots \dots \dots \dots \dots \dots \dots \dots \dots \dots \dots \dots \dots \dots \dots \dots . \dots \dots \dots \dots \dots [3.22]$$

The reduction in fill factor (FF) corresponding to total series resistance is given by:

$$\Delta FF = \frac{-I_{SC}}{V_{OC}} * R_S * FF_{ideal} \dots \dots \dots \dots \dots \dots \dots . \dots \dots \dots \dots \dots . . \dots \dots \dots [3.23]$$

The maximum power output can be calculated as: $P_{max} = V_{max} I_{max}$

Calculated maximum current output of solar PV panel at nominal temperature and solar radiation (at 25℃ and $1000 w/m^2$) could be expressed using equation (3.13) as

$$I_{mpp} = I_{phr} - I_{Or}\left[exp^{\left(\frac{V_{mpp}+R_S I_{mpp}}{nV_{t,r}}\right)} - 1\right] - \frac{V_{mpp} + I_{mpp}\, R_{mpp}}{R_{sh}} \dots \dots \dots . [3.24]$$

CHAPTER FOUR:

4. METHODOLOGY OF THE RESEARCH

4.1 Introduction

This chapter explains about cooling system design, construction of ice tank independently and combined with milk storage tank, total required ice mass calculation, mathematical modeling of phase change process using fixed grid (enthalpy) method and moving mesh method, mathematical equations for nodal temperature distribution of water and ice crystal growth as a function of time, total cooling load calculations, modeling of solar radiation, photovoltaic module material and type selection, total number of PV panel calculation.

4.2 Cooling System Design

Solar PV cooling system utilized a vapour-compression refrigeration cycle in order to produce the desired cooling and dehumidification. The evaporator, compressor, condenser and expansion device are four main components of the cycle.

To select appropriate size of all these components, first amount of heat load and cooling space geometry of the system depending on the amount of ice formed to cool needed milk during night will be determined.

4.2.1 Milk and Slab Ice Storage Tank Construction

The construction of milk and ice storage system consists of three layers of materials which are interior surface, external surface and insulation material. These three type of materials can be selected appropriately to build a refrigerated space which is a major factor in terms of energy saving. Several materials are considered to ensure good insulation and body stiffness for the construction of the storage system.

- Interior surface: - plastic panel (polypropylene, pp) material is selected for interior surface. This material has well resistant for impact and moisture, light weight, easy to clean and has enough strength for the system.
- External surface: -aluminum sheet material is selected for the external surface, due to its anticorrosive, light and capable of supporting the storage structure as a whole.
- Insulation material: - in order to reduce the heat leakage into the cold space (to reduce the cooled heat outflow from the refrigerated space or the hot heat inflow from the outside environment into the refrigerated space) appropriate selection of the cold insulation material is important.

There are vary of recent developed insulation materials which are polyurethane, nitrile rubber expanded, phenolic foam, synthetic rubber expanded, polyethylene foam, polypropylene and polypropylene. From these variety of insolation materials, Polyurethane is selected for many reasons. It is an excellent insulator, structurally strong, very light, safe, and affordable. Among all insulation materials, polyurethane foam insulation is the most commonly used for dairy and food industry. The material is used from medium to heavy – duty refrigeration systems to reduce heat gain and provide condensation control [40].

4.2.2 Milk and Slab Ice Storage Tank Sizing

The dimension of milk and slab ice storage tank are based on the amount of milk refrigerated during day time. Based on the amount of milk cooled during day time, the amount of ice can be estimated enough to keep the temperature of milk during night. This research is designed based on 50 liter of refrigerated milk with 4℃ minimum temperature and to keep this temperature during night by adding slab ice having equal cooling capacity bellow 4℃ to the transmission load through milk storage tank wall during night time around remote areas of Ethiopia. Specifically the site is located around Samara north-east of Ethiopia and 354 kilometer far from Addis Ababa. Before calculating the volume and mass of ice, the amount of transmission load through milk storage tank wall during night can be determined first by using the volume of milk and estimated ice mass:

4.2.3 Milk Tank Transmission Load Estimation

To determine the required mass of ice enough to keep 50 liter of milk with 4℃ temperature during night can be use the following relation from thermodynamics.

Heat gained by milk due to transmission load from the environment = heat gained by ice from milk during night

$$Q_{milk\ storage\ transmission} = Q_{ice} \dots\dots\dots\dots\dots\dots\dots\dots\dots\dots\dots\dots\dots\dots\dots. [4.1]$$

Slab ice can be absorb heat from milk until its temperature reaches the minimum milk temperature of 4℃. The transmission load can be estimated based on the refrigerated milk storage time which is starting from 5pm and all night time a total of 14 hours.

The transmission heat load is the major factor in the design of the refrigeration system. There are a number of factors that affect the transmission heat load in order to account in calculation. These are:

- Time: in long-term storage more heat will be escape from the system.
- Temperature difference: when temperature difference between refrigerated space and ambient is great, heat escaped into the system is more.
- Type of insulation: the thermal conductivity property of insulation material affects the heat removal rate through the wall.
- Thickness of insulation material and External area of milk and ice slab tank:

The sensible heat gain through the surface of milk and ice storage tank wall, ceiling and floor can be calculate as follows:

$$\mathrm{Q_{trans}} = \mathrm{U}A_{milk}(\mathrm{T}_{outside} - \mathrm{T_{inside}}) \dots\dots\dots\dots\dots\dots\dots\dots\dots\dots\dots\dots\dots\dots\dots [4.2]$$

$Where, \mathrm{Q_{trans}}$: Transmission cooling load $and\ U$: Overall heat transfer coefficient

A_{milk}: Milk tank outside surface area and it depends on its volume

The volume of the tank becomes sum of volume of milk and volume of ice and initially the volume of ice can be taken 25% of milk tank volume including free space.

$V_{milk} = 50\ liter = 0.001m^3 * 50 = 0.05m^3$, and its 25% becomes $0.0125m^3$

Total volume becomes $0.0625m^3$ with dimensions of 0.5m*0.3m*0.42m

$A_{milk} = 2(0.5 * 0.3) + 2(0.5 * 0.42) + 2(0.3 * 0.42) = 0.972m^2$:

The milk tank has $0.972m^2$ internal area, then the external surface area can be calculate by including the thickness of the material which are, outer aluminum cover 0.002m, inner plastic cover 0.003m thickness and insulation foam material 0.015m thickness and multiplying all by two. The figure bellow shows the section view of milk and ice storage tank represented by length and width of the tank.

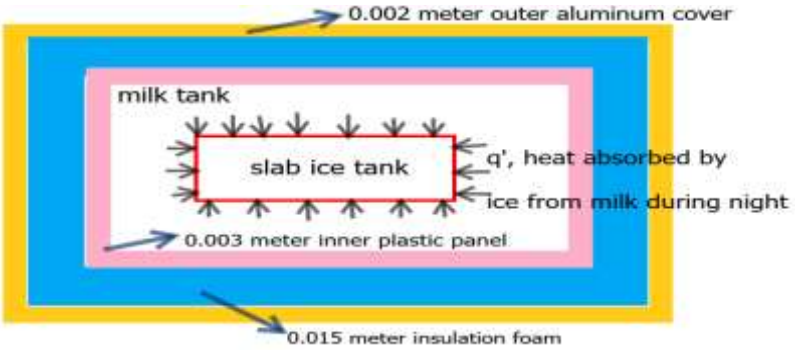

Figure 4-1. Two dimensional section view of milk and ice storage tank

$A_{milk} = 2(0.52 * 0.34) + 2(0.52 * 0.46) + 2(0.34 * 0.46) = 1.1448m^2$:

Floor, wall and roof outside area of the storage tank (m^2). The two wall surface areas are equal and the top and floor surface areas are also equal.

$\mathrm{T_{outside}} = 30°\mathrm{C}$: Outside air temperature, the ambient temperature of the location or site during night time.

$\mathrm{T_{inside}} = 4°\mathrm{C}$: Inside refrigerated milk temperature during night.

The overall heat transfer coefficient of the surface U can be calculate as follows by the following equation:

$$U = \frac{1}{\frac{1}{h_i} + \frac{X}{k} + \frac{1}{h_o}} \qquad [4.3]$$

Where, X: thickness of the insulator material wall (m)

K: thermal conductivity ($W/m.k$)

h_i *and* h_o: Inside and outside surface conductance respectively ($W/m^2.k$)

According to (ASHRAE, 2002) U factor for the flat parallel multi-surface with different thickness and properties can be calculate by using the following equation:

$$U = \frac{1}{\frac{x_1}{k_1} + \frac{x_2}{k_2} + \frac{x_3}{k_3}} \qquad [4.4]$$

By including h_i: inside surface conductance and h_o: outside surface conductance, we get the following.

$$U = \frac{1}{\frac{1}{h_i} + \frac{x_1}{k_1} + \frac{x_2}{k_2} + \frac{x_3}{k_3} + \frac{1}{h_o}} \qquad [4.5]$$

Where x_1, x_2 *and* x_3 : are the thicknesses of the materials 1, 2 and 3 respectively.

k_1, k_2 *and* k_3 : are thermal conductivity of the material 1, 2 and 3 respectively.

It is a very popular insulation material with available thickness of 10 to 15mm and density ranging from 35 to 50kg/m^3 with 0.016 to 0.023 $w/m.k$ thermal conductivity.

The material service temperature is in the range of $-180\ to\ 110℃$ [40]. The water vapour barriers are required on the cold sides of the insulation like aluminum foils of minimum 0.06mm thickness [40].

Table 4-1. Milk storage tank surface specification with thermal conductivity

Type of material	Thickness (m)	K (w/m.k)	h ($W/m^2.k$)
Plastic panel (inside)	0.003	0.22	5
Polyurethane expanded foam	0.015	0.023	
Aluminum sheet (outside)	0.002	237	30

$$U = \frac{1}{\frac{1}{5} + \frac{0.003}{0.22} + \frac{0.015}{0.023} + \frac{0.002}{237} + \frac{1}{30}}$$

$$U = 1.112159 W/m^2.k$$

$\mathrm{Q_{trans}} = 1.112159 w/m^2.k * 1.1448 m^2 (30-4)k$, during evening time:

$$\mathrm{Q_{trans}} = 33.11\mathrm{w}$$

$\mathrm{Q_{trans}} = 33.11\mathrm{w} * 14\mathrm{Hours} = 497\mathrm{Wh/day}$, within 14 hours of evening heat leakage.

$$\mathrm{Q_{trans}} = 33.11 \frac{\mathrm{J}}{\mathrm{sec}} * 14 * 3600\ \mathrm{sec} = 1{,}788\ \mathrm{kJ}$$

An additional or supplementary of 15 to 30% of ice transmission load can be incorporated to account as a safety factor [5].

$$Then, \qquad \mathrm{Q_{trans}} = 1.3 * 1{,}788\mathrm{kJ} = 2{,}324\mathrm{kJ}$$

Then, using equation (4.1) the amount of ice can be estimate as follows:

$$Qmilk, trns = m_{ice}\left[cp_{water}\left(T_{\min milk} - T_{fr}\right) + Q_L + Cp_{ice} * \Delta T_{ice}\right] \ldots\ldots [4.6]$$

$where,\ \mathrm{T_{min,milk}} = 4℃, \text{refrigerated milk temperature}$

$cp_{water} = 4180 \frac{J}{kg.k}, and\ cp_{ice} = 2025 \frac{J}{kg.k}, \text{Specific heat capacity of water and ice}$

$\Delta T_{ice} = (T_{fr} - T_L)$: Change of ice temperature below water freezing point.

$T_{fr} = 0℃, \quad T_{fr} = 0℃ \quad and \quad T_L = -4℃$: Freezing, phase change and average final temperature of water respectively.

$Q_L = 333700 \frac{J}{kg}$: Latent heat of fusion

From equation [4.6] by rearranging the ice mass we get:

$$m_{ice} = (Q_{milk,trns}) / \left[cp_{water}(T_{min,milk} - T_{fr}) + Q_L + Cp_{ice} * \Delta T_{ice}\right]$$

$$m_{ice} = \frac{2{,}324kJ}{4.180 \frac{kJ}{kg.k} * (4-0)k + 333.7 \frac{kJ}{kg} + 2.025 \frac{kJ}{kg.k} * (0-(-4))k}$$

$$m_{ice} = \frac{2{,}324kJ}{358.5kJ/kg} = 6.5\ KG$$

Then, the volume of the slab ice can be calculate by using the following relation:

$$\mathrm{m_{ice}} = V_{ice} * \rho_{ice}$$

$$\rho_{ice} = 918 \frac{kg}{m^3}, density of\ ice\ \ and\ V_{ice}: volume\ of\ ice$$

$$Volume_{ice} = \frac{m_{ice}}{\rho_{ice}} = \frac{6.5KG}{918\ kg/m^3} = 0.0071\ m^3 = 7.1L\ iter$$

The total volume of ice and milk storage system is:

$0.0071 + 0.05\ m^3 = 0.0571\ m^3$.

An additional or supplementary of 15% to 30% of ice volume can be incorporated to account as a safety factor.

Then the total volume of ice is : $1.3 * 0.0071\ m^3 = 0.0092\ m^3$

The volume of ice is less than the assumed value which is $0.0125\ m^3$, thus ice volume becomes $0.0092\ m^3$

Total volume of milk and ice becomes: - $0.0092\ m^3 + 0.05\ m^3 = 0.0592\ m^3$.

The size of the total cabinet becomes:

$$L * h * W, \qquad 0.31m * 0.45m * 0.425m = 0.0592\ m^3$$

$$Volume_{ice} = 0.0092\ m^3\ and$$

$$Mass\ of\ ice = V_{ice} * \rho_{ice} = 0.0092 * 920 = 8.5kg$$

The size of the ice tank only becomes:

$$L * h * w, \qquad 0.08m * 0.4m * 0.29m = 0.0092\ m^3$$

4.2.4 Thermal Expansion of Water

Thermal expansion is change in length, area or volume of storage tank material mass due to change of temperature. The volume of water increases during water solidification due to decreasing temperature and it causes decreasing of density of formed slab ice. For this reason amount of water volume inside ice storage tank will be decide based on thermal expansion of water. The slab ice storage tank size designed above was the final volume of water which is the volume of ice. Thus, volume of water must be less than this volume of ice to account its expansion. The initial volume of water can be determine by using thermal expansion of water in three dimensions or volume as follows:

$$\Delta V = 3\alpha v T = \beta V_i \Delta T$$

Where,$\Delta V = 0.0092m^3 - V_i$ change in volume of water in the storage tank

$3\alpha = \beta = 210 * 10^{-6}/℃$: The volume expansion coefficient, taken from standard volume expansion table

ΔT: Change in temperature of water from 33℃ to -4℃.

V_i: The initial volume of the water

$$\Delta V = 210 * 10^{-6}/℃ * V_i(33℃ - (-4)℃)$$

$$0.0092m^3 - V_i = 210 * 10^{-6}/℃ * V_i * 37℃$$

$$V_i = 0.00705m^3$$

This $0.00705m^3$ volume of free space is required in addition to water volume to form $0.0092m^3$ volume of ice. Thus, $0.00005m^3$ free space must be required for volume expansion of water during freezing.

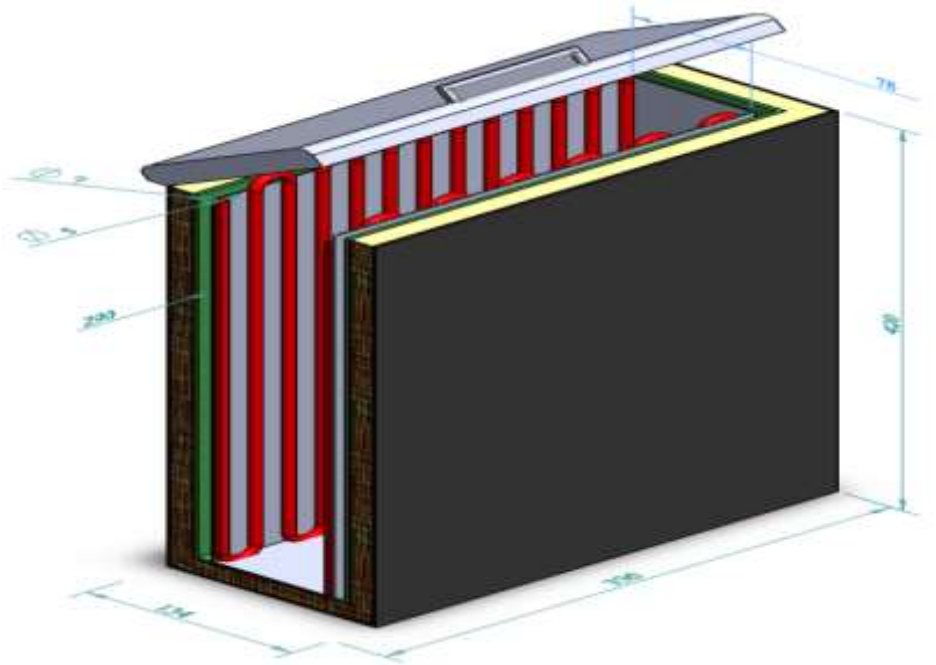

Figure 4-2. Isometric cut view of ice storage tank and Evaporator assembly

In day time milk tank and slab ice storage tank are placed independently. 50 litre of milk could be cooled using solar PV refrigeration system and during night 8.5 kilogram of ice could be added to remove transmission heat through milk wall. The slab ice tank could be placed at the middle of milk storage and surrounded by milk to absorb heat from milk.

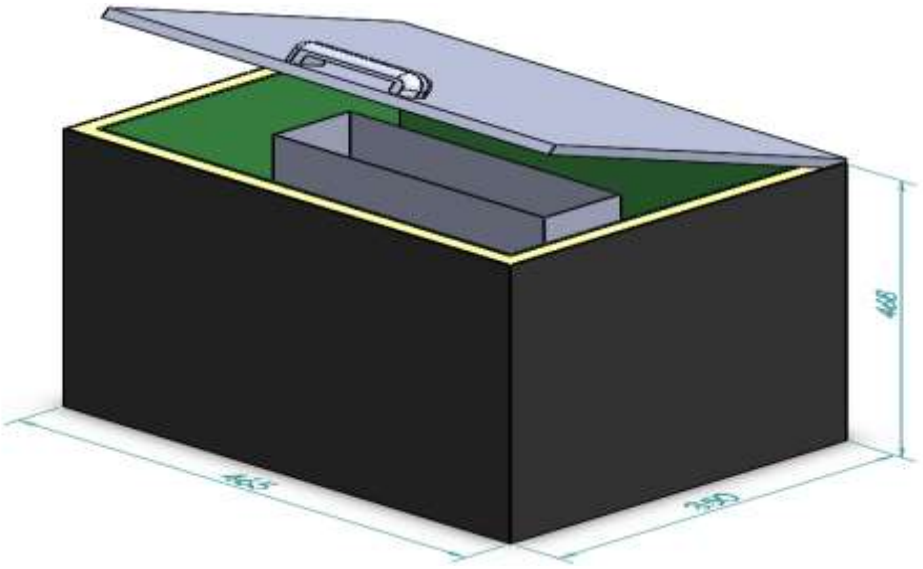

Figure 4-3. 3D view of combined milk and ice storage tank

4.3 Mathematical Modeling of PCM Solidification and Melting with Solving Methods

Solidification process is a transient heat transfer problem, which is described by non-linear partial differential equations. Stefan number (St) is a dimensionless number which means the sensitive heat relative to latent heat in phase change processes. The domain is divided into two distinct domains which are solid and liquid parts separated by a moving or interface boundary. For the moving boundary of phase change process both the phases exists and boundary of the phase change moves at a constant rate [41].

For the formation of slab ice, assume all sides of the slab tank are insulated and two internal opposite vertical sides are covered with the evaporator. The ice formation thickness increases in the horizontal (x) direction from each evaporator.

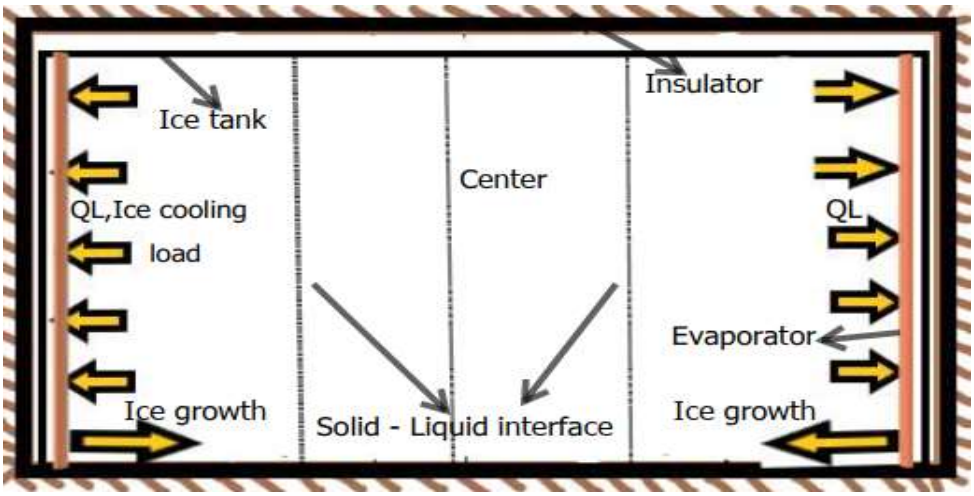

Figure 4-4. Schematic of water freezing process including the evaporator

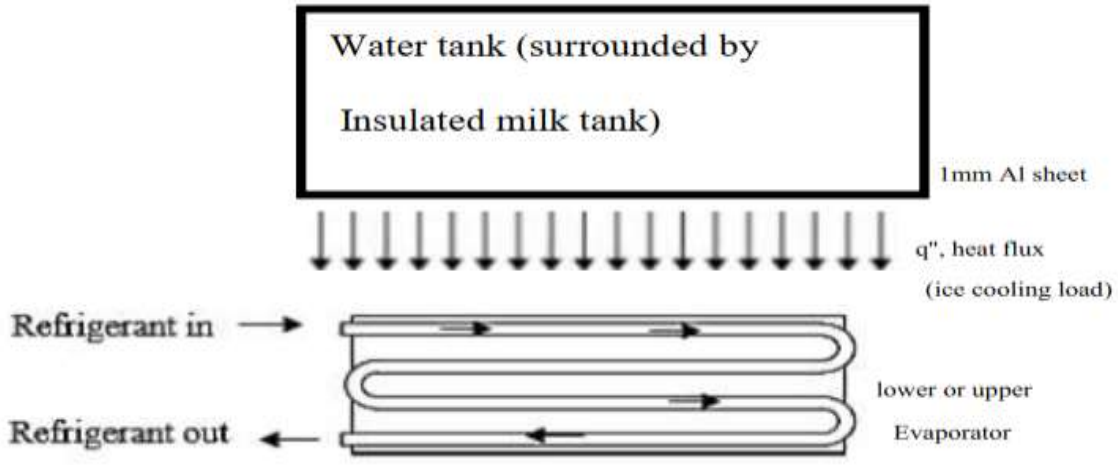

Figure 4-5. Representation of evaporator with refrigerant fluid inlet and outlet

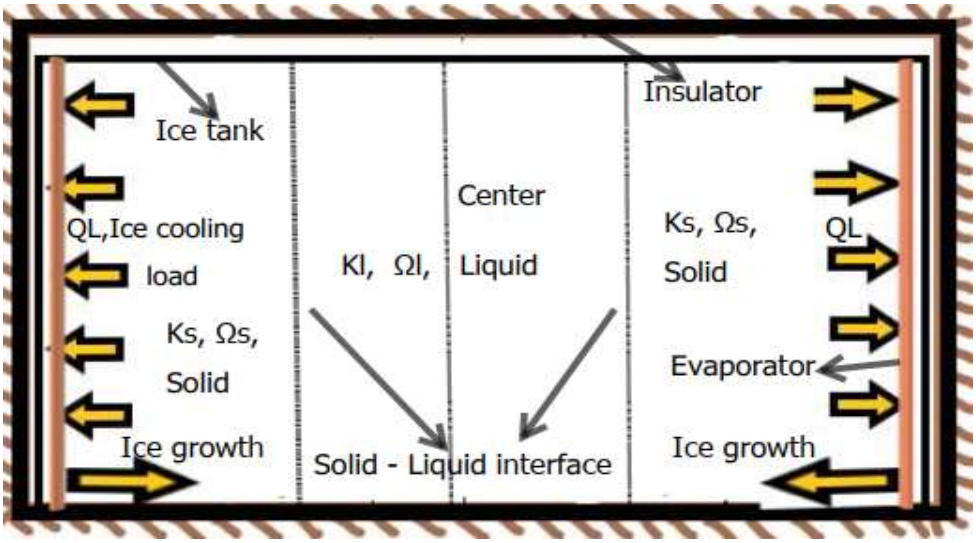

Figure 4-6 Water solidification in a rectangular capsule cooling from left and right surface of water tank

Figure 4.6 represents only the ice tank containing solid and liquid region and interface. The two distinct domains are Ω_s *and* Ω_l, where $\Omega_s + \Omega_l$. Considering the energy conservation in the domain, by considering one - dimensional case.

- k, ρ and c: specific heat, density and thermal conductivity of PCM
- h, thickness of the capsule Lt, solidification thickness of ice
- St, Stephan number S, Solid phase change material (ice)
- L, Liquid phase change material (water)
- T, temperature and t, time

The governing equations for heat equation along with the initial and boundary can be defined [41].

$$\rho_s c_s \frac{\partial T_s}{\partial t} = k_s \frac{\partial^2 T_s}{\partial x^2}, \qquad 0 \le x < y \ldots\ldots\ldots\ldots\ldots\ldots\ldots\ldots\ldots\ldots\ldots\ldots\ldots\ldots\ldots\ldots [4.7]$$

Equation [4.7], represents the heat conduction equation in the solid region.

$$\rho_l c_l \frac{\partial T_l}{\partial t} = k_s \frac{\partial^2 T_l}{\partial x^2}, \qquad y \le x < h \ldots\ldots\ldots\ldots\ldots\ldots\ldots\ldots\ldots\ldots\ldots\ldots\ldots\ldots\ldots\ldots [4.8]$$

Equation [4.8], represents the heat conduction equation in the liquid region.

The heat transfer in the solid by conduction in solidified portion is similar to the heat entering the interface by latent heat release at the interface and heat coming from liquid by

conduction. The complete explanation of phase change problem includes interface condition on phase change boundary Γ_{sl} [42]. $T_{sl} = T_f$

$$k_l\left(\frac{\partial T}{\partial x}\right)_l - k_s\left(\frac{\partial T}{\partial x}\right)_s = \rho_s Q_L \frac{ds}{dt}. on \ \ \Gamma_{sl} \ldots\ldots\ldots\ldots\ldots\ldots\ldots\ldots\ldots\ldots\ldots [4.9]$$

Where, Q_L, latent heat of fusion $T_{f,}$ phase change temperature

$\frac{ds}{dt}$, the interface velocity S, position of the interface

Equation [4.9], represents the Stefan condition at the solid – liquid interface region.

Temperature at the solid – liquid interface region can be expressed as:

$$T(X(t), t) = T_m, \quad then\ t > 0$$

The initial conditions of the model are:

$$T(X, 0) = T_s < T_m \quad for\ x > 0, x(0) = 0$$

The boundary conditions of the model are:

$$T(0, t) = T_l > T_m \quad for\ t > 0 \text{ And also } T(X, t) = T_s \quad for\ x \to \infty, t > 0$$

Where, $X(t)$, is the position of the melting interface (moving boundary) and T_m, T_s *and* T_l *are the melting, solid and liquid temperature respectivily*

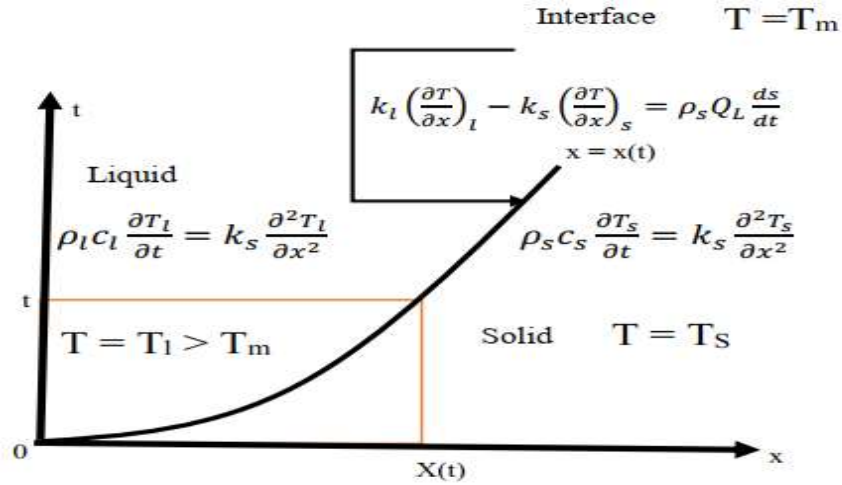

[Source, [42]]

Figure 4-7 Schematic representation of space time for two-phase Stefan problem

There are two numerical solving methods during the release or absorption of latent heat of fusion at the solid – liquid interface. These are: -

- Fixed mesh (enthalpy) method and
- Moving mesh methods or front tracking method.

4.3.1 Fixed Grid (Enthalpy) Method

A fixed grid method is an explicit method to calculate the unknown nodal temperature for the new time exclusively by using the unknown nodal temperature at the previous time with straightforward. The method approximated the heat flow equation by finite difference replacements for the derivatives to calculate the temperature on a fixed grid in the (x, t) plane. These are $T_{i,n}\ at\ X_i = i\Delta x$ and time $t_n = n\Delta t$. the moving boundary will be located between two adjacent grid points at any time $t_n = n\Delta t$. For instance $i_b\Delta x\ and\ (i_b + 1)\Delta x$ as shown below in the figure 4.8. [42]. This method can handle multidimensional problems efficiently without much difficulty.

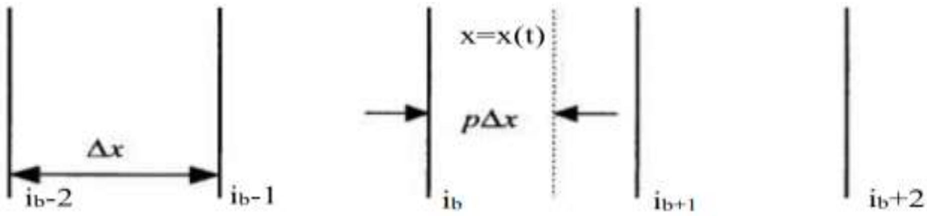

Figure 4-8 Moving boundary Positions in a fixed grid [Source, [42]]

Where, $\mathrm{i_b}$: Interface node index and X (t): positions of the liquid – solid interface.

P: Location of moving interface and i: any coordinate value

In this technique, properties are interpolated using nodal temperature of water at every time step. And also solid liquid phase interface can be calculated at every time step. A single energy conservation equation by using Fourier's law of heat conduction, is can be written for the whole domain: -

$$\frac{\partial H}{\partial t} = k\frac{\partial^2 T}{\partial x^2}, \qquad in\ \Omega \ldots\ldots\ldots\ldots\ldots\ldots\ldots\ldots\ldots\ldots\ldots\ldots\ldots\ldots\ldots\ldots [4.10]$$

Where, H enthalpy function or the total heat content, temperature T and thermal conductivity K.

Under the enthalpy based method, used to solve phase change problems based on direct solution system in a general way, the enthalpy H, can be expressed by the equation as follows: [43] [44].

$$H(T) = \int_{T_r}^{T} \rho C(T)\, dT, \dots\dots\dots\dots\dots\dots\dots\dots\dots\dots\dots\dots\dots\dots\dots\dots\dots\dots\dots\dots [4.11]$$

$\rho C(T)$: Is the volumetric heat capacity T_r : Is the reference temperature

In the case of phase change material with an isothermal phase change process the enthalpy function H can be defined as: [44] [43].

$$H(T) = \begin{cases} \int_{T_r}^{T} \rho C_S(T)dT\,, & when, T < T_f\ (solid\ phase) \dots\dots\dots\dots\dots\dots\dots [4.12a] \\ \int_{T_r}^{T_f} \rho C_S(T)dT + \rho Q_L + \int_{T_f}^{T} \rho c_l\,(T)dT\,, when, T > T_f\ (liquid). \dots [4.12b] \end{cases}$$

In the case of phase change material with non - isothermal phase change process the enthalpy function H including the mushy zone, can be defined as: [44].

$$H(T) = \begin{cases} \int_{T_r}^{T} \rho C_S(T)dT\,, & when, T \le T_{solidus}\ (solid\ phase) \dots\dots\dots\dots [4.13a] \\ & for\ mushy\ phase\ zone \\ \int_{T_r}^{T_{solidus}} \rho c_L(T)\, dT + \frac{\rho Q_L (T - T_{solidus})}{\Delta T}, when, T_{solidus} < T \le T_{liquidus} & [4.13b] \\ & for\ liquid\ phase \\ \int_{T_r}^{T_{solidus}} \rho C_S(T)dT + \rho Q_L + \int_{T_f}^{T} \rho c_L\,(T)dT\,, when,\ T > T_{liquidus} \dots\dots [4.13c] \end{cases}$$

Where, ρ is mass density, $\Delta T = T_{liquidus} - T_{solidus}$, c is specific heat, $Q_L\ is$ latent heat per unit mass, $T_f\ is$ freezing temperature, $T_r\ is$ reference temperature, S and L are the solid and liquid properties respectively and $T_{solidus}\ and\ T_{liquidus}$ are temperature of solid-mushy and mushy-liquid respectively. $\rho C_S(T)\ and\ \rho C_L(T)$, are the volumetric heat capacity for the solid and liquid phase respectively.

In the case of constant heat capacity and linear expression of liquid fraction function equation [4.12a and 4.12b] of H becomes as follows: [44].

$$H(T) = \begin{cases} \rho C_S(T - T_r), & when, T < T_f\ (solid\ phase) \dots\dots\dots\dots\dots\dots [4.14a] \\ & and \\ \rho C_S\big(T_f - T_r\big) + \rho Q_L + \rho C_L(T - T_f), & when, T > T_f\ (liquid\ ) \dots [4.14b] \end{cases}$$

In the case of constant heat capacity and linear expression of liquid fraction function equation [4.13a, 4.13b and 4.13c] of H becomes as follows: [44].

$$H(T) = \begin{cases} \rho C_S(T - T_r) & when, T \le T_{solidus}, \quad (solid\ phase) \\ & for\ mushy\ phase\ zone \\ \rho C_S(T_{solidus} - T_r) + \frac{\rho Q_L(T - T_{solidus})}{T_{liquidus} - T_{solidus}}, & when,\ T_{sol} < T \le T_{liq} \\ & for\ the\ liquid\ phase \\ \rho C_S(T_{solidus} - T_r) + \rho Q_L + \rho C_L(T - T_{liq}), & when, T > T_{liq} \end{cases} \quad \ldots [4.13a, 4.13b, 4.13c]$$

Where, T_{liq} – Liquidus temperature, T_{Sol} – Solidus temperature

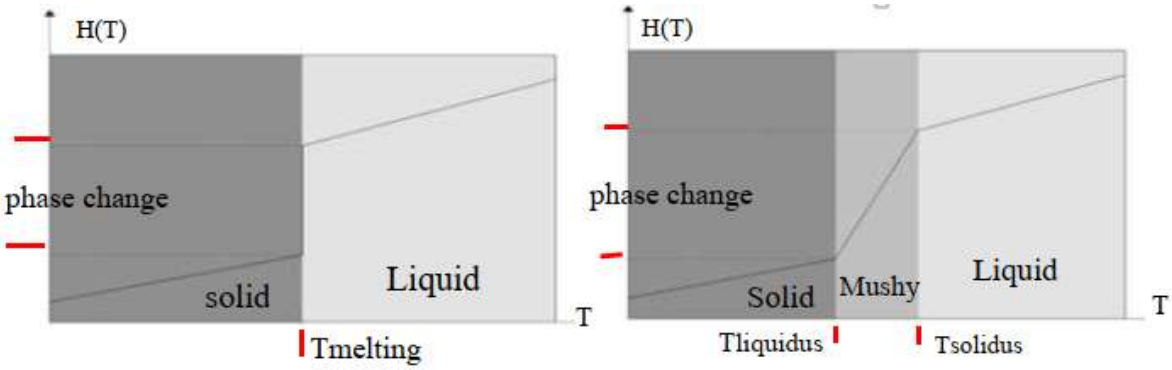

a. Isothermal phase change b. non-isothermal phase change [Source, [44]].

Figure 4-9. H-T behavior with constant heat capacity and using linear expressions of the liquid fraction function

The total latent heat of change Q_p^{total} of each control volume is:

$$Q_p^{total} = \int \rho\, Q_L dv \quad \ldots [4.14]$$

The phase change over the intervals of temperatures of T_S and T_L which are solidus and liquidus, respectively, can be defined as [45]:

$$H = \int_{T_r}^{T_S} \rho c_s\, dT + \int_{T_S}^{T} [\rho \frac{dQ_L}{dT} + \rho c_f] dT, \quad when, T_S \le T \le T_L \quad \ldots [4.15a]$$

$$H = \int_{T_r}^{T_S} \rho c_s\, dT + \rho Q_L + \int_{T_f}^{T_L} \rho c_f\, dT + \int_{T_L}^{T} \rho c_l\, dT, when, T > T_L \quad \ldots [4.15b]$$

Where, c_f – is the specific heat in the freezing interval

$Q_L -$ is the latent heat

$T_r -$ is the reference temperature below the solidus temperature.

Under the enthalpy method, the liquid fraction $fL(T)$ which is the amount of liquid or water content in the tank at the specific time can be calculate by using the following expressions [46]

$$fL(T) = \begin{cases} 0 & T < T_m\,, \quad solid \\ \dfrac{T - T_m}{T_s - T_m} & T_m \le T \le T_s, \quad mushy \\ 1 & T > T_s, \quad liquid \end{cases} \ldots\ldots\ldots\ldots\ldots\ldots [4.16a]$$

$$T_s, - solid\ phase\ temperature\ and \quad T_{m,} - melting\ temperature\ of\ ice$$

Or by using the $liquidus\ temperature, T_L\ and\ \ the$ solidus temperature, T_S

$$fL(T) = \begin{cases} 0 & T < T_S\,, \quad solid \\ \dfrac{T - T_{Solidus}}{T_{Liquidus} - T_{Solidus}} & T_S \le T \le T_L, \quad mushy \\ 1 & T > T_L, \quad liquid \end{cases} \ldots\ldots\ldots\ldots\ldots [4.16b]$$

$fL(T)$, is the liquid phase fraction as a function of temperature, the liquid phase fraction can take the values ranging from 0 up to 1 where $fL(T) = 0$ means the material is all in the solid phase, and

$fL(T) = 1$, means the material is all in the liquid phase, and

$fL(T) = \frac{T - T_{Solidus}}{T_L iquidus - T_{Solidus}}$, The material of these amount contains solid and liquid phases.

Among the fixed grid method, one of the most commonly used method is the effective heat capacity method. The method can be derived:

$$\frac{\partial H}{\partial t} = \frac{\partial H}{\partial T}\frac{\partial T}{\partial t} = k\frac{\partial^2 T}{\partial x^2}, \quad in\ \Omega \ldots\ldots\ldots\ldots\ldots\ldots\ldots\ldots\ldots\ldots\ldots\ldots\ldots\ldots [4.17]$$

From the standard heat equation, equation 4.14 can also be write:

$$\frac{\partial H}{\partial t} = c_{eff}, \quad \text{Where,} \quad c_{eff} - \text{the effective heat capacity.}$$

The effective heat capacity at the solid region can be expressed as:$equation[4.18a]$. the effective heat capacity at the solid liquid interface region (mushy zone) can be expressed

as: $equation[4.18b]$ and the effective heat capacity at the liquid region can be expressed as: $equation[4.18c]$ [45].

$$c_{eff} = \begin{cases} \rho c_s, & when\ T < T_S \ldots\ldots\ldots\ldots\ldots\ldots\ldots\ldots\ldots\ldots\ldots\ldots\ldots\ldots [4.18a] \\ \rho c_f + \dfrac{\rho_S Q_L}{T_L - T_S}, & when\ T_S < T < T_L \ldots\ldots\ldots\ldots\ldots\ldots\ldots [4.18b] \\ \rho c_l, & when\ T > T_L \ldots\ldots\ldots\ldots\ldots\ldots\ldots\ldots\ldots\ldots\ldots\ldots\ldots [4.18c] \end{cases}$$

The specific enthalpy H(T), as a function of temperature, by using the enthalpy method and the effective heat capacity found from above, is easy to handle a phase change material and the phase change range and the phase change range is express as follows [47].

$$H(T) = \begin{cases} C_s T, & when\ T < T_{solidus} \\ C_l T + \dfrac{Q_L (T - T_{solidus})}{\Delta T}, & when\ T_{solidus} < T < T_{liquidu} \ldots\ldots\ldots\ldots\ldots [4.19] \\ C_l T + Q_L, & when\ T > T_{liquidus} \end{cases}$$

Where, ρ is mass density, $\Delta T = T_{liquidus} - T_{solidus}$ C is the effective specific heat, $Q_L\ is$ latent heat per unit mass, $T_f\ is$ freezing temperature, $T_r\ is$ reference temperature, S and L are the solid and liquid properties respectively.

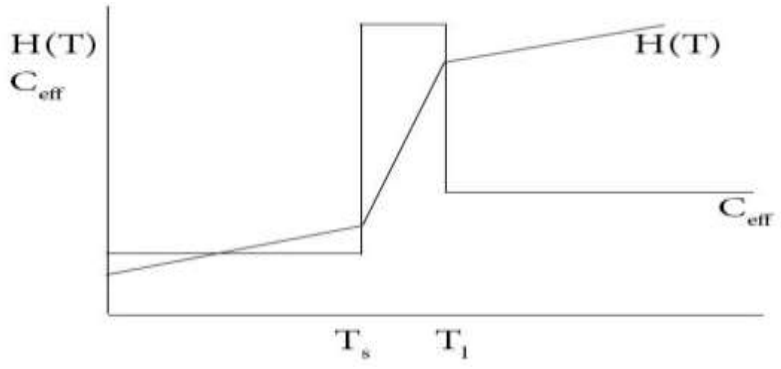

[Source: [45]]

Figure 4-10. Variation of enthalpy and effective heat capacity with temperature

The governing equation discretization of temperature distribution inside the water tank, when cooled from bottom by using one dimensional finite difference method during solidification are as follow:

- Assume the one dimensional heat conduction equation can be written as:

$$\rho c \frac{\partial T}{\partial t} = k \frac{\partial^2 T}{\partial x^2} \ldots\ldots\ldots\ldots\ldots\ldots\ldots\ldots\ldots\ldots\ldots\ldots\ldots\ldots [a]$$

4.3.1.1 Modeling of Transient Nodal Temperature Distribution of Water

By considering the heat conduction in a slab of thickness 2*0.04 meter, initially at a uniform temperature of water, applying heat flux at two vertical sides which are left and right surface of ice tank and all other sides are insulated. Assuming variable physical properties, such as thermal conductivity, density, and specific heat capacity, the generalized one dimensional heat flow, explicit transient heat conduction equation for slab, can be expressed as follows:

The nodal temperature of water can be expressed using explicit finite difference method, by taking three nodes, which are first node, interior node and last node inside water tank and assuming the heat flow is in the horizontal x-axis:

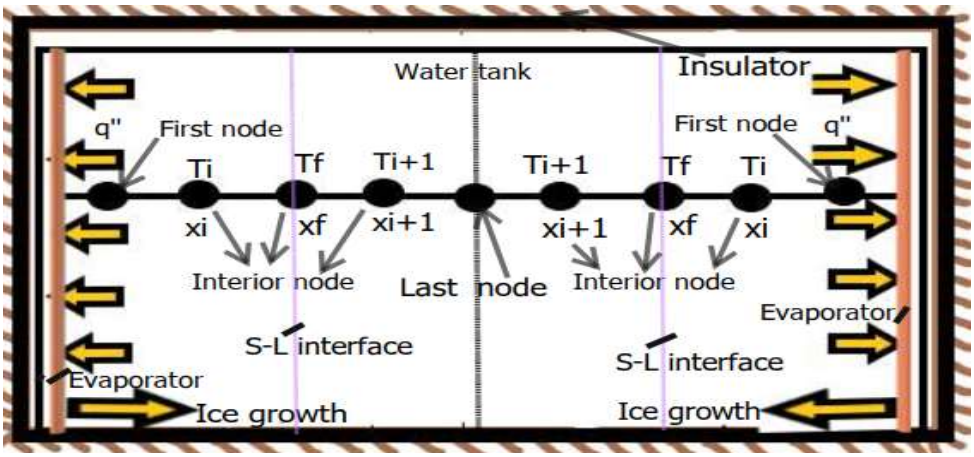

Figure 4-11 schematic of 1D heat flow, node location, from evaporator position

The mathematical equation is modeled by using transient, 1D, explicit finite difference method based on the geometry of ice slab tank and location of evaporator inside the tank. The equation can be formulate based on 0.4 meter height, 0.08 meter length and 0.29 meter width to form 8.5 kilogram 9.3 litre of ice slab. The evaporator covers two parallel vertical sides of the tank with 0.4*0.29 m^2 and 0.08 meter distance between two evaporators.

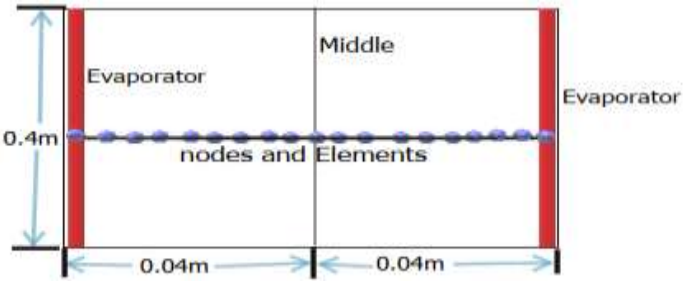

Figure 4-12. Two dimensional view of slab ice tank

a. For interior node (using explicit or forward difference method)

In explicit method or forward difference, the derivative is evaluated at the beginning of the time step or at n^{th} step. The one - dimensional transient conduction heat transfer equations using the explicit finite difference method for the interior nodes between the two right and left evaporators and the last node from each evaporator which is located at the center of the water tank shown below in the figure can be explain as follows:

For unsteady state heat conduction method the conservation of energy equation becomes:

$$\sum_{n=1}^{4} Q_{n\to(i,j)} + q(\Delta x.\Delta y.1) = \rho c(\Delta x.\Delta y.1)\frac{\partial T}{\partial t} \dots\dots\dots\dots\dots\dots\dots\dots\dots\dots\dots [4.20]$$

For the interior node, assuming no heat generation inside the system equation [4.20] becomes:

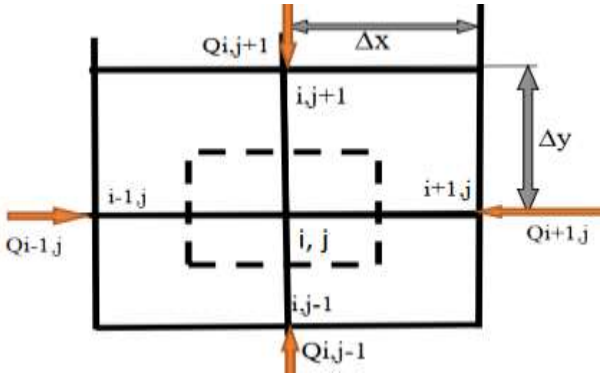

$$Q_{i+1,j} + Q_{i-1,j} + Q_{i,j+1} + Q_{i,j-1} = \rho c(\Delta x.\Delta y.1)\frac{\partial T}{\partial t} \dots\dots\dots\dots\dots\dots\dots [4.21]$$

In this case, the flow is one-dimension and assuming the flow is in the horizontal i direction, then equation [4.21] becomes:

$$Q_{i+1,j} + Q_{i-1,j} = \rho c(\Delta x.1)\frac{\partial T}{\partial t} \dots\dots\dots\dots\dots\dots\dots\dots\dots\dots\dots [a]$$

The rate of conduction heat transfer between nodes by consider unit depth and n refers to neighbor nodes are expressed as

$$Q_{i+1,j} = k(1)\frac{{T_{i+1,j}}^{n} - {T_{i,j}}^{n}}{\Delta x} \dots\dots\dots\dots\dots\dots\dots\dots\dots\dots\dots\dots [b]$$

$$Q_{i-1,j} = k(1)\frac{{T_{i-1,j}}^{n} - {T_{i,j}}^{n}}{\Delta x} \dots\dots\dots\dots\dots\dots\dots\dots\dots\dots\dots\dots\dots\dots [c]$$

Substituting equation [b] and [c] into equation [a] and rearranging we get:

$$\rho c\frac{{T_{i,j}}^{n+1} - {T_{i,j}}^{n}}{k\Delta t} = \frac{{T_{i+1,j}}^{n} + {T_{i-1,j}}^{n} - 2{T_{i,j}}^{n}}{\Delta x^2}$$

$${T_{i,j}}^{n+1} = {T_{i,j}}^{n} + \frac{k\Delta t}{\rho c\Delta x^2}\left({T_{i+1,j}}^{n} + {T_{i-1,j}}^{n} - 2{T_{i,j}}^{n}\right)$$

$${T_{i,j}}^{n+1} = \frac{k\Delta t}{\rho c\Delta x^2}\left({T_{i+1,j}}^{n} + {T_{i-1,j}}^{n}\right) + \left(1 - 2\frac{k\Delta t}{\rho c\Delta x^2}\right)T_{i,j}^{n} \dots\dots\dots\dots\dots [4.22]$$

b. For first node of the left water tank, heat flux towards the left side evaporator

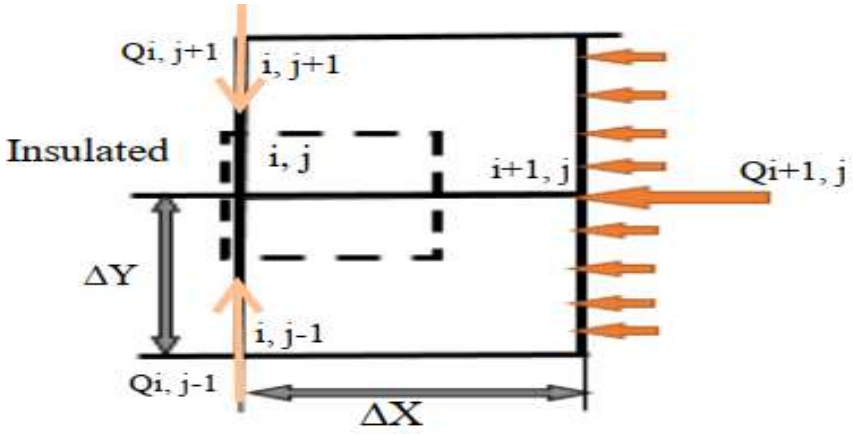

The energy balance equation for node at plane surface, with heat flux q'' can be given as:

$$Q_{i+1,j} + Q_{i,j-1} + Q_{i,j+1} + q'' = \rho c(\Delta x.\Delta y.1)\frac{\partial T}{\partial t} \dots\dots\dots\dots\dots\dots\dots [a]$$

But in this research case, there is no heat flow in the vertical direction and heat flow is only in the horizontal x-direction. By taking the left evaporator, equation [a] becomes:

$$Q_{i+1,j} + q'' = \rho c\left(\frac{\Delta x}{2}.1\right)\frac{\partial T}{\partial t} \dots\dots\dots\dots\dots\dots\dots\dots\dots\dots\dots [b]$$

$$Q_{i+1,j} = k(1)\frac{{T_{i+1,j}}^{n} - {T_{i,j}}^{n}}{\Delta x} \dots\dots\dots\dots\dots\dots\dots\dots\dots\dots\dots [c]$$

By substituting equation [c] and [d] into equation [b]

$$k(1)\frac{{T_{i+1,j}}^{n}-{T_{i,j}}^{n}}{\Delta x}+q''=\rho c\left(\frac{\Delta x}{2}.1\right)\frac{{T_{i,j}}^{n+1}-{T_{i,j}}^{n}}{\Delta t}$$

$${T_{i+1,j}}^{n}-{T_{i,j}}^{n}+\frac{1}{k}*q''*(\Delta x)=\frac{\rho c\Delta x^{2}}{2k\Delta t}({T_{i,j}}^{n+1}-{T_{i,j}}^{n})$$

Heat is absorbed from water to the evaporator, for this reason q'' is negative

$${T_{i,j}}^{n+1}=\frac{2k\Delta t}{\rho c\Delta x^{2}}\left({T_{i+1,j}}^{n}-\frac{\Delta x*q''}{k}\right)+\left(1-\frac{2k\Delta t}{\rho c\Delta x^{2}}\right){T_{i,j}}^{n}\ldots\ldots\ldots\ldots[4.23]$$

c. For the first node of the right water tank, with heat flux towards the right side of the evaporator

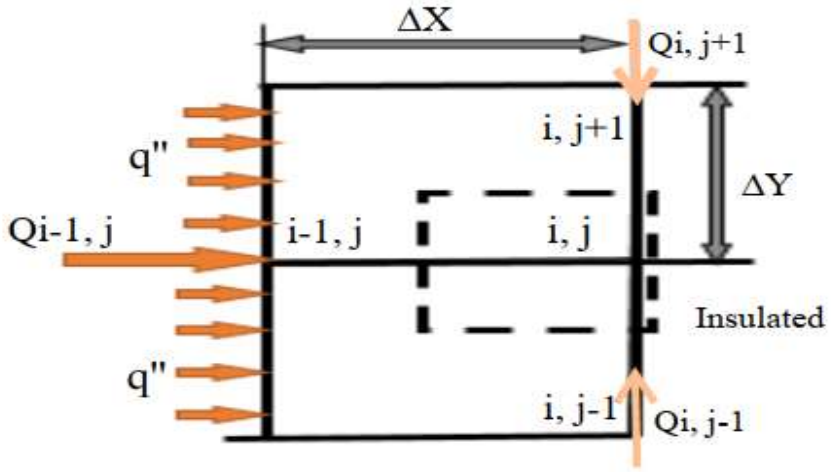

The energy balance equation at plane surface or boundary nodes, with heat flux q'' can be given as:

$$Q_{i,j+1}+Q_{i-1,j}+Q_{i,j-1}+q''=\rho c(\Delta x.\Delta y.1)\frac{\partial T}{\partial t}\ldots\ldots\ldots\ldots\ldots\ldots[a]$$

But in this research case, there is no heat flow in the vertical direction, and the heat flow is only in the horizontal x-direction, by taking the right side of the tank, so equation [a] becomes:

$$Q_{i-1,j}+q''=\rho c\left(\frac{\Delta x}{2}.1\right)\frac{\partial T}{\partial t}\ldots\ldots\ldots\ldots\ldots\ldots\ldots\ldots\ldots\ldots\ldots\ldots\ldots\ldots[b]$$

$$Q_{i-1,j}=k(1)\frac{{T_{i-1,j}}^{n}-{T_{i,j}}^{n}}{\Delta x}\ldots\ldots\ldots\ldots\ldots\ldots\ldots\ldots\ldots\ldots\ldots\ldots\ldots\ldots\ldots[c]$$

By substituting equation [c] and [d] into equation [b]

$$k(1)\frac{{T_{i-1,j}}^{n}-{T_{i,j}}^{n}}{\Delta x}+q''=\rho c\left(\frac{\Delta x}{2}.1\right)\frac{{T_{i,j}}^{n+1}-{T_{i,j}}^{n}}{\Delta t}$$

$${T_{i-1,j}}^{n}-{T_{i,j}}^{n}+\frac{1}{k}q''(\Delta x)=\frac{\rho c\Delta x^{2}}{2k\Delta t}({T_{i,j}}^{n+1}-{T_{i,j}}^{n})$$

Heat is absorbed from water to the evaporator, for this reason q'' is negative

$${T_{i,j}}^{n+1}=\frac{2k\Delta t}{\rho c\Delta x^{2}}\left({T_{i-1,j}}^{n}-\frac{\Delta x*q''}{k}\right)+\left(1-\frac{2k\Delta t}{\rho c\Delta x^{2}}\right){T_{i,j}}^{n}\ldots\ldots\ldots\ldots[4.28]$$

d. For the center node between right and left evaporator

This node is located at the center of ice tank and is the last node of both evaporators. At the center node, assume no heat transfer relation between these two left and right parts of the tank, the equation becomes:

At the mid plane node the equation is the same as equation (4.26) at the center node, but the node temperatures of ${T_{i-1,j}}^{n}\ and\ {T_{i+1,j}}^{n}$ are equal, ${T_{i-1,j}}^{n}={T_{i+1,j}}^{n}$.

Thus, the equation becomes: ${T_{i,j}}^{n+1}=\frac{k\Delta t}{\rho c\Delta x^{2}}\left(2*{T_{i-1,j}}^{n}\right)+\left(1-\frac{2k\Delta t}{\rho c\Delta x^{2}}\right){T_{i,j}}^{n}$

Or using the procedure, the equation can be formulate as follows:

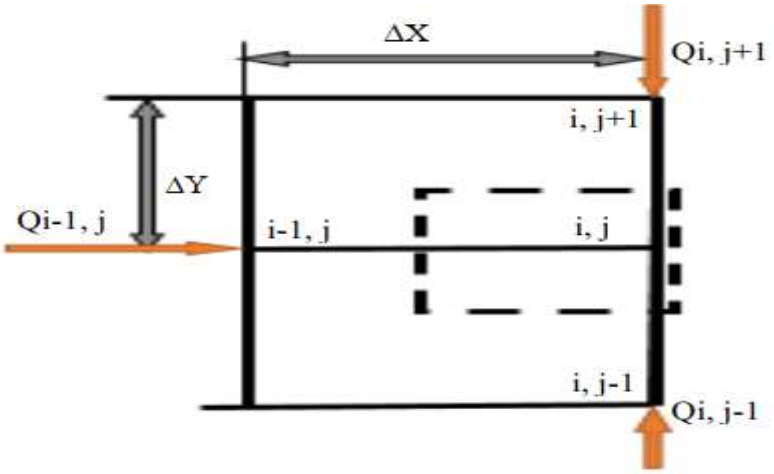

The energy balance equation for node at the center of the tank with no heat flux and convection can be given as:

$$Q_{i-1,j}+Q_{i,j+1}+Q_{i,j-1}=\rho c(\Delta x.\Delta y.1)\frac{\partial T}{\partial t}\ldots\ldots\ldots\ldots\ldots\ldots\ldots\ldots\ldots[a]$$

But in this research case, there is only heat flow in the horizontal x-direction, no heat flows in the vertical y-axis, and also one side is adiabatic, so equation [a] becomes:

$$Q_{i-1,j} = \rho c\left(\frac{\Delta x}{2}.1\right)\frac{\partial T}{\partial t} \ldots\ldots\ldots\ldots\ldots\ldots\ldots\ldots\ldots\ldots\ldots\ldots\ldots\ldots\ldots\ldots\ldots\ldots [a]$$

$$Q_{i-1,j} = k(1)\frac{{T_{i-1,j}}^{n} - {T_{i,j}}^{n}}{\Delta x} \ldots\ldots\ldots\ldots\ldots\ldots\ldots\ldots\ldots\ldots\ldots\ldots\ldots\ldots\ldots\ldots\ldots\ldots [b]$$

By substituting equation [b] into equation [a] and using 1D heat transfer equation

$$k(1)\frac{{T_{i-1,j}}^{n} - {T_{i,j}}^{n}}{\Delta x} = \rho c\left(\frac{\Delta x}{2}.1\right)\frac{{T_{i,j}}^{n+1} - {T_{i,j}}^{n}}{\Delta t}$$

$${T_{i-1,j}}^{n} - {T_{i,j}}^{n} = \frac{\rho c \Delta x^2}{2k\Delta t}({T_{i,j}}^{n+1} - {T_{i,j}}^{n})$$

$${T_{i,j}}^{n+1} = \frac{2k\Delta t}{\rho c \Delta x^2}\left({T_{i-1,j}}^{n}\right) + \left(1 - \frac{2k\Delta t}{\rho c \Delta x^2}\right){T_{i,j}}^{n} \ldots\ldots\ldots\ldots\ldots\ldots\ldots\ldots\ldots\ldots\ldots\ldots [4.29]$$

4.3.1.2 Solid Liquid Phase Interface Location Modeling

To calculate thickness of thin and thick ice growth, there are different equations derived by different researchers. The square root of freezing degree days is most commonly used method to calculate ice thickness floating [11]. By considering heat losses, the coefficients of thermal resistance between the ice top surface, the bulk temperature of air and heat flux to provide an analytical result both thin and thick ice growth, the equation is as follows:

$$X(t) = \left[\frac{2k}{\rho Q_L}(T_m - T_a)t + \left(\frac{k}{h}\right)^2\right]^{\frac{1}{2}} - \frac{k}{h} \ldots\ldots\ldots\ldots\ldots\ldots\ldots\ldots\ldots\ldots\ldots\ldots\ldots\ldots\ldots\ldots [4.30a]$$

Where, $X(t)$: $is\ the\ ice\ thickness, [m]$ $\quad and\ t$: $time\ [s]$

$$h: heat\ transfer\ coeefficient\ [w/m^2{}^{\circ}\mathrm{C}] and\ \rho: density\ of\ ice\ kg/m^3$$

$$k: thermal\ conductivity\ [w/m{}^{\circ}\mathrm{C}]\ and\ Q_L: heat\ of\ fusion\ [J/kg]$$

$$T_a: air\ temperature\ [{}^{\circ}\mathrm{C}] and\ T_m: melting\ point\ temperature\ [{}^{\circ}\mathrm{C}]$$

The distance of the solid-liquid interface from the end wall can be calculate as follows [22]:

$$S_x = \sqrt{\frac{2k_S(T_w - T_m)t}{-\rho(Q_L + C_l(T_i - T_m))}} \ldots\ldots\ldots\ldots\ldots\ldots\ldots\ldots\ldots\ldots\ldots\ldots\ldots\ldots\ldots\ldots\ldots\ldots\ldots\ldots [4.30b]$$

$$S_x = \left(\frac{2k}{\rho * QL}\right)^{\frac{1}{2}} * [(T_m - T_w) * t]^{\frac{1}{2}} \ldots\ldots\ldots\ldots\ldots\ldots\ldots\ldots\ldots\ldots\ldots\ldots\ldots\ldots\ldots\ldots\ldots\ldots\ldots\ldots [4.30c]$$

Where, S_x: *is the ice thickness,* $[m]$ *and* t: *time* $[s]$

T_i: *initial temperature* [℃]*and* ρ: *density of ice* kg/m^3

k: *thermal conductivity* $[w/m℃]$ *and* Q_L: *latent heat of fusion* $[J/kg]$

T_w: *wall temperature* [℃]*and* T_m: *solidification temperature* [℃]

The location of the solid-liquid interface can also be calculate by interpolation three consecutive nodes as shown figure (4.13) bellow:

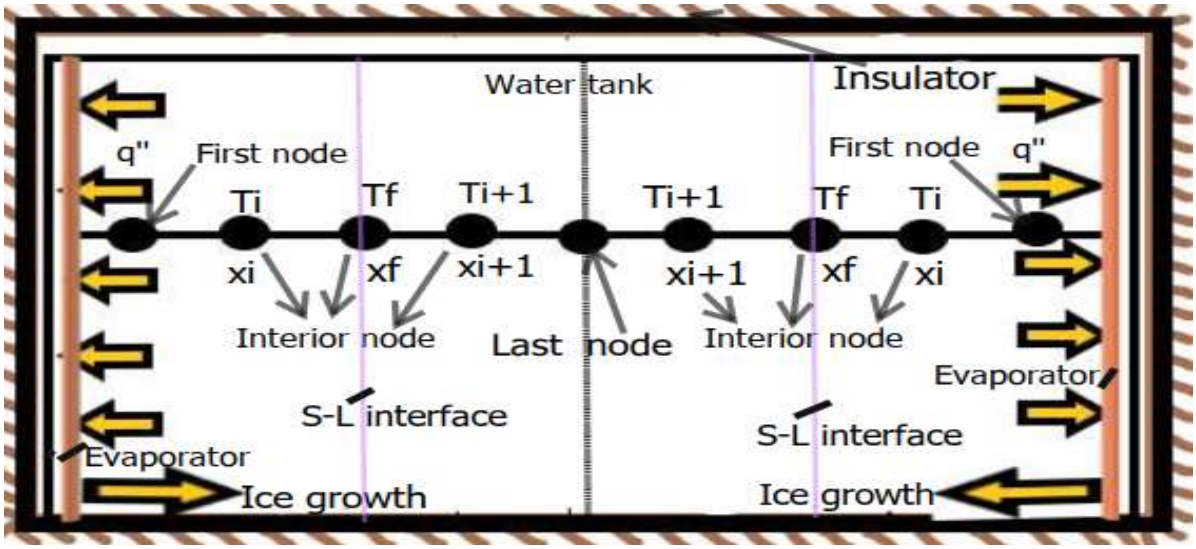

Figure 4-13: ice slab tank with milk storage space nodal temperature and interface location

The heat flux is due to the convective heat transfer between the refrigerant and evaporator tube, conduction heat transfer through the tube thickness, the convective heat transfer between the evaporator tube and water initially, conduction heat transfer through ice thickness and convective heat transfer between ice surface and water.

By using interpolation of nodal temperatures and nodal ice crystal formation, the final ice crystal growth can be formulate as follows:

$$X(t) = Xf = x_{i-1} + \frac{T_f - T_{i-1}}{T_{i+1} - T_{i-1}}(x_{i+1} - x_{i-1}) \dots\dots\dots\dots\dots\dots\dots\dots\dots\dots\dots\dots [4.30c]$$

Where, $x(t)\ is\ the\ solid - liquid\ interface, x_i$ is the initial ice thickness,

$$T_f = \frac{C_S + C_l}{2} + \frac{Q_L}{\Delta T} - \text{ is the finite temperature}$$

$$\Delta T = T_{Liquidus} - T_{Solidus}$$

$C_S\ and\ C_l$ are the fictitious specific heat for solid and liquid respectivily

The thermophysical properties ρ – density, k – thermal conductivity and cp-specific heat of the mushy region are the average properties, by using the expression bellow [48]:

$$\begin{cases} k_{mush} = k_s + f(T) * (k_l - k_s), \\ \quad and \\ \rho_{mush} = \rho_s + f(T) * (\rho_l - \rho_s) \dots\dots\dots\dots\dots\dots\dots\dots\dots\dots\dots\dots\dots\dots [4.30d] \\ Cp_{mush} = \dfrac{Q_L}{\Delta T} + \dfrac{C_S + C_L}{2} \end{cases}$$

$$where, liquid\ fraction, f(T) = \frac{T - T_{solidus}}{T_{liquidus} - T_{solidus}}\ , \qquad T_{solidus} \le T \le T_{liquidus},$$

The specific heat of the mushy region C_{mush} can be calculate using the latent heat of fusion Q_L and change in freezing temperature $\Delta T = T_{liquidus} - T_{solidus}$.

The explicit method is conditionally stable and has high accuracy. But the solution stability has restriction based on the values of time step and grid size. The values of time step and grid space can be limited based on the stability criteria for one dimensional explicit heat equation of each node, which is $F_o \le \frac{1}{2}$, $F_O = \frac{k\Delta t}{\rho c \Delta x^2}$

4.3.2 Moving Mesh (Backward Difference) Method

In implicit method or backward difference, the derivative are evaluated at the beginning of the end of time step or at n+1th step. The boundary separates two different phases which develops in a phase change problem moving in the matter during the process. At the moving boundary both the phases exists and boundary moves at a constant rate. Moving interface boundary problem is associated with time dependent boundary problem, where the positions of moving boundary must be determined as a function of time and space. In this

method solid – liquid regions are treated separately and phase change interface is explicitly determined as a moving boundary [41].

In this moving mesh technique, finite element method is used due to its two domains and uses transient non-linear heat transfer.

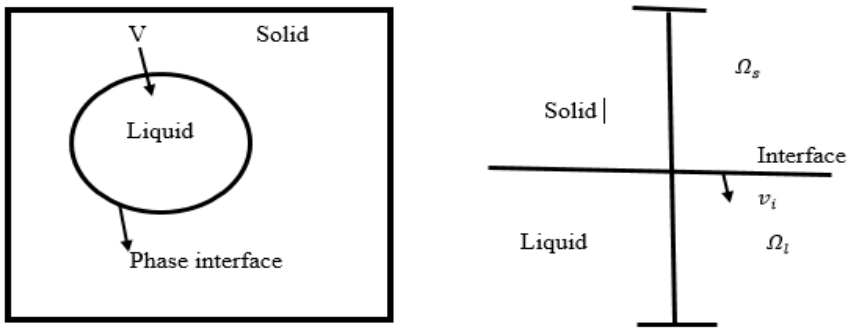

Figure 4-14 Schematic physical model of moving mesh system

The governing equations of the heat conduction along with the initial and boundary conditions can be defined as [41]:

At the interface, $T = T_f = T_{sl}$

$$\rho_s c_s \frac{\partial T_s}{\partial t} = k_s \frac{\partial^2 T_s}{\partial x^2}, \qquad 0 \le x < y \ldots\ldots\ldots\ldots\ldots\ldots\ldots\ldots\ldots\ldots\ldots\ldots\ldots\ldots\ldots [4.31]$$

$$\rho_l c_l \frac{\partial T_l}{\partial t} = k_s \frac{\partial^2 T_l}{\partial x^2}, \qquad y \le x < h \ldots\ldots\ldots\ldots\ldots\ldots\ldots\ldots\ldots\ldots\ldots\ldots\ldots\ldots\ldots [4.32]$$

These two equations, represents the heat conduction equation in the solid and the liquid region respectively.

The complete explanation of the problem includes the Stefan condition at the solid – liquid interface condition on the phase change boundary Γ_{sl}. $T_{sl} = T_f$

$$k(\frac{\partial T}{\partial x})_l - k\left(\frac{\partial T}{\partial x}\right)_s = \rho Q_L \frac{dx_i}{dt}, on \ \ \Gamma_{sl} \ldots\ldots\ldots\ldots\ldots\ldots\ldots\ldots\ldots\ldots\ldots\ldots\ldots\ldots [4.33]$$

Where, Q_L, latent heat of fusion T_f, phase change temperature

S, position of the interface $\frac{dx_i}{dt}$, the interface velocity

$$k_l(\frac{\partial T}{\partial x})_l - k_s\left(\frac{\partial T}{\partial x}\right)_s = \rho Q_L \frac{dx_i}{dt} \dots\dots\dots\dots\dots\dots\dots\dots\dots\dots\dots\dots\dots\dots [4.34]$$

$$k_l \frac{\partial T}{\partial x} = -k_l \frac{T_i - T_{i+1}}{\Delta x} \dots\dots\dots\dots\dots\dots\dots\dots\dots\dots\dots\dots\dots\dots [a]$$

$$k_s \frac{\partial T}{\partial x} = -k_s \frac{T_i - T_{i-1}}{\Delta x} \dots\dots\dots\dots\dots\dots\dots\dots\dots\dots\dots\dots\dots\dots [b]$$

$v * \Delta t = \Delta x$, Where v is the velocity of the interface and Δx is the mesh displacement, thus by substituting equation [a] and [b] in to equation [4.34] we get.

$$-k_l \frac{T_i - T_{i+1}}{\Delta x} - \frac{-k_s(T_i - T_{i-1})}{\Delta x} = \rho Q_L \frac{dx_i}{dt} \dots\dots\dots\dots\dots\dots\dots\dots [4.35]$$

$\frac{dx_i}{dt} = v_{int}, is\ the\ interface\ velocity\ and\ rearranging\ equation$ [4.35] we get:

$$v_{int} = \frac{dx_i}{dt} = \frac{\frac{-k_l(T_i - T_{i+1})}{\Delta x} - \frac{-k_s(T_i - T_{i-1})}{\Delta x}}{\rho Q_L}$$

$$\rho A \Delta x_i Q_L - heat\ rejected\ by\ the\ liquid\ during\ freezing$$

$\rho A \Delta x_i - \dot{m}$, mass flowrate and Q_L the latent heat of fusion.

We can use, $\frac{\Delta T}{\Delta t} = \frac{\partial x}{\partial t}\frac{\partial T}{\partial X} + \frac{\partial T}{\partial t}$, X is charging with time

This is from material derivatives

$$thus, \frac{\Delta T}{\Delta t} = \frac{\partial x}{\partial t}\left(\frac{\partial T}{\partial X}\right) + \frac{\partial T}{\partial t} \dots\dots\dots\dots\dots\dots\dots\dots\dots\dots\dots\dots\dots\dots [c]$$

Substituting equation [c] in to equation [4.31] and equation [4.32] we get the following equations: Equation [4.31] becomes

$$\rho_s c_s\left(\frac{\partial x}{\partial t}\frac{\partial T}{\partial X} + \frac{\partial T}{\partial t}\right) = k_s \frac{\partial^2 T}{\partial x^2} \dots\dots\dots\dots\dots\dots\dots\dots\dots\dots\dots\dots\dots\dots [4.36]$$

Equation [4.32] becomes

$$\rho_l c_l\left(\frac{\partial x}{\partial t}\frac{\partial T}{\partial X} + \frac{\partial T}{\partial t}\right) = k_l \frac{\partial^2 T}{\partial x^2} \dots\dots\dots\dots\dots\dots\dots\dots\dots\dots\dots\dots\dots\dots [4.37]$$

Rearranging equation [4.36] for the solid part and write $\frac{\partial x}{\partial t}\frac{\partial T}{\partial X} = v\frac{\partial T}{\partial x}$, we get

$$\frac{\partial T}{\partial t} = \frac{k_s}{\rho_s c_s}\frac{\partial^2 T}{\partial x^2} - v\frac{\partial T}{\partial x}$$

$$\frac{T_i^{n+1} - T_i^n}{\Delta t} = \frac{k_s}{\rho_s c_s}\left(\frac{T_{i+1}^n - 2T_i^n - T_{i-1}^n}{(\Delta x)^2}\right) - v_i\left(\frac{T_{i+1}^n - T_{i-1}^n}{2\Delta x}\right)$$

$$T_i^{n+1} = T_i^n + \frac{\Delta t k_s}{\rho_s c_s}\left(\frac{T_{i+1}^n - 2T_i^n - T_{i-1}^n}{(\Delta x)^2}\right) - \Delta t v_i\left(\frac{T_{i+1}^n - T_{i-1}^n}{2\Delta x}\right) \ldots\ldots\ldots\ldots [4.38]$$

Rearranging equation [4.37] for the liquid part and write $\frac{\partial x}{\partial t}\frac{\partial T}{\partial X} = v\frac{\partial T}{\partial x}$, and follow the same procedure like the solid part, we get

$$T_i^{n+1} = T_i^n + \frac{\Delta t k_l}{\rho_l c_l}\left(\frac{T_{i+1}^n - 2T_i^n - T_{i-1}^n}{(\Delta x)^2}\right) - \Delta t v_i\left(\frac{T_{i+1}^n - T_{i-1}^n}{2\Delta x}\right) \ldots\ldots\ldots\ldots [4.39]$$

The mesh velocity can be defined for both the solid and liquid part as follows:

For the solid, $at\ x_i = 0, v_i = 0,\ v_{mesh} = v_{inter}\left(\frac{x_i}{x_{interface}}\right)$

For the liquid, at $x_i = x_{interface}, v_i = v_{interface\ and\ at\ x_i = x_m,\ v_m}$

$$v_{mesh} = v_{inter}\left(\frac{x_m - x_i}{x_m - x_{interface}}\right)$$

$$where,\ v_{int} = \frac{\frac{-k_l(T_i - T_{i+1})}{\Delta x} - \frac{-k_s(T_i - T_{i-1})}{\Delta x}}{\rho Q_L}$$

For exact solutions of 1D phase change process of semi-infinite slab within the moving mesh approach, exact temperature distributions of the solid and liquid are as follows [49]:

Temperature for the solid

$$T_S(x,t) = T_C + (T_F - T_C)\frac{\mathrm{erf}(x^*)}{\mathrm{erf}(x_{SL}^*)}, when\ 0 < x^* < x_{SL}^* \ldots\ldots\ldots\ldots\ldots\ldots [4.40a]$$

Temperature for the liquid

$$T_L(x,t) = T_i + (T_F - T_i)\frac{\mathrm{erfc}\left(\sqrt{\alpha_S/\alpha_L x^*}\right)}{\mathrm{erfc}\left(\sqrt{\alpha_S/\alpha_L x_{SL}^*}\right)}, when\ x_{SL}^* < x^* < \infty \ldots\ldots\ldots\ldots\ldots [4.40b]$$

Where, erf (.) and erfc (.) are the error and complementary error functions, respectively.

$where, x^* = x/2\sqrt{\alpha_S t}$, -is the dimensionless position and

$\alpha = \frac{k}{\rho c}, is\ the\ thermal\ diffusivity,$ Which are calculated from mechanical properties for both solid $\alpha_S\ and\ liquid\ \alpha_L$ values. The values of dimensionless position of solid – liquid interface x_{SL}^* are obtained from the nonlinear algebraic equation:

$$\frac{T_F - T_i}{T_F - T_C}\frac{k_S}{k_L}\sqrt{\frac{\alpha_S}{\alpha_L}}\frac{\exp(-\left(\frac{\alpha_S}{\alpha_L}\right)(x_{SL}^*)^2)}{erfc(\sqrt{\alpha_S/\alpha_L}x_{SL}^*)} + \frac{\exp(-(x_{SL}^*)^2)}{\mathrm{erf}(x_{SL}^*)} - \frac{\sqrt{\pi x_{SL}^* L}}{C_S(T_F - T_C)} = 0 \ldots [4.40c]$$

Where, T_F - the freezing temperature, and $T_i\ is\ the\ initial\ temperature\ of\ water$ $T_C, is\ the\ cold\ or\ refrigrant\ temperature$

The implicit method is unconditionally stable. But, it has less accuracy and the solution oscillates for large time steps. The implicit solution is stable for all grid size and time step which is no restriction on using grid size and time stem for the computation.

4.4 Ice Refrigeration Load Estimation

The heat load estimation is important, to design and select the refrigeration equipment and to size solar PV panel. To find the total heat load in the cooling unit, the total amount of heat removed from the system during a certain period of time can be determined. This includes the heat leakage through the wall, heat removal from water and the heat remove from ice storage material systems.

4.4.1 Ice Tank Transmission Load Estimation

The sensible heat gain through the surface of the storage tank wall, ceiling and floor can be calculate as follows:

$$\mathrm{Q_{trans}} = \mathrm{U}A_{ice}(\mathrm{T}_{outside} - \mathrm{T_{inside}}) \ldots\ldots\ldots\ldots\ldots\ldots\ldots\ldots\ldots\ldots\ldots\ldots\ldots\ldots\ldots\ldots\ldots\ldots\ldots\ldots\ldots [4.41]$$

$Where, \mathrm{Q_{trans}}$: Transmission cooling load and U: Overall heat transfer coefficient

$A_{ice} = 2(0.4 * 0.08) + 2(0.4 * 0.29) + 2(0.08 * 0.29) = 0.342m^2$:

This is the internal surface area of ice tank, then the external surface area can be calculate by including the thickness of the material and also 8mm gap between ice tank and insulation tank, the area becomes:

$A_{ice} = 2(0.44 * 0.136) + 2(0.44 * 0.352) + 2(0.136 * 0.352) = 0.5252m^2$:

Floor, wall and roof outside area of the storage tank (m^2). The two wall surface areas are equal and the top and floor surface areas are also equal.

$\mathrm{T_{outside}} = 37°\mathrm{C}$ and $\mathrm{T_{inside}} = -4°\mathrm{C}$: Outside and average inside water temperature.

The overall heat transfer coefficient of the surface U can be calculate as follows by the following equation:

$$U = \frac{1}{\frac{1}{h_i} + \frac{X}{k} + \frac{1}{h_o}} \quad \text{[4.42]}$$

Where,x: thickness of tank wall (m) $and\ h_o$: Outside surface conductance $\left(\frac{W}{m^2.k}\right)$

K: thermal conductivity $\left(\frac{W}{m.k}\right)$ $and\ h_i$: Inside surface conductance $\left(\frac{W}{m^2.k}\right)$

According to (ASHRAE, 2002) U factor for the flat parallel multi-surface can be calculate by using the following equation:

$$U = \frac{1}{\frac{x_1}{k_1} + \frac{x_2}{k_2} + \frac{x_3}{k_3}} \quad \text{[4.43]}$$

Including $h_i\ and\ h_o$: inside and outside surface conductance respectively, becomes:

$$U = \frac{1}{\frac{1}{h_i} + \frac{x_1}{k_1} + \frac{x_2}{k_2} + \frac{x_3}{k_3} + \frac{1}{h_o}} \quad \text{[4.44]}$$

Where $x_1, x_2\ and\ x_3$: are the thicknesses of the materials 1, 2 and 3 respectively.

$k_1, k_2\ and\ k_3$: are the thermal conductivity of the material 1, 2 and 3 respectively.

It is a very popular insulation material with available thickness of 10 to 15mm and density ranging from 35 to $50kg/m^3$ with 0.016 to 0.023 $w/m.k$ thermal conductivity. The material service temperature is in the range of $-180\ to\ 110°\mathrm{C}$ [40].

The water vapour barriers are required on the cold sides of the insulation like aluminum foils of minimum 0.06mm thickness [40].

The water storage tank materials are similar with milk storage tank materials and the specification can be taken from table [4.1]. In addition to these independent tank made from aluminum and 1mm thickness is needed for water storage.

Type of material	Thickness (m)	K (w/m.k)	h ($W/m^2.k$)
Plastic panel (inside)	0.003	0.22	5
Polyurethane expanded foam	0.015	0.023	
Aluminum sheet (outside)	0.002	237	30
Aluminum sheet (ice tank)	0.001	237	30

$$U = \frac{1}{\frac{1}{5} + \frac{0.003}{0.22} + \frac{0.015}{0.023} + \frac{0.002}{237} + \frac{1}{30}}$$

$$U = 1.112159 W/m^2.k$$

$\mathrm{Q_{trans}} = 1.112159 w/m^2.k * 0.5252 m^2 (37 - (-4))k$, during ice forming period:

$$\mathrm{Q_{trans}} = 24\mathrm{w}$$

$\mathrm{Q_{trans}} = 24\mathrm{w} * 8\mathrm{Hours} = 192\mathrm{Wh/day}$, within 8 hours of heat leakage during ice forming.

$$\mathrm{Q_{trans}} = 192\mathrm{Wh/day}$$

4.4.2 Ice Product Cooling Load Estimation

The total cooling load energy Q_{ice} needed to produce the required ice to be evacuated from water cooled down from approximately ambient temperature to 0℃ which is the phase change temperature of water and then cool down it to its final temperature, the equation is [5]. The equation includes sensible heat loss from 33℃ temperature of water to its freezing temperature of 0℃, latent heat loss at the phase change temperature and sensible heat loss from phase change temperature to its final temperature.

$$Q_{ice} = \left[cp_{water}\left(T_{water} - T_{fr}\right) + Q_L + cp_{ice}\left(T_{fr} - T_L\right)\right] m_{ice} \ldots\ldots\ldots\ldots\ldots\ldots [4.45]$$

Where, $cp_{water} = 4180 \frac{J}{kg.k}$ and $cp_{ice} = 2025 \frac{J}{kg.k}$, heat capacity of water and ice

$T_{water} = 33℃, T_{fr} = 0℃$ and $T_L = -4℃$: The initial, freezing and final temperature of water respectively.

$m_{ice} = 8.5kg$, Mass of ice and $Q_L = 333700\frac{J}{kg}$, The enthalpy to freeze water

$$Q_{ice} = [4.18\,kJ/kg.k(33-0)k + 333.7k\,J/kg + 2.025kJ/kg.k(0-(-4))k]8.5kg$$

$$Q_{ice} = 4{,}087kJ$$

$Q_{ice} = \frac{4{,}087\,kJ}{(4*3600)second} = 284W$, within four hours ice formation time period of PV panel.

$$Q_{ice} = 284W * 4hours = 1419Wh/day$$

4.4.3 Ice Tank Material Cooling Load Estimation

During the slab ice formation period the heat that needs to be removed from the storage tank material can be calculate by summing up of the heat removed by insulation material, aluminum sheet and plastic panel.

$$Q_{s,t\,cooling} = Q_{insulation} + Q_{AL} + Q_{plastic} \ldots\ldots\ldots\ldots\ldots\ldots\ldots\ldots\ldots\ldots [4.46]$$

The amount of heat removed from each material is given by the same formula as follows:

The amount of heat that needs to be removed from the insulation material polyurethane expanded foam can be calculate as follows:

$$Q_{insulation} = m_{insu} * cp_{insu} * (T_{air} - T_{ma}) \ldots\ldots\ldots\ldots\ldots\ldots\ldots\ldots\ldots [a]$$

Amount of heat that needs to be removed from aluminum sheet can be calculate as follows:

$$Q_{Al} = m_{Al} * cp_{Al} * (T_{air} - T_{ma}) \ldots\ldots\ldots\ldots\ldots\ldots\ldots\ldots\ldots\ldots\ldots [b]$$

Amount of heat that needs to be removed from plastic panel can be calculate as follows:

$$Q_{plastic} = m_{plastic} * cp_{plastic} * (T_{air} - T_{ma}) \ldots\ldots\ldots\ldots\ldots\ldots\ldots [c]$$

By substituting the above equations [a, b and c] in to equation [5.8] becomes:

$$Q_{s,t\,cooling} = (T_{air} - T_{ma})[(m_{insu} * cp_{insu}) + (m_{Al} * cp_{Al}) + (m_{plastic} * cp_{plastic})]$$

$$m_{material} = V_{material} * \rho_{material}\ and\ V_{material} = A_{s.t} * thichness_{material}$$

Then mass of the material becomes:

$$m_{material} = A_{s,t} * t_{material} * \rho_{material}$$

Table 4-2. Storage tank material size and properties

S.N	Material	Areas [m^2]	Thickness [m]	Density [kg/m^3]	Specific heat capacity [J/kg.k]
1	Polyurethane	0.5252	0.015	50	1045
2	Aluminum sheet	0.5252	0.002	2702	903
3	Plastic panel (pp)	0.5252	0.003	920	1900

Source: Incropera, Lenntech, wiley and [40]

$$Q_{s,t\ cooling} = (T_{air} - T_{ma}) * A_{s,t}[(th_{insu} * \rho_{insu} * cp_{insu}) + (th_{Al} * \rho_{Al} * cp_{Al}) + (th_{plas} * \rho_{plas} * cp_{plas})]$$

$$Q_{s,t\ cooling} = (37 - (-4))k * 0.5252m^2 \left[\left(0.015m * 50\frac{kg}{m^3} * 1045\frac{J}{kg.k}\right) + \left(0.002m * 2702\frac{kg}{m^3} * 903\frac{J}{kg.k}\right) + \left(0.003m * 920\frac{kg}{m^3} * 1900\frac{J}{kg.k}\right)\right]$$

$$Q_{S,t} = 235kJ$$

The temperature lowered from atmospheric temperature to ice final temperature within five hours. So cooling load due to the storage tank becomes:

$$Q_{cooling,S,t} = \frac{235kJ}{4 * 3600} = 16W$$

$$Q_{cooling,S,t} = 16\,W * 4hours = 64Wh/day$$

4.4.4 Infiltration Load

Infiltration load refers to the sensible and latent heat gain due to air flow into the refrigerated space during opening of the storage tank in order to loading and unloading the ice product. To load water or ice product needs a short period of time. Thus, the infiltration load is assumed to be negligible in the calculation of the total heat load system.

4.4.5 Factor of Safety

An additional or supplementary of 15% to 30% of ice freezing load can be incorporated to account as a safety factor [5].

$$Q_S = 30\%\left(Q_{ice} + Q_{s,t}\right) \quad \text{[4.47]}$$

$$Q_S = 0.3((1419 + 64)Wh/day)$$

$$Q_S = 431Wh/day$$

The total cooling load including the 2watt condenser fan will be:

$$Q_{total} = Q_{trasm} + Q_{ice} + Q_{s,t} + Q_S + Q_{cond\ fan} \dots\dots\dots\dots\dots\dots\dots\dots\dots\dots\dots\dots [4.48]$$

$$Q_{total} = 24W + 284W + 16W + 0.3 * (284 + 16)W + 2W$$

$$Q_{total} = 416W$$

$$Q_{total} = 192Wh/day + 1419Wh/day + 64Wh/day + 431Wh/day$$

$$Q_{total} = 2{,}107Wh/day$$

4.5 Estimate Solar Radiation of the Site

To estimate the solar radiation at the site, the monthly average daily solar radiation on a horizontal plan, The Longitude =41° E, Latitude = 11.8° N, Elevation = 433m these are from the collected solar data of Semera, Declination, sunset hour angle, the extraterrestrial radiation and clearness index must be first analyzed. After doing these and specifying the day of the considered month, from the monthly solar radiation on a horizontal surface we calculate the monthly average daily diffuse solar radiation.

Then, calculate the coefficients the ratio of hourly to daily total solar radiation and the ratio of hourly diffuse radiation to total diffuse radiation on horizontal surface in order to determine the hourly global solar radiation on a horizontal surface and the hourly diffuse solar radiation respectively. And these two hourly solar radiation are important to calculate the beam radiation.

Finally the global hourly solar radiation on a tilted surface can be calculate by using all hours of the considered day. This is determined by repeated from the sunrise to the sunset of the day, taking into account the change in the value of the solar hour angle throughout the day. The total daily solar radiation is obtained by summing all values of it [50].

4.5.1 Declination Angle

It is the angular position of the sun at solar noon relative to the plane of the equator. The approximate equation of the declination is as follows [50]:

$$\delta = 23.45 \sin\left(360 * \frac{284 + n}{365}\right) \dots\dots\dots\dots\dots\dots\dots\dots\dots\dots\dots\dots\dots\dots\dots\dots\dots [4.49]$$

$$Where, n: is\ the\ nth\ day\ of\ the\ year\ and\ \delta: is\ declination\ of\ the\ sun$$

Table 4-3. Recommended average day of month and value of n by month within a year.

Month	n for i^{th} Day of Month	I^{th} day of the month	Julian day of the year	Declination in degrees
January	*i*	17	17	-20.92
February	31 + *i*	16	47	-12.95
March	59 + *i*	16	75	-2.42
April	90 + *i*	15	105	9.41
May	120 + *i*	15	135	18.79
June	151 + *i*	11	162	23.09
July	181 + *i*	17	198	21.18
August	212 + *i*	16	228	13.45
September	243 + *i*	15	258	2.22
October	273 + *i*	15	288	-9.60
November	304 + *i*	14	318	-18.91
December	334 + *i*	10	344	-23.05

Source: [50]

4.5.2 Solar and Sunset Hour Angle

The solar hour angle is the angular displacement of the sun west or east of the local meridian and it becomes positive in morning time, zero at solar midday and negative in the afternoon time. It can be calculate by the following [50]:

$$\omega = 15°(T_{Local} - 12) \dots\dots\dots\dots\dots\dots\dots\dots\dots\dots\dots\dots\dots\dots\dots\dots\dots\dots [4.50]$$

Where, T_{Local}: is the local time

The sunset hour angle is the solar hour angle corsponding to time when the sun sets. It can be calculete by the following equation:

$$cos\omega_S = -tan\varphi tan\delta \dots\dots\dots\dots\dots\dots\dots\dots\dots\dots\dots\dots\dots\dots\dots\dots\dots\dots [4.51]$$

Where, φ, is the latitude of the site (Semera)

The day length or the maximum sunshine hours S_{max} can be calculate by converting the sunset hour andle in to hour, $1h = 15°$ and using the relation as follows [51]:

$$the\ day\ length, \qquad S_{max} = (2/15)\omega_s$$

4.5.3 Extrattersterial Radiation

Extraterrestrial radian is the solar radiation incident outside the earth's atmosphere. H_O, The Extraterrestrial radian is given by the following equation:

$$H_O = \frac{24G_{SC}}{\pi}\left(1 + 0.033COS\left(2\pi\frac{n}{365}\right)\right) * (cos\varphi\ cos\delta\ sin\omega_S + \omega_S sin\varphi\ sin\delta)..[4.52]$$

Where, $G_{SC} = 1367w/m^2$, solar constant

4.5.4 Clearness Index

The daily clearness index K_t is the solar radiation ratio at the surface of the earth to the extraterrestrial radiation.

$$\overline{K}_t = \frac{\overline{H}}{\overline{H}_O} \ldots\ldots\ldots\ldots\ldots\ldots\ldots\ldots\ldots\ldots\ldots\ldots [4.53]$$

$\overline{H}$: The monthly average daily solar radiation on the horizontal surface.

$\overline{H}_O$: The monthly of extraterrestrial daily solar radiation

4.5.5 Hourly Diffuse Solar Radiation Calculation

The monthly average daily diffuse solar radiation $\overline{H}_d$ is the scattered solar radiation reaching the earth's surface and can be calculate by using the monthly average daily global horizontal solar radiation $\overline{H}$ and $\overline{K}_t$ *is between* 0.3 *and* 0.8 as follows [52]

$$\frac{\overline{H}_d}{\overline{H}} = 1.391 - 3.560\overline{K}_t + 4.189\overline{K}_t^2 - 2.137\overline{K}_t^3 \ldots\ldots\ldots\ldots\ldots .[4.53a]$$

This is when the sunset hour angle ω_S is less than 81.4° and

$$\frac{\overline{H}_d}{\overline{H}} = 1.391 - 3.560\overline{K}_t + 4.189\overline{K}_t^2 - 2.137\overline{K}_t^3 \ldots\ldots\ldots\ldots\ldots .[4.53b]$$

This is when the sunset hour angle ω_S is greater than 81.4°

In addition to this, the ratio of total diffuse radiation to hourly diffuse radiation on a horizontal surface r_d can be calculate as follows:

$$r_d = \frac{\pi}{24}\frac{cos\omega - cos\omega_S}{sin\omega_S - \omega_S cos\omega_S} \ldots\ldots\ldots\ldots\ldots\ldots\ldots\ldots [4.54a]$$

By using this r_d each hour of average day, the diffuse radiation H_d becomes:

$$H_d = r_d \bar{H}_d \ldots\ldots\ldots\ldots\ldots\ldots\ldots\ldots\ldots\ldots\ldots\ldots\ldots\ldots\ldots\ldots\ldots\ldots\ldots\ldots\ldots\ldots\ldots\ldots [4.54b]$$

4.5.6 Hourly Horizontal Solar Radiation Calculation

The ratio of hourly to daily solar radiation r_t used to determine the hourly solar radiation on the horizontal surface daily distribution H. r_t Can be calculate as follows [50]:

$$r_t = \frac{\pi}{24}(a + b\cos\omega)\frac{\cos\omega - \cos\omega_S}{\sin\omega_S - \omega_S\cos\omega_S} \ldots\ldots\ldots\ldots\ldots\ldots\ldots\ldots\ldots\ldots\ldots\ldots [4.55a]$$

Where, $a = 0.409 + 0.5019\sin(\omega_S - \frac{\pi}{3})$ and $b = 0.6609 + 0.4767\sin(\omega_S - \frac{\pi}{3})$

Then, $H = r_t \bar{H} \ldots\ldots\ldots\ldots\ldots\ldots\ldots\ldots\ldots\ldots\ldots\ldots\ldots\ldots\ldots\ldots\ldots\ldots\ldots\ldots\ldots\ldots\ldots\ldots [4.55b]$

4.5.7 Hourly Beam Solar Radiation Calculation

The beam solar radiation or direct normal solar radiation H_b is the incident solar radiation that directly reaches the earth's surface without significantly scattered and coming from the direction of the sunlight [52].

$$H_b = H - H_d \ldots\ldots\ldots\ldots\ldots\ldots\ldots\ldots\ldots\ldots\ldots\ldots\ldots\ldots\ldots\ldots\ldots\ldots\ldots\ldots\ldots\ldots\ldots\ldots [4.56]$$

4.5.8 Hourly Solar Radiation Calculation on a Tilted PV Surface

The hourly solar radiation on the tilted solar PV surface can be determined as follows [53]:

$$H_t = H_b R_b + H_d R_d + H\rho\left(\frac{1 - \cos\beta}{2}\right) \ldots\ldots\ldots\ldots\ldots\ldots\ldots\ldots\ldots\ldots\ldots\ldots [4.57]$$

$Where,$ ρ: is the reflectivity of the surrounding where the PV panel is located and its value normally taken 0.2 for the reflectivity of grass or concrete.

$\beta = Latitude - declination$: is the inclination angle of the PV panel

R_d: ratio of diffuse solar radiation on to a tilted surface to that of the horizontal surface

From Liu and Jordan model

$$R_d = \frac{1 + \cos\beta}{2} \ldots\ldots\ldots\ldots\ldots\ldots\ldots\ldots\ldots\ldots\ldots\ldots\ldots\ldots\ldots\ldots\ldots\ldots\ldots\ldots\ldots\ldots\ldots\ldots [4.58]$$

R_b: represents the ratio of average day of the beam solar radiation on a tilted surface to that of a horizontal surface and can be expressed as follows:

$$R_b = \frac{\cos\left((\varphi-\beta)\frac{\pi}{180}\right)\cos\left(\delta\frac{\pi}{180}\right)\cos(\omega)+\sin\left((\varphi-\beta)\frac{\pi}{180}\right)\sin(\delta\frac{\pi}{180})}{\cos\left(\delta\frac{\pi}{180}\right)\cos(\omega)\cos\left(\varphi\frac{\pi}{180}\right)+sin(\delta\frac{\pi}{180})\sin\left(\varphi\frac{\pi}{180}\right)}. \quad [4.59]$$

4.5.9 Daily Tilted Solar Radiation Calculation

$\overline{H_t}$: is the daily total radiation and obtained by summing individual hours by using the formula for the daily solar radiation bellow:

$$\overline{H_t} = \sum_{t_{sunrise}}^{t_{sunset}} H_t(t), \qquad (t = hour) \ldots\ldots\ldots\ldots\ldots\ldots\ldots\ldots\ldots\ldots\ldots\ldots\ldots\ldots [4.60]$$

Where, $t_{sunrise}\ and\ t_{sunset}$: is the sun rises and sun set time respectively.

These are determine by the following relations:

$$t_{sunrise} = 12 - Eqt + \frac{\left(L-\omega_S\frac{180}{\pi}\right)}{15} \ldots\ldots\ldots\ldots\ldots\ldots\ldots\ldots\ldots\ldots\ldots\ldots\ldots [4.61a]$$

And

$$t_{sunset} = 12 - Eqt + \frac{\left(L+\omega_S\frac{180}{\pi}\right)}{15} \ldots\ldots\ldots\ldots\ldots\ldots\ldots\ldots\ldots\ldots\ldots\ldots\ldots [4.61b]$$

$Where, L$: is longitude and Eqt is the equation of time

The equation of time can be express by using an approximate formula in minutes, given as follows:

$$Eqt = \frac{\left(0.123\cos\left((j+87)\frac{\pi}{180}\right)-\sin\left(2(j+10)\frac{\pi}{180}\right)\right)}{60} \ldots\ldots\ldots\ldots\ldots\ldots\ldots\ldots [4.62]$$

Where, j is the day of the considered mouth.

4.6 Solar PV Module System Sizing

In order to size the appropriate PV module to drive a compressor having a cooling capacity of more than 416W, the total peak watt that the PV module produces, the total estimated daily cooling load which is $Q_{total} = 2{,}107Wh/day$ calculated above and the estimated average solar radiation of the site are needed.

4.6.1 Photovoltaic Panel Types and Material Selection Criteria

PV cells are made of semiconductor materials. The major types of materials are crystalline and thin films, which vary from each other in terms of light absorption efficiency, energy conversion efficiency, manufacturing technology and cost of production. Crystalline material also classified poly crystalline and mono- crystalline materials.

a. Single crystalline material

In the PV industry single-crystal or mono-crystalline silicon cells are the most common material. It has a uniform molecular structure and high uniformity results in higher energy conversion efficiency, compared to non-crystalline materials. The higher a PV cell's conversion efficiency, the more electricity it generates for a given area of exposure to the sunlight. The conversion efficiency for single-silicon commercial modules ranges between 15-20%. Not only are they energy efficient, single-silicon modules are highly reliable for outdoor power applications [34].

b. Poly crystalline material

Consisting of small grains of single-crystal silicon, polycrystalline PV cells are less energy efficient than single-crystalline silicon PV cells. The grain boundaries in polycrystalline silicon delay the flow of electrons and decrease the power output of the cell. The energy conversion efficiency for a commercial module made of polycrystalline silicon ranges between 10 to 14%. Compared to single-crystalline silicon, polycrystalline silicon material is stronger and can be cut into 1/3 thickness of single-crystal material. It also has slightly lower wafer cost and less strict growth requirements. However, its lower manufacturing cost is leads to lower cell efficiency. The average price for a polycrystalline module made from cast and ribbon is slightly lower than that of a single-crystal module [34].

c. Thin film material

In a thin-film PV cell, a thin semiconductor layer of PV materials is deposited on low-cost auxiliary layer such as glass, metal or plastic foil. Since thin-film materials have higher light absorptivity than crystalline materials, the deposited layer of PV materials is extremely thin. Thinner layers of material yield significant cost saving. Also, the deposition techniques in which PV materials are scattered directly onto glass or metal substrate are cheaper. So the manufacturing process is faster, using up less energy and mass production is made easier than the ingot-growth approach of crystalline silicon. However, thin film PV

cells suffer from poor cell conversion efficiency due to non-single crystal structure, requiring larger array areas and increasing area-related costs such as mountings. Efficiency is in the range of only 7–13 percent [34].

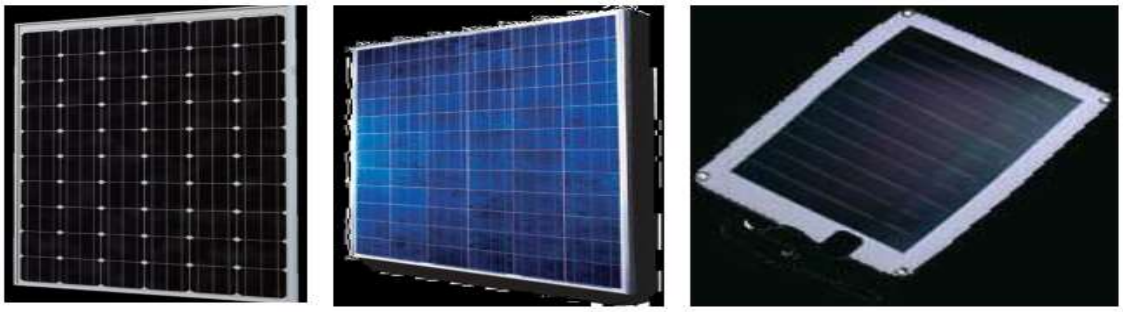

a. Mono-crystalline, b. poly crystalline c. amorphous or thin film panel

Figure 4-15. Different types of Solar Modules [source, [17]]

For this research mono-crystalline PV panel was selected due to its uniform molecular structure and high uniformity results in higher energy conversion efficiency, this leads to generate more electricity for a given area of exposure to the sunlight. And also it is highly reliable for outdoor power applications. The 220W, AS-6M24 PV panel was selected and the characteristics given by the manufacturer are list bellow in table 4.4. The manufacturer is worldwide energy and manufacturing USA Co. Ltd. Amerisolar.

Table 4-4. Electrical, mechanical and temperature characteristics of AS-6M24 PV at STC.

Electrical characteristics of AS-6M24 solar panel at STC (standard test condition**)**							
Nominal power (P_{max})	190W	195W	200W	105W	210W	215W	220W
Open circuit voltage (V_{OC})	30.2V	30.3V	30.4V	30.5V	30.6V	30.7V	30.8V
Short circuit current (I_{SC})	8.45A	8.58A	8.70A	8.82A	8.94A	9.05A	9.17A
Voltage at nominal power (V_{mp})	24.2V	24.3V	24.5V	24.6V	24.7V	24.8V	24.9V
Current at nominal power (I_{mp})	7.82A	8.0A	8.17A	8.34A	8.51A	8.67A	8.84A
Module efficiency (%)	14.55	14.94	15.32	15.70	16.09	16.47	16.85

Operating temperature	-40℃ to +85℃
Maximum system voltage	1000V DC
Maximum series fuse rating	15A
STC: Irradiance = $1000 W/m^2$, Cell temperature = 25℃ and AM (air mass) = 1.5	
Mechanical characteristics of AS-6M24 solar panel at STC	
Cell type	Mon crystalline 156x156mm
Number of cells	48(6x8)
Dimension of panel module	1316x992x35mm
Weight	15kg
Front cover	3.2mm low iron tempered glass with AR (anti-reflection) coating
Frame	Anodized aluminum alloy
Temperature characteristics of AS-6M24 solar panel at STC	
Nominal operating Cell temperature (NOCT)	45℃ ± 2℃
Temperature coefficient of (P_{max})	-0.43%/℃
Temperature coefficient of (V_{OC})	-0.33%/℃
Temperature coefficient of (I_{SC})	-0.056%/℃

Source: Amerisolar

Mono-crystalline photovoltaic module with 220W peak is selected for this slab ice formation design system from manufacturer.

4.6.2 Calculate the Total Power Demand and the Number of PV Panels

To calculate the size of the PV panel, first we calculate the total area in order to determine the total peak watt. The area of the PV panel can be determined by using the following equation [26] [54]:

$$PV_{Area} = \frac{total\ daily\ estimated\ energy\ demand}{G_{av} * \eta_{pv} * TCF} \ldots\ldots\ldots\ldots\ldots [4.63]$$

Where, $Q_{cooling\ load} = 2{,}107Wh/day$: total daily estimated demand

$G_{av} = 5kWh/m^2/day$: Average solar energy input per day

$\eta_{pv} = 16.85\%$: Module efficiency at reference temperature and insolation of 1kW/m^2 and taken from the manufacturer specification.

TCF: temperature correction factor, the temperature correction for maximum power

$$TCF = 1 - [\beta_{ref}(T_{cell} - T_{STC})]$$

Where, $\beta_{ref} = -0.43\%$ ℃: the temperature coefficient at maximum power STC

(Values taken from the manufacturer for mono − crystalline modules).

$T_{STC} = 25$℃: cell temperature at standard test condition given by the manufacturer.

T_{cell}: $cell\ temperature\ \ at\ cell\ operating\ temperature\ T_C$ [℃]

$$T_{cell} = T_{air} + \frac{NOCT - 20}{800} * G_{SC}$$

Where, $G_{SC} = 1000w/m^2$: $Solarradiation, taken\ from\ PV\ manufacturer.$

$T_{air} = 37$℃: Ambient temperature [℃]

$NOCT = 45$℃: Nominal operating cell temperature provided by the mono − crystalline PV manufacturer.

$$T_{cell} = 37℃ + \frac{45℃ - 20}{800} * 1000w/m^2 = 68℃$$

$$TCF = 1 - [0.0043(68℃ - 25℃)] = 0.8151$$

$$PV_{Area} = \frac{2.107\text{kWh/day}}{5kw\ h/m^2/day * 0.1685 * 0.8151} = \frac{2{,}035m\text{^}2}{0.687} = 3m^2$$

To determine the peak power output from the total PV module we use the following equation:

$$PV_{peak\ power} = PV_{Area} * \eta_{pv} * PSI$$

Where, PSI = $1000W/m^2$: PV peak power at the earth surface at peak solar intensity

$\eta_{pv} = 0.1685$: PV efficiency from manufacturer of selected mono crystalline module

$$PV_{peak\ power} = 3m^2 * 0.1685 * 1000W/m^2 = 500w$$

The output power of a single PV panel can be express as follows:

$$max.power\ of\ each\ panel = 220w$$

The number of PV module for the system, can be express by using the following equation:

$$NO\ of\ PV\ panels = \frac{pv_{\ peak\ power}}{max.power\ of\ each\ panel} \ldots\ldots\ldots\ldots\ldots\ldots\ldots\ldots [4.64]$$

$$NO\ of\ PV\ panels = \frac{500W}{220} = 2.3 = 3$$

CHAPTER FIVE

5. REFRIGERATOR COMPONENT SELECTION AND DESIGN

5.1 Introduction

This chapter explains about the refrigerator compressor selection which are compressor, condenser, evaporator and capillary tube, refrigeration system design and arrangements.

5.2 DC Compressor Selection

The DC compressor is used to increase the pressure and circulate the refrigerant in the refrigeration system. A compressor of refrigerator is a combination of mechanical compression part and an electrical motor. The electrical motor converts electrical energy to mechanical energy in a refrigeration compressor.

The selection of DC compressor depends on its less contribution to the greenhouse effect and its smooth start up ability during low availability of solar PV power mainly for solar PV powered compressor. For this specific application DC compressor is selected due to its ability to connect directly with PV panel without an external control system like invertor and capacitor or starting battery. This DC compressor is equipped with an adaptive energy optimizer control used to speed up the compressor from minimum to maximum speed during starting. This DC compressor can an ability to stop rotation when the PV panel cannot deliver sufficient power and try to start again at low speed and increases slowly, if the panel will starts power generating.

The selection of this refrigerator DC compressor size depends on the amount of cooling load required to produce enough ice to replace the heat absorbed by cold milk during night time in order to keep its temperature 4℃ within fourteen hours. The total cooling load which is $Q_{cooling} = 416\, watt$ in order to form slab ice and to keep the required milk effectively within the required time should be less than the selected compressor cooling capacity. CASCADE17-0244Y3 model, which is Masterflux Company product variable speed DC (VSDC), high back pressure is selected for the system as it has high cooling capacity of 618 Watt at -7℃ evaporator temperature which is greater than from the total cooling load of this system.

5.2.1 Technical Data Sheet of CASCADE17-0244Y3 VSDC Compressor and Control Unit

The CASCADE17-0244Y3 model compressor is ideally fit for PV powered stationary and movable applications. It has the voltage of 12, 24 or 48V DC power supply and the used refrigerant type of R-134a. This type of compressor is applicable for commercial refrigeration for foods and beverages, make and store ice and ac system. It is applicable for evaporator temperature range of -40℃ to 15℃ and condenser temperature range of 26.7℃ to 65.6℃. These compressor and control unit have the total weight of 6.67kg.

The feature of the control unit are 4-poles sensor-less/brushless variable speed BLDC motor controller,1.0-4.75V analog speed set input (resistor programmable for fixed speed) and the rpm range is 1800-4200.

All three tables bellow are shows that the performance of CASCADE17-0244Y3 compressor for different evaporating temperature at-ARI HBP test condition at 35℃ ambient temperature, 18.33℃ suction temperature, 8.33℃ sub-cooling and condenser temperature of 54.4℃. For all three tables the source is Masterflux.

Table 5-1. Compressor cooling capacity (W) for 24V at ARI -HBP test condition

	Evaporator temperature ℃						
RPM	−7℃	−1℃	2℃	4℃	7℃	10℃	13℃
1800	114	162	188	214	240	267	294
2400	158	219	250	283	316	350	384
3000	218	287	324	362	400	440	479
3600	273	350	391	432	475	519	563
4200	308	389	433	477	523	570	**618**

Source: Masterflux

Table 5-2 Compressor power consumption (W) for (24V) at ARI -HBP test condition

	Evaporator temperature ℃						
RPM	−7℃	−1℃	2℃	4℃	7℃	10℃	13℃
1800	83	92	97	101	106	110	114
2400	105	115	121	126	131	136	142
3000	129	143	150	157	165	173	181
3600	155	174	184	195	206	218	230
4200	181	209	224	239	255	272	290

Source: Masterflux

Table 5-3: Compressor Current consumption (Amp) for (24V) at ARI -HBP test condition

	Evaporator temperature ℃						
RPM	−7℃	−1℃	2℃	4℃	7℃	10℃	13℃
1800	3.45	3.85	4.04	4.22	4.40	4.57	4.73
2400	4.37	4.81	5.02	5.24	5.46	5.68	5.91
3000	5.38	5.94	6.24	6.54	6.86	7.19	7.54
3600	6.44	7.24	7.67	8.12	8.59	9.08	9.59
4200	7.56	8.70	9.32	9.96	10.63	11.33	12.07

Source: Masterflux

Table 5-4: CASCADE17-0244Y3 Compressor optional fixed resistor speed table

Resistor value(OHMS)	Motor speed(RPM)	Resistor (OHMS)	Motor speed (RPM)
200	1800	1090	3000
242	1900	1.4k	3200
287	2000	1.88k	3400
388	2200	2.58k	3600
510	2400	3.8k	3800
659	2600	6.36k	4000
847	2800	15.3k	4200

Master-flux Company provided more flexible performance equation shown below in terms of Y, which is the performance characteristics like refrigerant mass flow rate, cooling capacity, current consumption, power consumption of the (24V) CASCADE17-0244Y3 compressor at ARI HBP test condition (source Master flux).

$$Y = C_1 + C_2X_1 + C_3X_1^2 + C_4X_1^3 + C_5X_2 + C_6X_2^2 + C_7X_2^3 + C_8X_3 + C_9X_3^2 + C_{10}X_3^3 + C_{11}X_1X_2X_3 + C_{12}X_1^2X_2X_3 + C_{13}X_1X_2^2X_3 + C_{14}X_1X_2X_3^2 + C_{15}X_1X_2 + C_{16}X_1X_3 + C_{17}X_2X_3 + C_{18}X_1^2X_2 + C_{19}X_1X_2^2 + C_{20}X_1^2X_3 + C_{21}X_1X_3^2 + C_{22}X_2^2X_3 + C_{23}X_2X_3^2 \dots\dots, \dots\dots\dots\dots\dots\dots\dots\dots\dots\dots\dots\dots\dots\dots [5.1]$$

$X_1 =$ RPM and $X_2 =$ Evaporator temperature in degree Fahrenheit

$X_3 =$ Condenser temperature in degree Fahrenheit

$C_1 - C_{23}$: The performance coefficient of 24V CASCADE17-0244Y3 compressor like refrigerant mass flow rate, cooling capacity, current consumption, power consumption.

5.2.2 Evaporator and Condenser Temperature Selection

Based on the collected Metrological data the ambient temperature of Semera reaches 43℃. So that for this research refrigerator condenser must operate at a temperature greater than this value in order to release heat to the surrounding. So it will be appropriate to fix the condenser temperature to 49℃, which results 6℃ minimum temperature difference between the ambient and the operating temperature of the condenser.

For this system the selected compressor is applicable with maximum operating temperature of evaporator -7℃. Ice formation takes place below 0℃ temperature. From table 5.1 manufacturer specification the cooling capacity at 1800rpm is 294watt and at 4200rpm is 618watt with evaporator temperature of 13℃ and -7℃ evaporator temperature the cooling capacity is 308 watt. Thus, the total cooling load of the study is between these values which is 416w. Thus, possible minimum operating temperature of evaporator becomes -7℃. By using -7℃ and 49℃ evaporator and condenser operating temperature respectively and ideal vapour compression refrigeration system, R-134a refrigerant properties can be taken from saturated liquid and saturated vapour tables of R-134a.

Table 5-5: properties of R-134a with −7℃ evaporator temperature at state one

Properties	Liquid form	Vapour form	Mixed form
Enthalpy	$(h_{f1})\ 42.52\frac{kJ}{kg.k}$	$(h_{g1})\ 246.3kJ/kg$	$(h_{fg1})\ 203.8kJ/kg$
Entropy	$(S_{f1})0.16994\frac{kJ}{kg.k}$	$(S_{g1})\ 0.93549\frac{kJ}{kg.k}$	$(S_{fg1})\ 0.76569\frac{kJ}{kg.k}$
Pressure $P_1 = P_4$	225.76kpa		
Specific volume	$0.00075895\ m^3/kg$	$0.089077\ m^3/kg$	

For ideal case $S_1 = S_2 = 0.93549kJ/kg.k$

Then, by using entropy at condenser inlet and condenser temperature 49℃ from R-134a refrigerant superheated table the enthalpy is:

$$\left.\begin{matrix} T_2 = 49℃ \\ S_2 = 0.93549kJ/kg.k \end{matrix}\right\}, h_2 = 281.6kJ/kg\ and\ P_2 = P_3 = 1000kpa$$

At the inlet of expansion device by using the pressure P_3 and from R-134a refrigerant saturated liquid pressure table, the enthalpy at this system can be taken.

$$\left.\begin{matrix} P_3 = 1000kpa \\ Saturated\ liquid \end{matrix}\right\}, h_3 = h_{f3} = h_4 = 107.32kJ/kg\ and\ T_3 = 39.37℃, S_{f2} = 0.39189kJ/kg.k$$

For ideal case, $X_1 = 1(saturated\ vapour), X_3 = 0(saturated\ liquid)$

$$X_4 = \frac{h_4 - h_{f1}}{h_{fg1}} = \frac{107.32kJ/kg - 42.52kJ/kg}{203.8kJ/kg} = 0.32$$

5.2.3 Refrigerator Evaporator Equipment Selection and Design

The principal purpose of the evaporator is to remove heat from the refrigerated space and to maintain humidity by turning the liquid form of the refrigerant into its gaseous form by

vaporizing it. The evaporator tube was selected as Copper Tube Evaporators with Standard ASTM B301-145.

Table 5-6: Technical specification of the selected evaporator Copper tube

S,N	Material	Outer diameter	Wall thickness	Inside diameter	Thermal conductivity at (-7℃)
1	Copper	7mm	1mm	5mm	385W/m k
2	Standard name ASTM B301-145				

Heat Extracted by evaporator:

$$Q_E = m_r * (h_1 - h_4) \dots\dots\dots\dots\dots\dots\dots\dots\dots\dots\dots\dots\dots\dots\dots\dots\dots\dots\dots\dots [5.2]$$

Mass flow rate of refrigerant R-134a m_r can be calculate as follows:

$$m_r = \frac{Q_E}{(h_1 - h_4)} = \frac{0.416kw}{246.3kJ/kg - 107.32\ kJ/kg} = 0.002993kg/s$$

Q_{Evapo} Can also be calculate by using the total area of evaporator tube, the overall heat transfer coefficient and the logarithmic mean temperature difference in order to design the length of the evaporator tube from its area.

$$Q_e = U_e A_e * (T_{water} - T_e) \dots\dots\dots\dots\dots\dots\dots\dots\dots\dots\dots\dots\dots\dots\dots\dots\dots [5.3]$$

Where, Inlet temperature of water inside the water storage tank, $T_{water} = 33℃$

Evaporator temperature, ($T_e = -7$)

$$T_{water} - T_e = 33℃ - (-7℃) = 40℃$$

The overall heat transfer coefficient U_e can be express by summing up of convective heat transfer from water to slab ice outside surface, conduction heat transfer from outside ice surface to inside ice surface, conduction heat transfer from outside surface of tube to inside surface and convective heat transfer from inside tube to refrigerant.

The overall heat transfer coefficient of the system can be calculate as follows:

$$\frac{1}{U_e A_e} = \frac{1}{h_{water} A_{O,ice}} + \frac{X_{ice}}{K_{ice} A_{m,ice}} + \frac{X_{pipe}}{K_{Al} A_{mE}} + \frac{1}{h_r A_{iE}} \dots\dots\dots\dots\dots\dots\dots\dots [5.4]$$

Considering the inside tube area only and conduction heat transfer from outside surface of tube to inside surface and convective heat transfer from inside tube to refrigerant.

$$\frac{1}{U_{e\,i}} = \frac{X_{pipe} * A_{iE}}{K_{Al}(A_{iE} + A_{OE})/2} + \frac{1}{h_r} = \frac{X_{pipe} * L_E * \pi(D_{iE)}}{K_{Al}(L_E * \pi(D_{iE} + D_{OE}))/2} + \frac{1}{h_r}$$

$$\frac{1}{U_{e,i1}} = \frac{X_{pipe}(D_{iE)}}{K_{Al}(D_{iE} + D_{OE})/2} + \frac{1}{h_r} \ldots\ldots\ldots\ldots\ldots\ldots\ldots\ldots\ldots\ldots\ldots\ldots\ldots\ldots\ldots\ldots\ldots\ldots\ldots\ldots [5.5]$$

Considering convective heat transfer from water to the slab ice outside surface, conduction heat transfer from outside ice surface to the inside ice surface.

$$A_{o,ice} = A_{m,ice} = length * width\ of\ ice\ tank$$

$$\frac{1}{U_{e,i2}} = \frac{1}{h_{water}} + \frac{X_{ice}}{K_{ice}} \ldots\ldots\ldots\ldots\ldots\ldots\ldots\ldots\ldots\ldots\ldots\ldots\ldots\ldots\ldots\ldots\ldots\ldots\ldots\ldots [5.6]$$

$$U_{e,total} = U_{e,i1} + U_{e,i2} \ldots\ldots\ldots\ldots\ldots\ldots\ldots\ldots\ldots\ldots\ldots\ldots\ldots\ldots\ldots\ldots\ldots\ldots\ldots\ldots [5.7]$$

Where, $D_{OE}\ and\ D_{iE}$: outside and inside diameter of the evaporator pipe respectively.

$A_{OE},\ A_{iE}\ and\ A_{mE}$: Outside, inside and mean areas of the evaporator pipe respectively.

$X_{pipe}\ and\ X_{ice}$: is thickness of pipe and average ice respectively

$K_{Al} = 237\ and\ K_{ice} = 1.95$: - is thermal conductivity of aluminum pipe and ice respectively

h_r: The convective heat transfer coefficient on the refrigerant side and can be calculate depending on the flow type which are turbulent or laminar flow as follows [16]:

$$h_r = \frac{N_u * k_{mean,ref}}{2 * r_{iE}} \ldots\ldots\ldots\ldots\ldots\ldots\ldots\ldots\ldots\ldots\ldots\ldots\ldots\ldots\ldots\ldots\ldots\ldots\ldots\ldots [5.8]$$

$$k_{mean,ref}\ is\ conductive\ heat\ transfer\ coefficient\ of\ the\ refrigerant$$

$$r_{iE}\ is\ the\ inside\ diameter\ of\ the\ refrigerant\ pipe$$

The Nusselt number $N_{u,}$ depends on the Reynolds number R_e, and can be expressed as:

$$R_e = \frac{2 * \dot{m}_{ref}}{\pi * N_p * r_{iE} * \mu_{mean,ref}} \ldots\ldots\ldots\ldots\ldots\ldots\ldots\ldots\ldots\ldots\ldots\ldots\ldots\ldots\ldots\ldots\ldots [3.9]$$

$\dot{m}_{ref}$ *ie the refrigerant mass flowrate and* N_p *is number of tubes*

$\mu_{mean,ref}$ *is dynamic viscosity of refrigerant*

Table 5-7: Thermophysical properties of saturated liquid R -134a at evaporator temperature −7℃

S.N	Thermal conductivity	Dynamic viscosity	Density	Specific heat capacity	Pr, Prandtl number
1	$0.0952 W/m.k$	0.00029314 $N.s/m^2$	1317.9kg/m^3	1.323 $\frac{kJ}{kg.k}$	4.08

Source: Frank P. Incropera

Table 5-8: Thermophysical properties of saturated vapour R 134a at evaporator temperature −7℃

S.N	Thermal conductivity	Dynamic viscosity	Density	Specific heat capacity	Pr, Prandtl number
1	0.010665$W/m.k$	0.00001033 $N.s/m^2$	10.047 kg/m^3	0.8115 $\frac{kJ}{kg.k}$	

Source: ASHRAE Fundamentals Handbook, 2005

$$V_{mean} = \frac{\dot{V}_{refr}}{A_c}, \ and \qquad \dot{V}_{refr} = \frac{\dot{m}}{\rho_{mean,refr}}$$

A_c: is the cross sectional area of evaporator tube

$$A_c = \frac{1}{4}\pi D_{iE}^2 = \frac{1}{4} * 3.14 * (0.005m)^2 = 0.00001963m^2$$

$where, \dot{V}_{refr}$: is the volume flowrate of refrigerant fluid

Mean Dynamic viscosity can be calculate as follows:

Dynamic viscosity of saturated vapour R-134a, at evaporator temperature is equal to [55]:

$$\mu_{vapor} = \mu_{wall} = 0.00001033\ N.s/m^2$$

Dynamic viscosity of saturated liquid R-134a, when entering into the evaporator [55]:

$$\mu_{inlet} = x * \mu_{vapor} + (1 - x)\mu_{liquid}$$

$$\mu_{inlet} = 0.32 * 0.00001033 N.s/m^2 + (1 - 0.32)0.00029314\ N.s/m^2$$

$$\mu_{inlet} = 0.0002026 N.s/m^2$$

Dynamic viscosity of saturated vapour R-134a, leaving the evaporator [55]:

$$\mu_{outlet} = \mu_{vapor} = 0.00001033\ N.s/m^2$$

$$\mu_{mean} = \frac{\mu_{outlet} + \mu_{inlet}}{2} = \frac{0.00001033\ N.s/m^2 + 0.0002026 N.s/m^2}{2}$$
$$= 0.00010649 N.s/m^2$$

Mean density can be calculate as follows:

Density of saturated liquid R-134a, when entering into the evaporator:

$$\rho_{inlet} = x * \rho_{vapor} + (1 - x)\rho_{liquid}$$

$$\rho_{inlet} = 0.32 * 10.047\ \text{kg}/m^3 + (1 - 0.32)1317.9 kg/m^3$$

$$\rho_{inlet} = 900\ \text{kg}/m^3$$

Density of saturated vapour R-134a, leaving the evaporator:

$$\rho_{outlet} = \rho_{vapor} = 10.047\ \text{kg}/m^3$$

$$\rho_{mean} = \frac{\rho_{outlet} + \rho_{inlet}}{2} = \frac{10.047\ \text{kg}/m^3 + 900\ \text{kg}/m^3}{2} = 455\ \text{kg}/m^3$$

$$\dot{V}_{refr} = \frac{\dot{m}}{\rho_{mean,refr}} = \frac{0.002993 kg/s}{455\ \text{kg}/m^3} = 0.0000065776 m^3/s$$

Then, the mean velocity of the refrigerant fluid will be as follows:

$$V_{mean} = \frac{0.0000065776 m^3/s}{0.00001963 m^2} = 0.34 m/s$$

Mean thermal conductivity can be calculate as follows:

Thermal conductivity of saturated liquid R-134a, when entering into the evaporator:

$$k_{inlet} = x * k_{vapor} + (1 - x)k_{liquid}$$

$$k_{inlet} = 0.32 * 0.010665W/m.k + (1 - 0.32)0.0952W/m.k$$

$$k_{inlet} = 0.06815W/m.k$$

Thermal conductivity of saturated vapour R-134a, leaving the evaporator:

$$k_{outlet} = k_{vapor} = 0.010665W/m.k$$

$$k_{mean} = \frac{k_{outlet} + k_{inlet}}{2} = \frac{0.010665W/m.k + 0.06815W/m.k}{2} = 0.03941W/m.k$$

Mean specific heat capacity can be calculate as follows:

Thermal conductivity of saturated liquid R-134a, when entering into the evaporator:

$$Cp_{inlet} = x * Cp_{vapor} + (1 - x)Cp_{liquid}$$

$$Cp_{inlet} = 0.32 * 0.8115 \text{ kJ}//kg.k + (1 - 0.32)1.323\text{kJ}//kg.k$$

$$Cp_{inlet} = 1.15932 \text{ kJ}//kg.k$$

Thermal conductivity of saturated vapour R-134a, leaving the evaporator:

$$Cp_{outlet} = Cp_{vapor} = 0.8115 \text{ kJ}//kg.k$$

$$Cp_{mean} = \frac{Cp_{outlet} + Cp_{inlet}}{2} = \frac{0.8115 \text{ kJ}//kg.k + 1.15932\text{kJ}//kg.k}{2}$$
$$= 0.9854\text{kJ}//kg.k$$

The Nusselt number $N_{u,}$ depends on the Reynolds number R_e, and the Reynold number can be calculate as follows by guessing initial number of pipes and iterating, final value becomes 26:

$$R_e = \frac{2 * 0.002993}{\pi * 26 * 0.005 * 0.00010649} = 138$$

For laminar flow, when $R_e < 3200$, the nusselt number N_u is

$$N_u = 3.66 \ldots\ldots\ldots\ldots\ldots\ldots\ldots\ldots\ldots\ldots\ldots\ldots\ldots\ldots\ldots\ldots\ldots\ldots\ldots. [a]$$

For the flow, $3000 \leq R_e \leq 5 * 10^6$, the nusselt number N_u is

$$N_u = \frac{\frac{f}{8} * (R_e - 1000) * P_r}{1 + 12.7 * \left(\frac{f}{8}\right)^{0.5} (P_r^{\frac{2}{3}} - 1)}, 3000 \leq R_e \leq 5 * 10^6 \ldots\ldots\ldots\ldots [b]$$

$f, is\ the\ Darcy\ friction\ factor\ and\ can\ be\ expressed$:

$$f = ((0.79 * \log(R_e)) - 1.64^{-2} \ldots\ldots\ldots\ldots\ldots\ldots\ldots\ldots\ldots\ldots\ldots\ldots [c]$$

$P_r,\ is\ the\ prantel\ number\ and\ can\ be\ expressed$:

$$P_r = \mathrm{Pr}_{mean} = \frac{Cp_{mean} * \mu_{mean}}{K_{mean}} \ldots\ldots\ldots\ldots\ldots\ldots\ldots\ldots\ldots\ldots [d]$$

For turbulent flow when, $R_e \geq 5 * 10^6$, the nusselt number N_u is

$$N_u = 0.023 * {R_e}^{0.8} * {P_r}^{0.3} \ldots\ldots\ldots\ldots\ldots\ldots\ldots\ldots\ldots\ldots [e]$$

$$h_r = \frac{3.66 * 0.03941 W/m.k}{2 * 0.005m} = 15 W/m^2.k$$

$$\frac{1}{U_{e,i1}} = \frac{0.001m * 0.005m}{237 W/m.k(0.005m + 0.007m)/2} + \frac{1}{15 W/m^2 k}$$

$$\frac{1}{U_{e,i1}} = 0.00000351617 + 0.06933$$

$$U_{e,i1} = 15 w/m^2 k$$

$$\frac{1}{U_{e,i2}} = \frac{1}{81.2 w/m^2 k} + \frac{0.02m}{1.95 W/mk} = 44 w/m^2 k$$

Total overall heat transfer coefficient becomes, $59 w/m^2 k$

$$A_e = \frac{Q_e}{U_e * LMTD} = \frac{416 w}{40k * 59 w/m^2 k} = 0.176 m^2$$

$$A_e = \pi D_E L_e, from\ this\ L_{Evapo} = \frac{A_e}{\pi D_{iE}}$$

$$L_e = \frac{0.176 m^2}{3.14 * 0.005m} = 11m$$

The number of Evaporator tubes by considering the ice storage tank length and width 0.4x0.08x0.29m becomes:

$$N_E = \frac{L_{EVAPO}}{0.4m} = \frac{11m}{0.4} = 26$$

The evaporators are assembled on the two sides of the ice tank having 5.5m with 13 numbers of tubes on each side.

5.2.4 Refrigerator Condenser Equipment Selection and Design

The main function of forced air cooled condenser is to reject heat that is absorbed by the evaporator and that from the compressor by condensing refrigerant from its gaseous to its liquid state, by cooling it. 8mm steel tube condenser with standard GB/T 24187-2009 was selected with no coated low – carbon welded steel pipe manufactured by Changzhou city, Jiangsu.

Table 5-9: Technical specification of the selected condenser LC Steel tube

S,N	Material	Outer diameter	Wall thickness	Inside diameter	Thermal conductivity
1	LC steel	8mm	0.6 – 1mm=0.6mm	6.8mm	45w/m.k
2	Standard name - GB/T 24187-2009				

Source: Wushun

Heat rejected by condenser

$$Q_{Cond} = m_r(h_2 - h_3) \dots \dots \dots \dots \dots \dots \dots \dots \dots \dots \dots \dots \dots \dots \dots \dots \dots \dots \dots \dots \dots [5.10]$$

$$Q_{Cond} = 0.002993kg/s(281.6kJ/kg - 107.32kJ/kg) = 520w$$

Q_{Cond} Can also be calculate by using the total area of condenser tube, the overall heat transfer coefficient and the logarithmic mean temperature difference in order to design the length of the condenser tube from its area.

$$Q_{Cond} = UA_{Cond} * LMTD \dots \dots \dots \dots \dots \dots \dots \dots \dots \dots \dots \dots \dots \dots \dots . \dots \dots \dots [5.11]$$

Where, LMTD: Logarithmic Mean Temperature Difference

$$LMTD = \frac{\Delta T_1 - \Delta T_2}{\ln(\Delta T_1/\Delta T_2)} \dots\dots\dots\dots\dots\dots\dots\dots\dots\dots\dots\dots\dots\dots\dots\dots\dots\dots\dots\dots\dots\dots\dots\dots [5.12]$$

For forced air cooled temperature condenser:

Average air inlet temperature $T_{ia} = 37℃$

Condenser air outlet temperature $T_{oa} = 39$

Maximum condensing temperature ($T_{CondM} = 65.6℃$)

$$\Delta T_1 = T_{Cond} - T_{ia} = 55℃ - 37℃ = 28.6℃\,, \qquad and$$

$$\Delta T_2 = T_{Oa} - T_{ia} = 39℃ - 37℃ = 2℃$$

$$LMTD = \frac{28.6 - 2}{ln(28.6/2)} = 10℃$$

Equation [5.30] also express by summing up of convective heat transfer from air to outside surface of the tube, conduction heat transfer from outside tube to inside of the tube and convective heat transfer from inside tube to refrigerant.

The overall heat transfer coefficient of the system can be calculate as follows:

$$\frac{1}{UA_{Cond}} = \frac{1}{h_a A_{OCond}} + \frac{X_{th}}{K_{steel} A_{mCond}} + \frac{1}{h_r A_{iCond}} \dots\dots\dots\dots\dots\dots\dots\dots\dots\dots\dots\dots [5.13]$$

Considering the inside tube area only:

$$\frac{1}{U_i} = \frac{A_{iCond}}{h_a A_{OCond}} + \frac{X_{th} * A_{iCond}}{K_{steel}(A_{iCond} + A_{OCond})/2} + \frac{1}{h_r}$$

$$\frac{1}{U_i} = \frac{\pi D_{iCond} * L_{CON}}{h_a * \pi D_{OCond} * L_{CON}} + \frac{X_{th} * L_{CON} * \pi(D_{iCond})}{K_{steel}(L_{CON} * \pi(D_{iCond} + D_{OCond}))/2} + \frac{1}{h_r}$$

$$\frac{1}{U_i} = \frac{D_{iCond}}{h_a * D_{OCond}} + \frac{X_{th}(D_{iCond})}{K_{steel}(D_{iCond} + D_{OCond})/2} + \frac{1}{h_r} \dots\dots\dots\dots\dots\dots\dots\dots\dots\dots\dots\dots [5.14]$$

Where, $D_{OCond}\ and\ D_{iCond}$: outside and inside diameter of the condenser pipe respectively.

A_{OCond}, $A_{iCond}\ and\ A_{mCond}$: Outside, inside and mean areas of the condenser pipe respectively.

X_{th}: is thickness of pipe and K_{Steel} is thermal conductivity of steel pipe.

h_r: The convective heat transfer coefficient of the refrigerant inside the tube and can be calculate depending on the flow type which are turbulent or laminar flow as follows [5] [16]:

$$h_r = \frac{N_u * k_{ref}}{D_{iCond}} \ldots \ldots \ldots [5.15]$$

k_{ref} *is conductive heat transfer coefficient of the refrigerant*

D_{iCond} *is the inside diameter of the condenser pipe*

The Nusselt number $N_{u,}$ depends on the Reynolds number R_e, and can be expressed as:

$$R_e = \frac{v * \rho_{refr} * \dot{D}_{iCond}}{\mu_{ref}} \ldots \ldots \ldots [5.16]$$

Where, μ_{ref} *is dynamic viscosity of refrigerant* $- 134a$

ρ_{refr} *is the density of refrigerant* $- 134a$

v *is the velocity of the fluid/air*

Table 5-10: Thermophysical properties of saturated liquid R -134a at condenser temperature 49℃

S.N	Thermal conductivity	Dynamic viscosity	Density	Specific heat capacity	Pr, Prandtl number
1	0.07094$W/m.k$	0.00014408 $N.s/m^2$	1107.26 kg/m^3	1.5598 $\frac{kJ}{kg.k}$	3.18

Source: Frank P. Incropera

$$R_e = \frac{2m/s * 1107.26kg/m^3 * 0.0068m}{0.00014408N.s/m^2} = 104{,}516$$

For laminar flow, when $R_e < 3200$, for the flow, $3000 \le R_e \le 5 * 10^6$ and for turbulent flow when, $R_e \ge 5 * 10^6$.

For this research Re is 104,516 *in the interval of* $3000 \le R_e \le 5 * 10^6$

Then the nusselt number N_u is

$$N_u = \frac{\frac{f}{8} * (R_e - 1000) * P_r}{1 + 12.7 * \left(\frac{f}{8}\right)^{0.5} (P_r^{\frac{2}{3}} - 1)}, 3000 \leq R_e \leq 5 * 10^6 \ldots\ldots\ldots\ldots\ldots\ldots\ldots [5.17]$$

$f, is\ the\ Darcy\ friction\ factor\ and\ can\ be\ expressed$:

$$f = ((0.79 * \ln(R_e)) - 1.64)^{-2} \ldots\ldots\ldots\ldots\ldots\ldots\ldots\ldots\ldots\ldots\ldots\ldots\ldots\ldots\ldots [5.18]$$

$$f = ((0.79 * \ln(104{,}516)) - 1.64)^{-2} = 0.01782$$

$P_r = 3.3,\ is\ the\ prantel\ number\ and\ taken\ fron\ table\ R - 134a$:

$$N_u = \frac{\frac{0.01782}{8} * (104{,}516 - 1000) * 3.18}{1 + 12.7 * \left(\frac{0.01782}{8}\right)^{0.5} (3.18^{\frac{2}{3}} - 1)} = \frac{740.5}{1.6968} = 436$$

$$h_r = \frac{436 * 0.0709 W/m.k}{0.0068m} = 4{,}550 W/m^2.k$$

At the air side of the condenser with the compressed gas which flows through the condenser for a staggered tube rows, the equation expressions are as follows:

$$h_a = \frac{N_u * k_{air}}{D_{OCond}} \ldots\ldots\ldots\ldots\ldots\ldots\ldots\ldots\ldots\ldots\ldots\ldots\ldots\ldots\ldots\ldots\ldots\ldots [5.19]$$

$k_{air}\ is\ conductive\ heat\ transfer\ coefficient\ of\ outside\ air$

$D_{OCond}\ is\ the\ outside\ radius\ of\ the\ condenser\ pipe$

$$R_e = \frac{v_{air\ max} * \rho_{air} * \dot{D}_{OCond}}{\mu_{air}} \ldots\ldots\ldots\ldots\ldots\ldots\ldots\ldots\ldots\ldots\ldots\ldots [5.20]$$

$where, \quad \mu_{air}: is\ dynamic\ viscosity\ of\ air$

$\rho_{air}: is\ the\ density\ of\ outside\ air$

$v_{air\ max} = 5m/s: is\ the\ maximum\ velocity\ of\ the\ fluid/air$

Table 5-11: Thermophysical properties of air at outside condenser temperature 37℃

S.N	Thermal conductivity	Dynamic viscosity	Density	Specific heat capacity	Pr, Prandtl number
1	0.02704 $W/m.k$	0.0000189 $N.s/m^2$	1.1281kg/m^3	1.0074 $\frac{kJ}{kg.k}$	0.7056

Source: Frank P. Incropera

$$R_e = \frac{8m/s * 1.1281\ \text{kg}/m^3 * 0.008m}{0.00001893\ N.s/m^2} = 3{,}814$$

$$N_u = Pr^{0.36} * 0.4Re_{do}^{0.6} \ldots\ldots\ldots\ldots\ldots\ldots\ldots\ldots\ldots\ldots\ldots\ldots\ldots\ldots\ldots\ldots\ldots\ldots\ldots. [5.21]$$

$$N_u = 0.7056^{0.36} * 0.4 * 4{,}814^{0.6} = 50$$

$$h_a = \frac{50 * 0.02704W/m.k}{0.008m} = 168W/m^2.k$$

$$\frac{1}{U_i} = \frac{0.0068m}{168W/m^2k * 0.008m} + \frac{0.001m * 0.0068m}{45W/m^2k * (0.0068m + 0.008m)/2} + \frac{1}{4{,}550W/m^2k}$$

$$1/U_i = 0.0050598 + 0.00002042 + 0.00021977(w/m^2k)$$

$$U_i = 170.2\ (w/m^2k)$$

$$A_{iCond} = \frac{Q_{Cond}}{U * LMTD} = \frac{520W}{10k * 189w/m^2k} = 0.2754m^2$$

$$A_{iCond} = \pi D_{iCond} L_{CON}, from\ this\ L_{CON} = \frac{A_{Cond}}{\pi D_{iCond}}$$

$$L_{CON} = \frac{0.2754m^2}{3.14 * 0.0068m} = 13m$$

The number of condenser tubes by considering the height of the ice storage tank 0.4m and length of 0.29m are

$$N_{Cond} = \frac{L_{CON}}{0.4m} = \frac{13m}{0.4m} = 32$$

5.2.5 Refrigerator Capillary Tube Equipment Selection and Design

Capillary tubes with small internal diameter and its main function is to change the refrigerant pressure from high level to low ready to enter the evaporator. Its diameter varies from 0.5 to 2.28mm and commonly make up of from copper material [56].

$$h_3 = h_4 = 107.32kJ/kg$$

5.3 Energy Balance of the PV Module

Based on the ambient temperature the heat loss and heat gain both radiation and convection of the region can be formulated. This means heat from the PV surface to the surrounding will be lost when the ambient temperature is lower and heat energy will be gained when the ambient temperature is higher both for upper and lower side of the PV surface.

The PV energy balance of the system is given bellow:

$$m_{pv} * C_{pv} * \frac{(T_{pvf} - T_{pvi})}{dt} = A_{pv}(I_{pv} - E + 2(T_a * h_{cc}) - 2(T_{pvi} * h_{cc}) \ldots\ldots [5.22]$$

From the above equation the PV surface temperature at the final state can be expressed as follows:

$$T_{pvf} = T_{pvi} + \frac{(dt * A_{pv} * (I_{pv} - E + 2 * (T_a * h_{cc}) - 2 * (T_{pvi} * h_{cc})}{m_{pv} * C_{pv}} \ldots\ldots\ldots [5.23]$$

Where, m_{pv} mass of the PV module, C_{pv} PV specific heat, A_{pv} area of the PV module, dt change of time, T_{pvf} final state of PV temperature, T_{pvi} initial PV temperature, E electrical energy generation and I_{pv} solar enegy absorbed by module and arrived in the module.

$$h_{cc} = (h_{rad.pv} + h_{wind})$$

$h_{rad,pv}$: is the radiation heat loss of PV module and can be calculated as follows:

$$h_{rad,pv} = \in_{pv} * \sigma * \left(\frac{T_{pv}^4 - T_{sky}^4}{T_{pv} - T_{sky}}\right) \ldots\ldots\ldots\ldots\ldots\ldots\ldots\ldots\ldots\ldots\ldots\ldots\ldots\ldots\ldots [5.24]$$

Where, $\in_{pv}$ Emissivity of the PV module, T_{pv} PV temperature, σ Boltzmann constant and T_{sky} local air temperature.

$$T_{sky} = 0.0552T_a^{1.5}$$

h_{wind}: is the convective heat transfer coefficient at the upper and lower PV surface and can be calculate:

$$h_{wind} = 5.7 + 3.8v, \quad v: is\ the\ wind\ speed\ in\ m/s$$

5.3.1 Over All Energy Balance of the Refrigeration System

By using the first law of thermodynamics the energy balance between evaporator, condenser and compressor can express as follows:

$$Q_e = Q_{Cond} - W_{Comp} \dots \dots \dots \dots \dots \dots \dots \dots \dots \dots \dots \dots \dots \dots \dots \dots \dots \dots \dots \dots \dots \dots \dots \dots .. [5.25]$$

The evaporator cooling equation can also express as follows:

$$Q_e = A_e * U_e(T_{water} - T_e) \dots \dots \dots \dots \dots \dots \dots \dots \dots \dots \dots \dots \dots \dots \dots \dots \dots \dots \dots \dots \dots [5.26]$$

5.3.2 Hourly Ice Slab Temperature

The ice slab temperature is influenced by the cooling capacity of the evaporator

$$T_{ice} = T_O - \left(\frac{Q_{ice} - cp_{water} * m_{ice}(T_m - T_O) - m_{ice} * Q_L}{m_{ice} * Cp_{ice}}\right) \dots \dots \dots \dots \dots \dots \dots [5.27]$$

Where $T_{ice,final}$: the ice final temperature, and $T_{ice,in}$: is the inlet water temperature,

$$Q_{ice,} = Q_e - Q_{tank\ loss} - Q_{st} \dots \dots \dots \dots \dots \dots \dots \dots \dots \dots \dots \dots \dots \dots \dots [5.28]$$

Q_{ice} : is the heat gained by ice and $Q_{tank\ loss}$ is the storage tank heat loss

5.3.3 Milk Temperature Variation during Night

The milk temperature is influenced by the stored ice slab and the transmission heat leak in to the milk tank. And also it is affected by the heat flux absorbed through ice tank

$$Q_{milk} = Q_{milk\ trans} - Q_{ice\ tank} \dots \dots \dots \dots \dots \dots \dots \dots \dots \dots \dots \dots \dots \dots \dots [5.29]$$

$$Q_{milk}, \qquad milk\ cooling\ load,$$

$$Q_{milk\ trans}, transmission\ heat\ gain\ through\ milk\ tank$$

$$Q_{ice\ tank,}\ heat\ absorbed\ by\ ice\ through\ ice\ tank\ from\ milk$$

5.4 Cooling capacity By Using CASCADE17-0244Y3 Compressor Performance Equation and Performance Coefficient Values

The cooling capacity of the system could be formulated by using the performance equation and performance coefficient values of the selected compressor.

Table 5-12. Performance Coefficients (24V) - CASCADE17-0244Y3 VSDC ARI HBP

Coefficient	capacity (BTU/Hr)	Power (watt)	current (Amp)	Mass flow (Lbs. /Hr)
C1	-1.107663E+03	3.943455E+02	1.643106E+01	-9.435642E+00
C2	-1.300685E+00	-1.223476E-01	-5.097817E-03	-2.856467E-02
C3	2.056291E-04	2.942926E-05	1.226219E-06	4.165405E-06
.-	-	-	-	-
-	-	-	-	-
C22	-6.058412E-04	-4.793339E-04	-1.997224E-05	-6.54666E-06
C23	-8.010951E-03	2.484762E-04	1.035318E-05	-1.213048E-04

Unit conversion of compressor performance coefficient values for cooling capacity and mass flow rate of the refrigerant

1 Watt = 3.41214BTU /Hr (British thermal unit), and

1 kilogram per second = 7936.647pounds per hour

Performance equation of 24V CASCADE17-0244Y3 compressor at ARI HBP test condition

$$Y = C_1 + C_2X_1 + C_3X_1^2 + C_4X_1^3 + C_5X_2 + C_6X_2^2 + C_7X_2^3 + C_8X_3 + C_9X_3^2 + C_{10}X_3^3 + C_{11}X_1X_2X_3 + C_{12}X_1^2X_2X_3 + C_{13}X_1X_2^2X_3 + C_{14}X_1X_2X_3^2 + C_{15}X_1X_2 + C_{16}X_1X_3 + C_{17}X_2X_3 + C_{18}X_1^2X_2 + C_{19}X_1X_2^2 + C_{20}X_1^2X_3 + C_{21}X_1X_3^2 + C_{22}X_2^2X_3 + C_{23}X_2X_3^2 \dots\dots\dots\dots\dots\dots\dots\dots\dots\dots\dots\dots\dots\dots\dots\dots\dots\dots [5.30]$$

$X_1 =$ RPM

$X_2 =$ Evaporator temperature in degree Fahrenheit

$X_3 =$ Condenser temperature in degree Fahrenheit

$C_1 - C_{23}$: The performance coefficient of 24V CASCADE17-0244Y3 compressor like refrigerant mass flow rate, cooling capacity, current consumption, power consumption.

The useful electrical power coming from the solar PV panel to drive the DC compressor is given by:

$$E_{pv} = A_{pv} * H_C * \Delta(\sigma\tau) * \eta_{pv} * Pf * \left(\left(1 - T_{C,pv}\right) * \left(T_{pv} - T_{ref}\right)\right) \dots\dots\dots\dots [5.31]$$

Where, E_{pv} is the electrical energy generated, H_C is the solar radiation absorbed by the module, $\Delta(\sigma\tau)$ is difference between absorptivity and transitivity, Pf is packing factor, η_{pv} is efficiency of pv module, $T_{C,pv}$ is pv temperature coefficient, T_{pv} is PV temperature and T_{ref} is the module reference temperature. $T_{C,pv}$, $\Delta(\sigma\tau)$, η_{pv} and Pf are taken from the manufacturer datasheet of the selected mono-crystalline PV module.

The performance equation for compressor input power is equal to electrical energy generated from solar PV system and using column two performance coefficient values the equation becomes:

$$\begin{aligned} C_1 + C_2X_1 + C_3X_1^2 + C_4X_1^3 + C_5X_2 + C_6X_2^2 + C_7X_2^3 + C_8X_3 + C_9X_3^2 + C_{10}X_3^3 \\ + C_{11}X_1X_2X_3 + C_{12}X_1^2X_2X_3 + C_{13}X_1X_2^2X_3 + C_{14}X_1X_2X_3^2 + C_{15}X_1X_2 \\ + C_{16}X_1X_3 + C_{17}X_2X_3 + C_{18}X_1^2X_2 + C_{19}X_1X_2^2 + C_{20}X_1^2X_3 + C_{21}X_1X_3^2 \\ + C_{22}X_2^2X_3 + C_{23}X_2X_3^2 = PV\ electrical\ energy \dots\dots\dots\dots\dots\dots [5.32] \end{aligned}$$

Thus, using known values of $C_1 - C_{23}$, X_2 and X_3: the compressor rotational speed could be computed by using polynomial function with considering only for power consumption column.

Constant term with respect to X_1, X_1^2 and X_1^3

$$k = C_1 + C_5X_2 + C_6X_2^2 + C_7X_2^3 + C_8X_3 + C_9X_3^2 + C_{10}X_3^3 + C_{17}X_2X_3 + C_{22}X_2^2X_3 + C_{23}X_2X_3^2 + PV\ electrical\ energy$$

Coefficient of X_1,

$$K_1 = C_2X_1 + C_{11}X_1X_2X_3 + C_{13}X_1X_2^2X_3 + C_{14}X_1X_2X_3^2 + C_{15}X_1X_2 + C_{16}X_1X_3 + C_{19}X_1X_2^2 + C_{21}X_1X_3^2$$

Coefficient of X_1^2,

$$K_2 = C_3X_1^2 + C_{12}X_1^2X_2X_3 + C_{18}X_1^2X_2 + C_{20}X_1^2X_3$$

Coefficient of X_1^3, k3=$C_4X_1^3$

Then x1 (compressor rotational speed) it varies with solar radiation of the location, and the rotation becomes roots of the polynomial equation.

$$X1 = roots[K3 \quad K2 \quad K1 \quad K - PV\ Electrical\ energy] \ldots\ldots\ldots\ldots\ldots\ldots\ldots [5.33]$$

Then, the cooling capacity of the system can be computed from the compressor performance equation from equation [5.33] of the rotational speed.

$$\begin{aligned} Q_{cooling} = {} & C_1 + C_2X_1 + C_3X_1^2 + C_4X_1^3 + C_5X_2 + C_6X_2^2 + C_7X_2^3 + C_8X_3 + C_9X_3^2 + C_{10}X_3^3 \\ & + C_{11}X_1X_2X_3 + C_{12}X_1^2X_2X_3 + C_{13}X_1X_2^2X_3 + C_{14}X_1X_2X_3^2 + C_{15}X_1X_2 \\ & + C_{16}X_1X_3 + C_{17}X_2X_3 + C_{18}X_1^2X_2 + C_{19}X_1X_2^2 + C_{20}X_1^2X_3 + C_{21}X_1X_3^2 \\ & + C_{22}X_2^2X_3 + C_{23}X_2X_3^2 \ldots\ldots\ldots\ldots\ldots\ldots\ldots\ldots\ldots\ldots\ldots\ldots\ldots\ldots\ldots\ldots [5.34] \end{aligned}$$

The performance coefficient of the system

$$COP_{Ref} = \frac{Q_{cooling}}{E_{pv} * \eta_C} \ldots\ldots\ldots\ldots\ldots\ldots\ldots\ldots\ldots\ldots\ldots\ldots\ldots\ldots\ldots\ldots [5.35]$$

$$COP_{Ref} = \frac{Q_{cooling}}{A_{pv} * H_C * \Delta(\sigma\tau) * \eta_{pv} * Pf * \left(\left(1 - T_{C,pv}\right) * \left(T_{pv} - T_{ref}\right)\right) * \eta_C}$$

$$\eta_C = m_{flow\ rate} * w_{com}/E_{pv}, isentropic\ efficiency\ \ of\ compressor$$

$$\eta_C = (h_{2s} - h_1)/(h_{2s} - h_1), adiabatic\ efficiency\ compressor$$

For this research cooling load and mass flow rate of the refrigerant varies with electrical energy generated from solar PV system. For this reason performance coefficient depends on electrical energy generated from PV system. At maximum electrical energy, cooling load and mass flow rate of refrigerant becomes maximum and thus COP also maximum.

The performance coefficient can also expressed using thermodynamic cycle the refrigeration system

$$COP_{Ref} = \frac{Q_{cooling\ effect}}{work_{net\ in}} \ldots\ldots\ldots\ldots\ldots\ldots\ldots\ldots\ldots\ldots\ldots\ldots\ldots\ldots\ldots\ldots [5.36]$$

5.5 Part and Assembly Geometrical Modeling of the System

5.5.1 Part Drawing

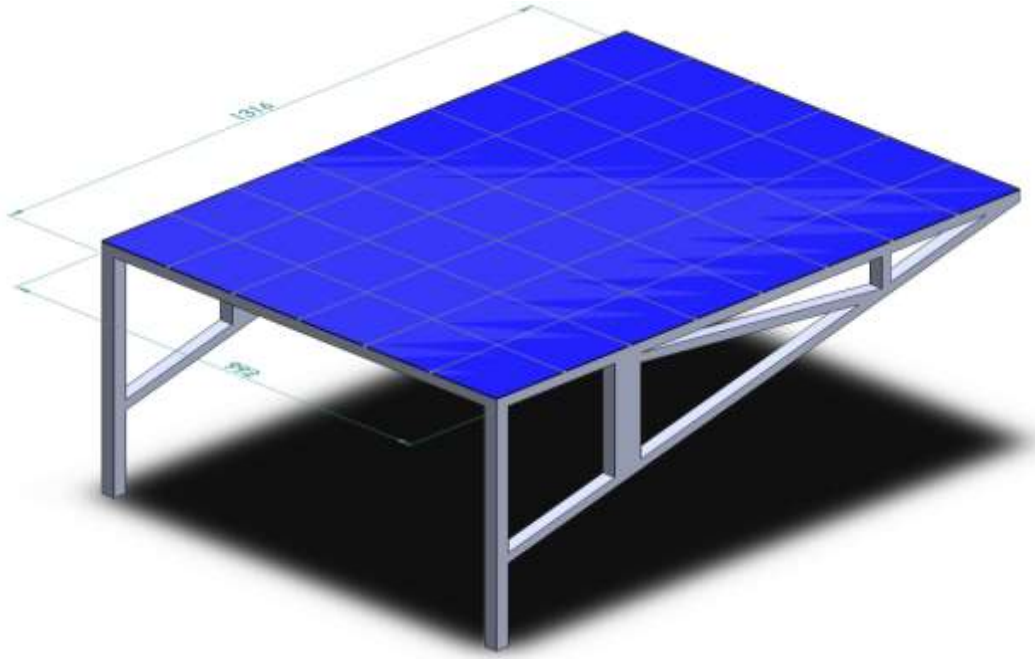

Figure 5-1. Photovoltaic panel with supporter

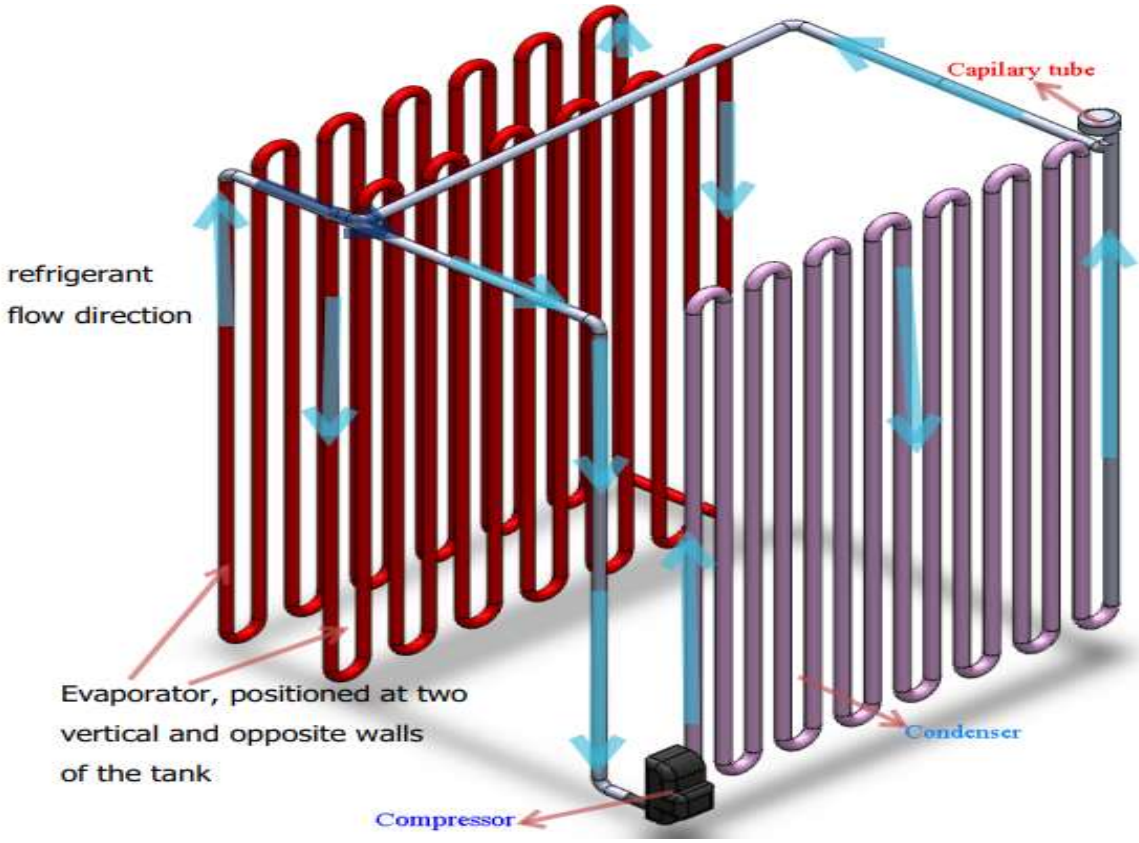

Figure 5-2. Evaporator, Condenser, Compressor and Capillary tube assembly

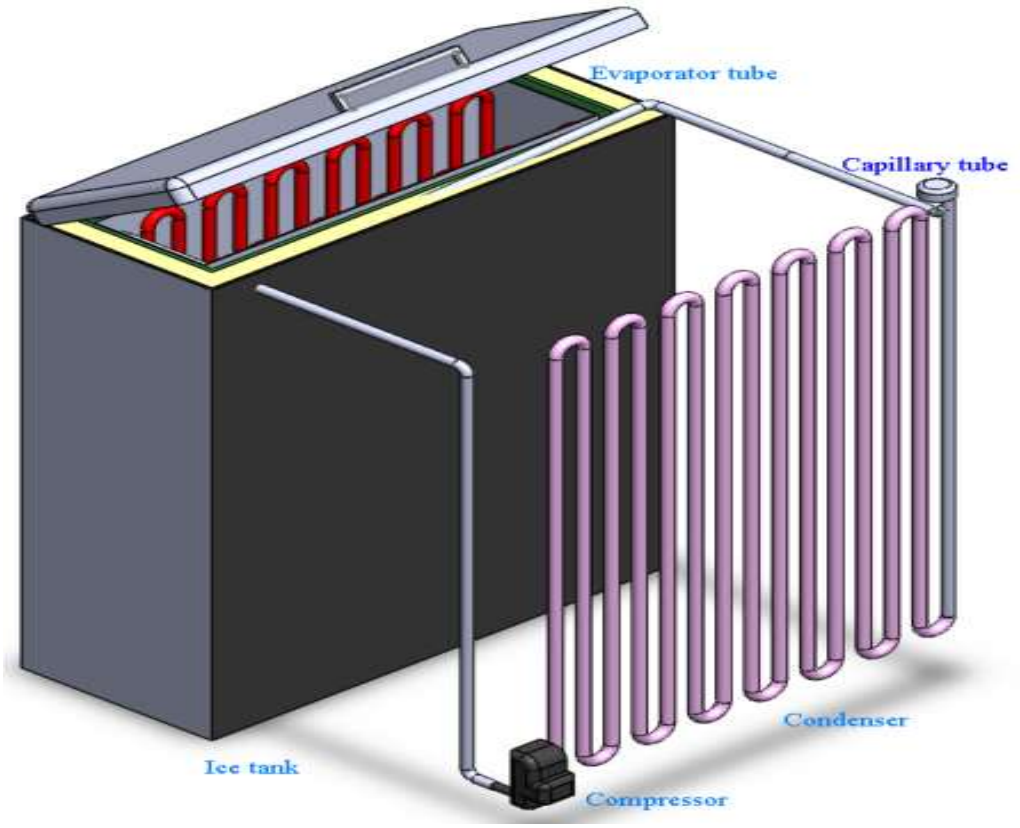

Figure 5-3. 3D drawing of slab ice storage tank with refrigerator components

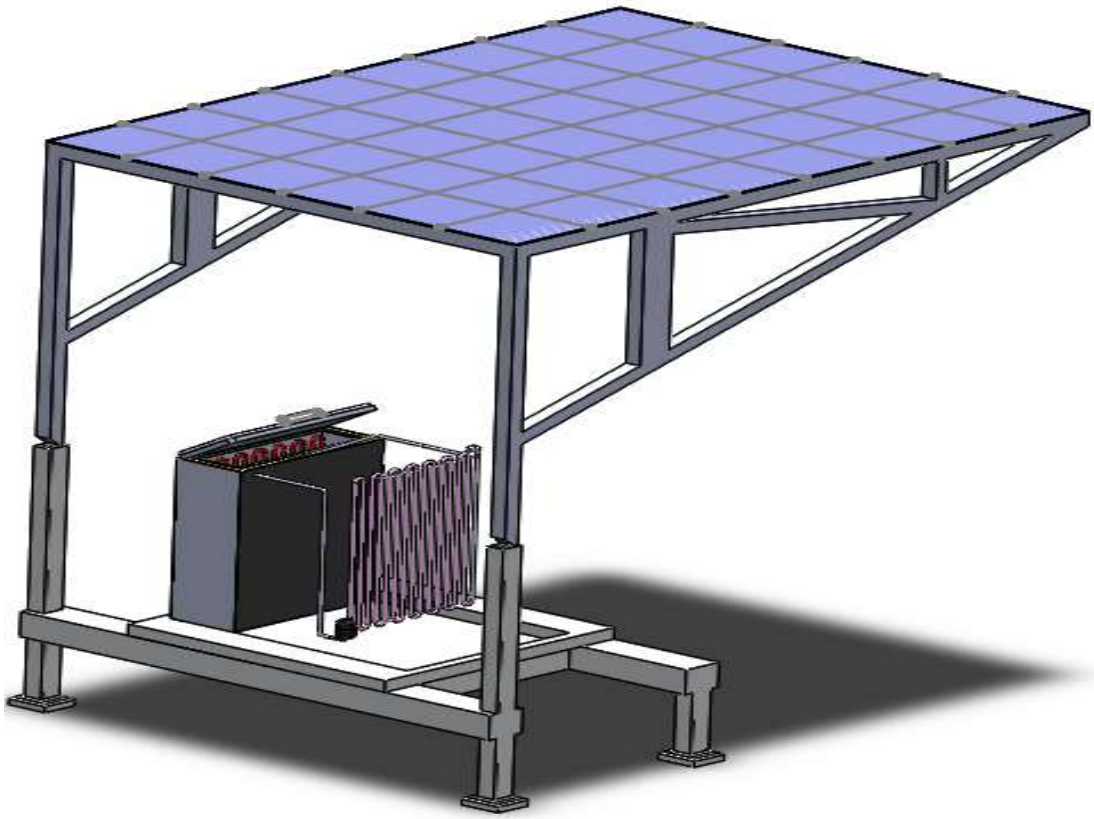

Figure 5-4. Assemble drawing of the whole system equipments

CHAPTER SIX

6. Result and Discussion

6.1 Introduction

This chapter explains about Matlab simulation results of nodal temperature distribution of water inside water tank, ice slab crystal growth with time variation, monthly average hourly solar radiation of Semera, monthly average hourly electrical generation from solar PV system, monthly average hourly PV surface temperature, monthly average hourly percentage of ice formation, monthly average hourly COP of the system and comparison of this result with experimental works.

6.2 Mat-Lab Simulation Results for Transient Ice Crystal Formation

6.2.1 Mat-Lab Simulation Results of Nodal Temperature Distribution of Water and Ice Crystal Growth with Time

Mat-lab code simulation results of the nodal temperature distribution in the water tank and the solid-liquid phase interface location (slab ice crystal growth) as a function of time for transient slab ice formation process are the following:

In the transient computational modelling of ice slab formation process, the results are obtained based on the following points.

- Ice freezer system has been designed that is able to form 8.5 kg of ice from 33℃ water and to cool 50 litre of milk at 4℃ temperature during night within 13 to 15 hours of time to balance the transmission heat gain through milk wall.
- Based on the ambient temperature of Semera Condenser temperature of 49℃ and evaporator temperature of -7℃ has been selected.
- Based on the total cooling load demand of 416 watt, CASCADE17-0244Y3 variable speed DC compressor and 4.6 m^2 area of AS-6M24, 220W power solar PV panel has been selected.

a. Mat-lab simulation result of nodal temperature distribution of water for Each Month

The transient nodal temperature distribution of water using 1D transient, explicit scheme of finite difference numerical method for selected months of December, March and August. These months are selected based the different values of cooling performance. Initially the

tank water is filled at 33℃ temperature and decreases with time. After five to seven hours the temperature of water in the tank decreases bellow 0℃ and it forms slab ice.

The minimum water temperature appears -6℃ nearest to the evaporator temperature -7℃ which is the minimum temperature of the system. Refrigerator working at the evaporator temperature of -7℃ and condenser temperature of 49℃ in order to freeze 0.4*0.08*0.29 m^3 or 9.3 Litre of water at initial temperature of 33℃ to cool 50 litre of milk during night.

The result were done by using half of the water tank. The total length of the water tank is 0.08 meter and divided in to 13 elements (grid space) with 14 nodes. Thus length of half tank is 0.04 meter with 6 grid space and 7 numbers nodes. The node temperature of water near to the evaporator decreases with less period of time and nodes far from the evaporator takes more time than the nearest node.

Since the computational method uses one-dimensional transient explicit which is conditionally stable but not unconditionally stable, that the value of time step and grid space not be chosen independently and the solution is not stable at all grid size and time step. The computational time also depend on change of time and grid size that decreasing these value, increases accuracy of the result and computational time.

For this reason the grid space could be selected based on the result accuracy and computational time. So using 7 numbers of nodes (6 grid size) and 50 change of time give a good result with appropriate computational time for the system. The computation also checked by using 14 grid size with 30 time step and it gives good result but the computation time increases. The computation was adjusted based on 1D interior node stability criteria $F_O \leq \frac{1}{2}$, $and\ F_O = \frac{k\Delta t}{\rho c \Delta x^2}$, by limiting the values of time step and grid space.

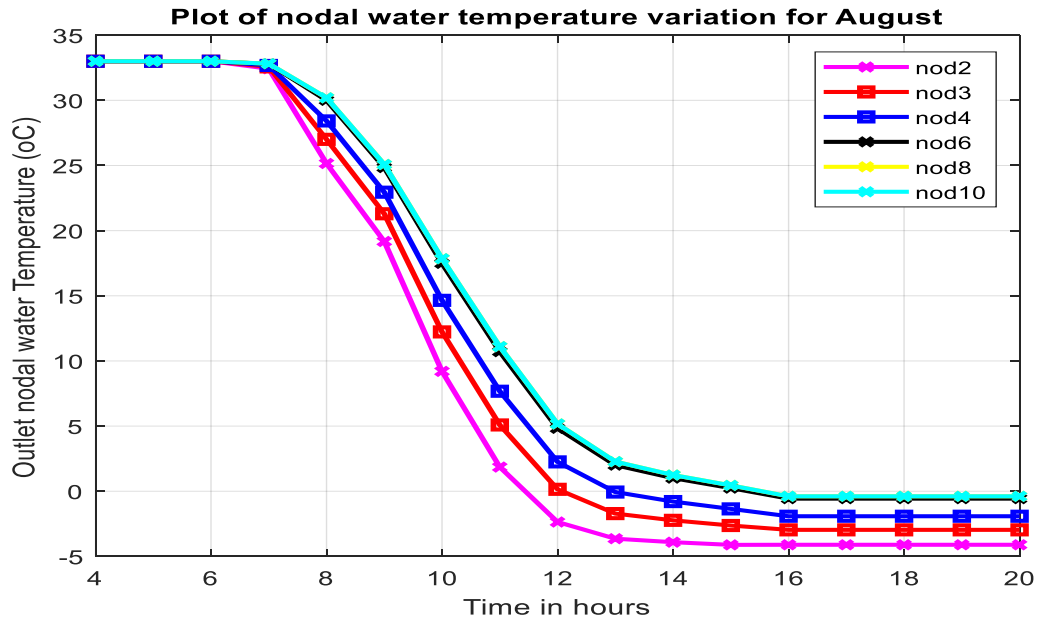

Figure 6-1. Monthly average hourly nodal temperature distribution of water for August

Figure 6.1 above shows nodal temperature distribution of water for less performed month of august and its temperature is below phase change temperature of water at 3 PM.

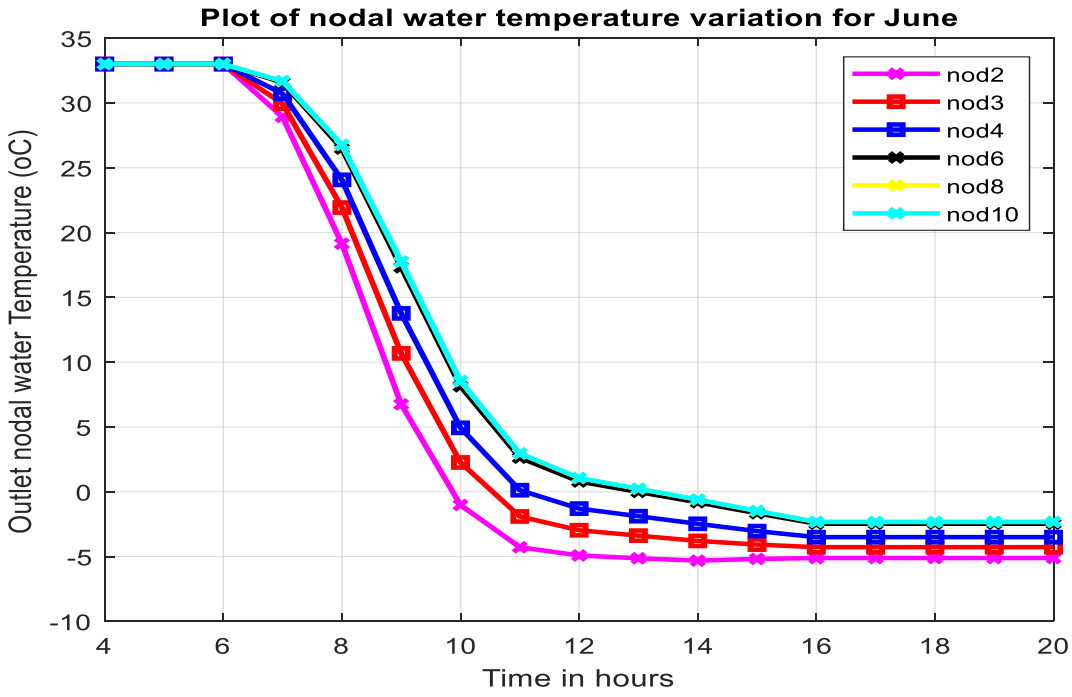

Figure 6-2. Monthly average hourly nodal temperature distribution of water for June

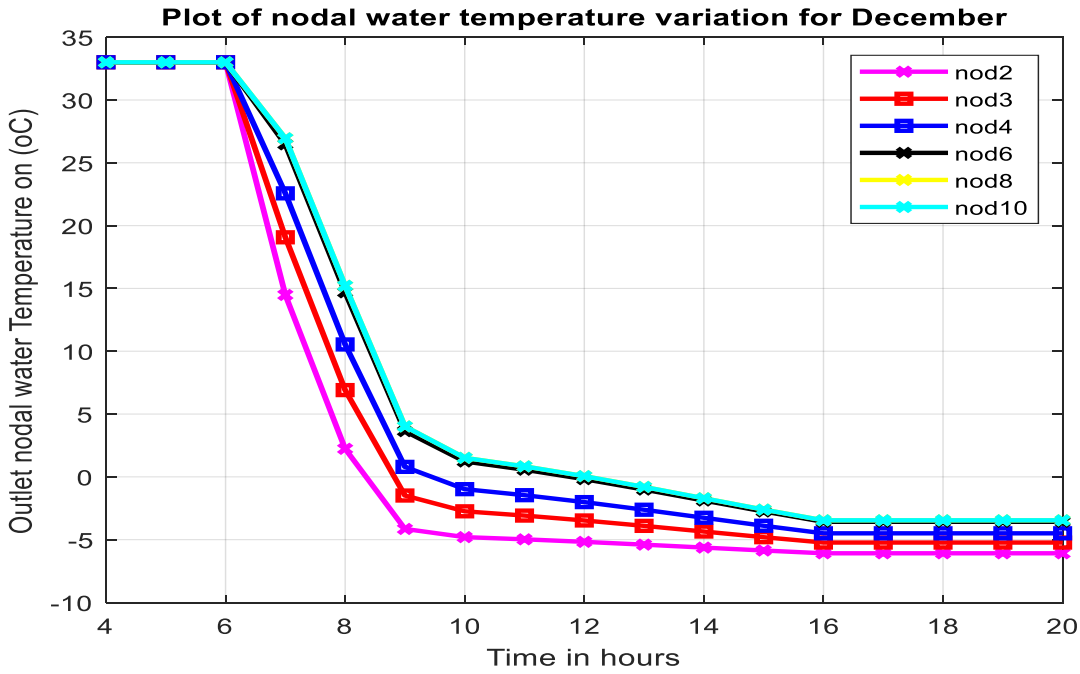

Figure 6-3. Monthly average hourly nodal temperature distribution of water for December

Figure 6.2 and 6.3 above shows nodal temperature distribution of water for moderate and highly performed months of June and December and its temperature is below phase change temperature of water at 1:30 PM and 12AM respectively.

b. Mat-lab simulation result of transient slab ice crystal growth in the water tank as a function of time

Initially the ice thickness is 0 meter and increases with time. After five to seven hours the slab ice crystal growth in the tank increases to 0.035 to 0.04. A rapid ice formation is occurred from 8AM to 3 PM hours of the day and ice crystal growth increases with time.

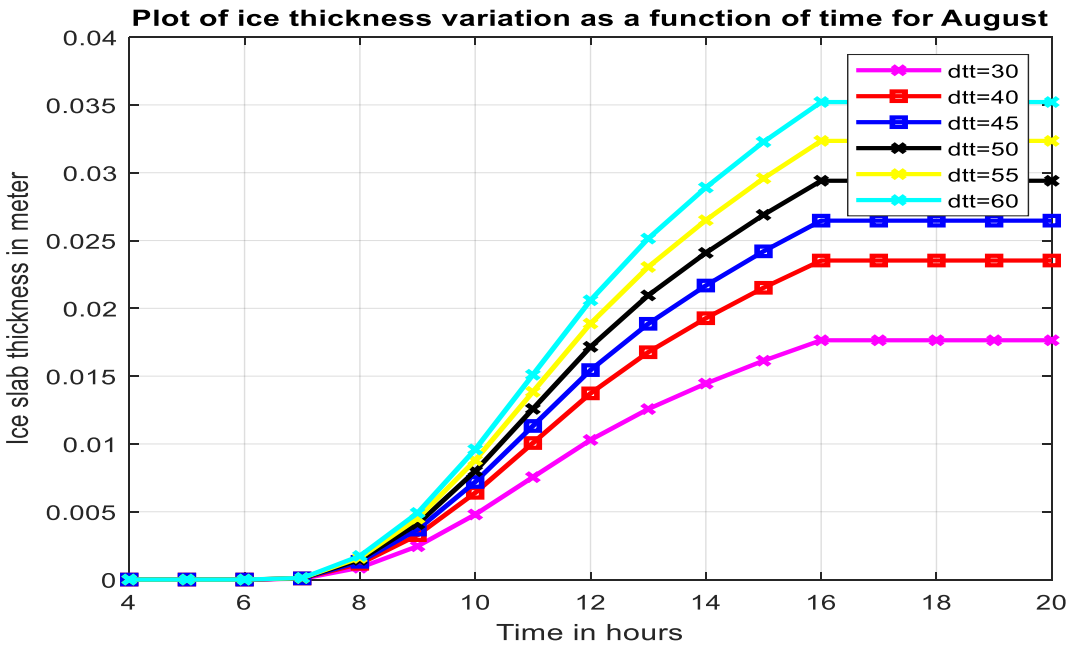

Figure 6-4. Monthly average hourly slab ice crystal growth for August

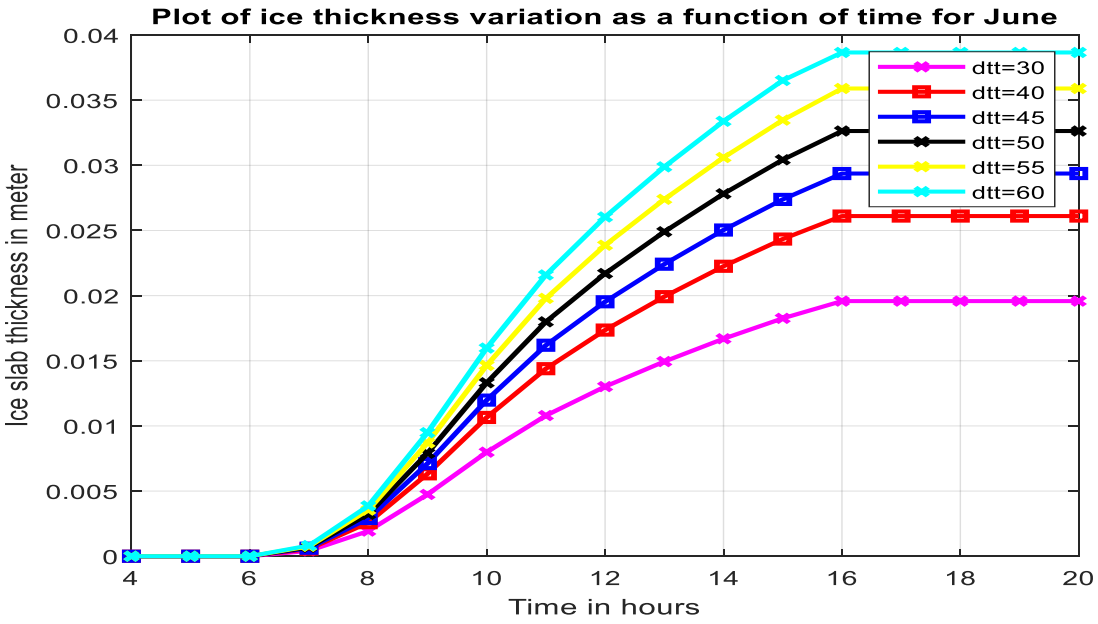

Figure 6-5. Monthly average hourly slab ice crystal growth for March

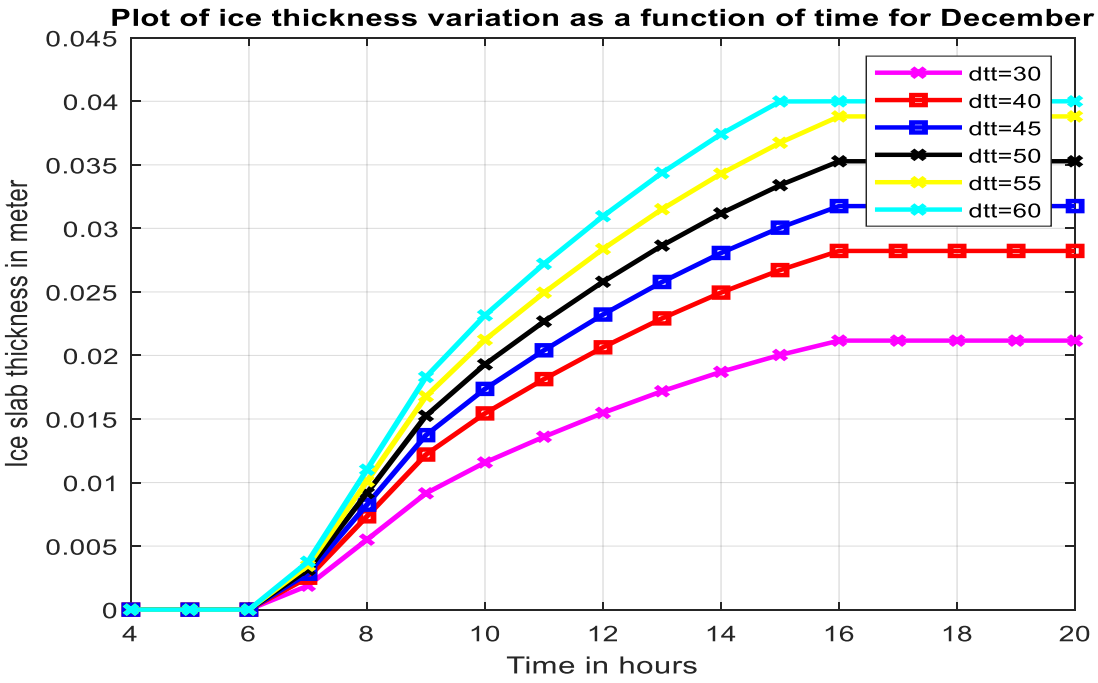

Figure 6-6. Monthly average hourly slab ice crystal growth for December

The figure 6.4, 6.5 and 6.6 above shows the transient slab ice crystal growth in the water tank and its variation as a function of time for less, moderate and highly performed months of August, June and December respectively. On the months of December and June 0.04 meter thickness ice crystal could be formed at 3PM and 4PM respectively and on August 0.035 meter thickness ice crystal could be formed at 4PM.

6.3 Performance Analysis of Slab Ice Formation Using Solar PV System at Semera

Mat-lab code hourly performance simulation results of transient slab ice formation process using solar photovoltaic system at the selected areas of Semera are the following:

6.3.1 Mat-Lab Simulation Result for Performance Analysis of Solar Radiation and Electrical Energy output

The performance of solar radiation on an inclined surface and electrical energy output at the selected place which is around Semera can be analyzed as follows:

a. Performance of Monthly average solar radiation on inclined PV surface

As shown in the figurer 6.7 bellow, monthly average solar radiation on inclined surface varies with time instantly where the highest radiation occurs at noon time when the sun

becomes overhead and the lowest radiation counts on the morning and at dawn time. Monthly point of view, December, April, November, May and February have the highest solar radiation while lowest in July, august and September.

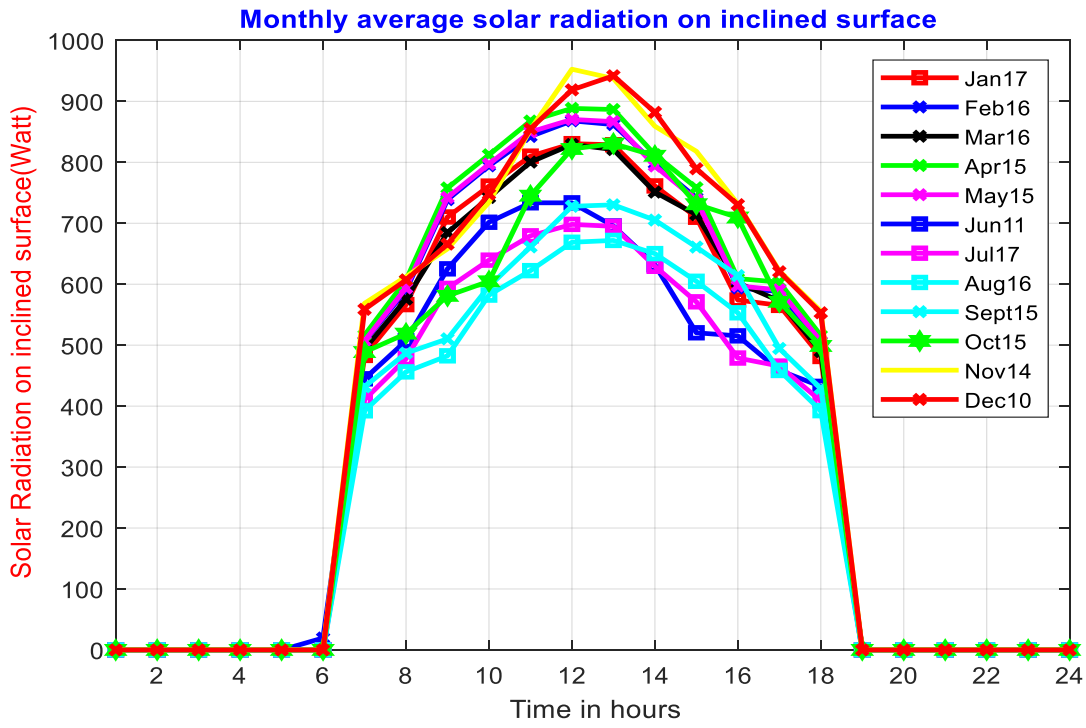

Figure 6-7. Monthly average solar radiation on inclined PV surface

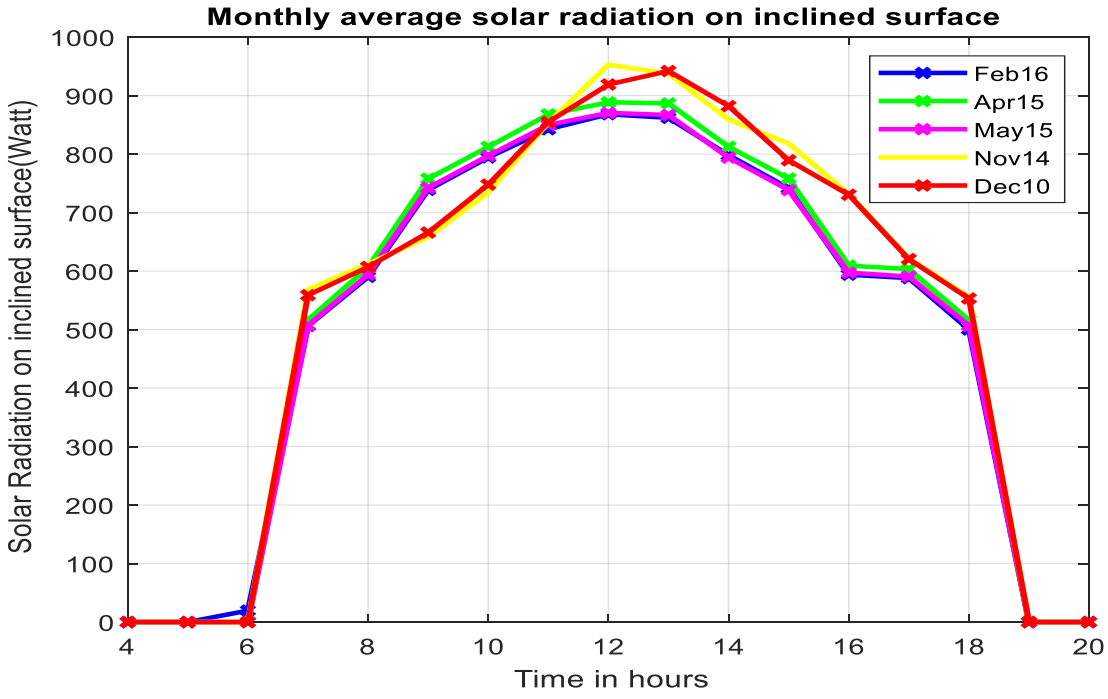

Figure 6-8. Available maximum solar radiation on inclined surface at Semera

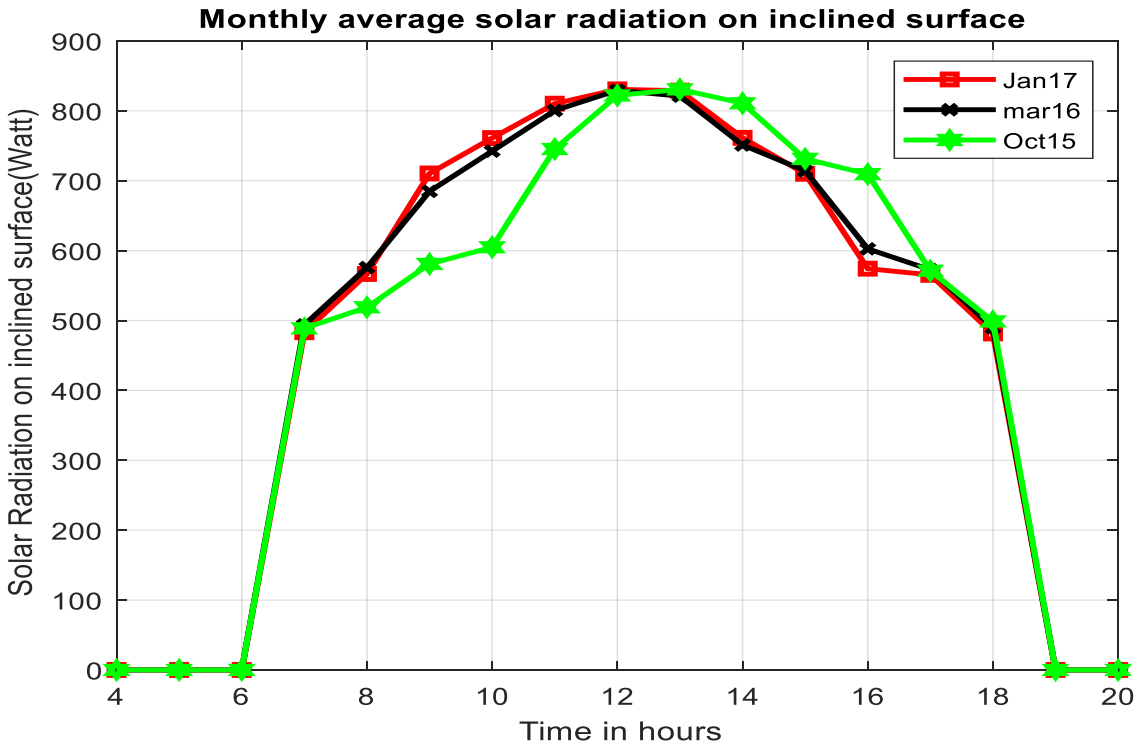

Figure 6-9. Available moderate solar radiation on inclined surface at Semera

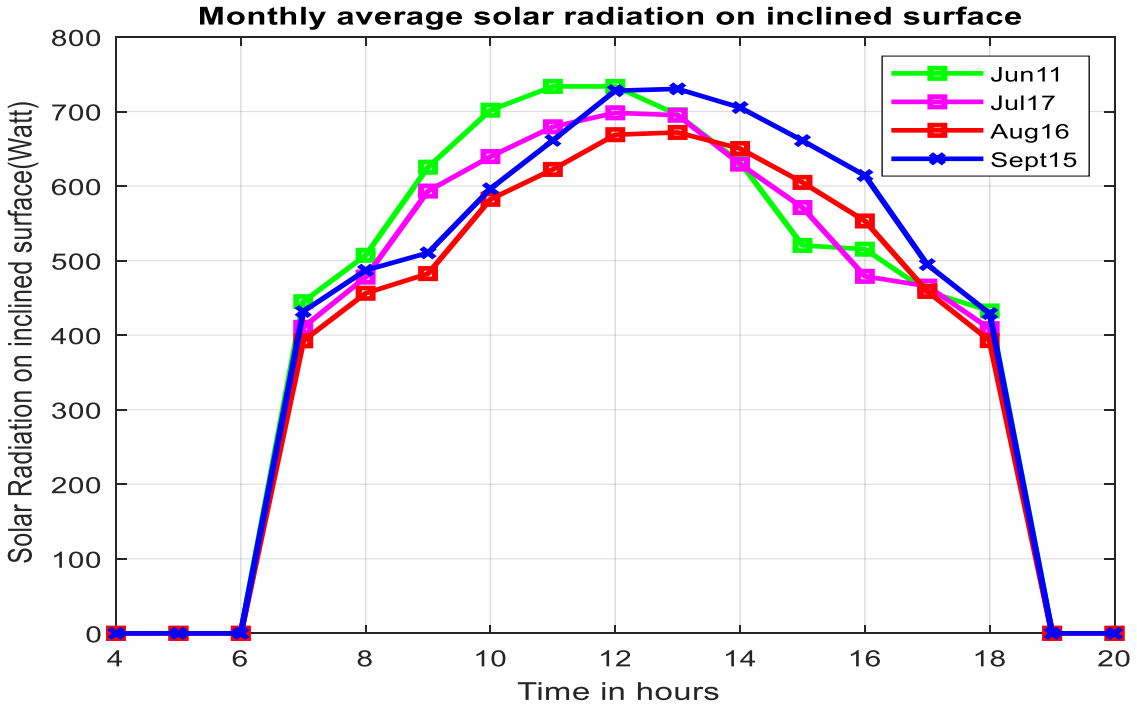

Figure 6-10. Available minimum solar radiation on inclined surface at Semera

Figure 6.8, 6.9 and 6.10 above represents high, moderate and less availability of monthly average solar radiation with 870 to 950 watt, 810 watt and 670 to 720 watt respectively.

b. Performance of Monthly average hourly Electrical Energy output of the system

As shown in figurer 6.11 bellow, the maximum electrical energy output of the system comes around 510 to 550Watt on the months of December, February, November, April and May and the minimum is in August around 390watt. Generally on the months of December, February, November and April, maximum electrical energy is harvested by the PV panel and on the months from June to September minimum electrical power can be harvested.

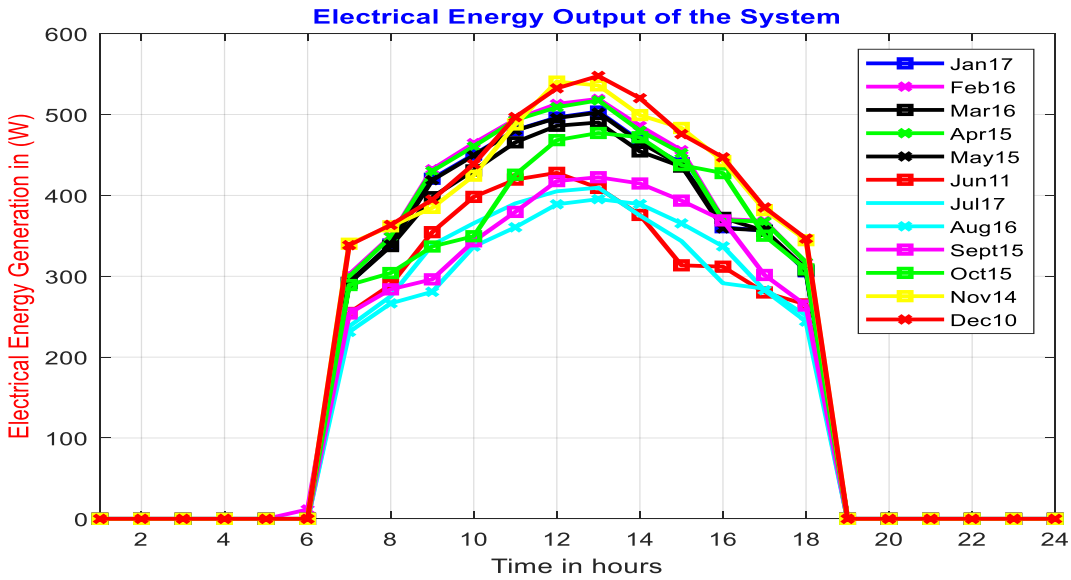

Figure 6-11. Hourly Electrical Energy output of the system

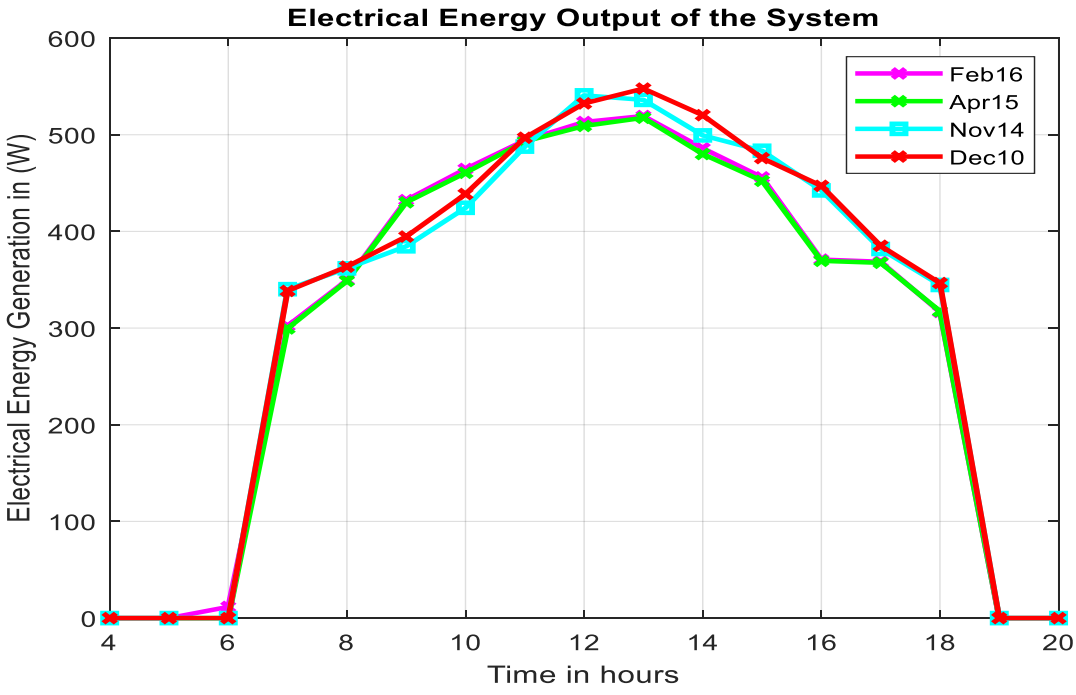

Figure 6-12. Available maximum Electrical Energy output on inclined surface at Semera

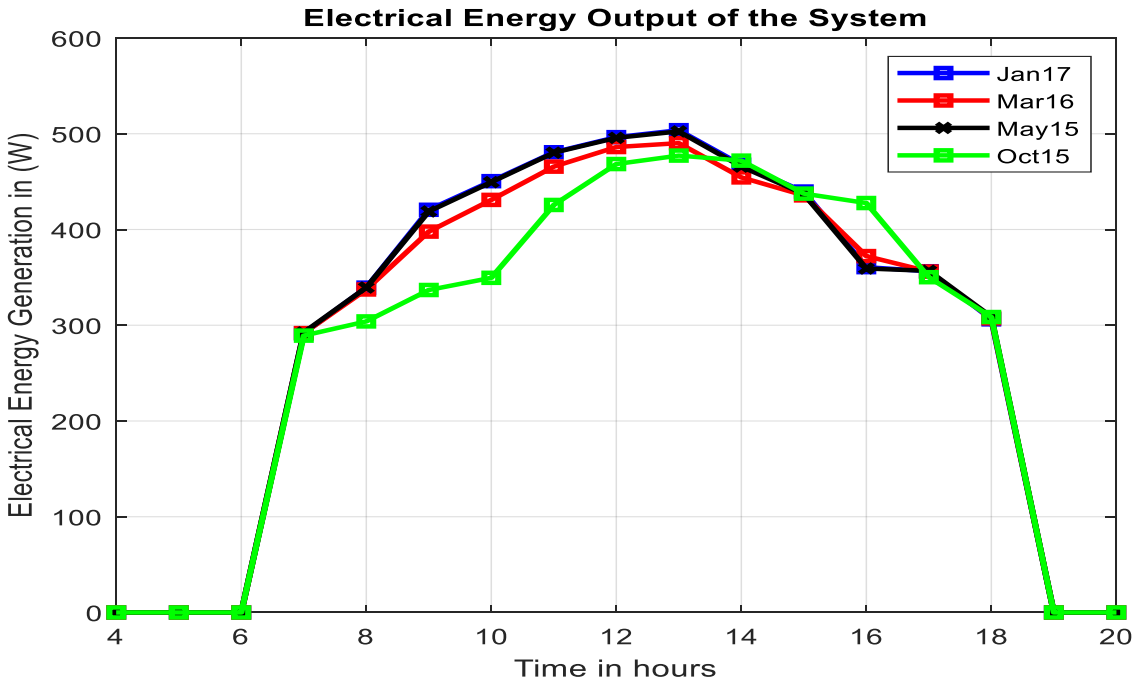

Figure 6-13. Available moderate Electrical Energy output on inclined surface at Semera

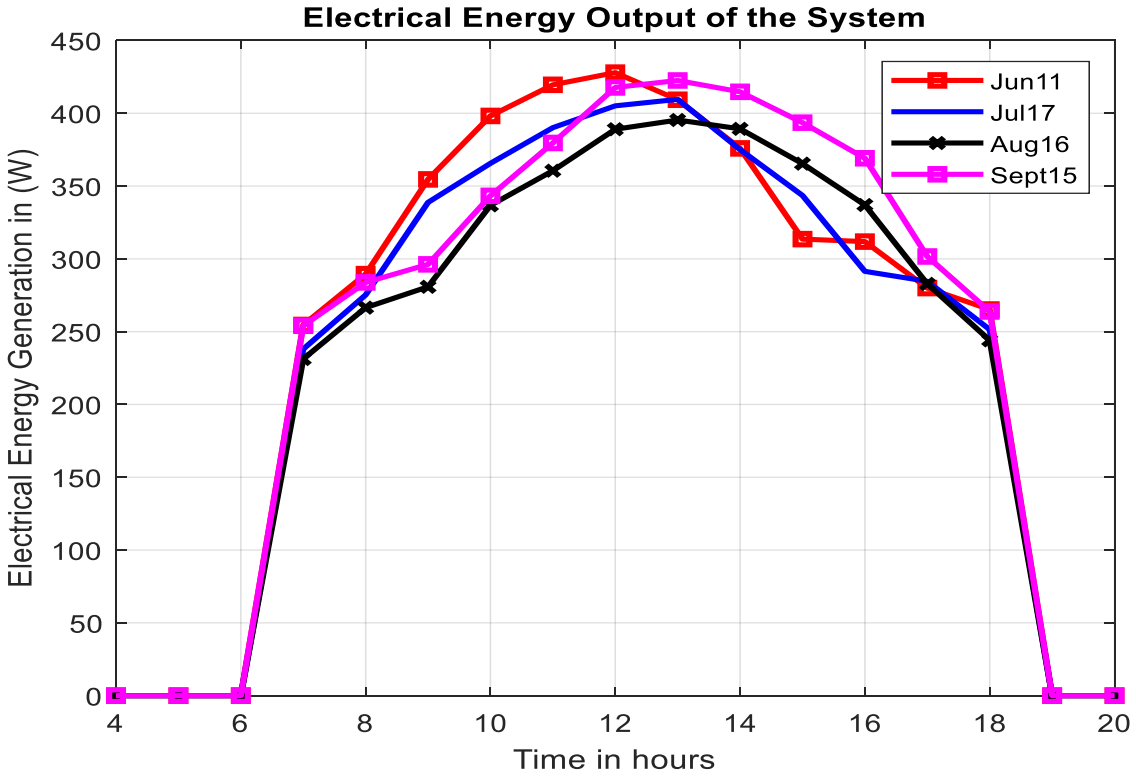

Figure 6-14. Available minimum Electrical Energy output on inclined surface at Semera

Figure 6.12, 6.13 and 6.14 above represents high, moderate and less availability of monthly average electrical energy generated from 4.6m^2 area solar PV panel with 510 to 550 watt, 480 to 500 watt and 390 to 425 watt respectively.

c. Monthly average hourly Photovoltaic panel surface temperature

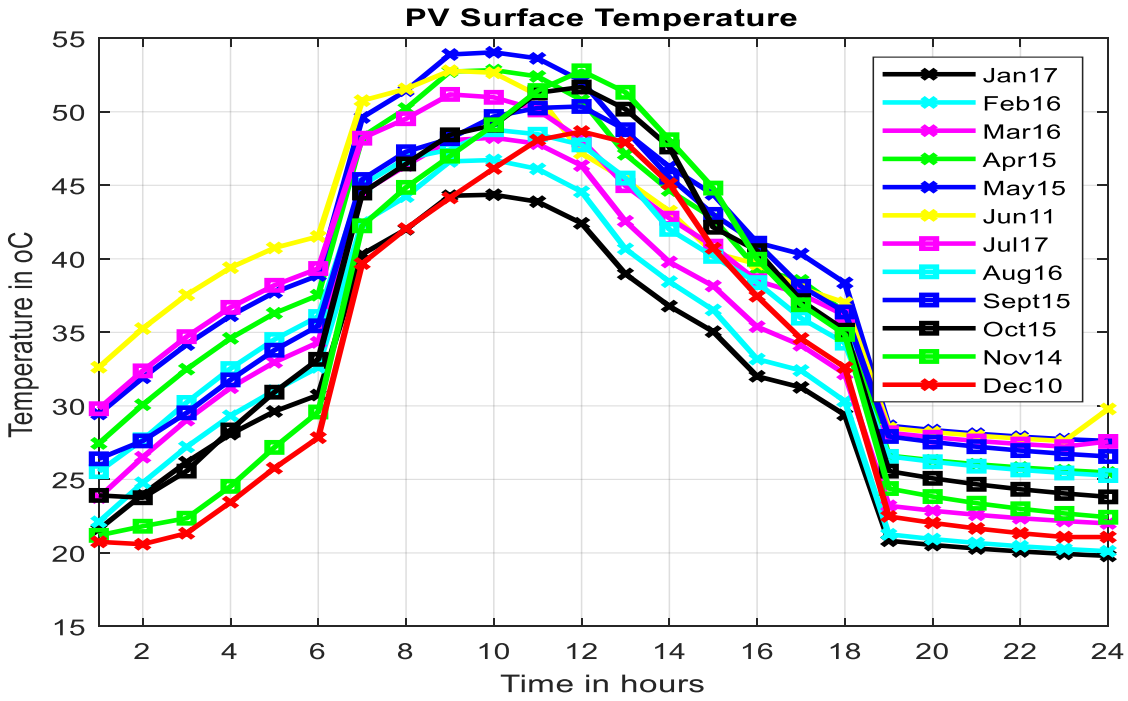

Figure 6-15. Monthly average Hourly Photovoltaic panel surface temperature

The fig 6.15 above shows the hourly PV surface temperature. The PV surface temperature is high at noon in the middle and low at the two opposite end of the graph which is in the morning and evening respectively. The minimum PV surface temperature during morning and evening is just around 20 to 30℃ as shown above figure and for the month of January is the minimum temperature during noon time around 43℃, also the maximum is around 53℃ on May which is good match for Semera region where maximum temperature appears on the months of May, June and April.

6.3.2 Performance Analysis of Water Temperature and Ice Formation

The performance of water temperature and ice slab crystal growth at the selected place which is around Semera can be analyzed as follows:

a. Performance analysis of Monthly average hourly nodal temperature of water

Temperatures of water in the storage tank by using daily values of average solar radiation for each months of a year were plotted in the figure below.

The figure 6.16 bellow shows the nodal temperature distribution in the water tank varies with each month of the year. The left and write evaporator attached on the water tank absorbs heat from the water. Initially the water is stored at 33℃ temperature and decreases

with time. Between the intervals of 7AM to 4PM hours the temperature of water in the tank decreases to 0℃ and it forms slab ice.

For the water temperature of 0ºc the maximum solar contribution to the heating load is archived during in the months of December, February, November, April and May respectively and the minimum is achieved during the summer season in the months of July, June, August and September respectively.

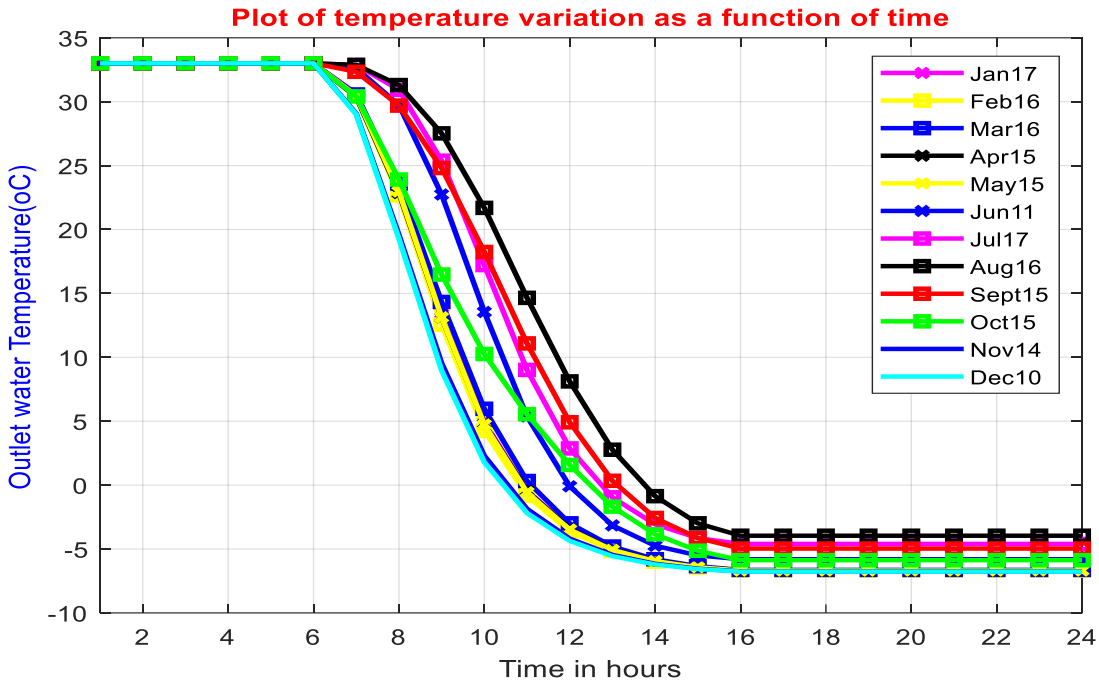

Figure 6-16. Monthly average hourly nodal temperature output of tank water

Temperature distribution of water in storage tank per a day:

- For the month of August, the temperature of water in the tank not achieved the required minimum values for six to seven hours of the day and thus moderate amounts of ice was formed.
- For months except August such as December, February, November, April and May the temperature of water in the tank below the water freezing point after 5 to 8 hours of the day and thus, the required amounts of slab ice was formed.

The maximum and minimum water temperature in storage tank was in December and August months respectively.

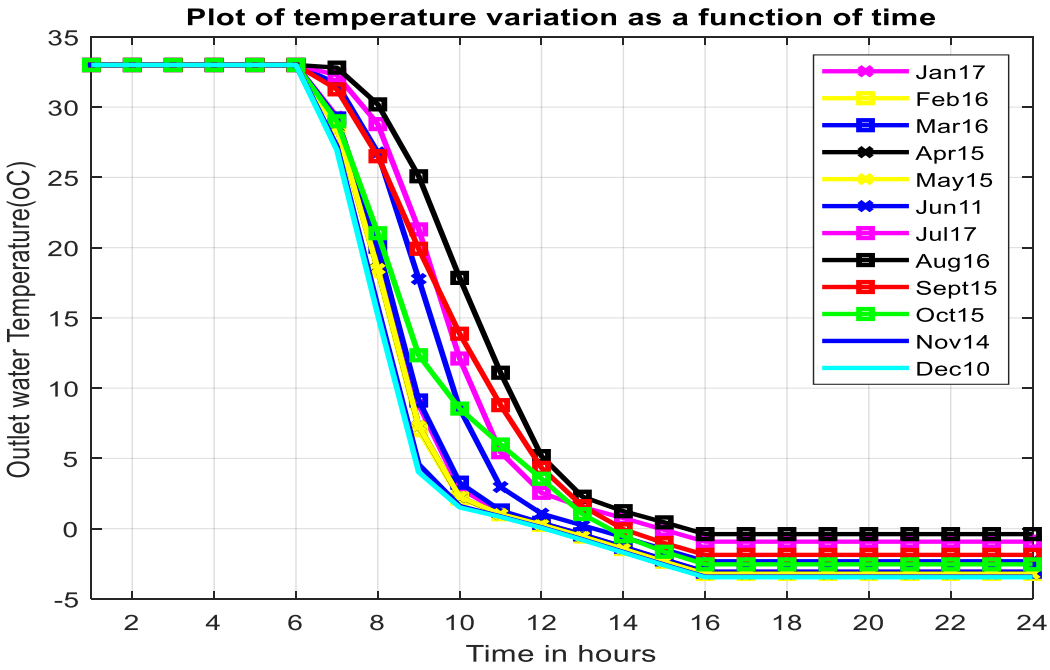

Figure 6-17. Monthly average hourly nodal temperature of water with maximum variation of solidus and liquidus temperature

Figure 6.17 above represents annual nodal temperature distribution of water using 2℃ and -4℃ liquidus and solidus temperature respectively. At the non-isothermal phase change process the temperature gradient differ from others.

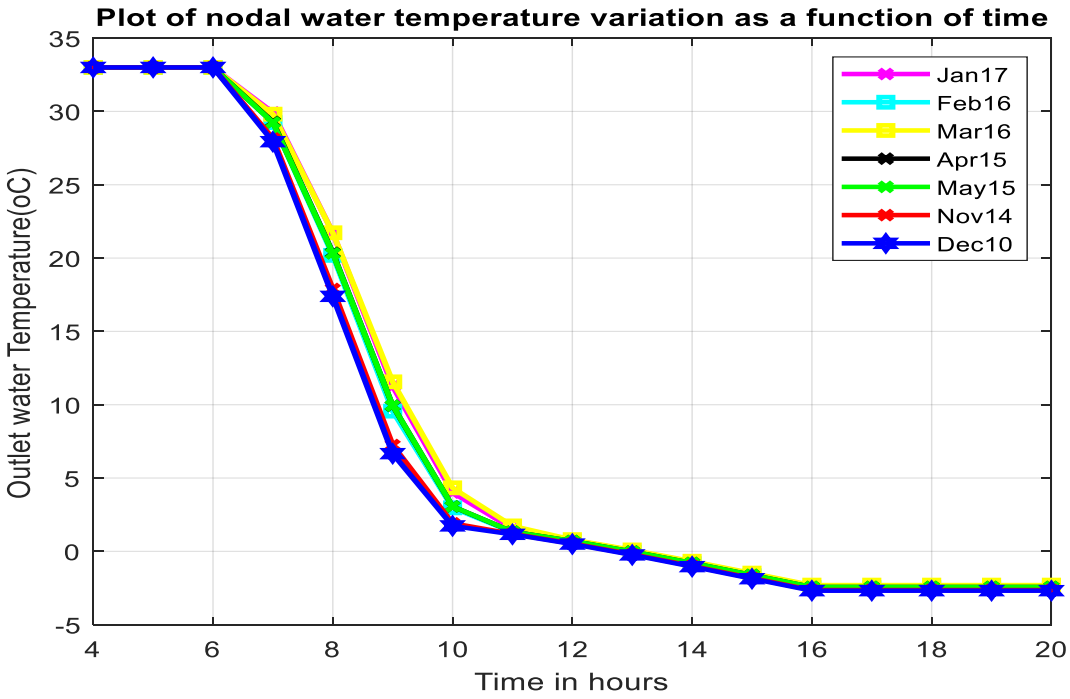

Figure 6-18. Average water temperature output of highly performed months at Semera

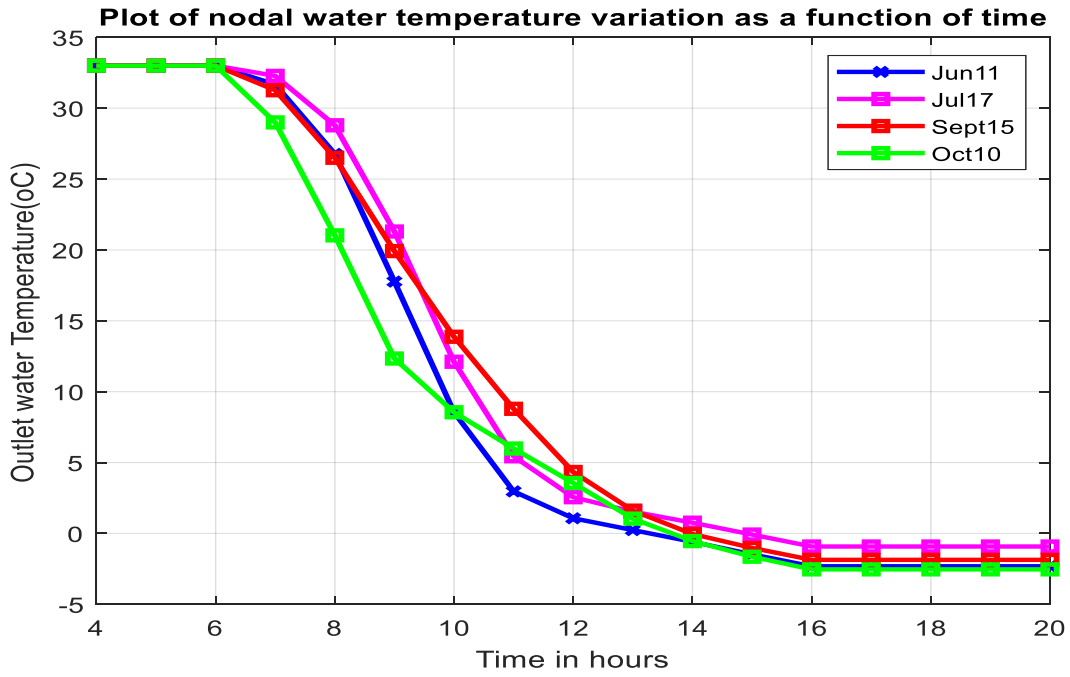

Figure 6-19. Average water temperature output of moderately performed months

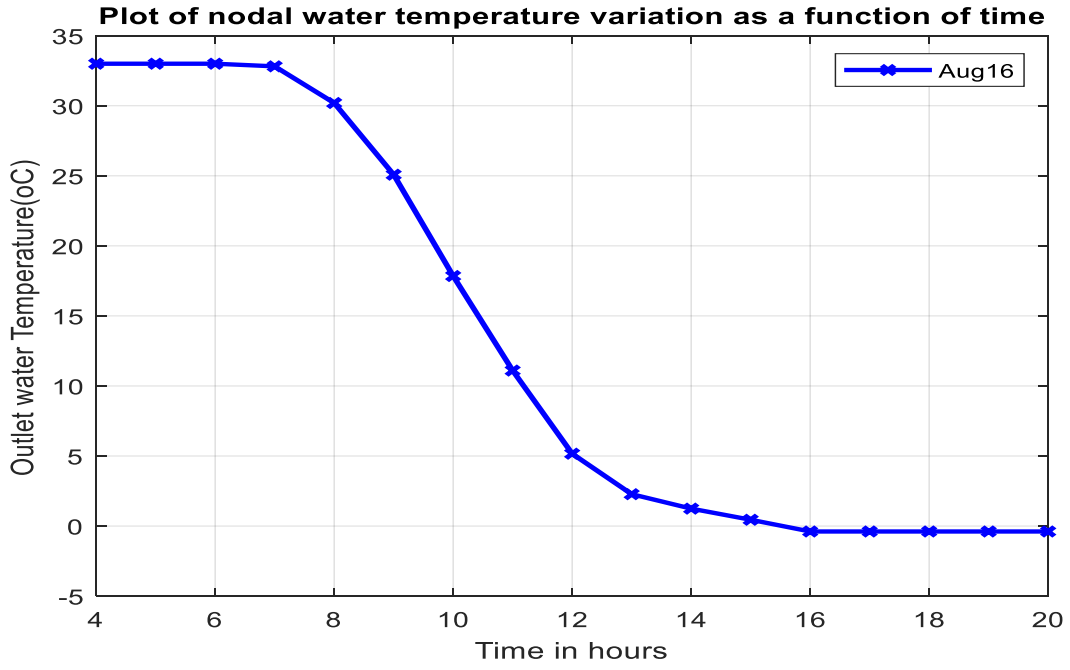

Figure 6-20. Average water temperature output of less performed months at Semera

Figure 6.18, 6.19 and 6.20 above shows nodal temperature distribution of water for high, moderate and less performed months and the temperature is below phase change temperature of water at 12AM, 1:30 PM and 3:30PM respectively.

b. Performance analysis of Monthly average hourly slab ice thickness growth

The figure 6.21 bellow shows the slab ice thickness growth from one side of half water tank and its variation with each month of the year by using the average values of monthly solar radiation.

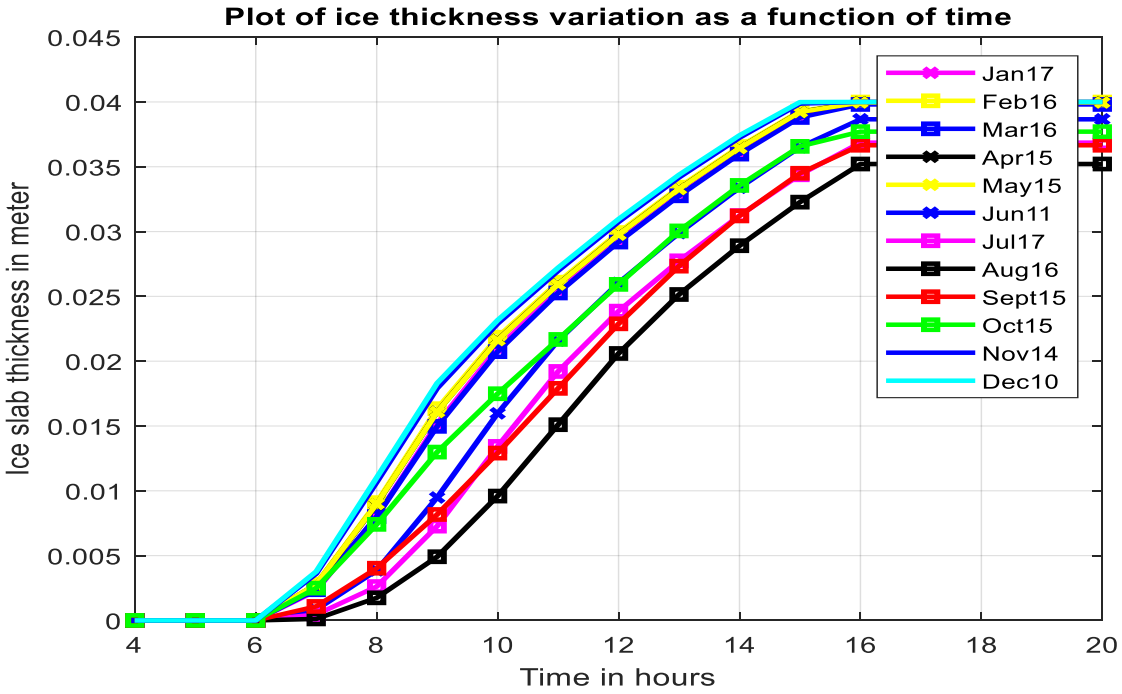

Figure 6-21. Monthly average hourly slab ice crystal growth

The left and right evaporator attached on the water tank absorbs heat from the water. Initially the ice thickness is 0 meter and increases with time. After 4 to 7 hours the slab ice thickness in the tank increases to 0.04 meter for maximum value and 0.036 meter for minimum values.

For the slab ice formation in the water tank the maximum solar radiation contribution to the heating load is archived during in the months of December, February, November, April and May respectively and the minimum is achieved in the months of August with 0.036 meter ice thickness.

The ice thickness growth in storage tank per a day:

- For June, July, October and September months, the system can achieved almost the required ice thickness which is 0.039 meter and for August month 0.036 meter slab ice can be formed in the tank form 7 AM to 4 PM hours of the day.

- For December, January, February, November, April, May and March months the required ice with 0.04 meter thickness was formed in the tank from 7 AM to 3PM hours of the day.

The maximum and minimum slab ice thickness in storage tank was in December and August months respectively.

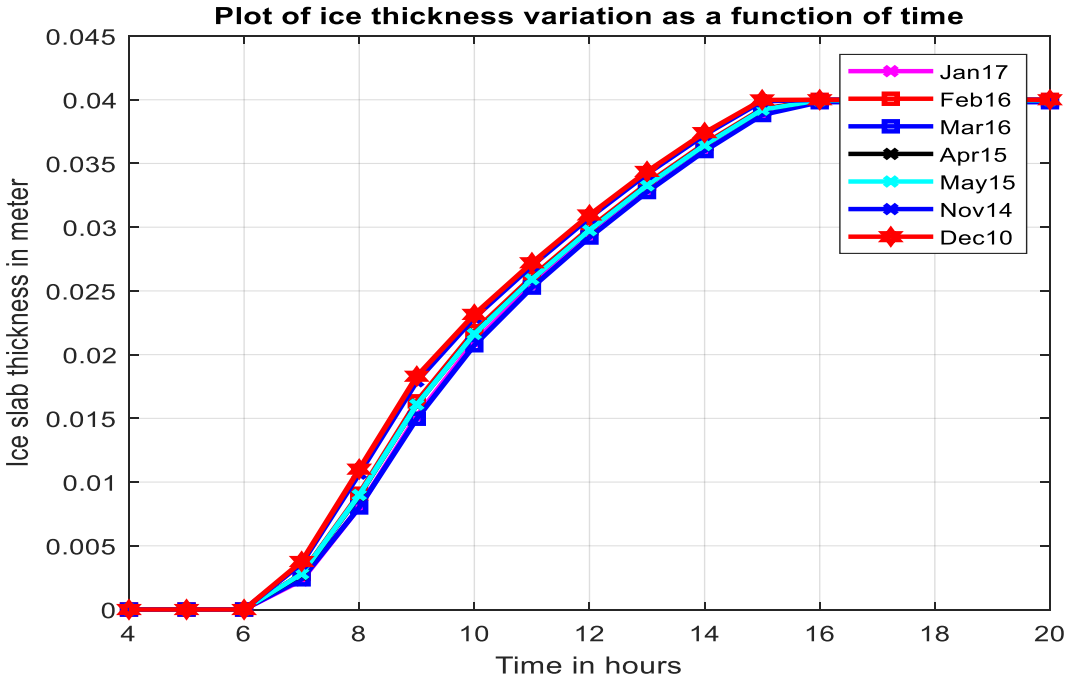

Figure 6-22. Average slab ice crystal growth of highly performed months at Semera

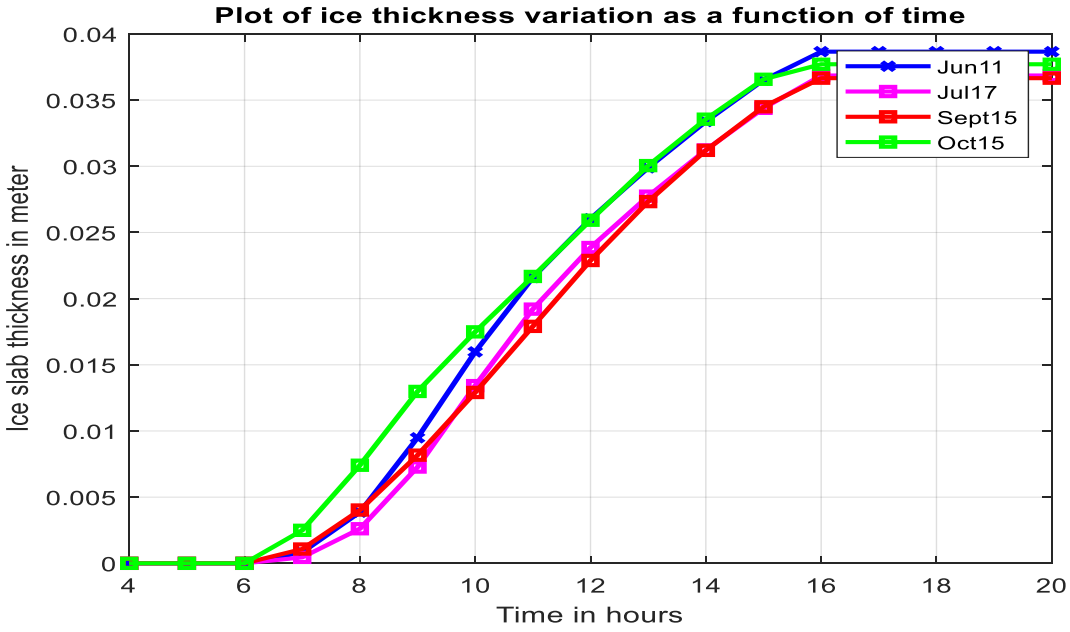

Figure 6-23. Average slab ice crystal growth of moderately performed months at Semera

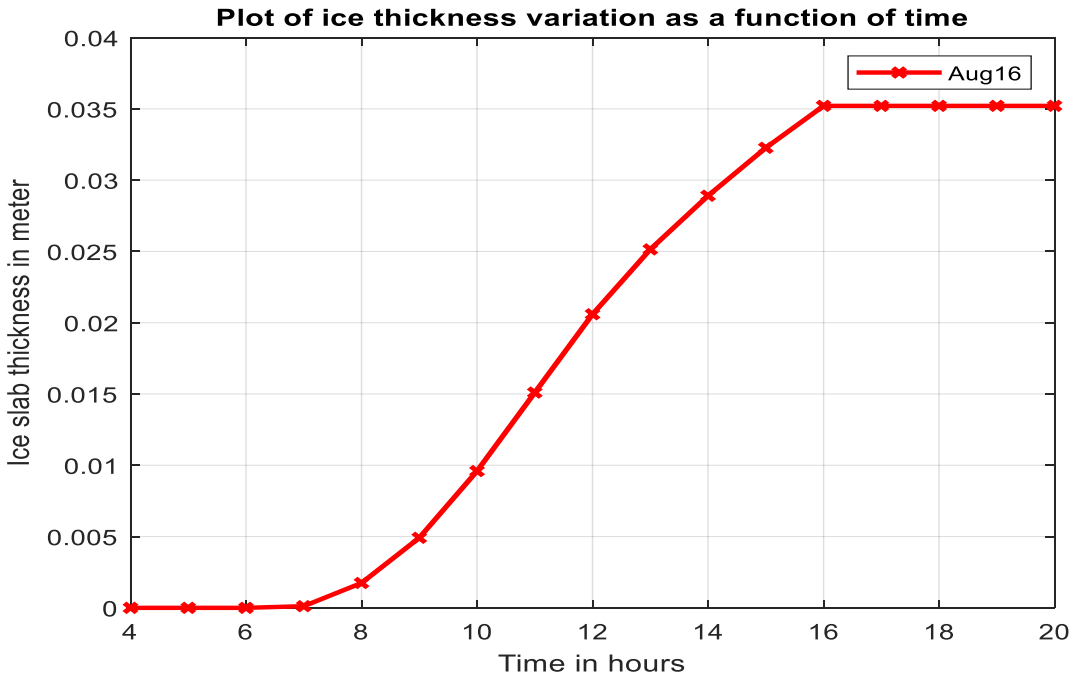

Figure 6-24. Average slab ice crystal growth of less performed months at Semera

Figure 6.22, 6.23 and 6.24 above shows ice slab crystal growth for high, moderate and less performed months with 0.04 meter, 0.085 meter and 0.035 meter thickness at 3PM, 4PM and 4PM respectively.

6.3.3 Monthly Average Hourly COP and Ice Formation Percentage

a. Performance Analysis of Monthly Average Hourly Percentage of Ice Formation

The figure 6.25 bellow shows the percentage of solid ice formation for the average values of each month in the year. As soon as the compressor is operating the water temperature decreases but ice formation starts after three to four hours due to convection heat transfer inside water tank. The slab ice formation starting from 8AM and ending at 4PM within 7 to 8 hours. All months of the year except August changes 98% water in to solid ice. In the months of January, December, November, April, March, May and February 100% of the water form slab ice and June, July, September and October 98% of water forms ice and in August 94% of water forms slab ice.

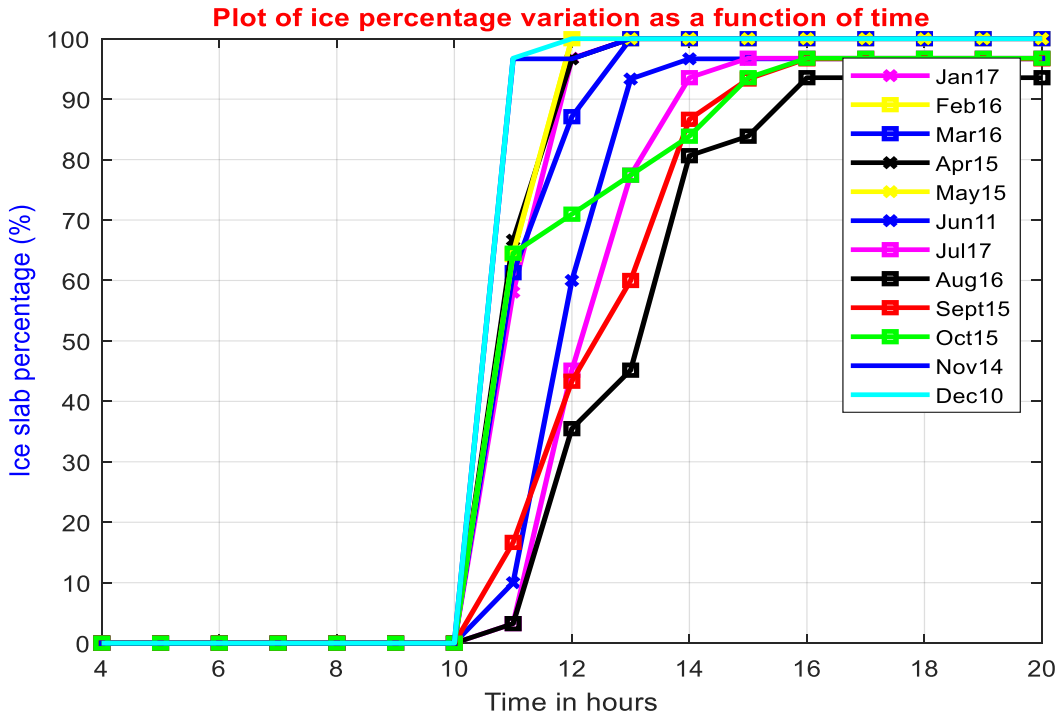

Figure 6-25. Monthly Average Hourly Percentage of Ice Crystal Formation

b. Monthly average hourly coefficient of performance of the system

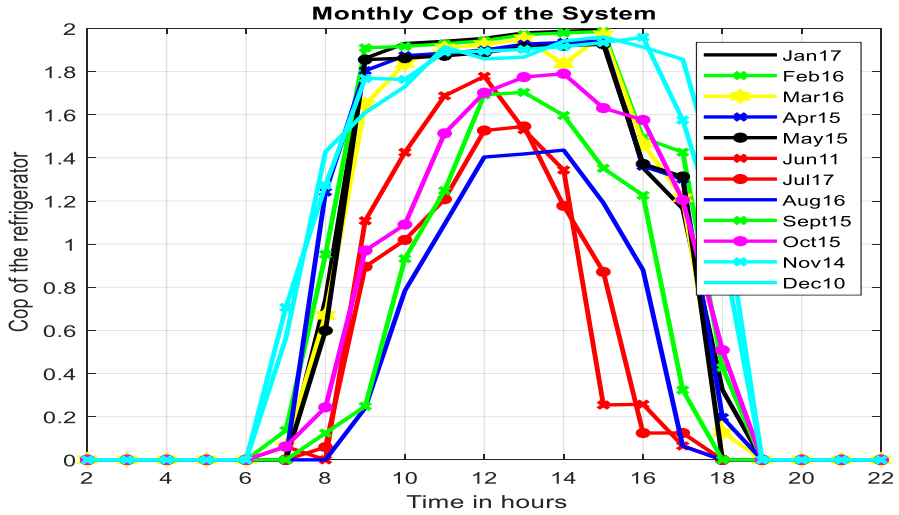

Figure 6-26. Monthly average hourly coefficient of performance of the system

The figure 6.26 above shows coefficients of performance of the system throughout a year. The computation was simulated based on cooling load and mass flow rate variation as a function of solar PV electrical energy. The maximum COP of the system is 2 from 9AM morning to 5PM afternoon on the months of January, February, April, March, November, December and May and the minimum is ranging from 0 to 1.4 on the months of August, July, September, June and October.

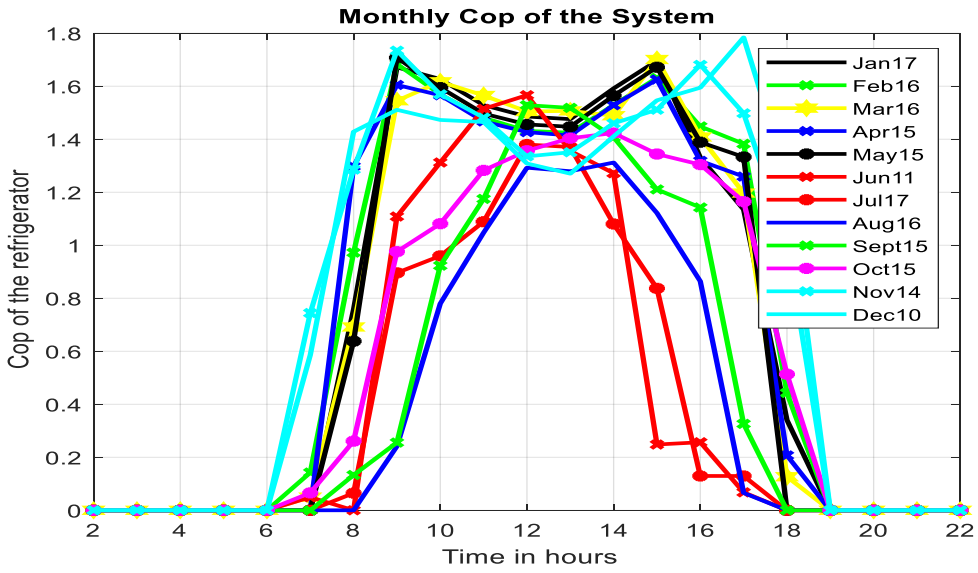

Figure 6-27. Monthly average hourly coefficient of performance for constant cooling

Figure 6.27 above shows coefficient of performance of the system by using constant cooling and mass flow rate throughout a year.

Table 6-1. Cop of the system using compressor specification tabulated values

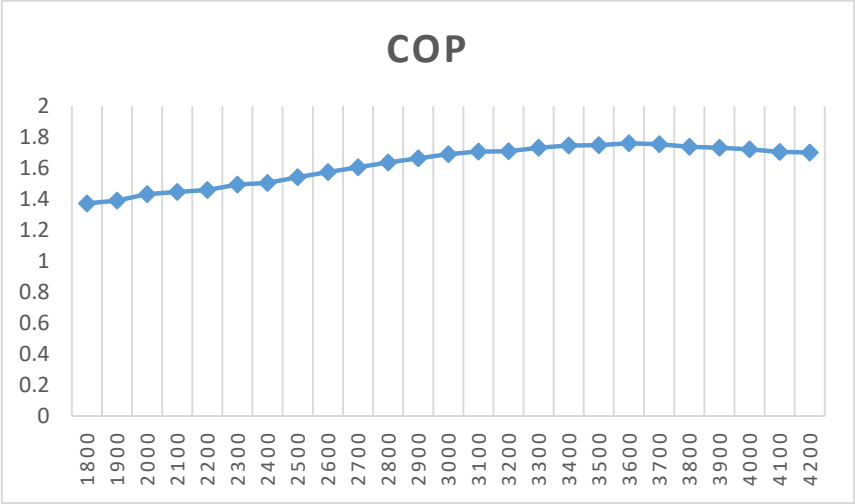

6.4 Validation of the computational result

The computation result could be compared with other experimental research work. Petros J. [1] studied experimentally and the system is capable to produce 4.5kg ice with 3KWh/m^2 and 17 kg of ice with 7.5 KWh/m^2 per day. In this research 8.5kg of ice is produced with 5KWh/m^2 per day and using interpolation gives 10kg ice which variation of 1.5kg ice. The variation is due to solar radiation of the location, which is in this system the computation uses the monthly average daily solar radiation and ice formation varies with each month of the year. Thus, 8.5 kg of ice is minimum amount of ice produced within a year.

CHAPTER SEVEN

7. Conclusion and Recommendation

7.1 Conclusion

The slab ice formation system for milk cooling, which is directly powered by a photovoltaic array was designed and simulated using Matlab code. The solar data for Semera region has been collected and analyzed from Ethiopian Metrology Agency and the hourly solar radiation data was used for the simulation of monthly average solar radiation on inclined surface, PV surface temperature, electrical energy output of the PV, transient nodal temperature variation of water, ice crystal formation and percentage of solid ice formation has been obtained by using MATLAB code simulation. In addition to these electrical characteristics of the AS-6M24, 220W power and 4.6 m^2 PV panel area was enough to run the CASCADE17-0244Y3 variable speed DC compressor and hourly performance of slab ice formation system was investigated by using the monthly average solar radiation data and using cooling load calculated from performance coefficient and performance equation integrated with electrical energy generated from solar pv system. In addition to this, implementation of this technology was vital especially in the areas where grid supply is unavailable or at long distance as most milk production areas, in order to preserve the milk for better use. From the Matlab simulation result minimum water temperature for each month of the year were observed between -6℃ which is for highly performed months and -3℃ for minimum performance months. And also ice crystal growth from minimum thickness of 0.036 meter to maximum thickness of 0.04 meter throughout the year.

7.2 Recommendation

In this paper, mathematical modeling of phase change material solidification and PV components and MATLAB simulation for the hourly performance evaluation of the system has been done by using batch ice making system.

The following points are recommended for future work:

- ✓ Experimental analysis of the prototype is needed to validate the theoretical modeling on the performance of the PV ice formation.

- ✓ Mathematical modeling of phase change material solidification and MATLAB simulation for hourly performance evaluation of the system by using continuous ice making system.
- ✓ For higher output of the PV panel, it is better to design a solar panel that follows tracking system to enhance the harvesting of solar irradiation for higher electricity production.
- ✓ For this research numerical model of water solidification was based on transient explicit conduction type heat transfer inside the tank, but for more accuracy of the result natural convection type of heat transfer also consider inside the water tank.

References

[1] Petros J. Axaopoulos, Michael P. Theodoridis, "Design and experimental performance of a pv Ice maker without battery," *Solar energy,* p. 1360 – 1369, 2009.

[2] D. MacPhee, "performance investigation of various cold thermal energy storage," University of Ontario Institute of Technology, 2008.

[3] S. Heimann, "Renewable Energy in Ethiopia, 13 Months of Sunshine for a sustainable development," addis ababa, 2007.

[4] A. M. A., "experimental study of a multi - purpose photovoltaic refrigeration system," *International journal of physical sciences,* vol. 67, pp. 46-57, 2011.

[5] A. Nasir, A. Mohammed, A. S. Adegoke, H. T. Abdulkarim, "Design and Performance Evaluation of an Ice Block Making Machine," *ARPN Journal of science and technology,* vol. 3, 2013.

[6] Rodrigo A. Jordan, Luís A. B. Cortez, Vivaldo Silveira Jr., Mário E. R. M. Cavalcanti- Mata, Fellipe D. de Oliveira, "Modelingand testing of an ice bankfor milk cooling after milking," *Journal of the brazilian Association of Agricultural engineering,* vol. 38, pp. 510-517, 2018.

[7] Robert Foster, Brian Jensen, Brian Dugdill, Bruce Knight,, Abdul Faraj, Johnson Kyalo Mwove, and Wendy Hadley, "Solar Milk Cooling: Smallholder Dairy Farmer Experience in Kenya," in *Solar World Congress*, korea, Daegu, 2015.

[8] Amrat lal Basediya & D. V. K. Samuel & Vimala Beera, "Evaporative cooling system for storage of fruits and vegetables - a review," *journal of Food Science Technology) ,* p. 429–442, 2013.

[9] Mohamed A.M. Ahmed, Simeon Ehui, and Yemesrach Assefa, "Dairy Development in Ethiopia," International Food Policy Research Institute, Washington, DC 20006 U.S.A., 2004.

[10] I. F. Titiladunayo, R. A. Shittu, "Design of a Microcontroller Based Automated Ice-cube Making Machine," *International Journal of Engineering and Applied Sciences (IJEAS),* vol. 5, no. 10, 2018.

[11] G. D. Ashton, "Thin Ice Growth," *Water resources research,* vol. 25, pp. 564-566 , 1989.

[12] L. G. SOCACIU, "Thermal Energy Storage with Phase Change Material," *Leonardo Electronic Journal of Practices and Technologie,* pp. 75-92, 2012.

[13] Akhil Johnson, Dr.J. Hussain, "Numerical Analysis of Thermal Storage Systems Using Phase Change Material," *International Journal of Mechanical and Industrial Technology,* pp. 85-97, 2016.

[14] Atul Sharma, V.V. Tyagi, C.R. Chen, Buddhi , "Review on thermal energy storage with phase change materials and applications," *Renewable and Sustainable Energy Reviews,* vol. 13, pp. 318-345, 2009.

[15] V. R. VOLLER AND C . R. SWAMINATHAN, "fixed grid techniques for phase change problems: A review," *international journal for numerical methods in Engineering ,* vol. 30, pp. 875-898, 1990.

[16] THEODORE L. BERGMAN, ADRIENNE S. LAVINE, FRANK P. INCROPERA, DAVID P. DEWITT, Fundamentals of mass and heat transfer, Los Angeles, Notre Dame.

[17] Antonio Caggiano , Christoph Mankel and Eddie Koenders, "Reviewing Theoretical and Numerical Models for PCM-embedded Cementitious Composites," *Buildings ,* p. 26, 2018.

[18] ANANE, SOLOMON KOFI, "Development of an energy efficient stand-alone solar photovoltaic DC refrigerator for off-grid communities," Kwame Nkrumah University of Science and Technology, Kumasi, Ghana, 2015.

[19] L. Hosseini, "Design and Analysis of a Solar Assisted Absorption Cooling System Integrated with Latent Heat Storage," Delft University of Technology, Delft, 2011.

[20] Yongfeng Xu, Ming Li, and Reda Hassanien Emam Hassanien, "Energy Conversion and Transmission Characteristics Analysis of Ice Storage Air Conditioning System Driven by Distributed Photovoltaic Energy System," *International journal of photo energy,* p. 17, 2016.

[21] Y. F. Xu, M. Li, X. Luo, Y. F. Wang, Q. F. Yu, H. E. Hassaniem, "performance analysis of ice storage air conditioning system driven by distributed photovoltaic energy," *Bulgarian Chemical Communications,* vol. 48, p. 165 – 172., 2016.

[22] Ahmet FERTELLİ, Orhan BÜYÜKALACA and Alper YILMAZ, "Ice formation around a horizontal tube in a rectangular vessel," *J. of Thermal Science and Technology,* vol. 29, no. 2, pp. 75 -87, 2009.

[23] P. Lamberg, "Approximate analytical model for two-phase solidification problem in a finned phase-change material storage," *Applied Energy,* no. 77, p. 131–152, 2004.

[24] Anish Modi, Anirban Chaudhuri, Bhavesh Vijay, Jyotirmay Mathur, "Performance analysis of solar photovoltaic operated domestic refrigerator," *applied energy,* vol. 86, p. 2583 – 2591, 2009.

[25] Xie. J., Yuan. C.,, "Numerical study of thin layer ring on improving the ice formation of building thermal storage system," *Applied thermal engineering,* vol. 69 (1), pp. 46-54, 2014.

[26] Y. Yusufoglu, T. Apaydin, S. Yilmaz, H.O. Paksoy,, "Improving performance of household refrigerators by incorporating phase change materials.," *International journal of refrigeration,* vol. 57, pp. 173 - 185, 2015.

[27] Asmaa Ahmed M. El-Bahloul, Ahmed Hamza H. Alia, Shinichi Ookawara, "Performance and sizing of solar driven dc motor vapor compression refrigerator with thermal storage in hot

arid remote areas," *International Conference on Solar Heating and Cooling for Buildings and Industry,* vol. 70, p.) 634 – 643, 2015.

[28] V. V. Truong, "Direct numerical simulations of solidification with effects of density difference," *Vietnam Journal of Mechanics,* vol. 38, p. 193 – 204 , 2015.

[29] Victor Torres – Toledo, Klaus Meissner, Alberto Coronas, Joachim Muller., "Performance characterization of small milk cooling with ice storage for pv application," *International journal of refrigeration,* vol. 60, p. 81 – 91, 2015.

[30] Ismail, K., P. Silva, and F. Lino, "Enhancement of solidification of PCM Around finned tubes, modeling and validation," vol. 06, pp. 49-63, 2016.

[31] Victor Torres – Toledo, Klaus Meissner, Philip Taschner, Santiago Martinez – Ballester, Joachim Muller., " Design and performance of a small – scale solar ice maker based on a DC – freezer and an adaptive control unit," *Solar energy,* vol. 139, pp. 139 - 443, 2016.

[32] Jannesari, H., Abdollahi. N, "Experimental and numerical study of thin ring and annular fin effects on improving the ice formation in ice-on-coil thermal energy storage system," *Applied energy,* vol. 189, pp. 369-384., 2017.

[33] S. Bakhshipour, M.S. Valipour , Y. Pahamli, "Parametric analysis of domestic refrigerators using PCM heat exchanger," *International journal of refrigeration ,* vol. 87, pp. 1-13, 2017.

[34] Hani Hussein Sait, "Design and analysis of flooded tube for cold energy storage," *international journal of refrigeration,* vol. 94, pp. 151-160, 2018.

[35] O. Mah, "Fundamentals of Photovoltaic Materials," *National Solar Power Reasearch Institute, Inc.,* 1998.

[36] Mboumboue Edouard, Donatien Njomo, "Mathematical Modeling and Digital Simulation of PV Solar Panel using MATLAB Software," *International Journal of Emerging Technology and Advanced Engineering,* vol. 3, no. 9, 2013.

[37] Wafaa ABD EL-BASIT1, Ashraf Mosleh ABD El–MAKSOOD, Fouad Abd El-Moniem Saad SOLIMAN, "Mathematical Model for Photovoltaic Cells," *Leonardo Journal of Sciences,* vol. 23, pp. 13-28, 2013.

[38] P. Simhachalam, "Design Analysis of Photovoltaic (Cell, Module, Array) By Using Matlab/Simulink," *Imperial Journal of Interdisciplinary Research (IJIR),* vol. 2, no. 7, 2016.

[39] Ravi Prakash, Sandeep Singh, "Designing and Modelling of Solar Photovoltaic Cell and Array," *IOSR Journal of Electrical and Electronics Engineering,* vol. 11, pp. 35-40, 2016.

[40] M.B. Eteiba, E.T. El Shenawy, J.H. Shazly and A.Z. Hafez, "A Photovoltaic (Cell, Module, Array) Simulation and Monitoring Model using MATLAB/GUI Interface," *International Journal of Computer Applications ,* vol. 69, 2013.

[41] Gajanan Deshmukh, Preeti Birwal, Rupesh Datir and Saurabh Patel, "Thermal Insulation Materials: A Tool for Energy Conservation," *Journal of Food processing technology ,* vol. 8, p. 5, 2017.

[42] P. Bhargavi, Dr. Radha Gupta, Dr. K. Rama Narasimha, "Effect of Stefan number on Temperature distribution, solidification thickness and solidification rate in a closed encloser".

[43] Henry Huy and Stavros A Argyropoulos, "Mathematical modelling of solidification and melting: a review," *Modelling Simul. Mater. Sci. Eng.,* vol. 4, p. 371–396, 1996.

[44] Maneeratana, Rotchana Prapainop and Kuntinee, "Simulation of ice formation by the finite volume method," *Songklanakarin J. Sci. Technol,* vol. 26, pp. 55-70, 2004.

[45] Robert Dyja, Elzbieta Gawronska, Andrzej Grosser, Piotr Jeruszka and Norbert Sczygiol, "Comparison of Different Heat Capacity Approximation in Solidification Modeling," *Proceedings of the World Congress on Engineering and Computer Science,* vol. 2, 2015.

[46] Anna Machniewicz, Dariusz Heim , "Modeling of latent heat storage in PCM modified components," *Technical Transection ,* 2014.

[47] Mehmet Esen and Teoman Ayhan, "Development of a model compatible with solar assisted cylindrical energy storage tank a n d variation of stored energy with time for different phase change materials," *Elsevier Science Ltd ,* vol. 37, 1996.

[48] J. Dallaire, "modeling of solid liquid phase change: the effects of density variation on phase change material solidification," in *Laval university*, 2017.

[49] M. N. Ozisik, Heat Conduction, wiley-Interscience, 1993.

[50] Ismail Baklouti, Zied Driss and Mohamed S. Abid, "Estimation of solar radiation on horizontal and inclined surfaces in Sfax, Tunizia," *ResearchGate ,* p. 13, 2012.

[51] M. Ravi Kumar, B. Bala Sai Babu, M. Seshu, "Estimation of Average Solar Radiation on Horizontal and Tilted Surfaces for Vijayawada Location," *IOSR Journal of Electrical and Electronics Engineering,* vol. 11, no. 3, pp. 43-53, 2016.

[52] K. Parkavi Kathirvelu, B. Viswanathan, "Estimation of Optimum Tilt Angle of PV Panel for Maximum Energy Harvesting," *International Journal of Electrical and Computer Engineering (IJECE),* vol. 6, p. 10, 2016.

[53] Tamps C, Coulson L., "Solar radiation incident upon Solar radiation incident upon," *Solar Energy,* p. 19, 1977.

[54] Unwaha, J.I Jones, N. D. Musa, A.J., "Design of Off - Grid Solar Photovoltaic (PV) System for Cottage hospital," *Journal of Energy Technologies and Policy,* vol. 6, 2016.

[55] Seyedeh Sepideh Ghaffari & Seyed Ali Jazayeri, "The Design of a Shell-Tube Heat Exchanger as Evaporator an Absorption Chiller Cycle to Reduce the Temperature of the Air Entering a

Diesel Engine Operating at Full Load Engine Medium," *Modern Applied Science,* vol. 9, 2015.

[56] NARALE P.D. BHOSALE SAGAR S. DHUMAL VISHAL B, BHOSALE DNYANESHWAR S and KHARADE KALYAN B, "Design and analysis of domestic refrigerator usinglpg cylinder," *International Journal of Research Publications in Engineering and Technology,* vol. 3, 1017.

[57] Håkon Selvnes1, Yosr Allouche1, Alexis Sevault2, Armin Hafner1, "CFD modeling of ice formation and melting in horizontally cooled and heated plates," in *Advances in Thermal Energy Storage*, Norway.

APPENDIX

Appendix-A: Thermophysical properties of water, ice and R-134a

Thermophysical properties of matter (in this case ice and refrigerant -134a), from heat transfer book (incropera, fundamentals of heat and mass transfer)

Description/ Composition	**Temperature (k)**	**Density, ρ $\frac{kg}{m^3}$**	**Thermal Conductivity, k $w/m.k$**	**Specific Heat, C_p $J/kg.k$**
Ice	273	920	1.88	2040
	253	…	2.03	1945
Leather (sole)	300	998	0.159	…
Paper	300	930	0.180	1340
Paraffin	300	900	0.240	2890

Saturated liquid R-134a (C2H2F4) Thermophysical properties

T(k)	ρ, kg/m^3	$C_{p.}$ $kJ/kg.k$	$\mu, 10^{-6}$, $N.s/m^2$	$v, 10^{-6}$, m^2/s	$k, 10^{-3}$, $w/m.k$	$\alpha, 10^{-6}$, m^2/s	Pr	$\beta, 10^{-3}$, k^-,
R-134a								
230	1426.8	1.249	0.04912	0.3443	112.1	0.629	5.5	2.02
240	1397.7	1.267	0.04202	0.3006	107.3	0.606	5.0	2.11
260	1337.1	1.308	0.03166	0.2368	97.9	0.560	4.2	2.36
270	1305.1	0.02775	0.2127	93.4	0.537	0.537	4.0	2.53
280	1271.8	1.361	0.02443	0.1921	89.0	0.514	3.7	2.73
290	1236.8	1.393	0.02156	0.1744	84.6	0.491	3.5	2.98

300	1199.7	1.432	0.01905	0.1588	80.3	0.468	3.4 3	3.30
310	1159.9	1.481	0.01680	0.1449	76.1	0.443	3.3	3.73
320	1116.8	1.543	0.01478	0.1323	71.8	0.417	3.2	4.33
330	1069.1	1.627	0.01292	0.1209	67.5	0.388	3.1	5.19
340	1015.0	1.751	0.01118	0.1102	63.1	0.355	3.1	6.57

Properties of common liquids, solids and foods

	Boiling data at 1atm		Freezing data		Liquid properties		
Substance	Normal boiling point (℃)	Latent heat of vaporization h_{fg} kJ/kg	Freezing point ℃	Latent heat of fusion $h_{if,}$ kJ/kg	Temperature ℃	Density (ρ) $,\frac{kg}{m^3}$	Specific heat C_p $kJ/kg.k$
ammonia	-33.3	1357	-77.7	322.4	-33.3	682	4.43
Octane	124.8	306.3	-57.5	180.7	20	703	2.10
R.134a	-26.1	217.0	-96.6	-	-50	1443	1.23
					-26.1	1374	1.27
					0	1295	1.34
					25	1207	1.43
Water	100	2257	0.0	333.7	0	1000	4.22
					25	997	4.18
					50	988	4.18
					75	975	4.19

Thermophysical properties of saturated water

Tempe-rature	Pressure	Specific Volume		Heat of Vaporization	Specific heat $kJ/kg.k$		Viscosity $N.s/m^2$	
T, (k)	P (bars)	$v, 10^3$ $\frac{m^3}{kg}$	v_g $\frac{m^3}{kg}$	h_g kJ/kg	$C_{p.}$	$C_{p.g}$	μ, 10^{-6},	μ_g, 10^{-6},
273.15	0.00611	1	206.3	2502	4.217	1.854	1750	8,02
285	0.01387	1	99.4	2473	4.189	1.861	1225	8.49
295	0.02617	1.002	51.94	2449	4.181	1.868	959	8.89
305	0.04712	1.005	29.74	2426	4.178	1.877	769	9.29

Thermal Conductivity, $w/m.k$		Prandtl Number		Surfaces tension N/m	Expansion coeff- k^-,
$k, 10^{-3}$	$k_g, 10^{-3}$,	pr	pr_g	$\alpha, 10^{-3}$	$\beta, 10^{-3}$,
569	18.2	12.9	0.815	75.5	-68.05
590	18.9	8.81	0.833	74.3	114.1
606	19.5	6.62	0.849	72.7	227.5
620	20.1	5.2	0.865	70.9	320.6

Appendix-B: Performance Coefficients (24V) - CASCADE17-0244Y3 VSDC ARI HBP

Coefficient	capacity (BTU/Hr)	Power (watt)	current (Amp)	Mass flow (Lbs/Hr)
C1	-1.107663E+03	3.943455E+02	1.643106E+01	-9.435642E+00
C2	-1.300685E+00	-1.223476E-01	-5.097817E-03	-2.856467E-02

C3	2.056291E-04	2.942926E-05	1.226219E-06	4.165405E-06
C4	-4.706144E-08	-2.445508E-10	-1.018962E-11	-7.435971E-10
C5	-7.624835E+01	-3.826043E+00	-1.594184E-01	-1.22214E+00
C6	1.678044E-01	4.168358E-02	1.736816E-03	2.49009E-03
C7	-8.433469E-04	3.524107E-05	1.468377E-06	-1.285188E-05
C8	7.156981E+01	-7.588050E+00	-3.161687E-01	1.008043E+00
C9	-8.933099E-01	5.706575E-02	2.37774E-03	-1.319664E-02
C10	3.539651E-03	-1.815833E-04	-7.56597E-06	5.237502E-05
C11	-4.128949E-04	-3.801532E-05	-1.583972E-06	-6.920254E-06
C12	-4.984281E-08	6.986678E-09	2.911116E-10	-6.890584E-10
C13	-1.084624E-06	2.132993E-07	8.88747E-09	-1.17853E-08
C14	2.881196E-06	-3.587806E-08	-1.494920E-09	4.61944E-08
C15	1.522813E-02	3.822661E-03	1.592776E-04	2.726404E-04
C16	1.794408E-02	1.206820E-03	5.028417E-05	3.516805E-04
C17	1.602984E+00	2.213781E-02	9.224086E-04	2.472096E-02
C18	5.350873E-06	-5.583706E-07	-2.326544E-08	7.28394E-08
C19	1.647996E-04	-2.041318E-05	-8.505493E-07	1.97087E-06
C20	1.730062E-06	-2.468870E-07	-1.028696E-08	1.98959E-08
C21	-1.230301E-04	1.131317E-06	4.713821E-08	-1.980280E-06
C22	-6.058412E-04	-4.793339E-04	-1.997224E-05	-6.54666E-06
C23	-8.010951E-03	2.484762E-04	1.035318E-05	-1.213048E-04

Appendix-C: Performance equation of 24V CASCADE17-0244Y3 compressor at ARI HBP test condition

$$Y = C_1 + C_2X_1 + C_3X_1^2 + C_4X_1^3 + C_5X_2 + C_6X_2^2 + C_7X_2^3 + C_8X_3 + C_9X_3^2 + C_{10}X_3^3 + C_{11}X_1X_2X_3 + C_{12}X_1^2X_2X_3 + C_{13}X_1X_2^2X_3 + C_{14}X_1X_2X_3^2 + C_{15}X_1X_2 + C_{16}X_1X_3 + C_{17}X_2X_3 + C_{18}X_1^2X_2 + C_{19}X_1X_2^2 + C_{20}X_1^2X_3 + C_{21}X_1X_3^2 + C_{22}X_2^2X_3 + C_{23}X_2X_3^2$$

1 Watt = 3.41214BTU /Hr (British thermal unit), and

1 kilogram per second = 7936.647pounds per hour

$X_1 =$ RPM

$X_2 =$ Evaporator temperature in degree Fahrenheit

$X_3 =$ Condenser temperature in degree Fahrenheit

$C_1 - C_{23}$: The performance coefficient of 24V CASCADE17-0244Y3 compressor like refrigerant mass flow rate, cooling capacity, current consumption, power consumption.

Appendix-C: 2D view of system major components

a. Slab Ice tank

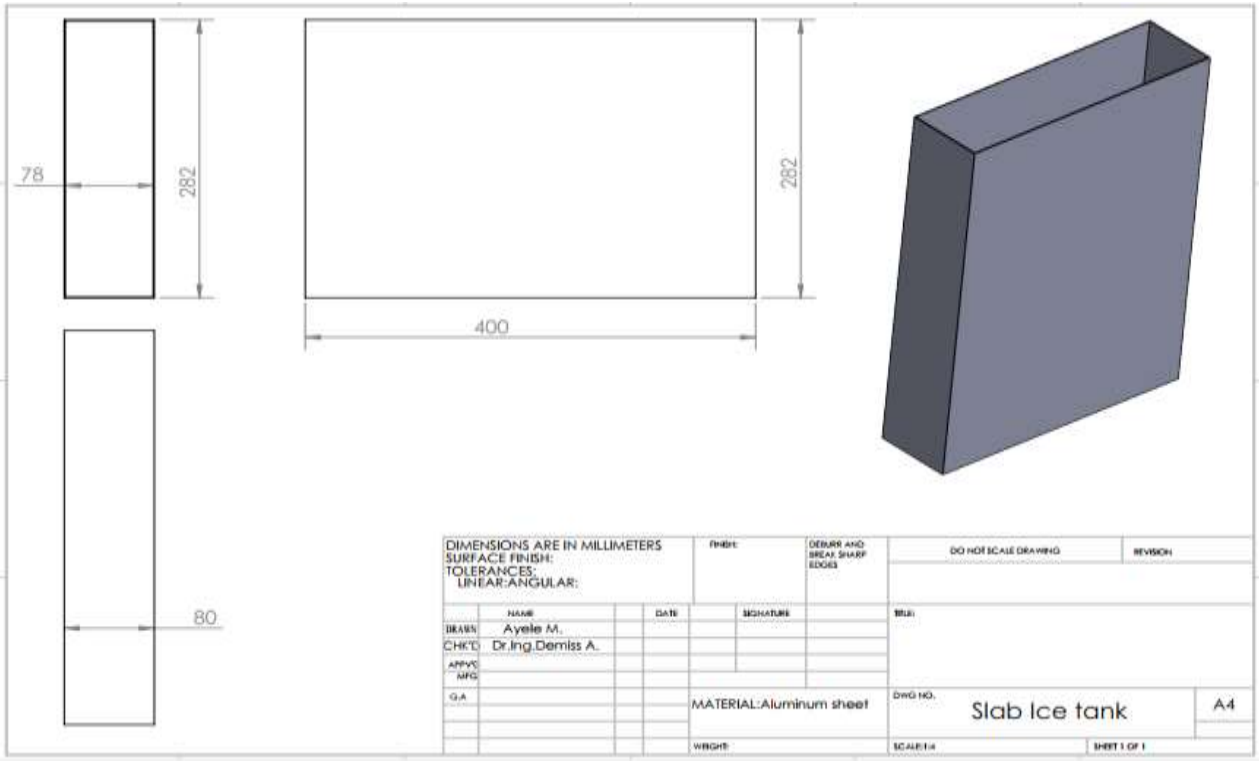

b. Slab Ice tank Insulation foam

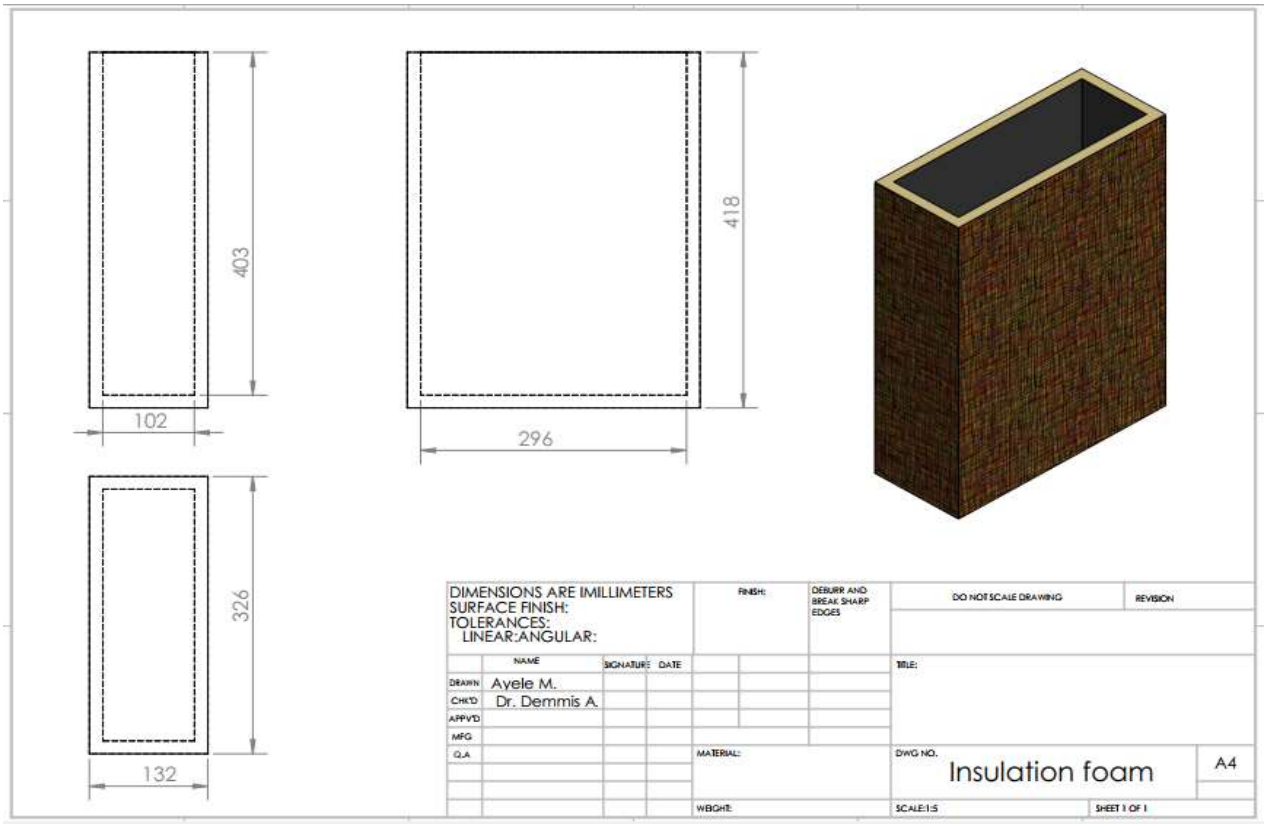

c. Slab Ice tank outer cover Aluminum sheet

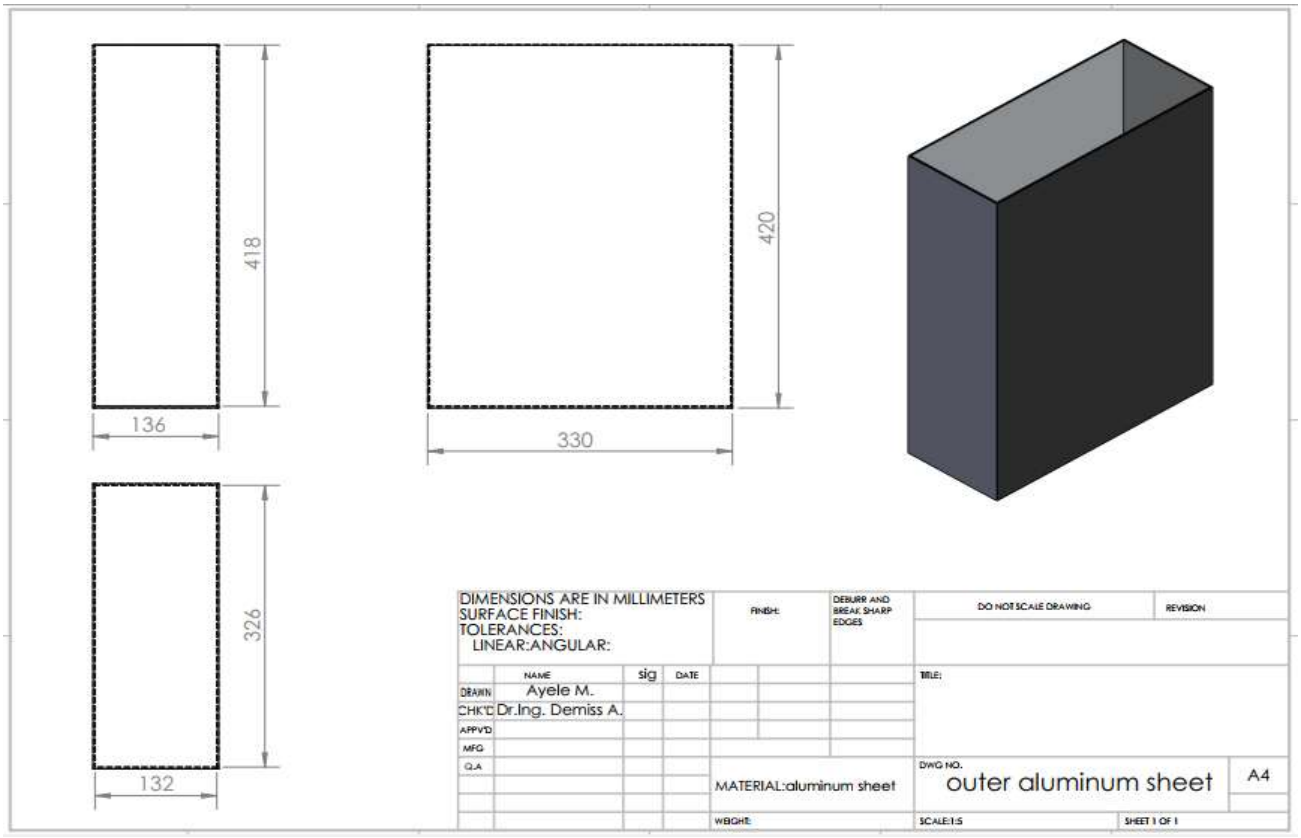

d. Slab Ice tank Inner cover plastic panel

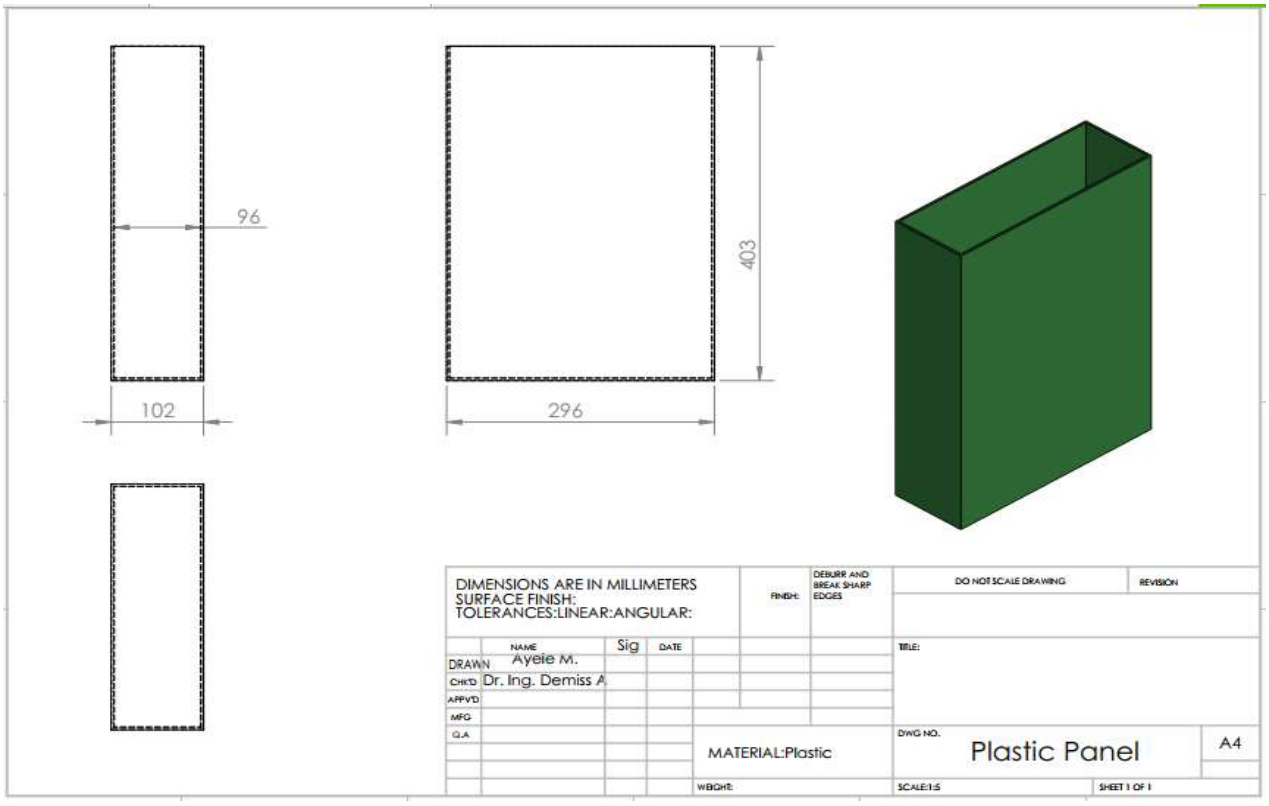

e. One side Evaporator for ice formation

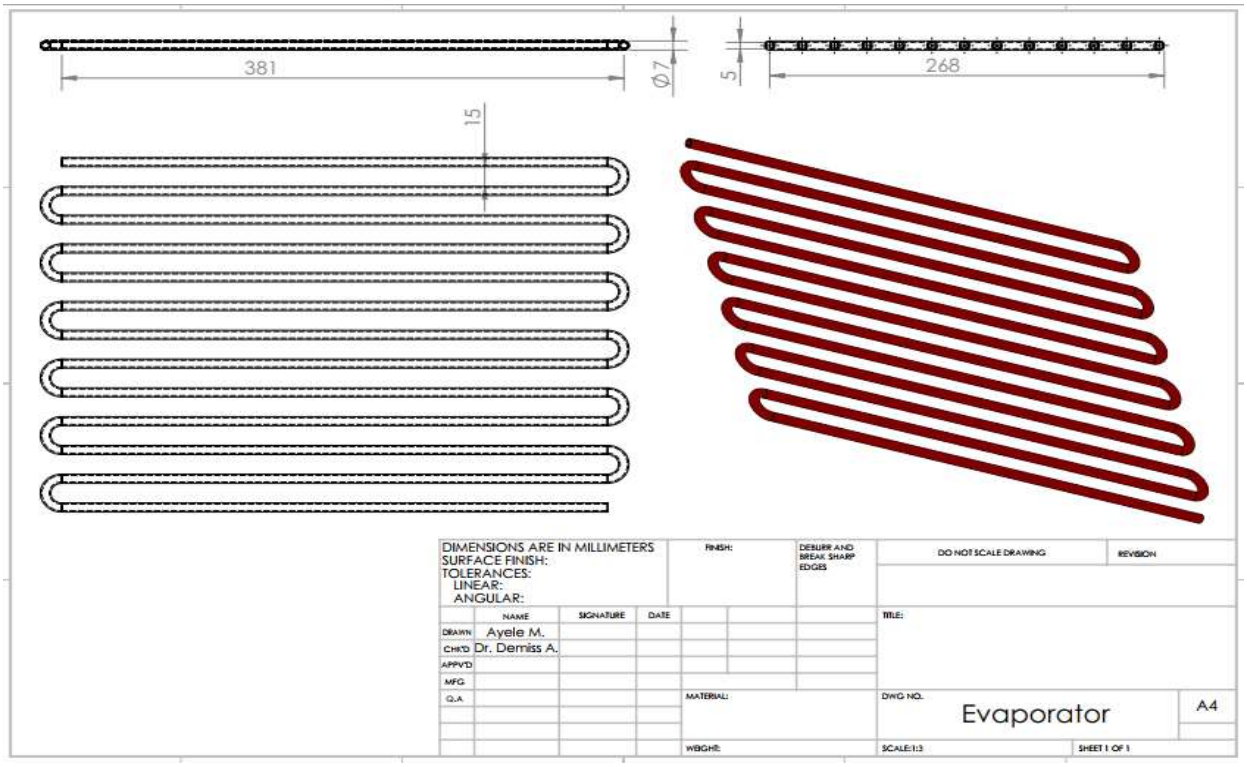

f. Condenser for ice formation

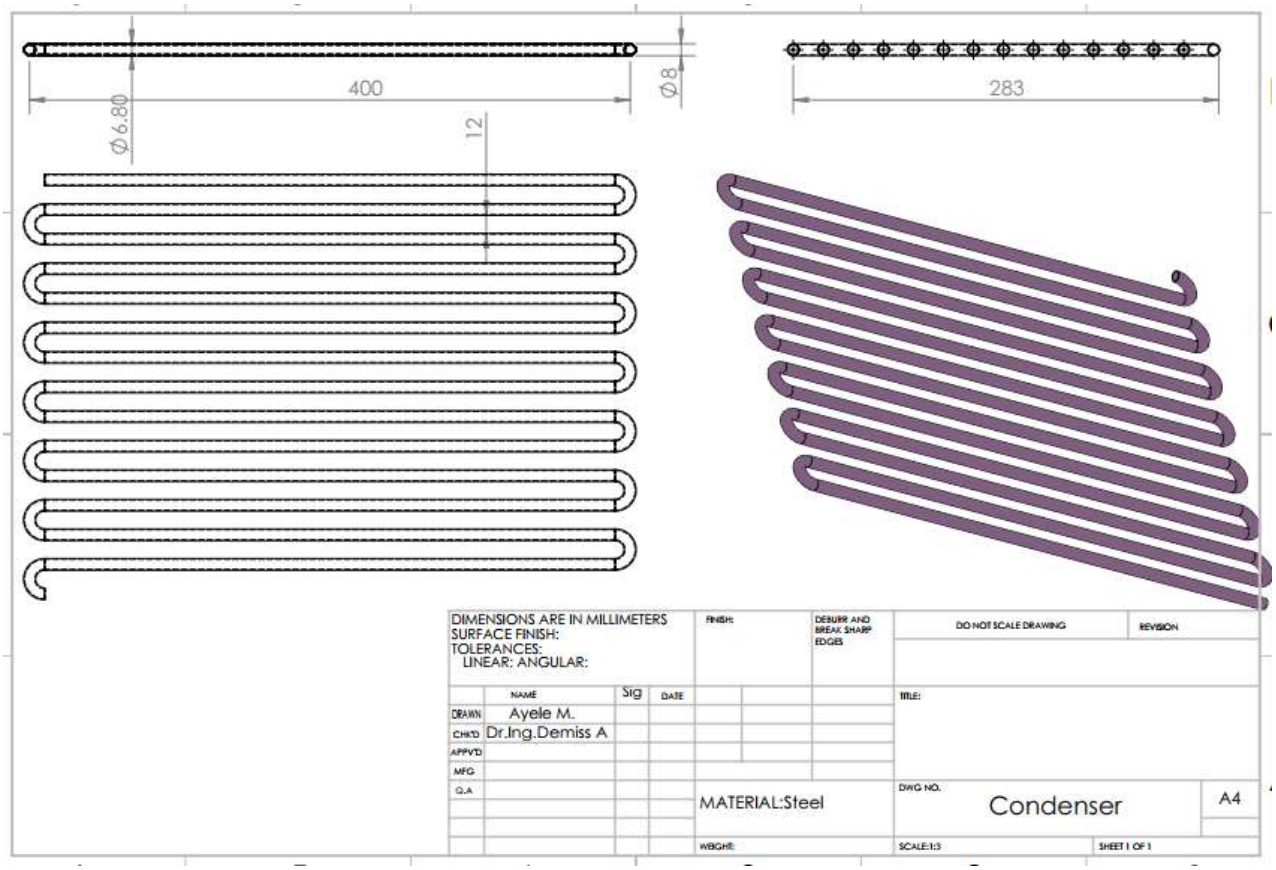

g. Solar panel

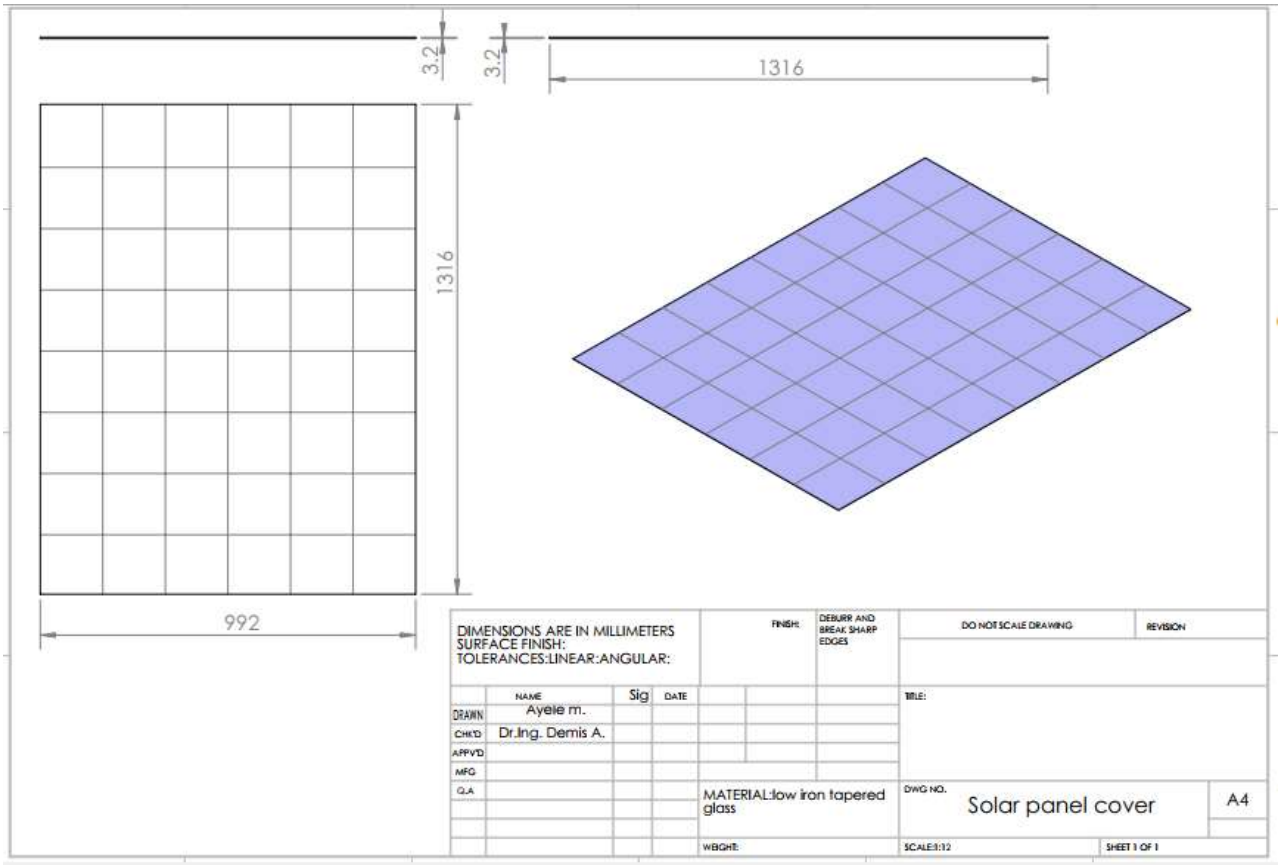

Appendix – D: Mat-lab code developed to model monthly average hourly solar radiation, PV surface temperature, electrical energy output, nodal temperature distribution of water, ice crystal formation with time, COP of the system and percentage of ice formation

```
clc
clear
close all
T2=49; %%%% condenser temperature in [0C]
Te=-7; %%% Temperature of evaporator in [0C]
Tmilk=33;%%%day time milk temperature in [0C]
Tm=4;%%%%required minimum milk temperature in [0C]
Tff=0;%%% phase change temperature in [0C]
Twater=33;%%% Initial temperature of water in the ice tank in [0C]
Tmm=18.5;%%%%% average milk temperature between 33 and 4 0c in 0c
Tff1=16.5;%%%%% average water temperature between 33 and 0 0c  in 0c
Mm=51.75; %%%mass of the milk in [kg]
Mice=8.5; %%%mass of the ice in [kg]
%%% Thermophysical properties of r-134a at refrigerant temperature
cprl=1323; %%%%% Specific heat of saturated liquid refrigerant (J/Kg.k)
rhorl=1317.9; %%%%%%density of saturated liquid refrigerant [kg/m3]
dyrl = 0.00029314; %%%%%Dynamic viscosity of saturated liquid refrigerant(kg/m s)
krl=0.0952; %%%%% thermal conductive of saturated liquid refrigerant(w/mk)
prl=4.04;%%%%% Prandtl number of saturated liquid refrigerant
```

```
cprv=811.5; %%%% Specific heat of saturated vapour refrigerant (J/kg.k)
rhorv=10.047 ; %%%%density of saturated vapour refrigerant [kg/m3]
dyrv = 0.00001033; %%%%Dynamic viscosity of saturated vapour refrigerant(kg/m s)
krv=0.010665; %%%%% thermal conductive of saturated vapour refrigerant(w/mk)
cprm=985.4; %%%%% Specific heat of saturated L-V refrigerant (J/Kg.k)
rhorm=455; %%%mean density of saturated L-V refrigerant [kg/m3]
dyrm =0.00010649; %%%%mean dynamic viscosity of saturated L-V refrigerant(kg/ms)
krm=0.03941; %% mean thermal conductive of saturated L-V refrigerant(w/mk)
prm=3.2; %%%%mean Prandtl number for saturated L-V refrigerant inside tube
mr = 0.002993; %%%%Mass flow rate of refrigerant (kg/s)
Vefc= 0.76; %%%%volumetric efficiency of the compressor
Mc=0.55; %%%%overall efficiency of compressor
Vcon=0.93; %%%%overall condenser efficiency
Vc= 9.63*10^-6; %%%%clearance volume of the compressor [m^3]
v1=0.099516; %%%%saturated specific volume of the refrigerant at compressor inlet
m^3/kg
s1=935.49; %%%%entropy at compressor inlet J/Kg.k
Tpv=0.035; %%%%Thickness of the PV module in [m]
Bti=0.015; %%%%Back insulation thickness in [m]
Trpv=0.1; %%%%Transmitivity of the PV module
hi=5; %%%%inner heat transfer coefficient storage tank w/m^2.k
ho=30; %%%%outer heat transfer coefficient storage tank w/m^2.k
sti = 0.015; %%%%  milk and ice storage tank insulation thickness in [m]
ki=0.023; %%%%thermal conductivity of storage insulator W/m.k
xp=0.003;%%% thickness of plastic panel in [m]
kp=0.22; %%%% thermal conductivity of plastic panel W/m.k
xAl=0.002;%%%% thickness of aluminum sheet m
kAl=237; %%% thermal conductivity of aluminum sheet W/m.k
Tair=37; %%% atmospheric air in [0C]
rhoi=50;%%%density of insulation [kg/m^3]
Cpi=1045;%%%%specific heat of insulation [J/kg.k]
rhoAl=2702;%%%density of aluminum [kg/m^3]
cpAl=903;%%%specific heat of aluminum [J/kg.k]
rhop=920;%%%%density of plastic [kg/m^3]
cpp=1900;%% specific heat of plastic J/kg.k
Xpipe=0.001; %%%thickness of evaporator pipe [m]
kcu=385;%%%%thermal conductivity of copper pipe W/m.k
Kice=2.5; %%thermal conductivity of ice W/m.k
cpair=1004;%% Specific heat capacity of air at temperature in J/kg.k
epv=0.83; %%%%Emissivity of the PV module
apv=0.9; %%%%Absorbability of PV module
egpv=0.9;%%% emissivity of glass
tapv=0.93; %%Difference b/n Absorptivity and Transmitivity of Module
eef=((1/epv)+(1/egpv)-1)^-1; %%%%Effective emissivity of PV
pf=0.9; %%%%Packing Factor
Tfp=-0.0043; %%%%Temperature coefficient of PV module
Nepv=0.1685; %%%%Nominal efficiency of PV module
Trf=25; %%%%Reference Temperature
ka=0.026; %%%%Thermal conductivity of air [W/m.k]
kpv=1.56; %%%%Thermal conductivity of pv W/m.k
```

```
Grho=0.2; %%%%Ground reflection
cg=1278.95; %%%%Glass specific heat
cppv=677; %%%% PV specific heat capacity  J/kg.k
mpv=15; %%%%mass of PV kg
Vw=3; %%%%wind speed m/s
beta=11.8*pi/180;%%% inclination angle
Lo =41;%% longitude of the site ° E
El = 433; %%%%elevation of the site m
phi=11.8*pi/180; %%Latitude of the site Semera
sigma=5.67e-8; %%Boltzmann constant
Tai=20; %%Initial Temperature of the atmosphere [0C]
Apv=4.60; %%%% Solar PV unit area m^2
Xice=0.02; %%% average thickness of ice [m]
%%% ice slab solidification temperature distribution
%%%Geometry parameters
%%% One side vertical surface area of the ice slab tank (m^2)
A1=0.29*0.4; %%%% 0.116m^2
%%% Two side vertical surface area of the ice slab tank (m^2)
A2=2*(0.29*0.4); %%%% 0.232m^2
%%% Total surface area of ice tank contact with milk in m^2
Aice=(2*(0.08*0.4)+2*(0.29*0.4))+0.08*0.29;%%% 0.3192m^2
tice=0.001;%%% thickness of ice tank aluminum in m
ht=0.4; %% height of the ice slab tank (m)
Vice=0.0092; %%%%% volume of ice slab tank (m^3)
Vmilk=0.0592; %%%%% volume of milk tank (m^3)
Lt = 0.04; %% half-length of ice tank (m)
Ltt=0.08;%%%total length of ice tank [m]
m=7; %%%%number of nodes in horizontal direction for half tank
mm=14;%%%%number of nodes in horizontal direction for total tank size
Np=26; %%%%% number of tube
Asti=0.5252; %%% outer surface area of storage ice tank [m^2]
%%% outer surface area of storage milk tank [m^2]
Astm=2*(0.45*0.31) +2*(0.45*0.425) +2*(0.31*0.425);
Ae=0.176; %%%area of the evaporator [m^2]
Ac=0.00001963; %%%% evaporator cross-section area [m^2]
doe=0.007; %%%outer diameter of the evaporator in [m]
die=0.005; %%%%inner diameter of the evaporator in [m]
Le=11; %%%% evaporator length in [m]
%%% heat transfer coefficient
TIQsolar=0; %%%%Initialization of solar radiation
vref=mr/rhorm;%%%refrigerant flow rate
Vmean=vref/Ac; %%% refrigerant mean velocity m/s
Re=2*mr/(pi*dyrm*die*Np); %%% Reynolds number of the tube flow refrigerant
Nu=3.66;%%% nusselt member
hr=(Nu*krm)/(2*die) ;%%% heat transfer coefficient of L-V refrigerant W/m^2 k
Tfinal=-4;%%%average final ice temperature in oC
TElec=0;
deltt=60;%%%% time step
%% Performance Coefficients (24V) - CASCADE17-0244Y3-ARI HBP
%%% column-1 capacity (BTU/Hr), column-2 power (watt), column-3 current (A)
```

```
%%% and column-4 mass flow (Lbs/Hr)
C=[-1.107663E+03   3.943455E+02   1.643106E+01   -9.435642E+00;
    -1.300685E+00   -1.223476E-01   -5.097817E-03   -2.856467E-02;
     2.056291E-04   2.942926E-05   1.226219E-06   4.165405E-06;
    -4.706144E-08   -2.445508E-10   -1.018962E-11   -7.435971E-10;
    -7.624835E+01   -3.826043E+00   -1.594184E-01   -1.22214E+00;
     1.678044E-01   4.168358E-02   1.736816E-03   2.49009E-03;
    -8.433469E-04   3.524107E-05   1.468377E-06   -1.285188E-05;
     7.156981E+01   -7.588050E+00   -3.161687E-01   1.008043E+00;
    -8.933099E-01   5.706575E-02   2.37774E-03   -1.319664E-02;
     3.539651E-03   -1.815833E-04   -7.56597E-06   5.237502E-05;
    -4.128949E-04   -3.801532E-05   -1.583972E-06   -6.920254E-06;
    -4.984281E-08   6.986678E-09   2.911116E-10   -6.890584E-10;
    -1.084624E-06   2.132993E-07   8.88747E-09   -1.17853E-08;
     2.881196E-06   -3.587806E-08   -1.494920E-09   4.61944E-08;
     1.522813E-02   3.822661E-03   1.592776E-04   2.726404E-04;
     1.794408E-02   1.206820E-03   5.028417E-05   3.516805E-04;
     1.602984E+00   2.213781E-02   9.224086E-04   2.472096E-02;
     5.350873E-06   -5.583706E-07   -2.326544E-08   7.28394E-08;
     1.647996E-04   -2.041318E-05   -8.505493E-07   1.97087E-06;
     1.730062E-06   -2.468870E-07   -1.028696E-08   1.98959E-08;
    -1.230301E-04   1.131317E-06   4.713821E-08   -1.980280E-06;
    -6.058412E-04   -4.793339E-04   -1.997224E-05   -6.54666E-06;
    -8.010951E-03   2.484762E-04   1.035318E-05   -1.213048E-04];
Tc=49; %%%temperature of Condenser in 0c
TE=-7; %%%temperature of Evaporator in 0c
h1=246300; %%%enthalpy at compressor inlet J/kg
h2=281600; %%%enthalpy at compressor outlet J/kg
h3=107320; %%% enthalpy at condenser inlet J/kg
h4=h3; %%%enthalpy at evaporator inlet J/kg
Wcom=h2-h1; %%%% isentropic work of the compressor in J/KG
x2=(TE*9/5)+32; %%%conversion of Evaporator temperature into Fahrenheit
x3=(Tc*9/5)+32; %%%conversion of condenser temperature into Fahrenheit
%%% constant terms with respect to x1, x1^2 and x1^3
kk=C(1,2)+C(5,2)*x2+C(6,2)*(x2)^2+C(7,2)*(x2)^3+C(8,2)*x3+C(9,2)*(x3)^2+...
C(10,2)*(x3)^3+C(17,2)*x2*x3+C(22,2)*(x2)^2*x3+C(23,2)*x2*(x3)^2;
%%%%%% coefficients of x1
kk1=C(2,2)+C(11,2)*x2*x3+C(13,2)*(x2)^2*x3+C(14,2)*x2*(x3)^2+C(15,2)*x2+...
C(16,2)* x3+C(19,2)*(x3)^2+C(21,2)*(x3)^2;
%%%%%% coefficients of x1^2
kk2=C(3,2)+C(12,2)*x2*x3+C(18,2)*x2+C(20,2)*x3;
%%%%%% coefficients of x1^3
kk3=C(4,2);
%%%% solar radiation
data1=zeros(24,3);
open=('GBR.xlsx');
Z=xlsread(open);
%%Data given for the global radiation, diffuse radiation and ambient temperature for 24
hours of each day for all day in the year
for j=1:365
```

```
data1(:,:,j)=Z(j+(23*(j-1)):j*24,:);
end
%%%%%%%%%%%%%%%%%%%%%%%%%%%%%%%%
 TFt=zeros(365,24);%% Last node Temperature of the water in storage tank
 TFt2=zeros(365,24);%% 2nd node Temperature of the water in storage tank
 TFt4=zeros(365,24);%% 4thnode Temperature of the water in storage tank
 TFt6=zeros(365,24);%% 6th node Temperature of the water in storage tank
 TFt8=zeros(365,24);%% 8th node Temperature of the water in storage tank
TFt10=zeros(365,24);%% Last node Temperature of the water in storage tank
xFt=zeros(365,24);%%last node Temperature of the water in storage tank
Ict=zeros(365,24);%%% solar energy generated from inclined pv panel
Tpt=zeros(365,24);%%Temperature of the pv
Et=zeros(365,24);%%electrical energy
omega=zeros(1,24);%%hour angle
decl=zeros(365,1);%% declination angle
copi=zeros(365,24);%% coefficient of performance
Tm1=zeros(365,24);%%Temperature of the milk during night
x1a = zeros(365,24); %% Ice thickness after one hour
x2a = zeros(365,24);%% Ice thickness after two hour
x3a = zeros(365,24);%% Ice thickness after three hour
x4 = zeros(365,24);%% Ice thickness after four hour
x5 = zeros(365,24);%% Ice thickness after five hour
x6= zeros(365,24);%% Ice thickness after six hour
%%imposition of initial condition
for r=1:m
T(1:r,1) = Twater; %%the initial temperature of water
x1a(1:r,1) =0; %% the initial ice thickness
x2a(1:r,1) =0; %% the initial ice thickness
x3a(1:r,1) =0; %% the initial ice thickness
x4(1:r,1) =0; %% the initial ice thickness
x5(1:r,1) =0; %% the initial ice thickness
x6(1:r,1) =0; %% the initial ice thickness
end
%Finite difference method explicitly discretization
%%%define property (thermal conductivity)
 %% variables
Tsolidus=-4; %% solidus temperature [0C]
Tliquidus=2; %% liquidus temperature [0C]
TSolidus=-0.35; %% solidus temperature [0C]
TLiquidus=0.35; %% liquidus temperature [0C]
s = 700; %%Number time steps
dt = 50; %%dt is time intervals
time=zeros(1,s+1);
time(1) = 0;
%%% thermal conductivity
ks = 2.5; %%%solid phase thermal conductivity (W/m.0C)
kl = 0.65; %%liquid phase thermal conductivity (W/m.0C)
%%%%define property (density)
rhos = 918; %%Solid phase density (kg/m^3)
rhol = 999; %%% liquid phase density (kg/m^3)
```

```
%%%%Specific heat capacity
cps = 2025; %%%Solid phase Specific heat capacity (J/kg.0C)
cpl = 4180; %%%liquid phase Specific heat capacity (J/kg.0C)
QL = 333700; %%%Latent heat of fusion (J/kg)
dTf=Tliquidus-Tsolidus; %%% freezing temperature interval(0c)
%%%%change in ice length
dx = Lt/(m-1);
%%%%%%%%%%%%%%%%%%%%%%%%%%%%
for n=1:365
decl(n)=(pi/180)*(23.45*sin((2*pi/365)*(284+n)));%%%Calculation of the declination
angle
end
for ii=1:24
omega(ii)=(ii-12)*15*pi/180; %%%Calculation of the hour-angle for each hour of the
day
end
for i=1:365
Grr=data1(:,1,i);
Drr=data1(:,2,i);
Taa=data1(:,3,i);
for j=1:24
Gr=Grr(j);%%Global solar radiation wh/m2
Dr=Drr(j);%%diffuse solar radiation wh/m2
Tx=Taa(j);%%ambient temperature
Ta=Tx;%%Ambient Temperature
Tpi=Tx+3;%% initial PV temperature
Tsky=Ta-6;%% sky temperature
pp=(cosd(phi-beta))*cosd(decl(i))*cosd(omega(j))+sind(decl(i))*(sind(phi-beta));
hh=(cosd(phi)*cosd(decl(i))*cosd(omega(j))+(sind(decl(i))*sind(phi)));
%%the ratio of average day of the beam solar radiation on a tilted surface to that of a
horizontal surface
Rb=pp/hh;
%%the beam solar radiation
Gb=Gr-Dr;
%%%the ratio of diffuse solar radiation on to a tilted surface to that of the horizontal
surface
Rd=0.5*(1+cosd(beta));
In=Rb*Gb+Dr*Rd+(0.5*Grho*((1-cosd(beta))*Gr));
%%% solar Energy arrived in the module and absorbed by module
Ic=In*apv;
Tf=(Tai+Tx)/2;%%%Film Temperature
Ve=2/(Tai+Tx);%%%Volume Expansion coefficient
hc1=2.8+3*Vw;%%%convective heat transfer coefficient at the top of the PV
%%%Radiation heat transfer b/n air and PV module
hr1=epv*sigma*(Tpi^4-Tsky^4);
a12=hc1+hr1;
Ut=((1/(hc1+hr1)))^-1; %%%top heat loss
Ul=Ut+a12;
%%%Initial Temperature of the PV
Tpm = 30 + 0.0175*(Ic-150) + 1.14*(Ta -25);
```

```
%%%Electrical Energy generation
Eg=Ic*Apv*tapv*pf*Nepv*((1-0.0045*(Tpi-Trf)));
%%PV surface temperature
Tp1=Tpi+(deltt*Apv*(Ic-Eg+(a12*Ta*2)-(a12*Tpi*2)))/(mpv*cppv);
end
end
%%Main Program
for i=1:365
Grr=data1(:,1,i);
Drr=data1(:,2,i);
Taa=data1(:,3,i);
 for y=2:s+1
T(r,y-1)=33;
T(r,y)=33;
x1a(r,y)=0;
x2a(r,y)=0;
x3a(r,y)=0;
x4(r,y)=0;
x5(r,y)=0;
x6(r,y)=0;
x1a(r,y-1)=0;
x2a(r,y-1)=0;
x3a(r,y-1)=0;
x4(r,y-1)=0;
x5(r,y-1)=0;
x6(r,y-1)=0;
 end
for j=1:24
Gr=Grr(j);
Dr=Drr(j);
Tx=Taa(j);
Ta=Tx;
pp=(cosd(phi-beta))*cosd(decl(i))*cosd(omega(j))+sind(decl(i))*(sind(phi-beta));
hh=(cosd(phi)*cosd(decl(i))*cosd(omega(j))+(sind(decl(i))*sind(phi)));
%%%the ratio of average day of the beam solar radiation on a tilted surface to that of a
horizontal surface
Rb=pp/hh;
if Rb<0
Rb=0.5;
end
Gb=Gr-Dr; %%% the beam solar radiation
%%%the ratio of diffuse solar radiation on to a tilted surface to that of the horizontal
surface
Rd=0.5*(1+cosd(beta));
In=Rb*Gb+Dr*Rd+(0.5*Grho*((1-cosd(beta))*Gr));
Ic=In*apv; %%%solar Energy arrived in the module and absorbed by module
if Ic<0
Ic=0;
end
Tp1=Tpi+(deltt*Apv*(Ic-Eg+(a12*Ta*2)-(a12*Tpi*2)))/(mpv*cppv);
```

```
TIQsolar=TIQsolar+In;
for jj=1:60
Tf=(Tai+Ta)/2; %Film Temperature
Ve=2/(Tai+Ta); %Volume expansion coefficient
Tsky=Ta-6; % sky temperature
hc1=2.8+3*Vw; %convective heat transfer coefficient at the top of the glass
hr1=epv*sigma*(Tp1^4-Tsky^4); %Radiation heat transfer b/n glass and PV module
Ut=((1./(hc1+hr1)))^-1; %%%top heat loss from the pv
a12=hc1+hr1;
Ul=Ut+a12; %Over all heat transfer coefficient of pv
%%%Initial Temperature of the PV module
Tpm =30+0.0175.*(Ic-150)+1.14*(Ta -25);
TElec=TElec+Eg*deltt/3600000;
tstep=60;
hwater=81.2;%%% water convective heat transfer coefficient W/m^2.k
%%%%overall heat transfer coefficient evaporator tube
Ue1=1/(Xpipe*die/(kcu*(die+doe)/2)+1/hr);
%%% overall heat transfer coefficient storage tank W/m^2.k
Ue2=1/(1/hwater +Xice/Kice);
%%% overall heat transfer coefficient evaporator and storage tank W/m^2 k
Ue=Ue1+Ue2;
%%% overall heat transfer coefficient for tank W/m^2.k
Ust=1/(1/hi +xp/kp +sti/ki +xAl/kAl +1/ho);
%%% overall heat transfer coefficient for ice tank to milk W/m^2.k
hii=5;
Um=1/(1/hii+tice/kAl+1/hwater);
%% Electrical Energy generation of the PV module
Eg=Apv*Ic*tapv*pf*Nepv*(1-0.0045*(Tp1-Trf));
%%% PV Surface Temperature
Tp1=Tpi+(deltt*Apv*(Ic-Eg+(a12*Ta*2)-(a12*Tpi*2)))/(mpv*cppv);
Tpi=Tp1;
Qcond=mr*(h2-h3);%%%% heat removal from condenser [watt]
%%%heat loss from milk and ice tank during milk cooling
Qstlossm=Astm*Ust*(Ta-Tm);
%%%heat loss from milk and ice tank during ice formation in watt
Qstlossi=Asti*Ust*(Ta-Tff1);
%%% storage tank material cooling load
Qst1=(Ta-Tff1)*Asti*((sti*rhoi*Cpi)+(xAl*rhoAl*cpAl)+(xp*rhop*cpp));
Qst=Qst1/(5*3600);%%%storage tank material cooling load in [watt]
%%% evaporator cooling capacity in [watt]
Qe=Ue*Ae*(Twater-Te);
 Wc=(h2-h1);%%% compressor work in watt
z=0;
%% roots of the performance equation relative to x1
aa=[kk3  kk2  kk1  (kk-Eg)];
x11=roots(aa);
x11=-x11(imag(x11)==0 & x11<122);
%%%%%% performance equation
for x1=length(x11)
 z=z+1;
```

```
Y=C(1,:)+C(2,:).*x1+C(3,:).*(x1).^2+C(4,:).*(x1).^3+C(5,:).*x2+C(6,:).*(x2).^2+...
C(7,:).*(x2).^3+C(8,:).*x3+C(9,:).*(x3).^2+C(10,:).*(x3).^3+C(11,:).*x1.*x2.*x3+...
C(12,:).*(x1).^2.*x2.*x3+C(13,:).*x1.*(x2).^2.*x3+C(14,:).*x1.*x2.*x3.^2+...
C(15,:).*x1.*x2+C(16,:).*x1*x3+C(17,:).*x2.*x3+C(18,:).*(x1).^2.*x2+...
C(19,:).*x1.*(x2).^2+C(20,:).*(x1).^2.*x3+C(21,:).*x1.*(x3).^2+...
C(22,:).*(x2).^2.*x3+C(23,:).*x2.*(x3).^2;
%%%performance Coefficient value of cooling capacity(watt)
%%% one Watt = 3.41214BTU/Hr (British thermal unit)
%%% one kilogram per second = 7936.647pounds per hour
Q(z,1)=Y(1)/3.41214;
%%%performance Coefficient value of mass flow rate(kg/s)
Q(z,4)=Y(4)/7936.6;
QE=(Q(z,4)*(h1-h4));
EG=Q(z,4)*(h2-h1);
%% Minimum operating power of the compressor
if Eg<280
  Q(z,1)=0;
end
if j>6 && j<18
  %% half cooling load and it varies with Eg in watt
Qeem=(Q(z,1)-Qstlossi-Qst)/2;
%% constant cooling load in watt
Qec=(Qe-Qstlossi-Qst);
%%cooling load with w/m^2
Qem=Qeem/Ae;
end
%%heat removed by the one side or lower evaporator only
if j>6 && j<18
qe=Qem;
else
    qe=0;
end
%% Minimum operating power of the compressor
if Eg<280
  qe=0;
end
effc(z)=(Q(z,4)*Wc)/(Eg);%%Isentropic efficiency of the compressor
if Eg<350
cop(z)=0;
else
cop(z)=(Qec)/(Eg*Mc); %% coefficient of performance
end
end
real k;%%thermal conductivity (W/m.0C)
%% calculation of k
if(T(r,y)>Tliquidus)
 k=kl;
elseif(T(r,y)<Tsolidus)
        k=ks;
    else
```

```
    k=ks+(kl-ks)*(T(r,y)-Tsolidus)/(Tliquidus-Tsolidus);
end
real rho;%%%density (kg/m^3)
%%%%%% calculation of rho
if(T(r,y)>Tliquidus)
 rho=rhol;
elseif(T(r,y)<Tsolidus)
       rho=rhos;
   else
    rho=rhos+(rhol-rhos)*(T(r,y)-Tsolidus)/(Tliquidus-Tsolidus);
end
real cp; %%%Specific heat capacity (J/kg.0C)
cpmush=QL/dTf;%%%Specific heat capacity in the mush region(J/kg.0C)
%%%calculation of cp
if(T(r,y)>Tliquidus)
 cp=cpl;
elseif(T(r,y)<Tsolidus)
       cp=cps;
   else
    cp=cpmush;
end
%%% calculation of alfa
alfal= kl/(rhol*cpl);%%% alfa value for liquid phase
alfas= ks/(rhos*cps);%%% alfa value for solid phase
alfarm = krm/(rhorm*cprm);%%% alfa value for refrigerant
real alfa; %%%values of alfa
if(T(r,y)>Tliquidus)
 alfa=alfal;
elseif(T(r,y)<Tsolidus)
  alfa=alfas;
   else
alfa=(ks+(kl-ks)*(T(r,y)-Tsolidus)/(Tliquidus-Tsolidus))./((rhos+(rhol-rhos)*(T(r,y)-
Tsolidus)/(Tliquidus-Tsolidus))*cpmush);
end
Bi = hr*dx/krm;%%% Biot number
%%% calculation of FO dimensionless time (Fourier number)
Fol = dt*alfal/((dx)^2);%%%%%Fo value for liquid phase
Fos = dt*alfas/((dx)^2);%%% Fo value for solid phase
Form = dt*alfarm/((dx)^2); %%%% Fo value for refrigerant
real Fo; %%%values of Fo
if (T(r,y)>Tliquidus)
  Fo=Fol;
elseif (T(r,y)<Tsolidus)
       Fo=Fos;
else
 Fo=dt*((ks+(kl-ks)*(T(r,y)-Tsolidus)/(Tliquidus-Tsolidus))./((rhos+(rhol-rhos)*(T(r,y)-
Tsolidus)/(Tliquidus-Tsolidus))*cpmush))/(dx)^2;
end
%%%define Bii
Biis=(dx)/ks;
```

```
Biil=(dx)/kl;
Biir=(dx)/krm;
real Bii; %%%values of alfa
if(T(r,y)>Tliquidus)
 Bii=Biil;
elseif(T(r,y)<Tsolidus)
       Bii=Biis;
   else
Bii=(dx)./(ks+(kl-ks)*(T(r,y)-Tsolidus)/(Tliquidus-Tsolidus));
end
%% Separating Thermophysical properties of water and refrigerant by nodes
real Foo; %%%values of Foo
for r = 1:m
if r<=m && r>1
  Foo=Fo;
  Bo=Bii;
else
 Foo=Form;
 Bo=Biir;
end
end
%%imposition of initial condition
for r=1:m
T(1:r,1) = Twater; %%the initial temperature of water
end
%%% water tank nodal temperature distribution calculation
for y = 2:s+1
 for r=1:m
  if j<=6
  T(r,y)=33;
  end
 if (j>6 && j<17)
   T(r,y-1)=T(r,y);
 if r==1
T(1,y) = (2*Foo.*(T(r+1,y-1)-(Bo*qe))+(1-2*Foo).*T(r,y-1));
%%%finding values of T of the first node
  elseif r==m
T(m,y)=(2*Foo*(T(r-1,y-1))+(1-2*Foo)*T(r,y-1));
  %%%finding values of T of the last node
  else
T(r,y) =(Foo*(T(r+1,y-1) + T(r-1,y-1)) + (1-2*Foo)*T(r,y-1));
  %%finding values of T of the interior node
  end
 end
 if T(r,y)>33
  T(r,y)=Twater; %% Maximum water temperature
 end
 if T(r,y)<Te %% Minimum evaporator temperature
  T(r,y)=Te;
 end
```

```
end
end
%% Slab ice thickness calculation using moving mesh method
% for y=2:s+1
if j>0&& j<17
 x1a(r,y-1)=x1a(r,y);
 x2a(r,y-1)=x2a(r,y);
 x3a(r,y-1)=x3a(r,y);
 x4(r,y-1)=x4(r,y);
 x5(r,y-1)=x5(r,y);
 x6(r,y-1)=x6(r,y);
  for  r=2:m-1
 %%% solid liquid phase interface velocity
vint=((-kl*(T(r,y)-T(r+1,y))./dx)-(-ks*(T(r,y)-T(r-1,y))./dx))./(rhos*QL);
 for r=1:m
  for dtt=30:60 %% The desired ice production time in hours
       if dtt==30
x1a(r,y)=x1a(r,y-1)+vint*dtt;  %%% ice thickness growth
       elseif dtt==40
x2a(r,y)=x2a(r,y-1)+vint*dtt;
      elseif dtt==45
 x3a(r,y)=x3a(r,y-1)+vint*dtt;
      elseif dtt==50
  x4(r,y)=x4(r,y-1)+vint*dtt;
      elseif dtt==55
  x5(r,y)=x5(r,y-1)+vint*dtt;
      elseif dtt==60
 x6(r,y)=x6(r,y-1)+vint*dtt;
      end
  end
 end
  end
end
 if x6(r,y)<0
    x6(r,y)=0;
 end
  if x6(r,y)>0.04 %% Maximum slab ice thickness in m
   x6(r,y)=0.04;
  end
  if x5(r,y)>0.04
   x5(r,y)=0.04;
  end
    if x4(r,y)>0.04
   x4(r,y)=0.04;
  end
%%% percentage of liquid water
 for r=1:m
  if j>0&& j<17
 if (T(r,y)>Tliquidus)
  sf(r,y)=1;   %% all solid ice
```

```
 elseif (T(r,y)<TSolidus)
  sf(r,y)=0;    %% all liquid water
 else
  sf(r,y)=(T(r,y)-TSolidus)/(Tliquidus-TSolidus); %% Mushy Zone (b/n Tliquidus-
Tsolidus)
  end
  end
 end
Ict(i,j)=Ic;
Tpt(i,j)=Tp1;
Et(i,j)=Eg;
TFt(i,j)=T(r,y);
TFt2(i,j)=T(2,y);TFt3(i,j)=T(3,y);TFt4(i,j)=T(4,y);TFt6(i,j)=T(6,y);TFt8(i,j)=T(7,y);...
TFt10(i,j)=T(m,y);
xFt(i,j)=x6(r,y);
xFt1(i,j)=x1a(r,y);xFt2(i,j)=x2a(r,y);xFt3(i,j)=x3a(r,y);xFt4(i,j)=x4(r,y);xFt5(i,j)=x5(r,y);..
..
xFt6(i,j)=x6(r,y);
copi(i,j)=cop(z);
sFt(i,j)=sf(r,y);
end
end
end
%%%%%%%%%%%%%%%%%%%%%%%%%%%%%%%%%%%
%%% Matlab plotting
Tqsolar=sum (sum (TIQsolar));
Telec=sum (sum (TElec));
%%%%%%%%%%%%%%%%%%%%%%%%%%%%%%%%%%%
%%% Monthly average solar radiation on inclined surface
J1=Ict(1:31,:);F2=Ict(32:59,:);M3=Ict(60:90,:);A4=Ict(91:120,:);m5=Ict(121:151,:);...
j6=Ict(152:181,:);ju7=Ict(182:212,:);Au8=Ict(213:243,:);S9=Ict(244:273,:);...
O10=Ict(274:304,:);N11=Ict(305:334,:);D12=Ict(335:365,:);
%%%%using average values average monthly radiation
IclJa17=sum(J1)./31;IclF16=sum(F2)./28;IclM16=sum(M3)./31;IclA15=sum(A4)./30;...
IclM15=sum(m5)./31;IclJ11=sum(j6)./30;IclJu17=sum(ju7)./31;IclAu16=sum(Au8)./31;..
.
IclS15=sum(S9)./30;IclO15=sum(O10)./31;IclN14=sum(N11)./30;IclD10=sum(D12)./31;
%%%%%%%%%%%%%%%%%%%%%%%%
tt=1:24;
plot(tt,IclJa17,'r-s',tt,IclF16,'b-x',tt,IclM16,'k-x',tt,IclA15,'g-x',tt,IclM15,'m-x',...
tt,IclJ11,'b-s',tt,IclJu17,'m-s',tt,IclAu16,'c-s',tt,IclS15,'c-x',tt,IclO15,'g-h',tt,IclN14,'-y',...
tt,IclD10,'r-x','linewidth',2);
xlabel(' Time in hours','linewidth',2)
ylabel(' Solar Radiation on inclined surface(Watt)')
title('Monthly average solar radiation on inclined surface ')
legend('Jan17','Feb16','Mar16','Apr15','May15','Jun11','Jul17','Aug16','Sept15',...
'Oct15','Nov14','Dec10')
grid on
xlim([1 24])
pause
```

```
clf
%%% Monthly average solar radiation for maximum months
FI2=Ict(32:59,:);AI4=Ict(91:120,:);mI5=Ict(121:151,:);NI11=Ict(305:334,:);...
DI12=Ict(335:365,:);
%%% using average values average monthly radiation
IclF16=sum(FI2)./28;IclA15=sum(AI4)./30;IclM15=sum(mI5)./31;...
 IclN14=sum(NI11)./30;IclD10=sum(DI12)./31;
%%%%%%%%%%%%%%%%%%%%%%%
tt=1:24;
plot(tt,IclF16,'b-x',tt,IclA15,'g-x',tt,IclM15,'m-x',tt,IclN14,'-y',tt,IclD10,'r-x','linewidth',2);
xlabel(' Time in hours','linewidth',2)
ylabel(' Solar Radiation on inclined surface(Watt)')
title('Monthly average solar radiation on inclined surface ')
legend('Feb16','Apr15','May15','Nov14','Dec10')
grid on
xlim([4 20])
pause
clf
%%%Monthly average solar radiation for months having moderate radiation
JI1=Ict(1:31,:);MI3=Ict(60:90,:);O10=Ict(274:304,:);
%%%%% using average values average monthly radiation
IclJa17=sum(JI1)./31;IclM16=sum(MI3)./31;IclO15=sum(O10)./31;
%%%%%%%%%%%%%%%%%%%%%%%
tt=1:24;
plot(tt,IclJa17,'r-s',tt,IclM16,'k-x',tt,IclO15,'g-h','linewidth',2);
xlabel(' Time in hours','linewidth',2)
ylabel(' Solar Radiation on inclined surface(Watt)')
title('Monthly average solar radiation on inclined surface ')
legend('Jan17','mar16','Oct15')
grid on
xlim([4 20])
pause
clf
%%% Monthly average solar radiation for months having Minimum radiation
jI6=Ict(152:181,:);juI7=Ict(182:212,:);AuI8=Ict(213:243,:);SI9=Ict(244:273,:);
%%%%%%%%% using average values average monthly radiation
IclJ11=sum(jI6)./30;IclJu17=sum(juI7)./31;IclAu16=sum(AuI8)./31;...
IclS15=sum(SI9)./30;
%%%%%%%%%%%%%%%%%%%%%%%
tt=1:24;
plot(tt,IclJ11,'g-s',tt,IclJu17,'m-s',tt,IclAu16,'r-s',tt,IclS15,'b-x','linewidth',2);
xlabel(' Time in hours','linewidth',2)
ylabel(' Solar Radiation on inclined surface(Watt)')
title('Monthly average solar radiation on inclined surface ')
legend('Jun11','Jul17','Aug16','Sept15')
grid on
xlim([4 20])
pause
clf %%%% monthly average PV Surface Temperature
Jp1=Tpt(1:31,:);Fp2=Tpt(32:59,:);Mp3=Tpt(60:90,:);Ap4=Tpt(91:120,:);...
```

```
mp5=Tpt(121:151,:);jp6=Tpt(152:181,:);jup7=Tpt(182:212,:);....
Aup8=Tpt(213:243,:);Sp9=Tpt(244:273,:);Op10=Tpt(274:304,:);...
Np11=Tpt(305:334,:);Dp12=Tpt(335:365,:);
%%% using average values average monthly radiation
TpJa17=sum(Jp1)./31;Tpf16=sum(Fp2)./28;Tpm16=sum(Mp3)./31;...
Tpap15=sum(Ap4)./30;Tpma15=sum(mp5)./31;TpJ11=sum(jp6)./30;...
Tpju17=sum(jup7)./31;TpAu16=sum(Aup8)./31;Tps15=sum(Sp9)./30;...
Tpo15=sum(Op10)./31;TpN14=sum(Np11)./30;TpD10=sum(Dp12)./31;
%%%%%%%%%%%%%%%%%%%%%%%%
tt=1:24;
plot(tt,TpJa17,'k-x',tt,Tpf16,'c-x',tt,Tpm16,'m-x',tt,Tpap15,'g-x',tt,Tpma15,'b-x',...
tt,TpJ11,'y-x',tt,Tpju17,'m-s',tt,TpAu16,'c-s',tt,Tps15,'b-s',tt,Tpo15,'k-s',...
tt,TpN14,'g-s',tt,TpD10,'r-x','linewidth',2)
grid on
legend('Jan17','Feb16','Mar16','Apr15','May15','Jun11','Jul17','Aug16','Sept15',...
'Oct15','Nov14','Dec10')
title('PV Surface Temperature');
xlabel('Time in hours');
ylabel('Temperature in oC');
xlim([1 24])
pause
clf
%%% monthly average PV Surface Temperature for maximum radiation
Ac4=Tpt(91:120,:);mc5=Tpt(121:151,:);jc6=Tpt(152:181,:);
%%%%%% using average values average monthly radiation
Tpap15=sum(Ac4)./30;Tpma15=sum(mc5)/31;TpJ11=sum(jc6)./30;
%%%%%%%%%%%%%%%%%%%%%%%%
tt=1:24;
plot(tt,Tpap15,'g-x',tt,Tpma15,'b-x',tt,TpJ11,'y-x','linewidth',2)
grid on
legend('Apr15','May15','Jun11')
title('PV Surface Temperature');
xlabel('Time in hours');
ylabel('Temperature in oC');
xlim([1 24])
pause
clf
%%% monthly average PV Surface Temperature for moderate radiation
juc7=Tpt(182:212,:);Auc8=Tpt(213:243,:);Sc9=Tpt(244:273,:);...
Oc10=Tpt(274:304,:);Nc11=Tpt(305:334,:);
%%%% using average values average monthly radiation
Tpju17=sum(juc7)./31;TpAu16=sum(Auc8)./31;Tps15=sum(Sc9)./30;...
Tpo15=sum(Oc10)./31;TpN14=sum(Nc11)./30;
%%%%%%%%%%%%%%%%%%%%%%%%
tt=1:24;
plot(tt,Tpju17,'m-s',tt,TpAu16,'c-s',tt,Tps15,'b-s',tt,Tpo15,'k-s',...
tt,TpN14,'g-s','linewidth',2)
grid on
legend('Jul17','Aug16','Sept15','Oct15','Nov14')
title('PV Surface Temperature');
```

```
xlabel('Time in hours');
ylabel('Temperature in oC');
xlim([1 24])
pause
clf
%%% monthly average PV Surface Temperature for minimum radiation
Jc1=Tpt(1:31,:);Fc2=Tpt(32:59,:);Mc3=Tpt(60:90,:);Dc12=Tpt(335:365,:);
%%% using average values average monthly radiation
TpJa17=sum(Jc1)/31;Tpf16=sum(Fc2)./28;Tpm16=sum(Mc3)./31;...
TpD10=sum(Dc12)./31;
%%%%%%%%%%%%%%%%%%%%%%%%
tt=1:24;
plot(tt,TpJa17,'k-x',tt,Tpf16,'c-x',tt,Tpm16,'m-x',tt,TpD10,'r-x','linewidth',2)
grid on
legend('Jan17','Feb16','Mar16','Dec10')
title('PV Surface Temperature');
xlabel('Time in hours');
ylabel('Temperature in oC');
xlim([1 24])
pause
clf %% monthly average Electrical Energy Generation
Jn1=Et(1:31,:);Fn2=Et(32:59,:);Mn3=Et(60:90,:);An4=Et(91:120,:);...
mn5=Et(121:151,:);jn6=Et(152:181,:);jun7=Et(182:212,:);Aun8=Et(213:243,:);...
Sn9=Et(244:273,:);On10=Et(274:304,:);Nn11=Et(305:334,:);Dn12=Et(335:365,:);
%%%% using average values average monthly radiation
EJa17=sum(Jn1)./31;EF16=sum(Fn2)./28;EM16=sum(Mn3)./31;...
EA15=sum(An4)./30;EMa15=sum(mn5)./31;EJ11=sum(jn6)./30;...
Eju17=sum(jun7)./31;EAu16=sum(Aun8)./31;ES15=sum(Sn9)./30;...
EO15=sum(On10)./31;EN14=sum(Nn11)./30;ED10=sum(Dn12)./31;
%%%%%%%%%%%%%%%%%%%%%%%%
tt=1:24;
plot(tt,EJa17,'b-s',tt,EF16,'m-x',tt,EM16,'k-s',tt,EA15,'g-x',tt,EMa15,'k-x',...
tt,EJ11,'r-s',tt,Eju17,'c-',tt,EAu16,'c-x',tt,ES15,'m-s',tt,EO15,'g-s',tt,EN14,'y-s',...
tt,ED10,'r-x','linewidth',2)
grid on
legend('Jan17','Feb16','Mar16','Apr15','May15','Jun11','Jul17','Aug16','Sept15',...
'Oct15','Nov14','Dec10')
title ('Electrical Energy Output of the System');
xlabel('Time in hours');
ylabel('Electrical Energy Generation in (W)');
xlim([1 24])
pause
clf
%%monthly average Electrical Energy Generation for months having maximum radiation
Fe2=Et(32:59,:);Ae4=Et(91:120,:);Ne11=Et(305:334,:);De12=Et(335:365,:);
%%% using average values average monthly radiation
EF16=sum(Fe2)./28;EA15=sum(Ae4)./30;EN14=sum(Ne11)./30;...
ED10=sum(De12)./31;
%%%%%%%%%%%%%%%%%%%%%%%%
tt=1:24;
```

```
plot(tt,EF16,'m-x',tt,EA15,'g-x',tt,EN14,'c-s',tt,ED10,'r-x','linewidth',2)
grid on
title ('Electrical Energy Output of the System');
xlabel('Time in hours');
ylabel('Electrical Energy Generation in (W)');
legend('Feb16','Apr15','Nov14','Dec10')
xlim([4 20])
pause
clf %%% monthly average Electrical Energy Generation for months having moderate values
Jx1=Et(1:31,:);Mx3=Et(60:90,:);me5=Et(121:151,:);Ox10=Et(274:304,:);
%%% using average values average monthly radiation
EJa17=sum(Jx1)./31;EM16=sum(Mx3)./31;EMa15=sum(me5)./31;...
EO15=sum(Ox10)./31;
%%%%%%%%%%%%%%%%%%%%%%%%
tt=1:24;
plot(tt,EJa17,'b-s',tt,EM16,'r-s',tt,EMa15,'k-x',tt,EO15,'g-s','linewidth',2)
grid on
legend('Jan17','Mar16','May15','Oct15')
title ('Electrical Energy Output of the System');
xlabel('Time in hours');
ylabel('Electrical Energy Generation in (W)');
xlim([4 20])
pause
clf %%%%%%%%%%%%%%%%%%%%%%%%
%%monthly average Electrical Energy Generation for months having minimum values
jr6=Et(152:181,:);jur7=Et(182:212,:);Aur8=Et(213:243,:);Sr9=Et(244:273,:);
%%%% using average values average monthly radiation
EJ11=sum(jr6)./30;Eju17=sum(jur7)./31;EAu16=sum(Aur8)./31;ES15=sum(Sr9)./30;
%%%%%%%%%%%%%%%%%%%%%%%%
tt=1:24;
plot(tt,EJ11,'r-s',tt,Eju17,'b-',tt,EAu16,'k-x',tt,ES15,'m-s','linewidth',2)
grid on
title ('Electrical Energy Output of the System');
xlabel('Time in hours');
ylabel('Electrical Energy Generation in (W)');
legend('Jun11','Jul17','Aug16','Sept15')
xlim([4 20])
pause
clf %%%performance of monthly average hourly water temperature distribution
%%%%plots at last nodes temperature distribution
Jw1=TFt(1:31,:);Fw2=TFt(32:59,:);Mw3=TFt(60:90,:);Aw4=TFt(91:120,:);...
mw5=TFt(121:151,:);jw6=TFt(152:181,:);juw7=TFt(182:212,:);...
Auw8=TFt(213:243,:);Sw9=TFt(244:273,:);Ow10=TFt(274:304,:);...
Nw11=TFt(305:334,:);Dw12=TFt(335:365,:);
%%%%% Using average values monthly solar radiation
TFJa17=sum(Jw1)./31;TFF16=sum(Fw2)./28;TFMa16=sum(Mw3)./31;...
TFA15=sum(Aw4)./30;TFm15=sum(mw5)./31;TFj11=sum(jw6)./30;...
TFJu17=sum(juw7)./31;TFAu16=sum(Auw8)./31;TFS15=sum(Sw9)./30;...
TFO15=sum(Ow10)./31;TFN14=sum(Nw11)./30;TFD10=sum(Dw12)./31;
```

```
%%%%%%%%%%%%%%%%%%%%%%%%%%%%
tt=1:24;
plot(tt,TFJa17,'m-x',tt, TFF16,'y-s',tt,TFMa16,'b-s',tt,TFA15,'k-x',...
tt, TFm15,'y-x',tt,TFj11,'b-x',tt,TFJu17,'m-s',tt,TFAu16,'k-s',...
tt,TFS15,'r-s',tt,TFO15,'g-s',tt,TFN14,'b-',tt,TFD10,'c-','linewidth',2);
grid on ;
xlabel('Time in hours');
ylabel('Outlet water Temperature(oC)');
title ('Plot of temperature variation as a function of time');
legend('Jan17','Feb16','Mar16','Apr15','May15','Jun11','Jul17','Aug16','Sept15',...
'Oct15','Nov14','Dec10')
xlim([1 24])
pause
clf  %%%% hourly water nodal temperature distribution for each month
%%%%plots at nodes temperature distribution within a day for (January)
Jz2=TFt2(1:31,:);Jz3=TFt3(1:31,:);Jz4=TFt4(1:31,:);Jz6=TFt6(1:31,:);...
Jz8=TFt8(1:31,:);Jz10=TFt10(1:31,:);
%%% Using average values monthly solar radiation
TFJ2=sum(Jz2)./31;TFJ3=sum(Jz3)./31;TFJ4=sum(Jz4)./31;...
TFJ6=sum(Jz6)./31;TFJ8=sum(Jz8)./31;TFJ10=sum(Jz10)./31;
%%%%%%%%%%%%%%%%%%%%%%%%%%%%
tt=1:24;
plot(tt,TFJ2,'m-x',tt, TFJ3,'r-s',tt,TFJ4,'b-s',tt,TFJ6,'k-x',...
tt, TFJ8,'y-x',tt,TFJ10,'c-x','linewidth',2);
grid on ;
xlabel('Time in hours');
ylabel('Outlet nodal water Temperature (oC)');
title ('Plot of nodal water temperature variation for January');
legend('nod2','nod3','nod4','nod6','nod8','nod10')
xlim([4 20])
pause
clf   %%% hourly water nodal temperature distribution for each month
%%%plots at nodes temperature distribution within a day for (February)
Fz2=TFt2(32:59,:);Fz3=TFt3(32:59,:);Fz4=TFt4(32:59,:);...
Fz6=TFt6(32:59,:);Fz8=TFt8(32:59,:);Fz10=TFt10(32:59,:);
%%% Using average values monthly solar radiation
TFF2=sum(Fz2)./28;TFF3=sum(Fz3)./28;TFF4=sum(Fz4)./28;....
TFF6=sum(Fz6)./28;TFF8=sum(Fz8)./28;TFF10=sum(Fz10)./28;
%%%%%%%%%%%%%%%%%%%%%%%%%%%%
tt=1:24;
plot(tt,TFF2,'m-x',tt,TFF3,'r-s',tt,TFF4,'b-s',tt,TFF6,'k-x',...
tt,TFF8,'y-x',tt,TFF10,'c-x','linewidth',2);
grid on ;
xlabel('Time in hours');
ylabel('Outlet nodal water Temperature (oC)');
title ('Plot of nodal water temperature variation February');
legend('nod2','nod3','nod4','nod6','nod8','nod10')
xlim([4 20])
pause
clf  %%%% hourly water nodal temperature distribution for each month
```

```
%%%%plots at nodes temperature distribution within a day for (March)
Mz2=TFt2(60:90,:);Mz3=TFt3(60:90,:);Mz4=TFt4(60:90,:);...
Mz6=TFt6(60:90,:);Mz8=TFt8(60:90,:);Mz10=TFt10(60:90,:);
%%% Using average values monthly solar radiation
TmF2=sum(Mz2)./31;TmF3=sum(Mz3)./31;TmF4=sum(Mz4)./31;....
TmF6=sum(Mz6)./31;TmF8=sum(Mz8)./31;TmF10=sum(Mz10)./31;
%%%%%%%%%%%%%%%%%%%%%%
tt=1:24;
plot(tt,TmF2,'m-x',tt,TmF3,'r-s',tt,TmF4,'b-s',tt,TmF6,'k-x',...
tt,TmF8,'y-x',tt,TmF10,'c-x','linewidth',2);
grid on ;
xlabel('Time in hours');
ylabel('Outlet nodal water Temperature (oC)');
title ('Plot of nodal water temperature variation March');
legend('nod2','nod3','nod4','nod6','nod8','nod10')
xlim([4 20])
pause
clf  %%% hourly water nodal temperature distribution for each month
%%%%plots at nodes temperature distribution within a day for (April)
Ap2=TFt2(91:120,:);Ap3=TFt3(91:120,:);Ap4=TFt4(91:120,:);...
Ap6=TFt6(91:120,:);Ap8=TFt8(91:120,:);Ap10=TFt10(91:120,:);
%%% Using average values monthly solar radiation
TFAp2=sum(Ap2)./30;TFAp3=sum(Ap3)./30;TFAp4=sum(Ap4)./30;...
TFAp6=sum(Ap6)./30;TFAp8=sum(Ap8)./30;TFAp10=sum(Ap10)./30;
%%%%%%%%%%%%%%%%%%%%%%
tt=1:24;
plot(tt,TFAp2,'m-x',tt, TFAp3,'r-s',tt,TFAp4,'b-s',tt,TFAp6,'k-x',...
tt, TFAp8,'y-x',tt,TFAp10,'c-x','linewidth',2);
grid on ;
xlabel('Time in hours');
ylabel('Outlet nodal water Temperature (oC)');
title ('Plot of nodal water temperature variation for April');
legend('nod2','nod3','nod4','nod6','nod8','nod10')
xlim([4 20])
pause
clf  %%% hourly water nodal temperature distribution for each month
%%%%plots at nodes temperature distribution within a day for (May)
mz2=TFt2(121:151,:);mz3=TFt3(121:151,:);mz4=TFt4(121:151,:);...
mz6=TFt6(121:151,:);mz8=TFt8(121:151,:);mz10=TFt10(121:151,:);
%%%%%% Using average values monthly solar radiation
TFm2=sum(mz2)./31;TFm3=sum(mz3)./31;TFm4=sum(mz4)./31;...
TFm6=sum(mz6)./31;TFm8=sum(mz8)./31;TFm10=sum(mz10)./31;
%%%%%%%%%%%%%%%%%%%%%%%%%%%%%%%%
tt=1:24;
plot(tt,TFm2,'m-x',tt, TFm3,'r-s',tt,TFm4,'b-s',tt,TFm6,'k-*',tt, TFm8,'y-x',...
tt,TFm10,'c-*','linewidth',2);
grid on ;
xlabel('Time in hours');
ylabel('Outlet nodal water Temperature (oC)');
title ('Plot of nodal water temperature variation for May');
```

```
legend('nod2','nod3','nod4','nod6','nod8','nod10')
xlim([4 20])
pause
clf  %% hourly water nodal temperature distribution for each month
%%%%plots at nodes temperature distribution within a day for (June)
jz2=TFt2(152:181,:);jz3=TFt3(152:181,:);jz4=TFt4(152:181,:);...
jz6=TFt6(152:181,:);jz8=TFt8(152:181,:);jz10=TFt10(152:181,:);
%%% Using average values monthly solar radiation
TFj2=sum(jz2)./30;TFj3=sum(jz3)./30;TFj4=sum(jz4)./30;...
TFj6=sum(jz6)./30;TFj8=sum(jz8)./30;TFj10=sum(jz10)./30;
%%%%%%%%%%%%%%%%%%%%%%%%
tt=1:24;
plot(tt,TFj2,'m-x',tt, TFj3,'r-s',tt,TFj4,'b-s',tt,TFj6,'k-x',tt, TFj8,'y-x',...
tt,TFj10,'c-x','linewidth',2);
grid on ;
xlabel('Time in hours');
ylabel('Outlet nodal water Temperature (oC)');
title ('Plot of nodal water temperature variation for June');
legend('nod2','nod3','nod4','nod6','nod8','nod10')
xlim([4 20])
pause
clf  %%% hourly water nodal temperature distribution for each month
%%%%plots at nodes temperature distribution within a day for (July)
juz2=TFt2(182:212,:);juz3=TFt3(182:212,:);juz4=TFt4(182:212,:);...
juz6=TFt6(182:212,:);juz8=TFt8(182:212,:);juz10=TFt10(182:212,:);
%%%%%%%%% Using average values monthly solar radiation
TFju2=sum(juz2)./31;TFju3=sum(juz3)./31;TFju4=sum(juz4)./31;...
TFju6=sum(juz6)./31;TFju8=sum(juz8)./31;TFju10=sum(juz10)./31;
%%%%%%%%%%%%%%%%%%%%%%%%%%%%
tt=1:24;
plot(tt,TFju2,'m-x',tt, TFju3,'r-s',tt,TFju4,'b-s',tt,TFju6,'k-x',tt,TFju8,'y-x',...
tt,TFju10,'c-x','linewidth',2);
grid on ;
xlabel('Time in hours');
ylabel('Outlet nodal water Temperature (oC)');
title ('Plot of nodal water temperature variation for July');
legend('nod2','nod3','nod4','nod6','nod8','nod10')
xlim([4 20])
pause
clf %%%%% hourly water nodal temperature distribution for each month
%%%%plots at nodes temperature distribution within a day for (August)
au2=TFt2(213:243,:);au3=TFt3(213:243,:);au4=TFt4(213:243,:);...
au6=TFt6(213:243,:);au8=TFt8(213:243,:);au10=TFt10(213:243,:);
%%%%% Using average values monthly solar radiation
TFau2=sum(au2)./31;TFau3=sum(au3)./31;TFau4=sum(au4)./31;...
TFau6=sum(au6)./31;TFau8=sum(au8)./31;TFau10=sum(au10)./31;
%%%%%%%%%%%%%%%%%%%%%%%%%%%%
tt=1:24;
plot(tt,TFau2,'m-x',tt, TFau3,'r-s',tt,TFau4,'b-s',tt,TFau6,'k-x',...
tt, TFau8,'y-x',tt,TFau10,'c-x','linewidth',2);
```

```
grid on ;
xlabel('Time in hours');
ylabel('Outlet nodal water Temperature (oC)');
title ('Plot of nodal water temperature variation for August');
legend('nod2','nod3','nod4','nod6','nod8','nod10')
xlim([4 20])
pause
clf  %%%%% hourly water nodal temperature distribution for each month
%%%%plots at nodes temperature distribution within a day for (September)
Sz2=TFt2(244:273,:);Sz3=TFt3(244:273,:);Sz4=TFt4(244:273,:);...
Sz6=TFt6(244:273,:);Sz8=TFt8(244:273,:);Sz10=TFt10(244:273,:);
%%%%%%%%%%%%%%%%%% Using average values monthly solar radiation
TFS2=sum(Sz2)./30;TFS3=sum(Sz3)./30;TFS4=sum(Sz4)./30;...
TFS6=sum(Sz6)./30;TFS8=sum(Sz8)./30;TFS10=sum(Sz10)./30;
%%%%%%%%%%%%%%%%%%%%%%%%%%%%%
tt=1:24;
plot(tt,TFS2,'m-x',tt, TFS3,'r-s',tt,TFS4,'b-s',tt,TFS6,'k-x',tt, TFS8,'y-x',...
tt,TFS10,'c-x','linewidth',2);
grid on ;
xlabel('Time in hours');
ylabel('Outlet nodal water Temperature (oC)');
title ('Plot of nodal water temperature variation for september');
legend('nod2','nod3','nod4','nod6','nod8','nod10')
xlim([4 20])
pause
clf  %%% hourly water nodal temperature distribution for each month
%%%%plots at nodes temperature distribution within a day for (October)
Oz2=TFt2(274:304,:);Oz3=TFt3(274:304,:);Oz4=TFt4(274:304,:);...
Oz6=TFt6(274:304,:);Oz8=TFt8(274:304,:);Oz10=TFt10(274:304,:);
%%% Using average values monthly solar radiation
TFO2=sum(Oz2)./31;TFO3=sum(Oz3)./31;TFO4=sum(Oz4)./31;...
TFO6=sum(Oz6)./31;TFO8=sum(Oz8)./31;TFO10=sum(Oz10)./31;
%%%%%%%%%%%%%%%%%%%%%%%%%%%%%
tt=1:24;
plot(tt,TFO2,'m-x',tt, TFO3,'r-s',tt,TFO4,'b-s',tt,TFO6,'k-x',tt, TFO8,'y-x',...
tt,TFO10,'c-x','linewidth',2);
grid on ;
xlabel('Time in hours');
ylabel('Outlet nodal water Temperature(oC)');
title ('Plot of nodal water temperature variation for October');
legend('nod2','nod3','nod4','nod6','nod8','nod10')
xlim([4 20])
pause
clf  %%% hourly water nodal temperature distribution for each month
%%%%plots at nodes temperature distribution within a day for (December)
Dz2=TFt2(335:365,:);Dz3=TFt3(335:365,:);Dz4=TFt4(335:365,:);...
Dz6=TFt6(335:365,:);Dz8=TFt8(335:365,:);Dz10=TFt10(335:365,:);
%%% Using average values monthly solar radiation
TFD2=sum(Dz2)./31;TFD3=sum(Dz3)./31;TFD4=sum(Dz4)./31;...
TFD6=sum(Dz6)./31;TFD8=sum(Dz8)./31;TFD10=sum(Dz10)./31;
```

```
%%%%%%%%%%%%%%%%%%%%%%%
tt=1:24;
plot(tt,TFD2,'m-x',tt, TFD3,'r-s',tt,TFD4,'b-s',tt,TFD6,'k-x',...
tt, TFD8,'y-x',tt,TFD10,'c-x','linewidth',2);
grid on ;
xlabel('Time in hours');
ylabel('Outlet nodal water Temperature on (oC)');
title ('Plot of nodal water temperature variation for December');
legend('nod2','nod3','nod4','nod6','nod8','nod10')
xlim([4 20])
pause
clf  %%% hourly water temperature distribution
%%%water temperature distribution for months having maximum cooling capacity
Jv1=TFt(1:31,:);Fv2=TFt(32:59,:);Mv3=TFt(60:90,:);Av4=TFt(91:120,:);...
mv5=TFt(121:151,:);Nv11=TFt(305:334,:);Dv12=TFt(335:365,:);
%%%%using average values of monthly solar radiation
TFJa17=sum(Jv1)./31;TFF16=sum(Fv2)./28;TFMa16=sum(Mv3)./31;...
 TFA15=sum(Av4)./30;TFm15=sum(mv5)./31;TFN14=sum(Nv11)./30;...
 TFD10=sum(Dv12)./31;
tt=1:24;
plot(tt,TFJa17,'m-x',tt, TFF16,'c-s',tt,TFMa16,'y-s',tt,TFA15,'k-x',...
tt,TFm15,'g-x',tt,TFN14,'r-x',tt,TFD10,'b-h','linewidth',2);
grid on ;
xlabel('Time in hours');
ylabel('Outlet water Temperature(oC)');
title ('Plot of nodal water temperature variation as a function of time');
legend('Jan17','Feb16','Mar16','Apr15','May15','Nov14','Dec10')
xlim([4 20])
pause
clf %% hourly water temperature distribution
%%%water temperature distribution for months having moderate cooling capacity
jv6=TFt(152:181,:);juv7=TFt(182:212,:);Sv9=TFt(244:273,:);...
 Ov10=TFt(274:304,:);
%%%%using average values of monthly solar radiation
TFj11=sum(jv6)./30;TFJu17=sum(juv7)./31;TFS15=sum(Sv9)./30;...
TFO15=sum(Ov10)./31;
%%%%%%%%%%%%%%%%%%%%%%%
tt=1:24;
plot(tt,TFj11,'b-x',tt,TFJu17,'m-s',tt,TFS15,'r-s',tt,TFO15,'g-s','linewidth',2);
grid on ;
xlabel('Time in hours');
ylabel('Outlet water Temperature(oC)');
title ('Plot of nodal water temperature variation as a function of time');
legend('Jun11','Jul17','Sept15','Oct10')
xlim([4 20])
pause
clf  %%% hourly water temperature distribution
%%%plots of water temperature distribution for months with minimum cooling load
Auv8=TFt(213:243,:);
%%%%%using average values of monthly solar radiation
```

```
TFAu16=sum(Auv8)./31;
%%%%%%%%%%%%%%%%%%%%%%%%%
tt=1:24;
plot(tt,TFAu16,'b-x','linewidth',2);
grid on ;
xlabel('Time in hours');
ylabel('Outlet water Temperature(oC)');
title ('Plot of nodal water temperature variation as a function of time');
legend('Aug16')
xlim([4 20])
pause
clf  %%% solid-liquid interface location modeling
%%%plot for ice crystal growth
Jh1=xFt(1:31,:);Fh2=xFt(32:59,:);Mh3=xFt(60:90,:);Ah4=xFt(91:120,:);...
mh5=xFt(121:151,:);jh6=xFt(152:181,:);juh7=xFt(182:212,:);...
Auh8=xFt(213:243,:);Sh9=xFt(244:273,:);Oh10=xFt(274:304,:);...
Nh11=xFt(305:334,:);Dh12=xFt(335:365,:);
%%%%using average values of monthly solar radiation
xFJa17=sum(Jh1)./31;xFF16=sum(Fh2)./28;xFMa16=sum(Mh3)./31;...
xFA15=sum(Ah4)./30;xFm15=sum(mh5)./31;xFj11=sum(jh6)./30;...
xFJu17=sum(juh7)./31;xFAu16=sum(Auh8)./31;xFS15=sum(Sh9)./30;...
xFO15=sum(Oh10)./31;xFN14=sum(Nh11)./30;xFD10=sum(Dh12)./31;
%%%%%%%%%%%%%%%%%%%%%%%%%
tt=1:24;
plot(tt,xFJa17,'m-x',tt,xFF16,'y-s',tt,xFMa16,'b-s',tt,xFA15,'k-x',...
tt,xFm15,'y-x',tt,xFj11,'b-x',tt,xFJu17,'m-s',tt,xFAu16,'k-s',...
tt,xFS15,'r-s',tt,xFO15,'g-s',tt,xFN14,'b-',tt,xFD10,'c-','linewidth',2);
grid on
xlabel('Time in hours');
ylabel('Ice slab thickness in meter');
title ('Plot of ice thickness variation as a function of time');
legend('Jan17','Feb16','Mar16','Apr15','May15','Jun11','Jul17','Aug16','Sept15',...
'Oct15','Nov14','Dec10')
xlim([4 20])
pause
clf  %%%%% hourly ice crystal growth for each month
%%%%plots of ice formation variation with time within a day for (January)
Jy1=xFt1(1:31,:);Jy2=xFt2(1:31,:);Jy3=xFt3(1:31,:);Jy4=xFt4(1:31,:);...
 Jy5=xFt4(1:31,:);Jy6=xFt6(1:31,:);
%%% Using average values monthly solar radiation
xFJ1=sum(Jy1)./31;xFJ2=sum(Jy2)./31;xFJ3=sum(Jy3)./31;...
xFJ4=sum(Jy4)./31;xFJ5=sum(Jy5)./31;xFJ6=sum(Jy6)./31;
%%%%%%%%%%%%%%%%%%%%%%%%%
tt=1:24;
plot(tt,xFJ1,'m-x',tt, xFJ2,'r-s',tt,xFJ3,'b-s',tt,xFJ4,'k-x',...
tt, xFJ5,'y-x',tt,xFJ6,'c-x','linewidth',2);
grid on ;
xlabel('Time in hours');
ylabel('Ice slab thickness in meter');
title ('Plot of ice thickness variation as a function of time for January');
```

```
legend('dtt=30','dtt=40','dtt=45','dtt=50','dtt=55','dtt=60')
xlim([4 20])
pause
clf %%% hourly ice crystal growth for each month
%%plots of ice formation variation with time within a day for(February)
Fy1=xFt1(32:59,:);Fy2=xFt2(32:59,:);Fy3=xFt3(32:59,:);...
Fy4=xFt4(32:59,:);Fy5=xFt5(32:59,:);Fy6=xFt6(32:59,:);
%%% Using average values monthly solar radiation
xFF1=sum(Fy1)./28;xFF2=sum(Fy2)./28;xFF3=sum(Fy3)./28;...
xFF4=sum(Fy4)./28;xFF5=sum(Fy5)./28;xFF6=sum(Fy6)./28;
%%%%%%%%%%%%%%%%%%%%%%%%%%%%
tt=1:24;
plot(tt,xFF1,'m-x',tt, xFF2,'r-s',tt,xFF3,'b-s',tt,xFF4,'k-x',tt,xFF5,'y-x',...
tt,xFF6,'c-x','linewidth',2);
grid on ;
xlabel('Time in hours');
ylabel('Ice slab thickness in meter');
title ('Plot of ice thickness variation as a function of time for February');
legend('dtt=30','dtt=40','dtt=45','dtt=50','dtt=55','dtt=60')
xlim([4 20])
pause
clf %%% hourly ice crystal growth for each month
%%%plots of ice formation variation within a day for(March)
My1=xFt1(60:90,:);My2=xFt2(60:90,:);My3=xFt3(60:90,:);...
My4=xFt4(60:90,:);My5=xFt5(60:90,:);My6=xFt6(60:90,:);
%%% Using average values monthly solar radiation
xmF1=sum(My1)./31;xmF2=sum(My2)./31;xmF3=sum(My3)./31;...
xmF4=sum(My4)./31;xmF5=sum(My5)./31;xmF6=sum(My6)./31;
%%%%%%%%%%%%%%%%%%%%%%%%%%%%
tt=1:24;
plot(tt,xmF1,'m-x',tt, xmF2,'r-s',tt,xmF3,'b-s',tt,xmF4,'k-x',tt,xmF5,'y-x',...
tt,xmF6,'c-x','linewidth',2);
grid on ;
xlabel('Time in hours');
ylabel('Ice slab thickness in meter');
title ('Plot of ice thickness variation as a function of time for March');
legend('dtt=30','dtt=40','dtt=45','dtt=50','dtt=55','dtt=60')
xlim([4 20])
pause
clf  %%% hourly ice crystal growth for each month
%%plots of ice formation variation within a day for(April)
Apy1=xFt1(91:120,:);Apy2=xFt2(91:120,:);Apy3=xFt3(91:120,:);...
Apy4=xFt4(91:120,:);Apy5=xFt5(91:120,:);Apy6=xFt6(91:120,:);
%%% Using average values monthly solar radiation
xFAp1=sum(Apy1)./30;xFAp2=sum(Apy2)./30;xFAp3=sum(Apy3)./30;...
xFAp4=sum(Apy4)./30;xFAp5=sum(Apy5)./30;xFAp6=sum(Apy6)./30;
%%%%%%%%%%%%%%%%%%%%%%%%%%%%
tt=1:24;
plot(tt,xFAp1,'m-x',tt, xFAp2,'r-s',tt,xFAp3,'b-s',tt,xFAp4,'k-x',tt, xFAp5,'y-x',...
tt,xFAp6,'c-x','linewidth',2);
```

```
grid on ;
xlabel('Time in hours');
ylabel('Ice slab thickness in meter');
title ('Plot of ice thickness variation as a function of time for April');
legend('dtt=30','dtt=40','dtt=45','dtt=50','dtt=55','dtt=60')
xlim([4 20])
pause
clf  %% hourly ice crystal growth for each month
%%plots of ice crystal growth variation within a day for (May)
mf1=xFt1(121:151,:);mf2=xFt2(121:151,:);mf3=xFt3(121:151,:);...
mf4=xFt4(121:151,:);mf5=xFt5(121:151,:);mf6=xFt6(121:151,:);
%%% Using average values monthly solar radiation
xFm1=sum(mf1)./31;xFm2=sum(mf2)./31;xFm3=sum(mf3)./31;...
xFm4=sum(mf4)./31;xFm5=sum(mf5)./31;xFm6=sum(mf6)./31;
%%%%%%%%%%%%%%%%%%%%%%%%
tt=1:24;
plot(tt,xFm1,'m-x',tt, xFm2,'r-s',tt,xFm3,'b-s',tt,xFm4,'k-*',tt, xFm5,'y-x',...
tt,xFm6,'c-*','linewidth',2);
grid on ;
xlabel('Time in hours');
ylabel('Ice slab thickness in meter');
title ('Plot of ice thickness variation as a function of time for May');
legend('dtt=30','dtt=40','dtt=45','dtt=50','dtt=55','dtt=60')
xlim([4 20])
pause
clf  %%plots of ice formation variation within a day for (June)
jy1=xFt1(152:181,:);jy2=xFt2(152:181,:);jy3=xFt3(152:181,:);...
jy4=xFt4(152:181,:);jy5=xFt5(152:181,:);jy6=xFt6(152:181,:);
%%% Using average values monthly solar radiation
xFj1=sum(jy1)./30;xFj2=sum(jy2)./30;xFj3=sum(jy3)./30;...
xFj4=sum(jy4)./30;xFj5=sum(jy5)./30;xFj6=sum(jy6)./30;
%%%%%%%%%%%%%%%%%%%%%%%%
tt=1:24;
plot(tt,xFj1,'m-x',tt, xFj2,'r-s',tt,xFj3,'b-s',tt,xFj4,'k-x',tt, xFj5,'y-x',...
tt,xFj6,'c-x','linewidth',2);
grid on ;
xlabel('Time in hours');
ylabel('Ice slab thickness in meter');
title ('Plot of ice thickness variation as a function of time for June');
legend('dtt=30','dtt=40','dtt=45','dtt=50','dtt=55','dtt=60')
xlim([4 20])
pause
clf  %%% hourly ice crystal growth for each month
%%%plots of ice formation variation within a day for (July)
juz1=xFt1(182:212,:);juz2=xFt2(182:212,:);juz3=xFt3(182:212,:);...
juz4=xFt4(182:212,:);juz5=xFt5(182:212,:);juz6=xFt6(182:212,:);
%%%%% Using average values monthly solar radiation
xFju1=sum(juz1)./31;xFju2=sum(juz2)./31;xFju3=sum(juz3)./31;...
xFju4=sum(juz4)./31;xFju5=sum(juz5)./31;xFju6=sum(juz6)./31;
%%%%%%%%%%%%%%%%%%%%%%%%%%%
```

```
tt=1:24;
plot(tt,xFju1,'m-x',tt, xFju2,'r-s',tt,xFju3,'b-s',tt,xFju4,'k-x',...
tt,xFju5,'y-x',tt,xFju6,'c-x','linewidth',2);
grid on ;
xlabel('Time in hours');
ylabel('Ice slab thickness in meter');
title ('Plot of ice thickness variation as a function of time for July');
legend('dtt=30','dtt=40','dtt=45','dtt=50','dtt=55','dtt=60')
xlim([4 20])
pause
clf  %%% hourly ice crystal growth for each month
%%%plots of ice formation variation within a day for (August)
au1=xFt1(213:243,:);au2=xFt2(213:243,:);au3=xFt3(213:243,:);...
au4=xFt4(213:243,:);au5=xFt5(213:243,:);au6=xFt6(213:243,:);
%%% Using average values monthly solar radiation
xFau1=sum(au1)./31;xFau2=sum(au2)./31;xFau3=sum(au3)./31;...
xFau4=sum(au4)./31;xFau5=sum(au5)./31;xFau6=sum(au6)./31;
%%%%%%%%%%%%%%%%%%%%%%%%%%
tt=1:24;
plot(tt,xFau1,'m-x',tt, xFau2,'r-s',tt,xFau3,'b-s',tt,xFau4,'k-x',...
tt, xFau5,'y-x',tt,xFau6,'c-x','linewidth',2);
grid on ;
xlabel('Time in hours');
ylabel('Ice slab thickness in meter');
title ('Plot of ice thickness variation as a function of time for August');
legend('dtt=30','dtt=40','dtt=45','dtt=50','dtt=55','dtt=60')
xlim([4 20])
pause
clf  %%% hourly ice crystal growth for each month
%%%%plots of ice formation variation within a day for(September)
Sz1=xFt1(244:273,:);Sz2=xFt2(244:273,:);Sz3=xFt3(244:273,:);...
Sz4=xFt4(244:273,:);Sz5=xFt5(244:273,:);Sz6=xFt6(244:273,:);
%%%% Using average values monthly solar radiation
xFS1=sum(Sz1)./30;xFS2=sum(Sz2)./30;xFS3=sum(Sz3)./30;...
xFS4=sum(Sz4)./30;xFS5=sum(Sz5)./30;xFS6=sum(Sz6)./30;
%%%%%%%%%%%%%%%%%%%%%%%%%%
tt=1:24;
plot(tt,xFS1,'m-x',tt, xFS2,'r-s',tt,xFS3,'b-s',tt,xFS4,'k-x',...
tt, xFS5,'y-x',tt,xFS6,'c-x','linewidth',2);
grid on ;
xlabel('Time in hours');
ylabel('Ice slab thickness in meter');
title ('Plot of ice thickness variation as a function of time for September');
legend('dtt=30','dtt=40','dtt=45','dtt=50','dtt=55','dtt=60')
xlim([4 20])
pause
clf  %%% hourly ice crystal growth for each month
%%%plots of ice formation variation within a day for (October)
Oz1=xFt1(274:304,:);Oz2=xFt2(274:304,:);Oz3=xFt3(274:304,:);...
Oz4=xFt4(274:304,:);Oz5=xFt5(274:304,:);Oz6=xFt6(274:304,:);
```

```
%%%% Using average values monthly solar radiation
xFO1=sum(Oz1)./31;xFO2=sum(Oz2)./31;xFO3=sum(Oz3)./31;...
xFO4=sum(Oz4)./31;xFO5=sum(Oz5)./31;xFO6=sum(Oz6)./31;
%%%%%%%%%%%%%%%%%%%%%%%%%
tt=1:24;
plot(tt,xFO1,'m-x',tt,xFO2,'r-s',tt,xFO3,'b-s',tt,xFO4,'k-x',tt,xFO5,'y-x',...
tt,xFO6,'c-x','linewidth',2);
grid on ;
xlabel('Time in hours');
ylabel('Ice slab thickness in meter');
title ('Plot of ice thickness variation as a function of time for October');
legend('dtt=30','dtt=40','dtt=45','dtt=50','dtt=55','dtt=60')
xlim([4 20])
pause
clf %%% hourly ice crystal growth for each month
%%%plots of ice formation variation within a day for (December)
Dz1=xFt1(335:365,:);Dz2=xFt2(335:365,:);Dz3=xFt3(335:365,:);...
Dz4=xFt4(335:365,:);Dz5=xFt5(335:365,:);Dz6=xFt6(335:365,:);
%%% Using average values monthly solar radiation
xFD1=sum(Dz1)./31;xFD2=sum(Dz2)./31;xFD3=sum(Dz3)./31;...
xFD4=sum(Dz4)./31;xFD5=sum(Dz5)./31;xFD6=sum(Dz6)./31;
%%%%%%%%%%%%%%%%%%%%%%%%%
tt=1:24;
plot(tt,xFD1,'m-x',tt, xFD2,'r-s',tt,xFD3,'b-s',tt,xFD4,'k-x',tt, xFD5,'y-x',...
tt,xFD6,'c-x','linewidth',2);
grid on ;
xlabel('Time in hours');
ylabel('Ice slab thickness in meter');
title ('Plot of ice thickness variation as a function of time for December');
legend('dtt=30','dtt=40','dtt=45','dtt=50','dtt=55','dtt=60')
xlim([4 20])
pause
clf  %% hourly ice crystal growth analysis
%%%Ice crystal growth for highly performed months
Jk1=xFt(1:31,:);Fk2=xFt(32:59,:);Mk3=xFt(60:90,:);Ak4=xFt(91:120,:);...
mk5=xFt(121:151,:);Nk11=xFt(305:334,:);Dk12=xFt(335:365,:);
%%%using average values of monthly solar radiation
xFJa17=sum(Jk1)./31;xFF16=sum(Fk2)./28;xFMa16=sum(Mk3)./31;...
xFA15=sum(Ak4)./30;xFm15=sum(mk5)./31;xFN14=sum(Nk11)./30;...
xFD10=sum(Dk12)./31;
%%%%%%%%%%%%%%%%%%%%%%%%%
tt=1:24;
plot(tt,xFJa17,'m-x',tt, xFF16,'r-s',tt,xFMa16,'b-s',tt,xFA15,'k-x',...
tt, xFm15,'c-x',tt,xFN14,'b-x',tt,xFD10,'r-h','linewidth',2);
grid on
xlabel('Time in hours');
ylabel('Ice slab thickness in meter');
title ('Plot of ice thickness variation as a function of time');
legend('Jan17','Feb16','Mar16','Apr15','May15','Nov14','Dec10')
xlim([4 20])
```

```
pause
clf %%% hourly ice crystal growth analysis
%%%Ice crystal growth for moderately performed months
jk6=xFt(152:181,:);juk6=xFt(182:212,:);Sk6=xFt(244:273,:);...
Ok6=xFt(274:304,:);
%%%%using average values of solar radiation
xFj11=sum(jk6)./30;xFJu17=sum(juk6)./31;xFS15=sum(Sk6)./30;...
xFO15=sum(Ok6)./31;
%%%%%%%%%%%%%%%%%%%%%%%
tt=1:24;
plot(tt,xFj11,'b-x',tt,xFJu17,'m-s',tt,xFS15,'r-s',tt,xFO15,'g-s','linewidth',2);
grid on
xlabel('Time in hours');
ylabel('Ice slab thickness in meter');
title ('Plot of ice thickness variation as a function of time');
legend('Jun11','Jul17','Sept15','Oct15')
xlim([4 20])
pause
clf %%% hourly ice crystal growth analysis
%%%Ice crystal growth for moderate performance  month
Auk6=xFt(213:243,:);
%%%%using average values of monthly average solar radiation
xFAu16=sum(Auk6)./31;
%%%%%%%%%%%%%%%%%%%%%%%%%%
tt=1:24;
plot(tt,xFAu16,'r-x','linewidth',2);
grid on
xlabel('Time in hours');
ylabel('Ice slab thickness in meter');
title ('Plot of ice thickness variation as a function of time');
legend('Aug16')
xlim([4 20])
pause
clf  %%% monthly average cop of the system
Jq1=copi(1:31,:);Fq2=copi(32:59,:);Mq3=copi(60:90,:);Aq4=copi(91:120,:);...
mq5=copi(121:151,:);jq6=copi(152:181,:);juq7=copi(182:212,:);...
Auq8=copi(213:243,:);Sq9=copi(244:273,:);Oq10=copi(274:304,:);...
Nq11=copi(305:334,:);Dq12=copi(335:365,:);
%%% using average values monthly average solar radiation
copiJa17=sum(Jq1)./31;copiF16=sum(Fq2)./28;copiMa16=sum(Mq3)./31;....
copiA15=sum(Aq4)./30;copim15=sum(mq5)./31;copij11=sum(jq6)./30;...
copiJu17=sum(juq7)./31;copiAu16=sum(Auq8)./31;copiS15=sum(Sq9)./30;...
copiO15=sum(Oq10)./31;copiN14=sum(Nq11)./30;copiD10=sum(Dq12)./31;
%%%%%%%%%%%%%%%%%%%%%%%%%%
tt=1:24;
plot(tt,copiJa17,'k-',tt,copiF16,'g-x',tt,copiMa16,'y-h',tt,copiA15,'b-x',...
tt,copim15,'k-*',tt,copij11,'r-x',tt,copiJu17,'r-*',tt,copiAu16,'-b',...
tt,copiS15,'g-x',tt,copiO15,'m-*',tt,copiN14,'c-x',...
tt,copiD10,'c-','linewidth',2);
xlabel(' Time in hours')
```

```
ylabel(' Cop of the refrigerator')
title('Monthly Cop of the System')
legend('Jan17','Feb16','Mar16','Apr15','May15','Jun11','Jul17','Aug16',...
'Sept15','Oct15','Nov14','Dec10')
xlim([2 22])
grid on
pause
clf  %% Liquid water percentage of ice modeling
%%% decreasing of water percentage
JI1=sFt(1:31,:);FI2=sFt(32:59,:);MI3=sFt(60:90,:);AI4=sFt(91:120,:);...
mI5=sFt(121:151,:);jI6=sFt(152:181,:);juI7=sFt(182:212,:);...
AuI8=sFt(213:243,:);SI9=sFt(244:273,:);OI10=sFt(274:304,:);...
NI11=sFt(305:334,:);DI12=sFt(335:365,:);
%%%using average values of monthly solar radiation
sFJa17=sum(JI1)./31;sFF16=sum(FI2)./28;sFMa16=sum(MI3)./31;...
sFA15=sum(AI4)./30;sFm15=sum(mI5)./31;sFj11=sum(jI6)./30;...
sFJu17=sum(juI7)./31;sFAu16=sum(AuI8)./31;sFS15=sum(SI9)./30;...
sFO15=sum(OI10)./31;sFN14=sum(NI11)./30;sFD10=sum(DI12)./31;
%%%%%%%%%%%%%%%%%%%%%%%%%%
tt=1:24;
plot(tt,sFJa17,'m-x',tt,sFF16,'y-s',tt,sFMa16,'b-s',tt,sFA15,'k-x',...
tt,sFm15,'y-x',tt,sFj11,'b-x',tt,sFJu17,'m-s',tt,sFAu16,'k-s',...
tt,sFS15,'r-s',tt,sFO15,'g-s',tt,sFN14,'b-',tt,sFD10,'c-','linewidth',2);
grid on
xlabel('Time in hours');
ylabel('liquid water percentage (%)');
title ('Plot of water percentage variation as a function of time');
legend('Jan17','Feb16','Mar16','Apr15','May15','Jun11','Jul17',...
'Aug16','Sept15','Oct15','Nov14','Dec10')
xlim([4 20])
grid on
```